

# Numerical Modelling of the Interaction between Tidal Stream Turbines and the Benthic Environment

David Haverson



*A thesis submitted in partial fulfilment of the requirements  
for the award on an Engineering Doctorate*

THE UNIVERSITY OF EXETER

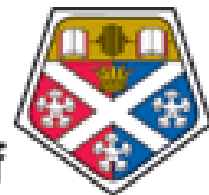
2017

# IDCORE

This thesis is submitted in partial fulfilment of the requirements for the award of an Engineering Doctorate, jointly awarded by the University of Edinburgh, the University of Exeter and the University of Strathclyde. The work presented has been conducted under the industrial supervision of Cefas as a project within the Industrial Doctoral Centre for Offshore Renewable Energy.




THE UNIVERSITY  
*of* EDINBURGH



University of  
**Strathclyde**

I declare that this was composed by myself and that the material presented, except where clearly indicated, is my own work. I declare that that the work has not been submitted for consideration as part of any other degree or professional qualification.

Signed:  \_\_\_\_\_

# Abstract

The tidal stream industry has seen large growth in recent years, and the number of pre-commercial scale devices currently being tested reflects this development. However, commercialising this technology whilst showing that their environmental impacts is minimal remains a challenge. The impact on benthic communities is not considered to be a key strategic consenting issue, yet it is anticipated that the benthic habitat will change as a result of the presence of tidal turbines. To date, only single tidal turbine devices have been installed to demonstrate the application of tidal stream technology but despite successful tests there are still uncertainties surrounding the quantitative impacts these turbines have on local benthic communities.

Unlike the wind industry, where physical effects of wind turbines have been catalogued through deployment of thousands of turbines, the tidal stream industry lacks these array scale quantitative data. Local impacts are known, but understanding the scale of the impacts and their relative significance of large arrays remains unknown. Tidal turbines (both single and arrays) interact with the hydrodynamics by decreasing the near field current flow directly in its wake through energy extraction and the drag caused by the physical structure. However, turbines may also affect the far field hydrodynamics, altering bed characteristics, sediment transport regimes and suspended sediment concentrations. As benthic habitats are closely linked to the physical seabed composition and the hydrodynamic conditions, the benthic environment is affected by to changes in the current flow. This thesis presents a series of studies investigating the interaction between tidal turbines and the benthic environment.

Based on the hydrodynamic modelling software, TELEMAC2D, a numerical model has been developed to investigate the hydrodynamic impact of a single tidal array at Ramsey Sound, Pembrokeshire as well as the cumulative impact of multiple tidal developments in the Irish Sea. Based on the results of the models, the hydrodynamic outputs were used as inputs to drive a species distribution model, based on the software MaxEnt, to investigate how the distribution of benthic species altered in the presence of a 10MW tidal array at Ramsey Sound. Results of the study showed the development would have a minimal negative impact on the benthic environment.



# Acknowledgements

Funding from the Energy Technologies Institute (ETI) and the RCUK Energy Programme for the Industrial Doctoral Centre for Offshore Renewable Energy (Grant number EP/J500847/1) is gratefully acknowledged.

This work was carried out on the High Performance Computing Cluster supported by the Research and Specialist Computing Support service at the University of East Anglia

I would like to thank my supervisory team Dr John Bacon (Cefas), Dr Helen Smith (University of Exeter), Dr Venki Venugopal (University of Edinburgh) and Dr Qing Xiao (University of Strathclyde) for their support, encouragement and guidance.

I am most grateful to my colleagues at Cefas notably Dr Liam Fernand, for his support and wisdom, Dr Anna Downie and Dr Alex Callaway, for their time and expertise on species distribution modelling, Dr Markus Diesing and Dr David Stephens, for their knowledge and data for the sediment distribution modelling.

I would like to thank Dr Paul Evans for the data he supplied for Ramsey Sound.

To my family, I thank you for your support and encouragement throughout the years that lead to me to where I am today.

Finally, to Rebecca, your unending love, support and patience over the course on my studies was immeasurable and without which I could not have succeeded.

*“When one tugs on a single piece of nature  
they find the rest of the world is attached to it.”*

*– John Muir*

# Table of Contents

Abstract.....	iv
Acknowledgements.....	v
List of Figures.....	xi
List of Tables.....	xvii
Abbreviations and Notations.....	xviii
1 Introduction .....	1
1.1 Introduction .....	1
1.2 Benthic Environment.....	4
1.3 Aims and Objectives.....	7
1.4 Overview of Thesis.....	9
2 Overview of Tidal Energy .....	11
2.1 Introduction .....	11
2.2 Tide Theory.....	11
2.3 Harnessing Tidal Energy.....	17
2.3.1 Tidal Barrages/Lagoons.....	17
2.3.2 Tidal Stream Turbines .....	20
3 Modelling Tidal Turbines .....	25
3.1 Introduction .....	25
3.2 Modelling Tidal Turbines .....	26
3.2.1 Solving Free Surface Flows.....	27
3.2.2 Representing Tidal Turbines.....	29
3.3 Hydrodynamic Modelling.....	31

3.3.1	TELEMAC-MASCARET Modelling System .....	32
3.3.2	Model Set-up .....	33
3.3.3	Wave Modelling with TOMAWAC .....	35
3.4	Conceptual Model .....	38
3.4.1	Idealised Channel Model .....	38
3.4.2	Dragfo.f Subroutine.....	42
3.4.3	Model Results.....	45
3.5	Summary.....	49
4	Modelling the hydrodynamic and morphological impacts of a tidal stream development: Case Study of Ramsey Sound, UK.....	51
4.1	Introduction .....	51
4.1.1	Ramsey Sound .....	52
4.2	Methodology.....	55
4.2.1	Numerical model.....	55
4.2.2	Modelling tidal turbines .....	57
4.3	Validation .....	58
4.3.1	Free Surface Elevations .....	59
4.3.2	Velocities .....	62
4.3.3	Harmonic Analysis .....	67
4.4	Results and Discussion.....	68
4.4.1	Array performance .....	68
4.4.2	Influence of tidal array .....	71
4.4.3	Hydrodynamic far field effects .....	74
4.4.4	Morphological effects due to tidal velocities.....	78
4.4.5	Morphological effect due to waves.....	87
4.5	Summary.....	92
5	Cumulative Impact Assessment of Tidal Energy in the Irish Sea .....	93
5.1	Introduction .....	93

5.2	Irish Sea Model .....	97
5.2.1	Model Domain.....	97
5.2.2	Modelling tidal turbines .....	98
5.3	Validation .....	100
5.3.1	Free surface elevations .....	100
5.3.2	Harmonic Analysis .....	105
5.3.3	Results.....	109
5.4	Northern Ireland Model.....	111
5.4.1	Model Domain.....	111
5.4.2	Validation .....	113
5.5	Results .....	119
5.6	Bed Shear Stress .....	125
5.7	Summary.....	129
6	Modelling the Benthic Environment.....	131
6.1	Introduction .....	131
6.2	Benthic Environment .....	131
6.2.1	Defining Benthic Environment .....	131
6.2.2	Role of Benthos in the Food Web.....	132
6.2.3	Anthropogenic Impact on the Benthic Environment.....	134
6.2.4	Habitat Mapping.....	135
6.2.5	Species Distribution Modelling.....	138
6.2.6	Species Distribution Modelling using MaxEnt .....	139
6.3	Modelling the Benthic Environment with MaxEnt .....	143
6.3.1	Benthic Species.....	143
6.3.2	MaxEnt Model Set-up .....	146
6.3.3	Predicting Grainsize Distribution.....	148
6.3.4	Predicting Sediment Fraction Distribution.....	149
6.4	MaxEnt Results and Validation .....	160

6.4.1	Validation.....	160
6.4.2	Results.....	163
6.5	Discussion.....	179
6.6	Summary.....	181
7	Discussion & Conclusions.....	183
7.1	Introduction.....	183
7.2	Modelling Tidal Turbines.....	183
7.3	Modelling the hydrodynamic morphological impacts of a tidal stream development in Ramsey Sound.....	185
7.4	Cumulative Impact Assessment of Tidal Energy in the Irish Sea.....	187
7.5	Modelling the Benthic Environment.....	188
7.6	Limitations & Further Research.....	191
7.7	Conclusion.....	193
8	Appendix A.....	196
9	Appendix B.....	198
10	Appendix B.....	202
11	Appendix B.....	204
12	Appendix B.....	206
	References.....	208

# Table of Figures

Figure 1-1: Map of sites of operational and potential wave and tidal energy extraction and device development.....	2
Figure 1-2: Relationship of the five numerical models developed to meet the research objectives. ....	10
Figure 2-1: Time series of tidal elevation recorded at the Milford Haven tide gauge, Wales. ....	12
Figure 2-2: Relative position of the Moon with respect to Earth and the Sun during a spring (top) and neap (bottom) cycle.....	13
Figure 2-3: Three potential operating regimes of a tidal barrage.....	18
Figure 2-4: The La Rance tidal barrage.....	19
Figure 2-5: Artist's impression of the 320 MW Swansea Bay tidal lagoon.....	20
Figure 2-6: The first tidal turbine, a 15kW proof of concept device, as developed by IT Power Consulting Ltd, deployed and tested in 1994 in Loch Linnhe, Scotland. ....	21
Figure 2-7: 300kW MCT Seaflow installed in 2003 off Lynmouth, Devon.....	22
Figure 2-8: 1.2MW MCT SeaGen installed in the Strangford Loch, Northern Ireland. ....	22
Figure 2-9: Selection of tidal current technologies.....	23
Figure 3-1: Schematic of idealised representation of tidal turbine. ....	30
Figure 3-2: Normalised force contributions of an idealised tidal turbine. The force is normalised to the total force at the rated velocity (2.25m/s).....	31
Figure 3-3: TEL Ltd DeltaStream device, (left) constructed 400kW full scale prototype, (right) artist impression of 1.2MW DeltaStream. ....	39
Figure 3-4: Power curve of 1.2MW DeltaStream device, using Plew & Stevens (2013) with $C_{T0} = 0.81$ and $C_{P0} = 0.27$ . The cut-in speed is 0.8 m/s with rated power occurring above 2.25 m/s. ....	39
Figure 3-5: Idealised channel finite element mesh. ....	40
Figure 3-6: Areas defining the drag of tidal turbines, modelled as (left) individual devices and (right) the whole array.....	41

Figure 3-7: Coordinate convention of variable NSOM, denoting coordinates of the quadrilateral defining the location of the turbines. ....	43
Figure 3-8: Velocity reduction with the tidal array represented as a) individual devices and b) the whole array. The black line represents where the flow speed has recovered to within 5% of the upstream velocity.....	46
Figure 3-9: Velocity (m/s) reduction across tidal array, down centre line of channel (m).....	47
Figure 3-10: One dimensional linear momentum actuator disc theory in an open channel flow, originally shown in Houlsby et al, 2008.....	48
Figure 3-11: Free surface elevation (m) showing the head drop across tidal array, down centre line of channel (m). ....	49
Figure 4-1: Constructed 400kW full scale prototype Tidal Energy Ltd DeltaStream device.....	53
Figure 4-2: Location of initial test site (bottom) and 10MW lease site (top), in red overlaying bathymetry. ....	54
Figure 4-3: Model computational domain with the locations of six tide gauges, two tidal diamonds and one bottom mounted ADCP used for validation.....	55
Figure 4-4: Array layout and location with respect to the lease site boundary (purple line), overlaying bathymetry. ....	58
Figure 4-5: Comparison of modelled free surface elevation and observations from BODC tide gauges. Black line represents $y=x$ relationship. ....	60
Figure 4-6: Location of ADCP transect with respect to the velocity modelled at the corresponding time step. ....	63
Figure 4-7: Line transect comparison of modelled and observed depth averaged tidal currents through Ramsey Sound. ....	63
Figure 4-8: Comparison of observed and modelled depth averaged velocities situated at $52^{\circ}10.6N$ $5^{\circ}52.3W$ . ....	65
Figure 4-9: Comparison between modelled and observed velocities at spring (top), neap (middle) and direction of spring velocities (bottom) of two tidal diamonds.....	66
Figure 4-10: Location of the UK ports used for harmonic analysis. ....	67
Figure 4-11: Device number convention.....	69
Figure 4-12: Total energy (MWh) produced over spring-neap cycle.....	69
Figure 4-13: Power production from the Device 1 (top) and Device 9 (bottom) representing the smallest and largest producing devices, respectively, over the	



30-day model run. Red dashed line represents the maximum instantaneous power production per device (1200 kW).....	70
Figure 4-14: Changes to the M2 tidal velocity constituents. The dashed lines represent contours of a 2% and 5% amplitude reduction. ....	72
Figure 4-15: Changes to the S2 tidal velocity constituents. The dashed lines represent contours of a 2% and 5% amplitude reduction. ....	73
Figure 4-16: Extracted streamlines showing eddies propagating north during a flood tide.....	75
Figure 4-17: Difference in velocity (m/s) between base case and turbine case over a single tidal cycle from low water to low water. ....	76
Figure 4-18: The zone of influence (black line), as characterised by the far field effects, of the 10 MW array at St David's Head.....	78
Figure 4-19: BGS Seabed Sediments using the Folk Classification. ....	79
Figure 4-20: Change in mean (top) and maximum (bottom) bed shear stress. ....	80
Figure 4-21: Predicted sediment maps during peak flood (left) and peak ebb (right).....	83
Figure 4-22: Predicted sediment maps during peak flood with no turbines (left) and 9 devices (right).....	85
Figure 4-23: Predicted sediment maps during peak ebb with no turbines (left) and 9 devices (right).....	86
Figure 4-24: TOMAWAC model computational mesh. The black dot represents the location of the wave record used to determine the model boundary conditions. ....	88
Figure 4-25: Significant wave height from Met Office WW3 hindcast model between 01/01/2000 to 31/12/2000. ....	89
Figure 4-26: Modelled wave height (left) and the resulting bed shear stress (right). ....	90
Figure 4-27: Bed shear stress dominance due to tidal velocities (red) and waves (blue). The black contour represents the extent of the reduction in maximum bed shear stress due to the presence of the tidal turbines. ....	91
Figure 5-1: Irish Sea model domain showing the locations of the tidal arrays (purple diamonds) and tide gauge locations (black squares) used for validation. ....	97
Figure 5-2: Tidal turbine technologies: a) DeltaStream, b) SeaGen-S, c) Openhydro, d) Hammerfest and e) Nautricity. ....	99

Figure 5-3: Comparison of observed and modelled free surface elevation. The black line represents a $y=x$ relationship with the dashed line representing a regression line of best fit. ....	101
Figure 5-4: Comparison of observed and modelled free surface elevation. The black line represents a $y=x$ relationship with the dashed line representing a regression line of best fit. ....	102
Figure 5-5: Maximum tidal range of the free surface elevations from the 30-day model base case. ....	104
Figure 5-6: Co-tidal charts of the amplitude (left) and the phase (right) of the M2 tidal constituent. ....	105
Figure 5-7: Comparison between modelled and observed M2 (left) and S2 (right) tidal constituent. ....	107
Figure 5-8: Comparison between modelled and observed M2 (left) and S2 (right) tidal constituents for tidal velocities. ....	108
Figure 5-9: The cumulative zones of influence for all 8 tidal projects, calculated using the range of difference. ....	110
Figure 5-10: Northern Ireland model domain. Locations of the tidal arrays are indicated in black dots. ....	111
Figure 5-11: Array layout of Fair Head (left) and Torr Head (right) overlaying peak spring velocity.....	112
Figure 5-12: Array layout of Mull of Kintyre overlaying peak spring velocity... ..	113
Figure 5-13: Comparison of observed and modelled free surface elevation. The black line represents a $y=x$ relationship with the dashed line representing a regression line of best fit. ....	114
Figure 5-14: Location of harmonic constituents extracted from TPXO database used for validation in purple diamonds and current observations in red squares. ....	115
Figure 5-15: Comparison between modelled and observed M2 (left) and S2 (right) tidal constituent. ....	116
Figure 5-16: Comparison between Northern Ireland and Irish Sea modelled M2 (left) and S2 (right) tidal constituent.....	117
Figure 5-17: Maximum tidal range of the free surface elevations from the 30-day model base case. ....	118
Figure 5-18: Comparison between modelled and observed tidal velocities at 55.46°N, 6.2333°W and 55.1167°N, 5.8883°W. ....	119

Figure 5-19: Range of difference for case 8 (all three projects). Black outlines represent turbine locations. ....	120
Figure 5-20: Zone of influence for case 2, only Fair Head.....	121
Figure 5-21: Zone of influence of case 3, only Torr Head. ....	121
Figure 5-22: Zone of influence of case 5, Fair Head and Torr Head. ....	122
Figure 5-23: Total power production for Fair Head (top) and Torr Head (bottom). The solid black line represents the power production from each array separately (case 2) and the solid orange represents both Fair Head and Torr Head operating concurrently (case 5). The dash black line represents the maximum total power output of each array. ....	124
Figure 5-24: Variation in maximum bed shear stress for case 8.....	125
Figure 5-25: Variation in mean bed shear stress for case 8. ....	126
Figure 5-26: Variation in maximum bed shear stress for case 2. The black contour represents the spatial extent of change for case 8. ....	127
Figure 5-27: Variation in mean bed shear stress for case 2. The black contour represents the spatial extent of change for case 8. ....	127
Figure 6-1: Role of benthos in cycling nutrients.....	133
Figure 6-2: Example breakdown of the EUNIS Habitat Classification .....	137
Figure 6-3: A hypothetical ROC curve of a trained model (red) and a random model (black). The closer the red line tends towards the top left corner the better the model is at discerning between suitable and unsuitable habitats. ....	142
Figure 6-4: The nine benthic species chosen for modelling: a) <i>Alcyonium digitatum</i> , b) <i>Axinella dissimilis</i> , c) <i>Bugula turbinata</i> , d) <i>Dendrodoa grossularia</i> , e) <i>Eunicella verucosa</i> , f) <i>Flustra foliacea</i> , g) <i>Nemertesia ramosa</i> , h) <i>Pachymatisma johnstonia</i> and i) <i>Raspailia ramosa</i> . ....	145
Figure 6-5: Predicted grainsize, determine by the smallest grainsize whose threshold of motion does not exceed the mean bed shear conditions.....	149
Figure 6-6: Simplified Folk classification based on the classification of Folk (1954). Sediments are classified according the fractions of mud, sand and gravel .....	150
Figure 6-7: Predicted gravel fraction distribution from BGS observations using Random Forest algorithm.....	152
Figure 6-8: Predicted sand fraction distribution from BGS observations using Random Forest algorithm.....	153

Figure 6-9: Predicted mud fraction distribution from BGS observations using Random Forest algorithm. ....	154
Figure 6-10: Comparison of observed and predicted additive log ratio of mud. The solid black line denotes a $y=x$ relationship with the dashed lines representing the 95% prediction intervals. ....	156
Figure 6-11: Comparison of observed and predicted additive log ratio of sand. The solid black line denotes a $y=x$ relationship with the dashed lines representing the 95% prediction intervals. ....	156
Figure 6-12: Comparison of observed and predicted gravel fraction. The solid black line denotes a $y=x$ relationship with the dashed line representing a regression line of best fit. ....	157
Figure 6-13: Comparison of observed and predicted sand fraction. The solid black line denotes a $y=x$ relationship with the dashed line representing a regression line of best fit.....	158
Figure 6-14: Comparison of observed and predicted mud fraction. The solid black line denotes a $y=x$ relationship with the dashed line representing a regression line of best fit.....	158
Figure 6-15: Histogram of gravel, sand and mud fraction of the BGS Observations. ....	159
Figure 6-16: BGS Seabed Sediments using the Folk Classification. ....	160
Figure 6-17: Response operating characteristic curves for <i>Pachymatisma johnstonia</i> . ....	161
Figure 6-18: Response operating characteristic curve for <i>Alcyonium digitatum</i> , <i>Axinella dissimilis</i> , <i>Bugula turbinata</i> , <i>Dendrodoa grossularia</i> , <i>Eunicella verucosa</i> , <i>Flustra foliacea</i> , <i>Nemertesia ramosa</i> , <i>Pachymatisma johnstonia</i> , <i>Raspailia ramosa</i> . ....	162
Figure 6-19: MaxEnt prediction of <i>Axinella dissimilis</i> .....	163
Figure 6-20: Combined predicted spatial distribution of <i>Axinella dissimilis</i> , with a confidence score of 0 (absent in all 10 predictions) to 10 (present in all 10 predictions).....	166
Figure 6-21: Combined predicted spatial distribution of <i>Alcyonium digitatum</i> , with a confidence score of 0 (absent in all 10 predictions) to 10 (present in all 10 predictions).....	166

Figure 6-22: Combines predicted spatial distribution of <i>Bugula turbinata</i> , with a confidence score of 0 (absent in all 10 predictions) to 10 (present in all 10 predictions).....	167
Figure 6-23: Combined predicted spatial distribution of <i>Dendrodoa grossularia</i> , with a confidence score of 0 (absent in all 10 predictions) to 10 (present in all 10 predictions).....	167
Figure 6-24: Combined predicted spatial distribution of <i>Eunicella verucosa</i> , with a confidence score of 0 (absent in all 10 predictions) to 10 (present in all 10 predictions).....	168
Figure 6-25: Combined predicted spatial distribution of <i>Flustra foliacea</i> , with a confidence score of 0 (absent in all 10 predictions) to 10 (present in all 10 predictions).....	168
Figure 6-26: Combined predicted spatial distribution of <i>Nemertesia ramosa</i> , with a confidence score of 0 (absent in all 10 predictions) to 10 (present in all 10 predictions).....	169
Figure 6-27: Combined predicted spatial distribution of <i>Pachymatisma johnstonia</i> , with a confidence score of 0 (absent in all 10 predictions) to 10 (present in all 10 predictions).....	169
Figure 6-28: Combined predicted spatial distribution of <i>Raspailia ramosa</i> , with a confidence score of 0 (absent in all 10 predictions) to 10 (present in all 10 predictions).....	170
Figure 6-29: Combined predicted habitat lost (blue) and created (red) of <i>Alcyonium digitatum</i> due to the presence of a 10 MW tidal array at St David's Head.....	171
Figure 6-30: Zonal boundary of bed shear stress change .....	172
Figure 6-31: Box and whisker plots of the total area of predicted spatial distribution from the ten replicants for each species.....	173
Figure 6-32: Box and whisker plots of the area of habitat lost due to the tidal stream array from the ten replicants for each species.....	174
Figure 6-33: Box and whisker plots of the area of habitat created due to the tidal stream array from the ten replicants for each species.....	175
Figure 6-34: Combined changes in habitat of all replicants and species.....	179

# Table of Tables

Table 2-1: List of selected tidal harmonics for the Port of Newlyn, (Cornwall, UK), from analysis of data for 1985-1997. ....	16
Table 3-1: Types of boundary conditions used with TELEMAC.....	34
Table 3-2: List of variables used to parameterise a tidal turbine in the dragfo.f subroutine.....	44
Table 4-1: Validation statistics of the six tide gauges. ....	62
Table 4-2: Validation statistics of the tidal diamonds.....	66
Table 4-3: Comparison between observed and modelled M2 constituent .....	68
Table 4-4: Comparison between observed and modelled S2 constituent.....	68
Table 4-5: Changes to the M2 and S2 tidal velocity constituents at the location of the devices. ....	74
Table 4-6: Mean threshold shear stress ( $\tau_{cr}$ ) conditions for the entrainment of various grain sizes (d) (from Berenbrock & Tranmer, 2008).....	81
Table 5-1: Characteristics of the five device technologies used to parameterise the turbines in the model, using the Plew & Stevens (2013) method. ....	100
Table 5-2: Validation statistics of the 16 tide gauges. ....	103
Table 5-3: Comparison between observed and modelled M2 constituent. ....	106
Table 5-4: Comparison between observed and modelled S2 constituents. ....	107
Table 5-5: Comparison of model validation with similar studies. ....	108
Table 5-6: Comparison of model validation of tidal currents with similar studies. ....	109
Table 5-7: The eight combinations of Fair Head Torr Head and Mull of Kintyre used to investigate their interaction. ....	113
Table 5-8: Comparison between observed and modelled M2 constituent. ....	115
Table 5-9: Comparison between observed and modelled S2 constituent.....	116
Table 5-10: Energy production of each tidal project for all 8 test cases. ....	122
Table 5-11: Percentage change in energy production for cases 5 – 8. ....	123

Table 6-1: Breakdown of the total number of observations of the nine modelled species into training and testing sets.....	146
Table 6-2: Validation of Random Forest model and test data .....	155
Table 6-3: Average area under curve of all replicants of all species. ....	161
Table 6-4: Threshold values used to determine presence/absence. ....	165
Table 6-5: Summary of the average change in habitat for all ten replicants...	176
Table 6-6: T-Score for the habitat lost and created for a species. ....	178

# Abbreviations & Notations

## Abbreviations

alr	Additive log-ratio
ADCP	Acoustic doppler current profiler
AUC	Area under curve
BGS	British Geological Survey
BODC	British Oceanographic Data Centre
EMEC	European Marine Energy Centre
EUNIS	European Nature Information
GAM	Generalised Additive Model
GARP	Genetic Algorithm for Rule set Production
GLM	Generalized Linear Model
LMADT	Linear momentum actuator disc theory
MCZ	Marine conservation zone
MPA	Marine protected area
MSE	Mean square error
OOB	Out-of-bag
RMSE	Root mean squared error
ROC	Response operator curve
SAC	Special area of conservation
SIF	Significant impact factor
TEL	Tidal Energy Ltd
UKHO	United Kingdom Hydrographic Office



## Notations

### Roman Letters:

$A$	Orbital wave amplitude
$A_r$	Rotor swept area
$A_s$	Structural swept area
$B$	Blockage ratio
$C_D$	Coefficient of drag
$C_P$	Coefficient of power
$C_{P0}$	Constant power coefficient
$C_T$	Coefficient of thrust
$C_{T0}$	Constant thrust coefficient
$d$	Grainsize
$d_{50}$	50 <sup>th</sup> percentile grainsize distribution
$D_*$	Dimensionless grainsize
$f_w$	Wave friction factor
$F_D$	Drag force
$F_r$	Froude number
$F_T$	Thrust force
$g$	Acceleration due to gravity, 9.81 m/s <sup>2</sup>
$h$	Depth
$H_S$	Significant wave height
$k_S$	Nikuradse bottom friction
$P_D$	Rated power
$R^2$	Coefficient of determination
$T$	Wave period

$u, v, w$	Velocity components in x, y, z-directions
$U$	Velocity magnitude
$U_C$	Rotor cut-in speed
$U_D$	Rotor rated speed
$U_w$	Wave orbital velocity
$y$	Observed values
$\bar{y}$	Mean of observed values
$\hat{y}$	Predicted values
$z_0$	Roughness length

#### Greek Letters:

$\rho$	Density of sea water
$\rho_s$	Density of sediment
$\rho_f$	Density of fluid
$\sigma^2$	Variance
$\nu$	Kinematic viscosity of water
$\tau$	Bed shear stress
$\tau_{cr}$	Threshold bed shear stress
$\tau_w$	Bed shear stress due to waves
$\theta_c$	Threshold shields parameter

# Chapter 1

## Introduction

### 1.1 Introduction

Renewable energy technologies can play an important role in mitigating the impact of climate change by replacing conventional sources of energy production, reducing greenhouse gas emissions (e.g. Luderer et al., 2014). The global installed capacity of all forms of renewable energy technologies was 1,849 GW, with 147 GW of newly installed capacity added in 2015 alone (REN21, 2016). 77% of this newly installed capacity came from wind and solar PV, primarily in the USA and China, with the rest predominantly from hydropower. Wave and tidal, make up only a small fraction of the total installed capacity: 0.0003% or 530 MW. The term 'tidal energy' encompasses both tidal stream technologies and tidal barrage/lagoon technologies. The majority of the current installed capacity of wave and tidal energy comes from two large-scale projects: the 240 MW La Rance tidal barrage, in France, and the 254 MW Sihwa Lake tidal barrage, in South Korea. There are a number of sites around the world being investigated and used for the development of wave and tidal technologies as well as large-scale extraction. Figure 1-1 shows the location of these sites, as summarised by Tethys (n.d.).

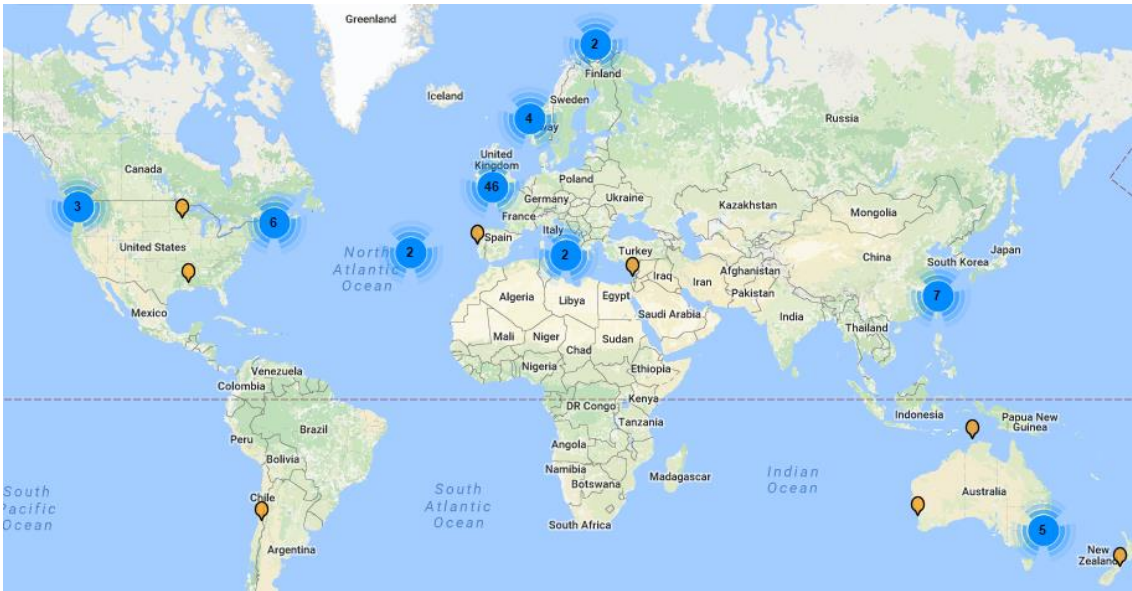


Figure 1-1: Map of sites of operational and potential wave and tidal energy extraction and device development. Figure sourced from Tethys website (<https://tethys.pnnl.gov/>).

In Asia, China has been harnessing tidal energy through tidal barrages since the 1970's. These include: the 0.25 MW Haishan tidal power plant, built in 1972, the 0.96 MW BaiShakou tidal power plant, built in 1978, and the 3.2 MW Jiangxia tidal power plant, built in 1985. In South Korea, the 1 MW Jindo Uldolmok tidal power plant was built in 2009, followed by the 254 MW tidal power plant at Sihwa in 2011. Tidal barrages are being further investigated in South Korea with a potential of 3.4 GW from four other sites: Garolim (520 MW), Incheon (1320 MW), Kanghai (840 MW) and Chonsu (720 MW) (Kim et al., 2012).

Outside of Asia, North America is another site with a large potential for tidal power, particularly the Bay of Fundy which has the largest tidal range in the world, >15m (Desplanque and Mossman, 2001). The first tidal power plant built in North America was the 20 MW Annapolis Royal tidal power plant, built in the mouth of the Bay of Fundy, Nova Scotia, in 1984. The Bay of Fundy, is also home to the Fundy Ocean Research Centre for Energy (FORCE) test site. FORCE is a grid-connected test facility for tidal stream devices. Since it opened in 2009, only one developer, OpenHydro, has installed a single device, which was deployed for approximately one year (FORCE, 2009).

Presently, Europe is at the forefront of development of marine energy, with 50% of the world's tidal energy developers and 45% of wave energy developers (Magagna and Uihlein, 2015). One of the reasons behind this is that the European

Shelf offers one of the best tidal and wave energy resource in the world. Europe has a theoretical wave power resource of 381 GW (Mork et al., 2010) and over 250 GW of tidal energy (Woolf et al., 2014). Within Europe, the UK has the largest potential of wave, tidal range and stream and has seen much of the research and development. This is in part to the success of the European Marine Energy Centre (EMEC) based in Orkney, Scotland. EMEC is a wave and tidal test site, whose template has been adopted internationally (Neill et al., 2017). It first opened the wave test facility in 2003 and the tidal test site in 2006. The first tidal devices tested at EMEC was by Openhydro in 2008. Since opening, it has tested nine different tidal stream devices (EMEC, n.d.). Subsequently, the first pre-commercial tidal stream array is being constructed in the Pentland Firth, Scotland. Within the UK there are currently 25 leases for tidal projects and 15 for wave projects (Crown Estate, n.d.). As such, the UK will be the main focus of the case studies within this study.

Currently, the UK has a target of reducing emissions by 80% by 2050 (Climate Change Act 2008). To meet this, the UK needs to invest in forms of renewable technologies which will provide efficient, economic and reliable energy sources for the future. It is estimated that the UK's technical tidal resource is 16 TWh/annum and that 30-50 GW installed capacity of wave and tidal energy could meet up to 20% of the UK electricity demand (UK Government, 2013). In 2011, it was expected that 18 GW of offshore wind and 300 MW wave & tidal would be installed by 2020 (Department of Energy & Climate Change, 2011). The offshore wind industry is on track to achieve this with over 5GW of offshore wind capacity already operational and a further 4.5GW under construction (Crown Estate, 2015). However, the wave and tidal industry is yet to develop beyond deploying single commercial-scale demonstration devices.

The commercial viability of a marine energy device is dependent on a sufficient available resource for power generation (O'Rourke et al., 2010; Dalton et al., 2010). Therefore, it is important for developers to fully understand the characteristics of the tidal environment in which the devices are deployed. This can be achieved through the use of tide gauges or Acoustic Doppler Current Profilers (ADCP) to record physical in-situ observations of tidal elevations and currents, respectively for a particular site. Tide gauges and ADCPs can provide long term time series of tidal elevations and tidal currents, respectively, but only

represent a very narrow footprint. ADCP transects can provide a profile of the tidal flow but only represent a narrow time frame. Multiple in-situ measurements can provide a broader understanding of the spatial and temporal variation in the tidal resource but this represents a potentially prohibitively capital expenditure. An alternative is to use well calibrated and validated numerical models, by physical and oceanographic measurements (Gunn and Stock-Williams, 2013).

Hydrodynamic numerical models solve a set of mathematical equations (such as the Navier-Stokes equations) which govern the physics of water movement in order to predict tidal elevations and currents in areas of interest (Abbot and Basco, 1997). They can be used to provide a number of different functions depending on the purpose and scale of the model. For example, large scale regional models, with a resolution on the order of kilometres, can be used for determining geographic resource hotspots. Small scale models, with a resolution on the order of tens of meters, can be used for detailed site assessment and device positioning.

## 1.2 Benthic Environment

As an island nation, the UK is intrinsically dependent on the value of its marine environment. In 2011, the estimated value of UK marine industries was £17 billion, with contributions from but not limited to shipping operations, research and development, construction, navigation and communication, ports and training (UK Marine Industries Alliance, 2011). It is recognised that the marine environment provides more than just economic value. The Millennium Ecosystem Assessment conducted by the World Health Organisation for the United Nations (World Health Organisation, 2005) established the linkages between the ecosystem services and human well-being. The report describes ecosystem services as the benefits people obtain from ecosystems. As a result, it was recognised there is a need to protect the marine environment. In 2013, the UK Government started designating Marine Conservation Zones (MCZ) in its territorial waters. The estimated benefit of the proposed designation of a network of MCZs in UK waters was estimated to be as high as £23.5 billion (Hussain et al., 2010). It is well understood that renewable energy can play an important role in tackling climate change and global warming. However, the marine environment is under increasing pressure from other anthropogenic sources, such as fishing,

drilling, mining, noise and pollution. Marine renewables need to be deployed sensitively to avoid creating further pressure on a system sensitive to changes (Moffitt et al., 2015).

To date, only single tidal stream devices have been installed to demonstrate the application of tidal stream technology (e.g. FORCE, 2009; EMEC, n.d.; Tidal Energy Ltd, 2015) but despite successful tests there are still uncertainties surrounding the quantitative impacts these machines have on local benthic communities. It is this uncertainty that dictates research and consenting priorities for regulators and planners. Collisions between turbine blades and marine mammals, birds or fish are considered to be the greatest issue delaying consent to marine renewable projects (ORJIP, 2015), despite there being little evidence of increased mortality (Frid et al., 2012, Roche et al., 2016). However, the impact on benthic communities is not considered to be a key strategic consenting issue (ORJIP, 2015). Yet, it is known that the benthic habitat will change as a result of tidal turbines. A small scale study of the benthic species assemblage response to the presence of OpenHydro's device deployed at the European Marine Energy Centre showed an increase in the species biodiversity and compositional differences within the device site (Broadhurst & Orme, 2014). In the absence of array scale developments, the interaction between tidal arrays and the benthic environment is still subject to speculation (Uihlein & Magagna, 2016).

Understanding the ecological impact of marine renewables is of increasing importance. Shields et al (2009) reviewed the strategic priorities for assessing ecological impacts of marine renewable devices with respect to the Pentland Firth. They detailed the ecological importance of the area for all components of the ecosystem, particularly feeding grounds for birds and fish spawning grounds. It also highlighted the lack of knowledge of the benthic communities in the area. Miller et al (2013) suggested the impact of a tidal development could be reduced by understanding the 'benthic footprint', defined as an area of marked effect or impact. Both Miller et al. (2013) and Shields et al. (2009) highlighted the potential risk of altering the concentration of suspended sediments, and that changes to the sediment transport regime represent a specific risk to benthic communities. Developers typically restrict the location of projects to be 1km away from designated protected areas. However, Ahmadian et al (2012) showed that suspended sediment concentrations were altered up to 15km from a tidal stream

array modelled in the Bristol Channel. Furthermore, Neill et al (2009) showed sediment patterns could change in the order of 50km from the point of energy extraction.

It is well understood that changes to the hydrodynamics and surface wave characteristics will alter other physical parameters, such as bed shear stress, which in turn alter sediment transport patterns, habitat equilibrium and the benthic environment. However, there is a shortage of published literature detailing the interaction of tidal turbines and the benthic environment. The changes in sediment transport, as shown by Ahmadian et al (2012) and Neill et al (2009), are likely to impact the benthic environment in a number of ways. Changes to the morphodynamics will lead to a change in the sediment class distribution leading to change in the physical benthic habitat. Similarly, an increase in sediment accumulation could lead to the burial of benthic species. This has been demonstrated in several studies (e.g. Rogers, 1990; Short & Wyllie-Echeverria, 1996). Although burial from increased sedimentation could lead to mortality, laboratory experiments show that some species can adapt to sediment burial (Hinchley et al., 2006). Due to the high flow speeds, tidal developments are typically situated in areas of medium to high suspended sediments (Robins et al, 2014). Filter feeders rely on nutrients in the suspended sediments. The presence of tidal turbines could lead to a reduction in suspended sediments through the reduction of tidal currents. Robins et al (2014) showed that the size of a proposed tidal development can be limited such that the reduction in suspended sediments is within the range of natural variability. As such, the impact to filter feeders can be minimised.

Whilst tidal stream turbines can alter the physical benthic environment, the turbine structures can themselves become part of the benthic environment. The support structure represents a hard substrate that can be colonised by seabed fauna and flora as an artificial habitat. Andersson et al (2009) showed through field experiments that concrete and steel support structures used for offshore wind farms were almost 100% covered after 1 year at sea. Whilst the support structures can increase local biodiversity through colonisation of native species, they have been shown to be favourable to colonisation from invasive non-native species (Glasby et al., 2007; Bulleri and Airoldi, 2005). These new benthic habitats may provide pathways for colonisation between regions that were



previously geographically isolated and spread non-native species. Whilst this has been shown on structures, such as oil platforms (Page et al., 2006), it has yet to be seen in marine renewables. This issue is not further investigated within this study.

### 1.3 Aims and Objectives

The tidal stream industry is still in its infancy but has great potential as a viable alternative energy source. Whilst multiple single devices have been tested, it is only just taking the first steps to deploy array scale projects. The marine environment is already under considerable pressure and tidal stream developments must show they can be operated without any additional determinantal effect on the environment. Furthermore, as the industry grows, determining the impact of single developments, in isolation, will not be sufficient. There is uncertainty as to how the lessons learned from the environmental interactions of single devices will translate to array-scale deployments. The principal aim of this study is to address that uncertainty and to investigate the interaction between tidal stream arrays and the benthic environment. This is achieved through a variety of modelling techniques, fulfilling the following objectives:

**Objective 1** *Develop a parameterisation of a tidal turbine to implement in a hydrodynamic numerical model and determine how best to represent tidal arrays in numerical models*

As the physical interaction of the tidal turbines with the hydrodynamics is the primary driver of change, it is important that this is correctly implemented. A conceptual hydrodynamic model of an idealised channel will be used to test and validate the implementation of the tidal turbines. Tidal arrays can be modelled at different scales meaning the interaction of the array and the hydrodynamics changes. The idealised channel model will be used to assess how the hydrodynamics respond to the representation of an array of tidal turbines to determine the most appropriate scale for energy extraction.

**Objective 2** *Develop a real world coastal hydrodynamic model of an area with a high potential of tidal energy for a single tidal array to determine the*

*extent and magnitude of change to the hydrodynamics and sedimentary processes due to the presence of a single tidal array.*

Whilst idealised test cases can provide important information, they are not representative of real world situations. High tidal flows are caused by the interaction of the hydrodynamics with local bathymetry leading to complex interactions with their surroundings. To understand the true impact of a tidal array, it needs to be assessed against these complex interactions. A validated coastal hydrodynamic model is required to provide a base line assessment before the influence of the tidal turbines is included. In order to understand the interaction between tidal turbines and the benthic environment, it is first important to understand how the devices interact with the physical environment. The coastal hydrodynamic model will be used to quantify the change in the hydrodynamics and how far the reach of the tidal array's influence extends. The principal effect of a tidal turbine is to alter the hydrodynamics. The principal change to the benthic environment is the change to the seabed through sedimentary processes. The coastal hydrodynamic model will be used to assess how the change in the hydrodynamics alters the morphodynamics.

**Objective 3** *Develop a regional hydrodynamic model of an area with a high potential of tidal energy for multiple tidal array to determine the extent and magnitude of change to the hydrodynamics due to the cumulative impact of multiple tidal arrays.*

As the tidal industry is in its infancy, the impact of testing single prototype devices does not pose a significant impact on the marine environment. However, as the tidal industry grows and more potential sites are developed, the potential for interaction between sites increases. A validated regional hydrodynamic model is required to provide a base line assessment before a cumulative impact assessment of multiple tidal arrays can be conducted. The regional hydrodynamic model will then be used to assess how far the influence of each tidal array extends to assess if there is any interaction between sites. For the sites that interact with one another, the impact of the interaction will be assessed through the change in power production along with how the hydrodynamics are altered due to the presence of the tidal arrays.

**Objective 4** *Develop a species distribution model of the benthic environment within the domain boundary of the coastal hydrodynamic model to determine the response of benthic species to the change in hydrodynamic and morphological conditions due to a tidal array.*

In order to assess the interaction of tidal turbines and the benthic environment, it is important to first understand which species are present and where they can be found. Tidal turbines pose the biggest threat to species that are sessile and cannot respond to changes in morphological conditions. An assessment will be made to determine which species are representative of the area encompassed by the coastal hydrodynamic model. A species distribution model will be developed to provide a base line assessment of the benthic environment. The species distribution model will be used to assess how distribution of benthic species alters due to the change in hydrodynamic and morphological conditions due to the presence of a tidal array, as modelled in the coastal hydrodynamic model.

## 1.4 Overview of Thesis

Five numerical models have been created in this study in order to complete the outlined research objectives. The study is broken down into a further seven chapters. Chapter 2 will provide an overview of tidal energy, through a summary of tidal theory and the development of technologies harnessing tidal energy. Chapter 3 will discuss and implement the parameterisation of tidal turbines in numerical hydrodynamic modelling, which will be tested through the use of the idealised channel model. Based on the results, Chapter 4 will develop a coastal model of Ramsey Sound in Pembrokeshire, Wales, to determine the spatial extent of hydrodynamic and morphological change around Ramsey Sound due to the presence of a single 10 MW tidal array situated of St David's Head. To assess the changes in bed shear stress due the tidal array, the bed shear stress due to waves were computed though the use of a wave model to provide a comparison and context to the changes. Chapter 5 will develop a regional model to assess the cumulative impact of eight tidal developments within the Irish Sea. As the regional model domain is computationally expensive to run, a smaller coastal model of Northern Ireland was developed to further investigate the tidal arrays that show interaction. Chapter 6 will discuss the benthic environment and

develop a species distribution modelling of the benthos around Ramsey Sound. Continuing with the work conducted in Chapter 4, the hydrodynamic and morphological impact of the 10 MW tidal array at St David’s Head will be introduced into the species distribution model to assess the impact of tidal turbines on the benthic environment. Finally, Chapter 7 will conclude the results of Chapters 3 to 6, summarising how the research objectives have been met. Figure 1-2 shows a flow diagram of how the five numerical models interlink, the chapters they can be found in and the research objectives they aim to achieve.

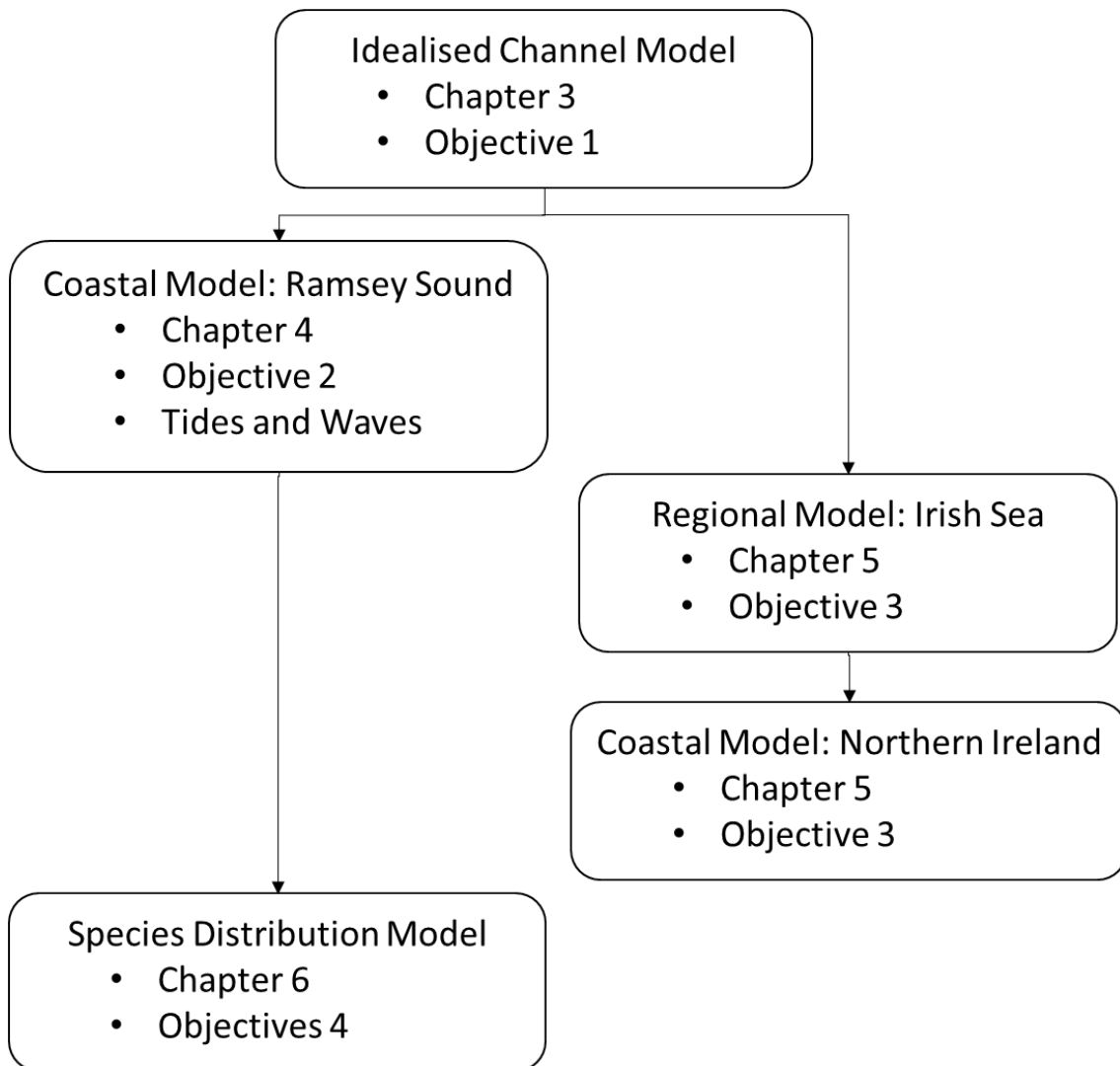


Figure 1-2: Relationship of the five numerical models developed to meet the research objectives.

# Chapter 2

## Overview of Tidal Energy

### 2.1 Introduction

The purpose of this chapter is to provide a background understanding of tidal theory. Whilst it is important to understand how a tidal stream turbine interacts with the hydrodynamics, it is equally important therefore to understand first how the tide works. A summary of tide theory is presented here explaining the key features and terminology. Furthermore, the chapter also details how tidal energy can be harnessed and the development of tidal turbine technology to the current state-of-the-art.

### 2.2 Tide Theory

Humans have been trying to understand the tides for centuries, but it was not until Isaac Newton formulated his theory of gravitational attraction, that the link between the relative position of the sun, moon and earth and motion of the tides was well understood. The term 'tide' is defined, according to Pugh (1987), as *"the periodic motions which are directly related to the amplitude and phase of periodic geophysical forces"*. There are many sources of geophysical forces, but the two main groups are gravitational tides and meteorological conditions (atmospheric pressure and winds acting on the sea surface). In addition to these forces, non-

linear effects due to the interaction between the motion of water and the seabed can alter the tides.

The vertical motion of the tide is described by the change in the elevation of the free surface due to the propagation of a tidal wave, whereas the horizontal motion is referred to as a tidal current. Tidal currents occur as a result of a gradient in the free surface due to the variation in the tidal elevation; water flows from areas with a higher elevation to a lower elevation. Tidal elevations are commonly recorded at tide gauge stations in coastal regions world-wide. A typical recorded tidal signal comprises a series of peaks and troughs representing high and low tide, centred around the mean sea level. High tide is when the tidal elevation is at the peak of the tidal cycle, and low tide is at the trough. Figure 2-1 shows an example time series of tidal elevation recorded at the Milford Haven tide gauge, in Pembrokeshire, UK.

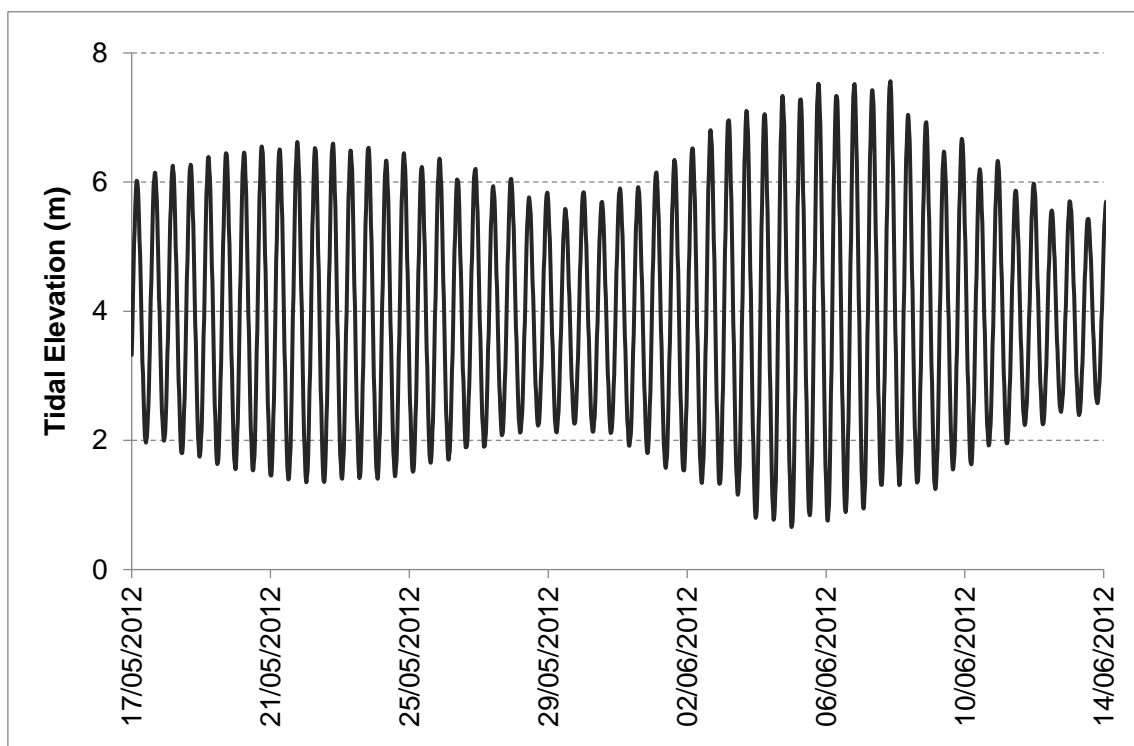


Figure 2-1: Time series of tidal elevation recorded at the Milford Haven tide gauge, Wales.

Figure 2-1 shows how the range between high and low tide varies over a 28-day period. This is due to the relative position of the Moon with respect to the Sun and Earth, shown in Figure 2-2. When the Moon and the Sun align the gravitational force exerted on the sea surface is at its peak. This results in the maximum tidal range known as the spring tide. When the Moon and Sun are out of alignment,

their position in relation to the Earth at 90° to each other, the components of tidal force partially cancel each other resulting in a smaller neap tide. The transition between the full spring-neap cycle occurs over a 28-day period.

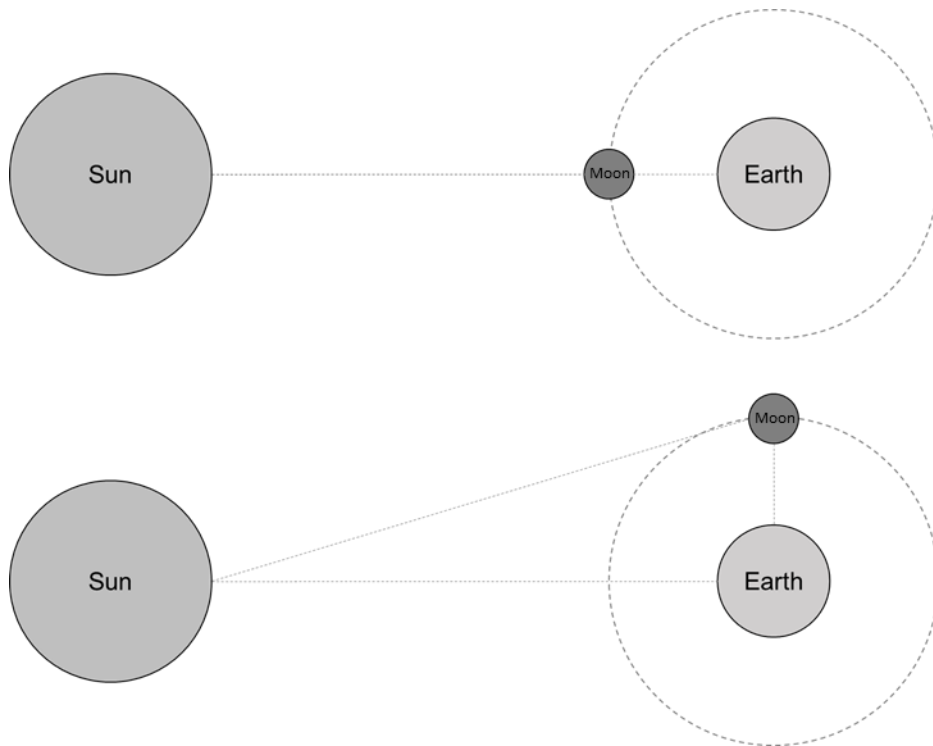


Figure 2-2: Relative position of the Moon with respect to Earth and the Sun during a spring (top) and neap (bottom) cycle.

The analysis of observational records has been one method used to make accurate predictions of water levels, namely for navigation and coastal flood defences (Parker, 2007). Using Pugh's definition, the periodic oscillations of the tide in the vertical can be described mathematically as:

$$Z(t) = H_x \cos(\omega_x t - g_x) \quad (2.1)$$

where  $Z$  is the free surface at time  $t$ ,  $H_x$  is the amplitude of the oscillation,  $\omega_x$  is the angular speed related to the period  $T_x$  and  $g_x$  is the phase lag with respect to a reference time zero. The tide is made up of the sum of multiple oscillations at different frequencies, each known as a tidal harmonic. Long term observational records can be analysed and the overall tidal signal separated into its different astronomical harmonics, each provided by a different astronomical body, as well as higher harmonics due to friction, bathymetry etc. The amplitude and phase of each tidal harmonic can be determined by performing a Fourier analysis on a time series of the full tidal motion. Doodson (1921) identified 388 different harmonics

of which the two principal harmonics are the semidiurnal lunar period,  $M_2$ , and the semidiurnal solar period,  $S_2$ . The  $M_2$  and  $S_2$  harmonics have a period of 12.42 hours and 12 hours, respectively. The different harmonics can be separated and grouped into species based upon their period. Table 2-1 lists some of the principal tidal harmonics for the Port of Newlyn (Cornwall, England). For illustration, Table 2-1 also shows the amplitude of each harmonic recorded at the Newlyn tide gauge and their relative percentage contribution to the overall tidal range, provided by the British Oceanographic Data Centre (BODC).

When a time series of tidal elevation is decomposed into its constituent harmonics, there remains a portion of the tidal signal that cannot be predicted by the astronomical tides. This proportion of the tidal signal is referred to as a residual and represents the meteorological forcing and other non-linear effects. The interaction of meteorological forcing and non-linear effects with the astronomical tides can lead to irregular patterns in the tidal record. Storm surges are one such example of meteorological conditions that can alter tidal elevations (Wadey et al., 2015). A storm surge is an increase in water depth above the normal astronomical tidal range caused by low atmospheric pressure. As the low pressure system moves, it causes the height in the sea level to change with it. When the system reaches the coast, the overall storm surge is the contribution of the normal tide, the storm tide and any waves or coastal setup (a rise in water level at the coast due to wind-driven surface waves).

In shallow waters, the local bathymetry can transfer energy through frictional effects to the higher-order harmonics with amplitudes larger than the astronomical components (Parker, 2007). When tidal waves propagate from the deep ocean onto the continental shelf, they can become distorted close to the coast by interactions with the shallow depths and local topography. As the tidal wave enters shallow water the speed of the wave decreases whereby the crest of the tide travels faster than the trough causing an asymmetry. Depending on the strength of the asymmetry it can lead to double tides, whereby there are multiple high waters during a flood phase, for example seen at Portland in Dorset, England (Bowers et al., 2013).

If the period of the tide matches the natural period of a bay or estuary that it is propagating into, it can cause a resonance effect leading to large tidal ranges. The natural period of oscillation is dependent on the length and depth of the



system. The Bristol Channel is an example of a resonant system, whereby the natural period of the channel resonates with the quarter wave length of the Atlantic tidal wave (Serhadlioglu, 2014). Large river flows can also cause nonlinear interactions and reduce the tidal range. During the flood tide, river flows oppose the flow of the tide leading to reduced current speeds and a shorter flood phase. During the ebb, the current is enhanced by the river flow leading to faster currents and a longer ebb phase.

Table 2-1: List of selected tidal harmonics for the Port of Newlyn, (Cornwall, UK), from analysis of data for 1985-1997.

Species	Symbol	Period (hr)	Description	Amplitude at Newlyn (m)	Percentage of Total Tidal Signal (%)
Zero-order	M <sub>sf</sub>	354.367	Lunisolar synodic fortnightly	0.003	0.09
First-order	K <sub>1</sub>	23.934	Lunar diurnal	0.063	1.98
	P <sub>1</sub>	24.066	Solar diurnal	0.021	0.66
	O <sub>1</sub>	25.819	Lunar diurnal	0.054	1.70
	Q <sub>1</sub>	26.868	Larger lunar elliptical diurnal	0.016	0.50
Second-order	K <sub>2</sub>	11.967	Lunisolar semidiurnal	0.165	5.19
	S <sub>2</sub>	12.000	Principal lunar	0.575	18.09
	M <sub>2</sub>	12.421	Principal solar	1.719	54.09
	N <sub>2</sub>	12.658	Larger lunar elliptical semidiurnal	0.331	10.42
Higher-order	MS <sub>4</sub>	6.102	Shallow water quarter diurnal	0.075	2.36
	M <sub>4</sub>	6.210	Shallow water overtides of principal lunar	0.114	3.59
	MN <sub>4</sub>	6.269	Shallow water quarter diurnal	0.042	1.32

## 2.3 Harnessing Tidal Energy

There are two principal methods for harnessing tidal energy: either by harnessing the energy from tidal elevations or from tidal currents. The difference between the two technologies will be discussed in detail in the subsequent sections. Both technologies technically utilise turbines to convert kinetic energy to electrical energy. However, after Chapter 2 the term ‘tidal turbine’ will solely refer to tidal stream devices, unless explicitly stated.

### 2.3.1 Tidal Barrages/Lagoons

Tidal energy has been harnessed in Europe since the Middle Ages, through the use of tidal mills (Minchinton, 1979). Tidal mills were early examples of a tidal barrage scheme whereby the energy is harvested from potential energy generated by the difference in tidal elevation either side of a structure. Tide mills were controlled by a sluice gate that allowed water to fill an enclosure on the flood tide which then closed on the turn of the tide. Once the tide level has reduced sufficiently, the sluice gate was opened and the escaping water turned the mill wheel. This method is an early example of an ebb mode operation.

A tidal barrage can be operated principally in three modes: ebb mode, flood mode and dual mode. The opposite of the ebb mode is the flood mode, where the sluice gate is closed during the ebb tide and water is allowed to flow into the enclosure during the flood tide. Modern tidal barrages were built to generate electricity. In some cases, modern tidal barrages run in a dual mode, generating electricity on both the flood and ebb tide. Some tidal barrages can use the turbines to pump water into the enclosure to further increase the head difference. Figure 2-3 shows the different operating regimes a tidal barrage could implement.

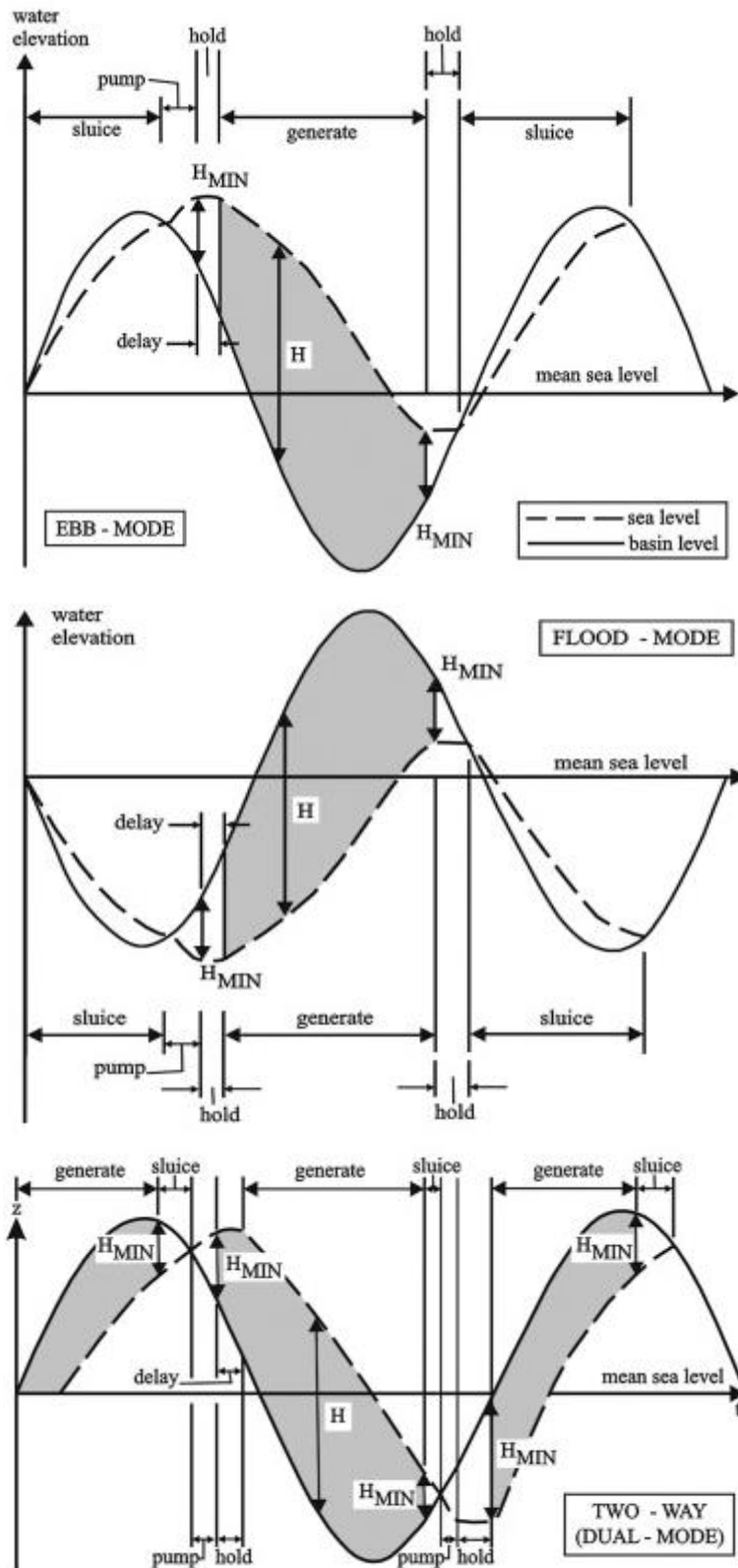


Figure 2-3: Three potential operating regimes of a tidal barrage. Figure originally from Yates et al. (2010).

Whilst tidal barrages for electricity generation were considered in the Bay of Fundy, Canada, in 1919 (Gordon and Longhurst, 1979) and the Severn Estuary,

UK, in 1933 (Ministry of Fuel and Power, 1945) the first tidal barrage to generate electricity commercially was the La Rance tidal barrage, France (Figure 2-4). Construction of the barrage started in 1960 and the scheme was operational by 1967. The 750m long dam was built across the mouth of the La Rance estuary and houses twenty-four 10 MW axial flow turbines which allow generation on both the flood and ebb tide. The design of the bulb turbines allows for water to be pumped into the estuary when the sluice gates are closed to increase the head difference (Retière, 1994).



Figure 2-4: The La Rance tidal barrage. Image copyright Tethys, sourced: *tethys.pnnl.gov*.

In the UK, the Bristol channel is considered an ideal site for a tidal barrage with the second largest tidal range in the world. There have been numerous studies into the feasibility of a tidal barrage in the Severn estuary, notably in 1981 by the Bondi Committee, in 1989 by the Severn Tidal Power Group and in 2007 by the UK Government. By 2010, prohibitive costs and significant impacts on the environment lead to the project being discounted (British Broadcasting Centre, 2010). In 2011, Corlan Hafren, a private sector consortium, investigated building a barrage with private sector money, but was again halted by 2014 (Shipton, 2014).

Conventional tidal barrages can be seen as dams across natural features, such as estuaries, to create a natural reservoir behind the structure. Alternatively, in areas with large a tidal range but no natural features, a fully enclosed structure can be built to create an artificial reservoir behind the retaining walls, known as tidal lagoons. The first tidal lagoon to be granted planning permission is the 320

MW tidal lagoon at Swansea Bay in South Wales, UK (Tidal Lagoon Power, 2015). An artist's impression of the Swansea Bay tidal lagoon is shown in Figure 2-5.



Figure 2-5: Artist's impression of the 320 MW Swansea Bay tidal lagoon. Image copyright of Tidal Lagoon Power, access from [www.tidallagoonpower.com](http://www.tidallagoonpower.com).

### 2.3.2 Tidal Stream Turbines

As well as harnessing energy from gradients in tidal range, tidal currents offer a second significant potential for power generation from tidal forces. It is only recently, in the latter part of the 20th century, that developers have begun developing technologies to harvest energy from tidal currents in the form of a tidal stream turbine, which will be referred to as a tidal turbine from this point onwards. A tidal turbine works using the same principles as an aircraft wing or wind turbine blades. The blades of the tidal turbine are shaped with an aerofoil cross-section. When the currents pass across the blade, thrust is generated by a pressure difference across the upper and lower surface causing the rotor to turn. That mechanical rotation is converted into electricity through a generator connected to the rotor's axle.

The first tidal turbine to harvest energy from tidal currents was a 15kW proof of concept prototype from IT Power Consulting Ltd. The prototype consisted of a two-bladed horizontal axis turbine with a rotor diameter of 3.5m. In 1994, the

turbine was mounted below a floating pontoon and tested in Loch Linnhe, Scotland, (Figure 2-6).



Figure 2-6: The first tidal turbine, a 15kW proof of concept device, as developed by IT Power Consulting Ltd, deployed and tested in 1994 in Loch Linnhe, Scotland. Images copyright of Marine Current Turbines Ltd, sourced: <http://www.british-hydro.org/>.

Following on from that test, in 1998, IT Power started development of the Seaflow turbine, a 300kW horizontal axis turbine with two blades, 11m in diameter. The device was fixed to the seabed through a 2m diameter cylindrical monopile. IT Power later established Marine Current Turbines Ltd (MCT) to develop the technology and hold the intellectual property rights (IT Power Consulting Ltd, n.d). In 2003, the 300kW Seaflow turbine was installed off Lynmouth, Devon, (Figure 2-7).



Figure 2-7: 300kW MCT Seaflow installed in 2003 off Lynmouth, Devon. Image copyright of Marine Current Turbines Ltd, sourced: [www.british-hydro.org](http://www.british-hydro.org).

MCT continued to develop the technology until 2008 where their first grid connected commercial scale device, the 1.2 MW MCT SeaGen, was installed in Strangford Loch, Northern Ireland. The SeaGen device consists of two 600kW horizontal axis rotors with two blades mounted on a support arm connected to a single cylindrical monopole support structure and is shown in Figure 2-8. The rotors have a diameter of 16m. Like the Seaflow device, the SeaGen allows for both rotors to be raised out of the water together for access.



Figure 2-8: 1.2MW MCT SeaGen installed in the Strangford Loch, Northern Ireland. Image copyright of Sea Generation Ltd sourced: [www.seageneration.co.uk](http://www.seageneration.co.uk).



MCT were the pioneers of the tidal current industry which has now grown to include a diverse range of developers and devices worldwide, as indicated by Figure 2-9.

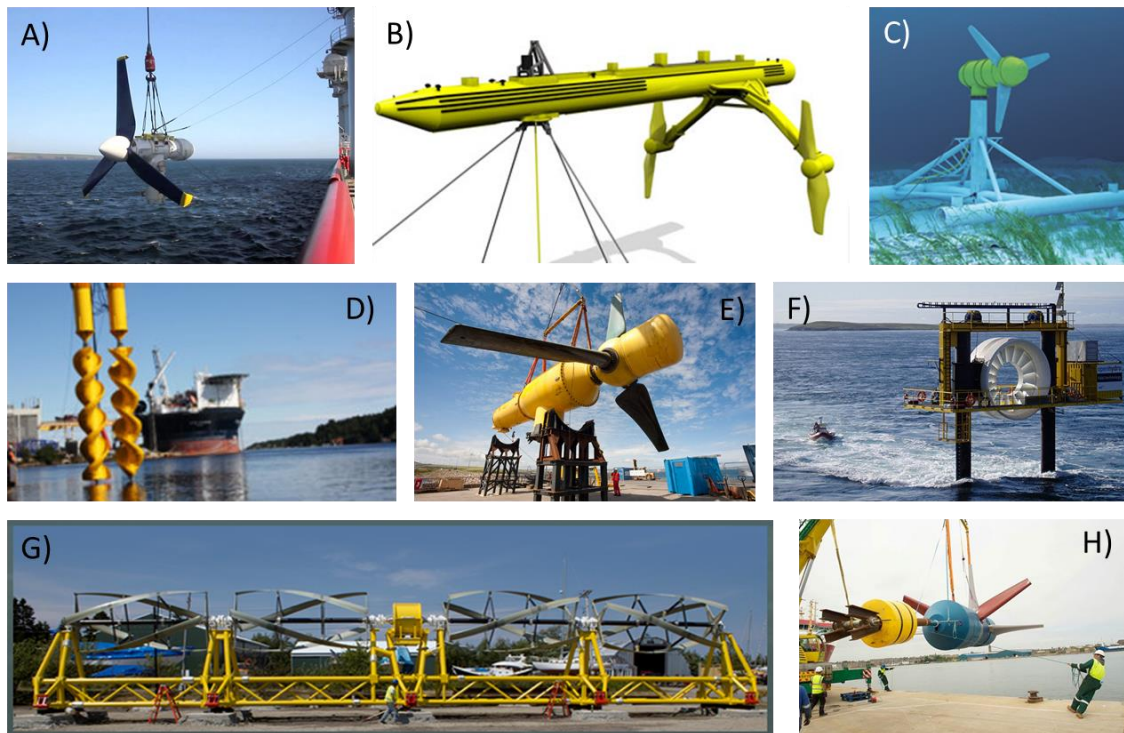


Figure 2-9: Selection of tidal current technologies: a) Atlantis Resources, b) ScotRenewables, c) Voith, d) Flumill, e) Tidal Generation, f) Openhydro, g) Ocean Renewable Power Company and h) Nautricity. Figure 1a copyright of Atlantis Resources Ltd, sourced: [www.atlantisresourcesltd.com](http://www.atlantisresourcesltd.com). Figure 1b copyright of Scotrenewables Tidal Power Ltd, sourced: [www.scotrenewables.com](http://www.scotrenewables.com). Figure 1c copyright of Voith, sourced: [www.voith.com](http://www.voith.com). Figure 1d copyright of Flumill AS, sourced: [www.flumill.com](http://www.flumill.com). Figure 1e copyright of Alstrom, sourced: [www.alstrom.com](http://www.alstrom.com). Figure 1f copyright of Openhydro, sourced: [www.openhydro.com](http://www.openhydro.com). Figure 1g copyright of OPRC LLC, sourced: [www.orpc.co](http://www.orpc.co). Figure 1h copyright of Nautricity Ltd, sourced: [www.nautricity.com](http://www.nautricity.com).

In 2006, the European Marine Energy Centre (EMEC) opened its Fall of Warness tidal test facility, in Orkney, to provide realistic tidal conditions to test full scale devices, with the potential to connect them to the electricity grid if required. Despite the variety of technologies, the market leading developers are now starting to converge towards a single design, a three bladed horizontal axis turbine with a rated power in excess of 1 MW, as evident by the turbines installed at EMEC. In 2010, Tidal Generation Ltd (TGL) deployed a 500kW three bladed horizontal axis turbine. In 2013, TGL was acquired by Alstrom, who subsequently developed a second generation 1 MW three bladed horizontal axis turbine, with

a turbine diameter of 18m. Later that year, the device was deployed using the existing support structure for the 500kW device already deployed at EMEC. In 2016, Alstrom was acquired by General Electricity (GE) and is developing a 1.5MW turbine. In 2011, Andritz Hydro Hammerfest deployed its 1 MW three bladed horizontal axis turbine, with a rotor diameter of 23m, at EMEC. In the same year, Atlantis Resources Corporation also deployed its 1 MW horizontal axis three bladed turbine with a rotor diameter of 18m. In 2016, Tidal Energy Ltd deployed their 400 kW three bladed horizontal axis turbine, with a rotor diameter of 12m, in Ramsey Sound, Wales. Whilst the Alstrom, Andritz, Atlantis and TEL turbines are all seabed mounted, Scotrenewables Tidal Power Ltd use a different approach by mounting two two-bladed rotors on a floating support structure. Their first 250 kW prototype with 8m blades was deployed at EMEC in 2011, for a limited period, and again in 2012 for a three-month deployment. Scotrenewables second generation device consists of two 1 MW two-bladed horizontal axis rotors with a 16m diameter and is currently at EMEC awaiting deployment.

Whilst most devices are converging towards the three bladed horizontal axis turbine, Openhydro have taken a different approach using a ducted open-centred, multi-bladed horizontal axis turbine, shown in Figure 2-9 (F). Openhydro were the first to deploy their device at the EMEC test facility when it opened in 2006 with a 250 kW prototype and a 6m rotor diameter. In 2013, Openhydro deployed a larger 16m diameter device at EDF's Paimpol-Brehat site in France. The device is the chosen turbine technology for the proposed 100 MW development at Torr Head in Northern Ireland which is due to start construction in 2017, subject to planning consent. The first operational commercial array of tidal turbines will be the MeyGen Project, situated in the Inner Sound of Pentland Firth, Scotland. The site is consented for a total of 400MW, with the turbines deployed in a number of phases. Phase 1a will comprise of one Atlantis turbine and three Andritz Hydro Hammerfest turbines, to prove the concept of constructing, operating and maintaining a tidal array. If successful, Phase 1b will deploy a further 80 MW with Phase 2 fulfilling the full site lease capacity. Construction of Phase 1a started in 2015, with the turbines expected to be commissioned by October 2016.

# Chapter 3

## Modelling Tidal Turbines

### 3.1 Introduction

To maximise the electrical output of a tidal turbine or array it needs to be sited at a location exposed to sufficient tidal energy. A cost-effective method for determining suitable locations is through the use of numerical models of hydrodynamic processes (Abbott and Basco, 1997). Large scale regional models can be used for determining geographic hotspots (e.g. Robins et al., 2015; Hashemi et al., 2015a), with finer small scale regional models used for detailed assessment (e.g. Robins et al., 2014; Martin-Short et al., 2015). The physical response to the presence of a tidal turbine on the hydrodynamics is a velocity reduction in the wake of the turbine due to energy extraction and the presence of the turbine (Bryden et al., 2006). Numerical modelling can be used to determine the magnitude of the velocity reduction and to what spatial extent it applies.

This chapter outlines the principles of hydrodynamic modelling and its use in determining the effect of tidal turbines on the flow. It will discuss the parameterisation of tidal turbines in numerical models. The parameterisation will be tested and validated through the use of a conceptual model of tidal flow. The experienced gained from operating the conceptual model will be taken forward for the use in the coastal and regional model.

## 3.2 Modelling Tidal Turbines

In order to understand the interaction between the tidal turbines and the benthic environment, it is first important to understand how the devices interact with the hydrodynamic environment. Numerical modelling of hydrodynamic flow is typically conducted with either two-dimensional or three-dimensional models. The advantage of a three-dimensional model is its ability to model the effects of density stratification due to temperature and salinity. However, the advantage of a two-dimensional model is it is less computationally demanding, running significantly faster than a three-dimensional one with the same model domain. If the hydrodynamic system is well mixed and non-stratified, then two-dimensional modelling is adequate.

Modelling a tidal turbine in 3D can give a very accurate representation of the turbine interaction. A coupled three-dimensional computational fluid dynamics model and blade element model can accurately resolve the complex changes in flow velocities around the turbine rotor and support structure. The model is able to determine the shape and size of the wake structure, as well as the turbulence generated. An example of this is shown in Masters et al (2013). However, these types of models are typically restricted to a single turbine in a domain that extends in the order of hundreds of meters. The resolution required by this modelling approach limits the model runs to a few rotations of the rotor. This approach is clearly too computationally expensive and not appropriate when regional or high resolution scale models extend in the order of hundreds of kilometres and run for 30 days. A 30-day model run is required so that a harmonic analysis of the tides can be conducted for validation of the model performance.

The method chosen for this study is to use a two-dimensional representation of the tidal turbine in a depth averaged flow model. A two-dimensional model offers significant time and cost savings and still provides the necessary information to conduct the research aims of this study. There are a number of ways to implement tidal turbines in depth averaged models. Early estimates of the potential power available in the Pentland Firth, (Black and Veatch, 2005), were made using the kinetic flux method. This method assumes the available power is a percentage of the undisturbed kinetic flux. However, this method came under scrutiny by Garrett and Cummins (2008) who showed that it does not accurately

represent the available power as it does not allow for the feedback effect of the turbine. The feedback effect is due to the fact that a turbine works by the water applying a force on the blade, causing it to rotate and generate rotary motion. This force on the blade results in a drag on the water causing a slowing of the flow around the turbine. An alternative method is to represent drag exerted by the turbines by locally increasing the bottom friction (e.g. Walkington and Burrows, 2009). However, applying a constant friction does not represent the operation of a tidal turbine over the tidal cycle as the thrust on the rotor is proportional to the velocity and will vary over the tidal cycle. A more effective method commonly used, is to model the drag effect of the turbine by applying an extra sink into the momentum equation governing the hydrodynamic model (e.g. Thiebot et al., 2015; Ahmadian et al., 2012; Neill et al., 2012).

### 3.2.1 Solving Free Surface Flows

The primary function of numerical hydrodynamic software packages, such as TELEMAC, is to compute the hydrodynamic processes by solving the Navier-Stokes equations for the dynamics of fluids. The two main equations solved are the mass conservation and continuity of momentum.

The mass conservation equation is given by:

$$\frac{\partial U}{\partial x} + \frac{\partial V}{\partial y} + \frac{\partial W}{\partial z} = 0 \quad (3.1)$$

and the continuity of momentum equation by:

$$\frac{\partial U}{\partial t} + U \frac{\partial U}{\partial x} + V \frac{\partial U}{\partial y} + W \frac{\partial U}{\partial z} = -\frac{1}{\rho} \frac{\partial p}{\partial x} + \nu \Delta(U) + F_x \quad (3.2)$$

$$\frac{\partial V}{\partial t} + U \frac{\partial V}{\partial x} + V \frac{\partial V}{\partial y} + W \frac{\partial V}{\partial z} = -\frac{1}{\rho} \frac{\partial p}{\partial y} + \nu \Delta(V) + F_y \quad (3.3)$$

$$\frac{\partial W}{\partial t} + U \frac{\partial W}{\partial x} + V \frac{\partial W}{\partial y} + W \frac{\partial W}{\partial z} = -\frac{1}{\rho} \frac{\partial p}{\partial z} - g + \nu \Delta(W) + F_W \quad (3.4)$$

where U, V and W are the three-dimensional velocity vectors in the x, y and z Cartesian coordinate system, t is time, g is gravity, p is pressure,  $\nu$  is the kinematic viscosity and F is the sum of the external forces acting on the water body in the x, y and z direction (Hervouet, 2007).

The Navier-Stokes equations presented here are used for solving non-hydrostatic three-dimensional flows. To solve two-dimensional flows, a depth-averaged variation of the Navier-Stokes equations known as the Saint-Venant equations can be used. The Saint-Venant equations were originally published by Saint-Venant (1871) but are still widely used today because of their importance in the use of calculating free surface flows in shallow waters. The Saint-Venant equations make a number of key assumptions:

1. Pressure is hydrostatic – the acceleration due to pressure is counterbalanced by gravity.
2. Vertical velocity is negligible.
3. The free surface and bottom surface are impermeable.
4. Water column is well mixed such that water density in the vertical is constant.

Using these assumptions, the Navier-Stokes equations are integrated with respect to depth from the bottom to the sea surface to form the following equations describing momentum in the x and y directions respectively:

$$\frac{\partial(hu)}{\partial t} + \frac{\partial(hu^2)}{\partial x} + \frac{\partial(huv)}{\partial y} = -gh \frac{\partial Z_s}{\partial x} + hF_x + \text{div}(hv_e \overrightarrow{\text{grad}}(u)) \quad (3.5)$$

$$\frac{\partial(hu)}{\partial t} + \frac{\partial(huv)}{\partial x} + \frac{\partial(hv^2)}{\partial y} = -gh \frac{\partial Z_s}{\partial y} + hF_y + \text{div}(hv_e \overrightarrow{\text{grad}}(v)) \quad (3.6)$$

where u and v are the vertically integrated horizontal components of the three-dimensional velocity vectors U and V,  $v_e$  is the effective diffusion of turbulent viscosity and dispersion (Hervouet, 2007). The momentum equations shown in Equations 3.5 & 3.5 can be broken down into the following terms:

$$\begin{array}{c}
\text{Convection} \qquad \text{Pressure Gradient} \qquad \text{Diffusion} \\
\hline
\frac{\partial(hu)}{\partial t} + \frac{\partial(hu^2)}{\partial x} + \frac{\partial(huv)}{\partial y} = -gh \frac{\partial Z_s}{dx} + hF_x + \text{div}(hv_e \overrightarrow{\text{grad}}(u)) \quad (3.7) \\
\hline
\text{Variation} \qquad \qquad \qquad \text{External Forces}
\end{array}$$

The variation component is a local acceleration of a control volume of fluid. The convection term is the advective rates of change due to motion. The pressure gradient is the direction and rate of pressure change around a point. The external forces are all the source terms and body forces, such as bottom friction, Coriolis forces, wind forcing etc. The final term is the diffusion of turbulence generated by the molecular agitation of the fluid.

The source term that can be used to introduce the effect tidal turbines is F, representing the external forces. F represents the sum of all the momentum source terms and body forces. The effect of the tidal turbine can be introduced as a new momentum sink term representing the drag exerted on the hydrodynamic flow.

### 3.2.2 Representing Tidal Turbines

As depth-averaged modelling is used throughout, the parameterisation of a tidal turbine is a two-dimensional representation of a three-dimensional object. A tidal turbine causes a change in momentum in two parts: thrust force produced by the rotor due to energy extraction and a drag force caused by the supporting structure, i.e.-

$$F_{TOTAL} = F_T + F_D = \frac{1}{2} \rho C_T A_r U^2 + \frac{1}{2} \rho C_D A_s U^2 \quad (3.8)$$

where U is the upstream velocity, ρ is the density of sea water, C<sub>T</sub> is the thrust coefficient, C<sub>D</sub> is the drag coefficient, A<sub>r</sub> is the swept area of the rotor and A<sub>s</sub> is the frontal area of the support structure, as shown in Figure 3-1.

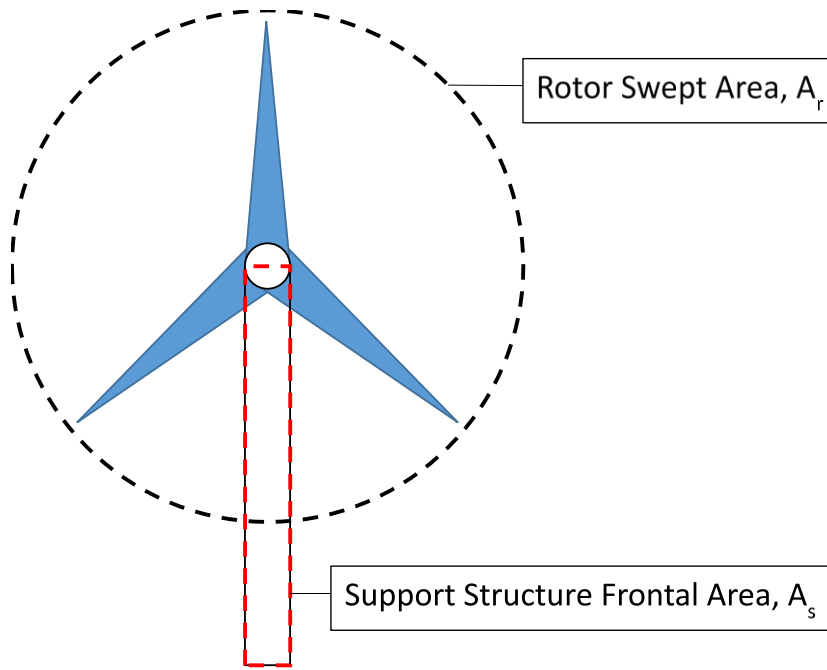


Figure 3-1: Schematic of idealised representation of tidal turbine.

The operation and output of the turbine is controlled by the pitch of the rotor blades, resulting in changes in the thrust and power coefficient. The methodology used to represent the operation of the tidal turbines is presented by Plew & Stevens (2013). Below the cut-in speed, the rotor produces no power, meaning that the thrust and power coefficient are zero, i.e.  $C_T = C_P = 0$ . Between the cut-in speed,  $U_C$ , and the rated speed,  $U_D$ , it is assumed the pitch of the rotor blade is fixed along with the tip speed ratio, resulting in a constant thrust and power coefficient,  $C_{T0}$  and  $C_{P0}$ . Above the rated speed, the pitch of the rotor blade is increased to reduce the power produced and maintain the rated power,  $P_D$ . The power coefficient is parameterised as:

$$C_P = \frac{2P_D}{\rho A_r U^3}, \quad U > U_D \quad (3.9)$$

For simplicity, Plew and Stevens (2013) assume a fixed relationship between the thrust and power coefficient, resulting in the thrust coefficient above rated speed being parameterised as

$$C_T = \frac{C_{T0}}{C_{P0}} \frac{2P_D}{\rho A_r U^3}, \quad U > U_D \quad (3.10)$$

It is important to model the full period of operation of the tidal turbine. Modelling a turbine as a constant drag term grossly misrepresents the forces exerted by the



rotor (Plew and Stevens, 2013). Similarly, by ignoring the drag caused by the support structure, the total force is under-represented, especially at higher flow velocities. Figure 3-2 shows the force exerted by an idealised turbine with the thrust from the rotor and the structural drag normalised to the total force at the rated velocity. It can be seen that as the flow velocity increases, the total force increases to its peak at rated velocity whereby the thrust from the rotor decreases. However, the drag from the support structure continues to increase, such that the total force reduces initially after rated velocity but then continues to rise again.

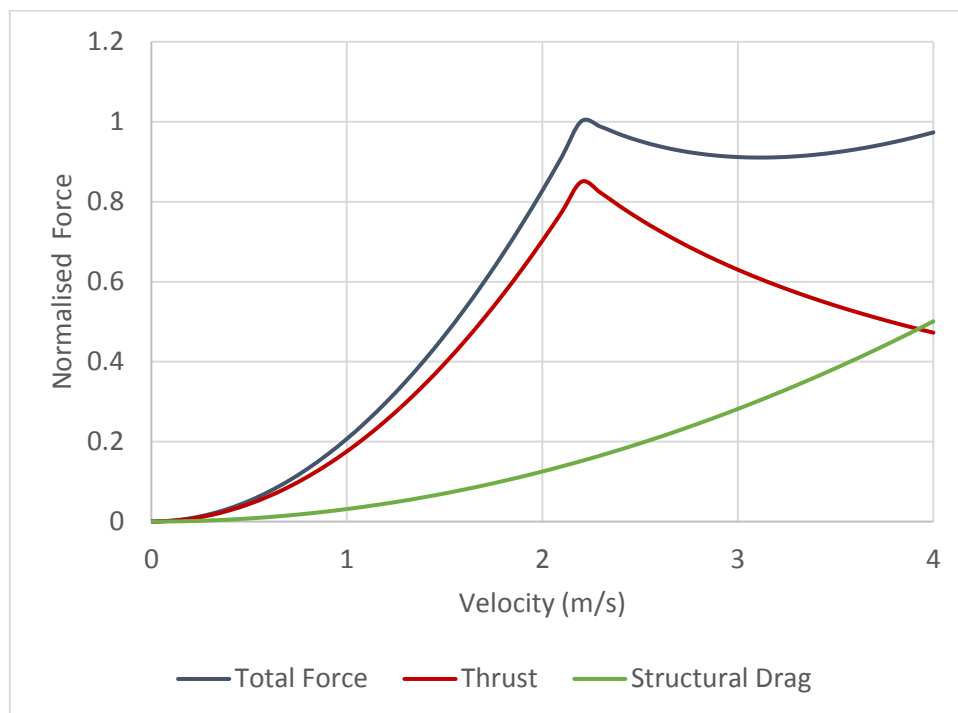


Figure 3-2: Normalised force contributions of an idealised tidal turbine. The force is normalised to the total force at the rated velocity (2.25m/s).

### 3.3 Hydrodynamic Modelling

There are a number of suitable software packages available for the modelling of hydrodynamic processes, i.e. TELEMAC2D, MIKE21, FLUIDITY, DELFT3D, FVCOM (Galland et al., 1991; Warren and Bach, 1992; Ford et al., 2004; Roelvink and Van Banning, 1995; Chen, Liu and Beardsley, 2003). Two that are widely used in the field of renewable energy are TELEMAC and MIKE ([www.opentelemac.org](http://www.opentelemac.org); [www.mikepoweredbydhi.com](http://www.mikepoweredbydhi.com)) (Thiebot et al., 2015; Ahmadian et al., 2012; O'Rourke et al., 2010; Easton et al., 2011). Both solvers are functionally similar in calculating free surface flows and show good agreement

between their individual capabilities (Samaras et al, 2016). The main difference between the two packages is MIKE is a licensable, commercial product and TELEMAC is available on an open-source licence. The advantage of using TELEMAC is that the source code is published and permits the code to be modified to the user's requirements. Whilst MIKE is capable of modelling tidal turbines, the parameterisation within the solver cannot be modified to ensure it is correctly representing the true effect. As such, TELEMAC has been chosen as the software package used to compute the hydrodynamics.

### 3.3.1 TELEMAC-MASCARET Modelling System

TELEMAC-MASCARET Modelling System is a suite of tools for the modelling of free surface flows (Hervouet, 2007). TELEMAC was originally developed as a commercial hydrodynamic code by the Research and Development Department of Electricité de France (EDF) for work relating to dams, reservoir management, thermal and nuclear power stations. In 2010, the TELEMAC-Consortium was founded for the distribution of TELEMAC as open-source software. Since becoming open-source, the use of TELEMAC has grown to over 4000 users worldwide leading to hundreds of publications (TELEMAC-MASCARET, n.d.). TELEMAC is written in FORTRAN and is capable of running on Windows, Linux and Unix operating systems.

The TELEMAC suite is integrated and made up of five hydrodynamic modules, three sediment transport modules and two pre/post-processing modules. Each module is capable of running independently but can also be internally coupled for more complex interactions. This is achieved through the use of a common geometry mesh. The TELEMAC modules are as follows:

- ARTEMIS Surface wave agitation in harbours
- MASCARET One-dimensional flows
- TELEMAC-2D Two-dimensional flows
- TELEMAC-3D Three-dimensional flows
- TOMAWAC Wave propagation in coastal waters
- SISYPHE Two-dimensional sediment transport
- SEDI-3D Three-dimensional sediment transport
- NESTOR Simulation of dredging
- STBTEL Grid interface
- POSTEL-3D Visualizing 2D sections of 3D flows

- WAQTEL Water quality

TELEMAC uses a finite element scheme. Finite element is an integral scheme for solving partial differential equations. One of the main advantages of TELEMAC is its use of finite element method used with an unstructured mesh with triangular elements. The model may be run in parallel mode using multiple processors simultaneously and reducing the computational time allowing for a more complex mesh where shallow bathymetry or areas of high topographic or hydrodynamic detail is needed (Moulinec et al., 2011). Complex coastlines can be more accurately represented and the model uses a varying resolution, with a higher node density in areas of interest and a lower density in other areas to speed up computational time by reducing the total number of nodes.

### 3.3.2 Model Set-up

TELEMAC requires a number of key input information in order to run. These include, but are not limited to:

- Steering file
- Geometry file
- Boundary conditions file
- Formatted data files
- Fortran file

The steering file is a text file that contains the keywords that defines the model set-up and parameters. These include the path names to the other input files, model run time, time step, output variables, etc.

The geometry file describes the finite element mesh and holds the bathymetry of the model domain. The model's output variables are written onto a mesh with the same geometry (node number and position) as the input geometry file. The geometry file was created using the freely available mesh generation software package BlueKenue, developed by the Canadian National Research Council as a pre/post-processing, analysis and visualization tool for hydraulic simulations ([www.nrc-cnrc.gc.ca](http://www.nrc-cnrc.gc.ca)). It is capable of creating and processing the input and output files for TELEMAC.

The boundary conditions file is a list of the node numbers around the boundary of the domain and for any islands within it. It describes the condition of each

boundary node, either closed or open and its type. The type of boundary condition is used to force a transfer of flux along the open boundary. The closed boundary allows no transfer of water across the boundary. There can be multiple combinations of differing types of boundary condition, as shown in Table 3-1.

Table 3-1: Types of boundary conditions used with TELEMAC.

Variable	Description
Depth condition	Open boundary with prescribed depth
	Open boundary with free depth
	Closed boundary (wall)
Flowrate or velocity condition	Open boundary with prescribed flowrate
	Open boundary with prescribe velocity
	Open boundary with free velocity
	Closed boundary with slip or friction
Tracer condition	Closed boundary with one or two null velocity components
	Open boundary with prescribed tracer
	Open boundary with free tracer
	Closed boundary (wall)

The information containing the prescribed forcing is obtained in two ways: a liquid boundary file or formatted data file. A liquid boundary file contains a time series of every parameter which changes on the boundary, such as surface elevation or velocity. Whilst it is possible to programme a unique value for each node along the boundary, the value is typically applied uniformly to each connected node on the corresponding open boundary. This is acceptable if the open boundary is small, such as a river input, or the value does represent the condition along the whole boundary. However, with large regional tidal domains this is not appropriate. In this case, the model can either be forced with a spatially varying boundary forcing using a formatted data file or use a modified Fortran file to program a function at each node. The formatted file approach is the method adopted in this study. The formatted data file is a text file with a user defined format. For the coastal and regional models described in the Chapter 1, the formatted data file contains the amplitude, phase and period of the separate harmonic tidal constituents at each boundary node. The harmonics are read using

a user-defined Fortran file and the spatially varying free surface elevation is calculated along the open boundary.

As TELEMAC is open source, users may modify or add additional code to perform functions that are not included in the base code. These alterations can be implemented in the user-defined Fortran file. At launch, the users Fortran code is recompiled and combined with the rest of TELEMAC and a new binary file produced. When a user-defined Fortran file is included in the model set-up, the subroutines in the user-defined Fortran file replace the corresponding original TELEMAC subroutines. The effect of the tidal turbines is introduced in TELEMAC, through the Fortran subroutine dragfo.f.

### 3.3.3 Wave Modelling with TOMAWAC

TOMAWAC is the wave propagation component of the TELEMAC-MASCARET suite and is used to model the production and propagation of sea surface waves. Waves are the oscillation in the free surface generated by wind blowing over the sea surface. Waves can be represented as sinusoidal movements much like the motion of tides, only whose period, or frequency, is much smaller (2.5-25 seconds). The condition of the sea surface, known as a sea state, can be represented with either regular or irregular waves. A regular sea state is made up of monochromatic waves represented as a sinusoidal wave with a single frequency that propagates in a single direction. An Irregular sea state is the combination of a range of monochromatic waves at different frequencies, over a range of propagation directions. An irregular sea state can thus be represented by the superposition of an infinite number of sinusoidal components where the free surface,  $\eta$ , is described by:

$$\eta(x, y, t) = \sum_{m=1}^M a_m \cdot \cos[k_m(x \cdot \sin\theta_m + y \cdot \cos\theta_m) - \omega_m \cdot t + \varphi_m] \quad (3.11)$$

where x and y are the spatial coordinate, t, is time, a is the wave amplitude,  $\omega$  is the wave frequency,  $\theta$  is the propagation direction and  $\varphi$  is the wave phase. k is the wave number and is yielded by the free surface wave linear dispersion relation,:

$$\omega^2 = g \cdot k \cdot \tanh(k \cdot d) \quad (3.12)$$

where  $\omega$  is the frequency and  $d$  is depth. TOMAWAC is a phased-averaged model and assumes the wave phases,  $\phi$ , are randomly distributed with a uniform probability density, over a range of 0 to  $2\pi$ . The energy per unit area of the irregular sea state is a continuous function of both frequency and propagation directions, whereby the directional spectrum of wave energy is represented by:

$$E(f, \theta) = \sum_f^{f+df} \sum_\theta^{\theta+d\theta} \frac{1}{2} \rho g a_m^2 \quad (3.13)$$

where  $\rho$  is density of water and  $g$  is gravitational acceleration. TOMAWAC models the generation and propagation of a sea state by solving the balance of the wave action density direction spectrum. The wave action density spectrum is defined by:

$$N = \frac{F}{\sigma} \quad (3.14)$$

where  $\sigma$  is the intrinsic angular frequency and  $F$  is the variance directional spectrum as defined by:

$$F(f, \theta) = \frac{E(f, \theta)}{\rho g} \quad (3.15)$$

The above equations provide a good representation of waves in deep water. However, as waves propagate into shallow waters, their sinusoidal profile becomes distorted by non-linear effects due to the interaction with the seabed. Shallow water are depths,  $h$ , smaller than the following criteria:

$$h = \frac{\lambda}{20} \quad (3.16)$$

where  $\lambda$  is the wavelength of a wave. As TOMAWAC is a phased-average model, the superposition of a number of sinusoidal components cannot represent the non-linear interactions. Instead, they are parameterised and introduced as source and sink terms. Some of the key terms are, but not limited to:

- Wind-driven wave generation
- Whitecapping-induced energy dissipation

- Bottom friction-induced energy dissipation
- Bathymetry breaking-induced energy dissipation
- Non-linear triad interactions
- Non-linear quadruplet interactions
- Interactions with unsteady currents

The wind-driven wave generation is the primary source of energy for the wave energy density distribution. Whitecapping is the dissipation of energy due to waves breaking as they become too steep. Bottom friction induced dissipation primarily occurs as waves interact with the seabed in shallow waters. Bathymetric breaking is due to waves shoaling in shallow water to the point where they become too steep and break. In shallow water, waves break when the wave height is 0.8 times larger than the depth. The non-linear triads describe a weak resonant interaction in shallow depths where two waves combine to form a third wave. Non-linear quadruplets are a resonant interaction of four wave components in deep water. If TOMAWAC is coupled with TELEMAC2D or 3D, then the interaction between the waves and tidal currents can be taken into account.

Combining the representation of the waves with the parameterised processes and non-linear interactions, the evolution of the wave action density direction spectrum on a computational domain can be expressed by:

$$\frac{\partial N}{\partial t} + \frac{\partial(\dot{x}N)}{\partial x} + \frac{\partial(\dot{y}N)}{\partial y} + \frac{\partial(\dot{k}_x N)}{\partial k_x} + \frac{\partial(\dot{k}_y N)}{\partial k_y} = Q(k_x, k_y, x, y, t) \quad (3.17)$$

where  $x$  and  $y$  are the spatial location for the position vector  $\vec{x}$ ,  $k_x$  and  $k_y$  are the components of the wave number vector  $\vec{k}$ ,  $t$  is time and  $Q$  is the combined source and sink terms.  $\dot{x}$ ,  $\dot{y}$ ,  $\dot{k}_x$  and  $\dot{k}_y$  are represented by:

$$\dot{x} = \frac{\partial \Omega}{\partial k_x} \quad \dot{y} = \frac{\partial \Omega}{\partial k_y} \quad \dot{k}_x = -\frac{\partial \Omega}{\partial x} \quad \dot{k}_y = -\frac{\partial \Omega}{\partial y} \quad (3.18)$$

where  $\Omega$  is the Doppler effect relationship between the absolute angular frequency,  $\omega$ , and the intrinsic angular frequency,  $\sigma$ , in the presence of a current,  $\vec{U}$ , denoted by:

$$\Omega(\vec{k}, \vec{x}, t) = \omega = \sigma + \vec{k} \cdot \vec{U} \quad (3.19)$$

As the same as TELEMAC, TOMAWAC requires a number of key input information in order to run. These include, but are not limited to:

- Steering file
- Geometry file
- Boundary conditions file
- Formatted data files
- Fortran file

The TOMAWAC input files act is the same way as the TELEMAC input files. The steering file is a text file that contains the keywords that defines the model set-up and parameters, although, the TOMAWAC steering file uses different keywords from TELEMAC. The same geometry file can be used for both TELEMAC and TOMAWAC. Whilst the boundary conditions file uses the same structure, a separate file is needed for TOMAWAC as only one value is used to describe the boundary as either a free boundary or a boundary with a prescribed value. To take either wind and/or currents into account, the user can provide values within either formatted files or binary files. The user may modify or add additional code to perform functions that are not included in the base code through the use of an additional Fortran file.

### 3.4 Conceptual Model

The role of the conceptual model is to demonstrate the parameterisation of the tidal turbines. Plew & Stephen's (2013) parameterisation represents the drag imposed by a single rotor. A tidal array is made up of multiple devices. In the numerical models the array can be represented as either the combined total drag of all devices spread over the total area of the array or as individual devices. The conceptual model will be used to test which method provides the best representation of the tidal array. The conceptual model will take the form of an idealised rectilinear channel with a uniform depth. The depth averaged model will be run using TELEMAC2D (v7p1).

#### 3.4.1 Idealised Channel Model

The turbines, used for this study, are based on the published figures of the TEL DeltaStream device (Tidal Energy Ltd, 2012) and the device is shown in Figure 3-3. Each device consists of three 400kW rotors with a diameter of 15m. Each



rotor reaches its rated power output at a current velocity of 2.25m/s. Based upon these parameters, the values for the constant power and thrust coefficients are  $C_{P0} = 0.29$  and  $C_{T0} = 0.8$ , and are used to create the power curve shown in Figure 3-4. The power curve represents sum the power generated from the three individual rotors. A 10MW array contains 9 devices with 27 rotors. The hub height is 14m. It has been assumed that the rotor has a cut-in speed of 0.8m/s. For simplicity, the support structure has been modelled as a cylindrical monopile with a diameter of 2m and a drag coefficient  $C_D = 0.9$ .



Figure 3-3: TEL Ltd DeltaStream device, left) constructed 400kW full scale prototype, right) artist impression of 1.2MW DeltaStream. Images copyright of TEL Ltd, sourced: [www.tidalenergyltd.com](http://www.tidalenergyltd.com).

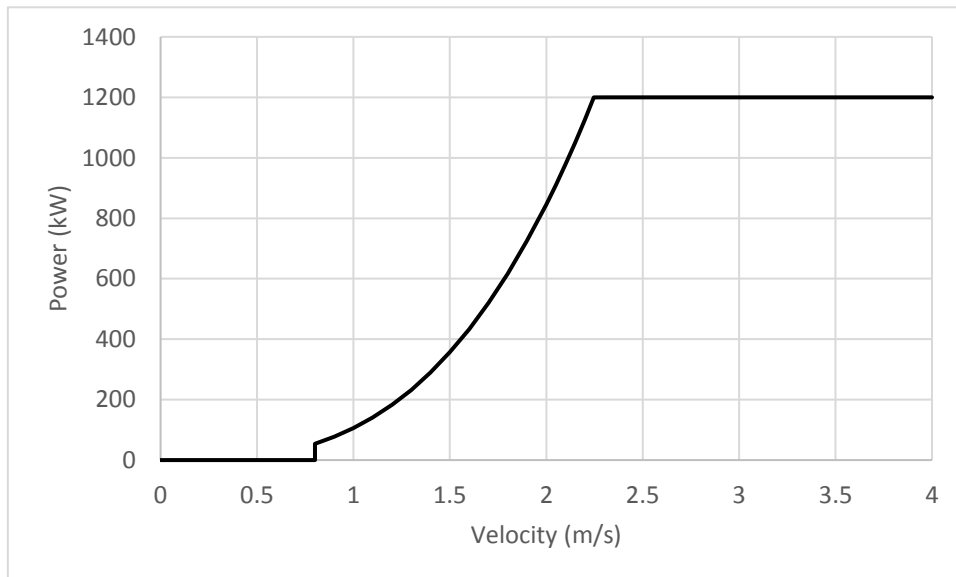


Figure 3-4: Power curve of 1.2MW DeltaStream device, using Plew & Stevens (2013) with  $C_{T0} = 0.81$  and  $C_{P0} = 0.27$ . The cut-in speed is 0.8 m/s with rated power occurring above 2.25 m/s.

As the resolutions of unstructured meshes are typically coarser than the modelled turbines, the total drag force of the entire array is spread over the area of several mesh elements and nodes. However, Kramer et al. (2014) showed that mesh

resolution can influence how much energy loss is represented by a model. As an unstructured mesh can result in elements of different sizes, the force applied to each element may be different within the same area defined as one turbine/array. Therefore, for the models presented, a regular mesh using triangular elements nested within the unstructured triangular mesh is used in the area where turbines are modelled, to ensure a uniform force distribution.

The idealised channel used was 14km in length and 3km wide. The tidal turbines were situated 4km downstream from the inflow boundary. An area of 600m by 400m, surrounding the tidal turbines, was discretised with a regular mesh with triangular elements of equal size (200m<sup>2</sup>). The rest of the mesh was discretised with an unstructured mesh with elements typically 1 km<sup>2</sup>. The mesh had a total of 20,982 nodes and 41,282 elements. The channel had a uniform depth of 35m. The finite element mesh is shown in Figure 3-5. The model was forced to provide a velocity of 2.7m/s from the upstream open boundary, flowing left to right.

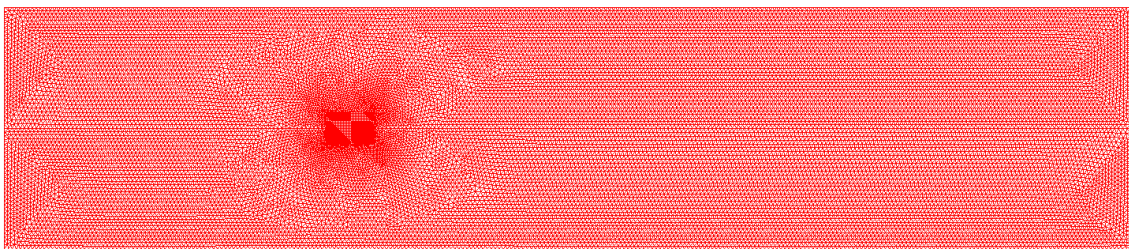


Figure 3-5: Idealised channel finite element mesh.

The Courant-Friedrich-Lewy (CFL) condition was used to determine the required time step of the model simulation. The CFL condition is used as a stability criterion whilst solving partial differential equations and in the one-dimension is defined as:

$$CFL = \frac{u\Delta t}{\Delta x} < 1 \quad (3.20)$$

where  $u$  is the local flow velocity at the grid element,  $\Delta t$  is the time step and  $\Delta x$  is the spatial discretisation (Trivellato and Castelli ,2014). For the idealised channel model, a time step  $t_s = 2s$  was used.

The model runs were performed on the High Performance Computing Cluster service at the University of East Anglia. The HPC consists of, but not limited to, 32 Ivy Bridge Dual 10 core E5-2670V2 2.5GHz processor systems (20 cores)

with 64GB of RAM. The Idealised Channel model (20,982 nodes) was run on a single node with 16 processors, with an initial model time of  $t = 24$  hours, taking approximately 45 minutes. After a spin-up period, to ensure flow through the channel was steady, the simulation was run for a model time  $t = 3$  hours, taking approximately 5 minutes.

Typically, the influence of the whole tidal array is modelled as a single area (e.g. Draper et al., 2014; Thiebot, 2015). However, this does not reflect the true influence. The mesh resolution of the idealised channel is too large for the model to simulate the inter-rotor effects of one device. However, it is small enough to model the intra-array effect of each device. Therefore, for comparison, the 10 MW array has been modelled as nine individual devices as well as the whole array modelled as one area, as shown in Figure 3-6. To represent one 1.2MW DeltaStream device, the force of all three rotors are combined and distributed over eight elements. Based on EMEC (2009) the devices were spaced ten rotor diameters downstream of each other and a lateral spacing of two and half rotor diameters.

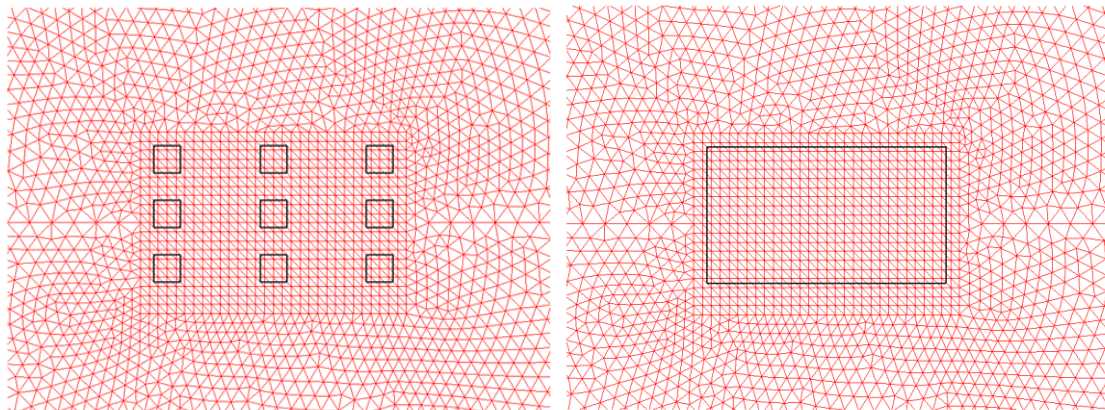


Figure 3-6: Areas defining the drag of tidal turbines, modelled as left) individual devices and right) the whole array.

TELEMAC offers a number of methods to represent the bottom friction. For this case study the Nikuradse law for bottom friction was applied as it allows the friction to be set according to a grain size distribution. Nikuradse bottom friction is defined as:

$$k_s = 30 z_0 \quad (3.21)$$

where

$$z_0 = \frac{d_{50}}{12} \quad (3.22)$$

$z_0$  is the roughness length and  $d_{50}$  is the grain diameter whereby 50% of the grains by mass are smaller (Soulsby, 1997). A constant friction coefficient of  $k_s = 0.01$  was chosen for the whole mesh, representing a gravel seabed with a  $d_{50} = 4\text{mm}$ .

TELEMAC provides different methods for modelling turbulence, such as constant viscosity, k- $\epsilon$  and Elder. The constant viscosity method uses a constant coefficient to represent the molecular viscosity turbulent viscosity and dispersion. The k- $\epsilon$  turbulence model solves the transport equation for turbulent energy,  $k$ , and turbulent dissipation,  $\epsilon$ . A depth averaged form of the k- $\epsilon$  model was developed by Rastogi and Rodi (1978). For the application of the k- $\epsilon$  turbulence model in TELEMAC, the velocity diffusivity is set to  $1 \times 10^{-06} \text{ m}^2/\text{s}$ , representing the kinematic viscosity of water. The k- $\epsilon$  turbulence model assumes the turbulence is isotropic. However, this does not always hold true (Wilson et al., 2002). The Elder model (Fischer et al., 1979) represents anisotropic turbulence where the viscosity values vary in the longitudinal,  $k_l$ , and transverse,  $k_t$ , directions. Based on a study by Moulin (1995), TELEMAC recommends the dimensionless dispersion coefficients be set to  $k_l = 6$  and  $k_t = 0.6$ . Despite the advances in representing turbulence, all numerical models have limitations and interpretation of results should be handled with care (Violeau et al., 2002). Both the k- $\epsilon$  and Elder model show similar predictive accuracy in channel models and are both better representations of turbulence compared to the constant viscosity (Wilson et al., 2002). Whilst the Elder model allows for a more accurate representation of anisotropic turbulence, it does require field measurements to calibrate the longitudinal and transverse viscosity values. The advantage of the k- $\epsilon$  model is that it does not require any calibration or validation. As field measurements are not available, a method that requires no calibration and provides similar predictive ability is preferable. As such, the k- $\epsilon$  turbulence model will be used in this study.

The TELEMAC steering file used for the Idealised Channel test case is shown in Appendix C.

### 3.4.2 Dragfo.f Subroutine

Dragfo.f is an empty user-programmable subroutine written in FORTRAN. The subroutine requires the user to include programming code to apply an extra drag

term in the momentum equation. The original dragfo.f subroutine is a “place holder” file and requires the user to program the function. If called without modification the subroutine has no influence on a model. In the case of modelling tidal turbines, the user has to write the code that calculates the total force exerted by the tidal turbine and define where the force is applied within the model domain. Rather than model the turbine as a point source, the total force is spread over a number of elements in the model mesh. The elements where the tidal turbines are implemented are defined by a quadrilateral where the number of nodes in the quadrilateral is defined by the variable NSOM. Here, the quadrilateral is defined by four nodes with Node 1 representing the bottom left corner, and counting anti-clockwise as shown in Figure 3-7.

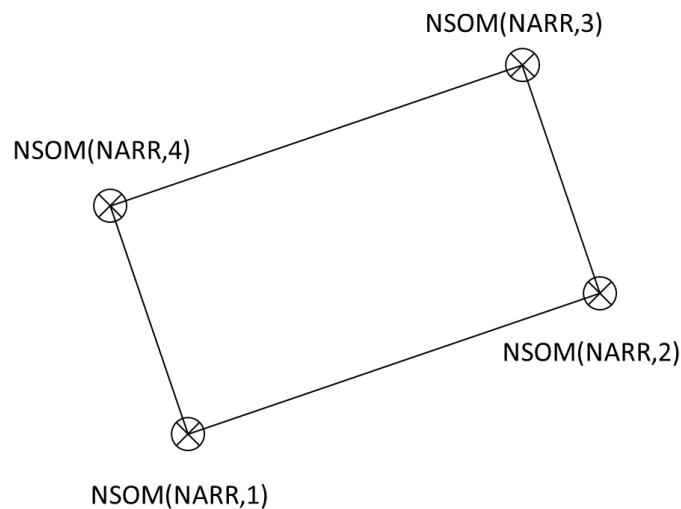


Figure 3-7: Coordinate convention of variable NSOM, denoting coordinates of the quadrilateral defining the location of the turbines.

TELEMAC can compute the hydrodynamics on a model domain using either a spherical or Cartesian coordinate system. When the mesh is specified in a spherical coordinate system, the coordinates are transformed into a Universal Mercator Cartesian system before any calculations are performed. Therefore, the coordinates defining the tidal turbine quadrilateral must be specified in Mercator format, and not as spherical latitude longitudes. A Mercator coordinate system was used for the idealised channel model. Whereas, a spherical coordinate system is used in the subsequent case studies.

For this study, the dragfo subroutine has been written to read a text file with the locations of the turbines and the turbine parameters. The main advantage of

writing the subroutine to read the text file is that it allows TELEMAT to apply multiple numbers of turbines in multiple areas with each area potentially representing different technology types, meaning it is more adaptable. The text file contains fifteen variables needed in the computation and are described in Table 3-2. The format structure of the text file is shown in Appendix A. The modified Fortran subroutine dragfo.f is shown in Appendix B.

Table 3-2: List of variables used to parameterise a tidal turbine in the dragfo.f subroutine.

Variable	Description
NARR	Number of arrays
NSOM	Number of points in quadrilateral
TARR	Type of array (1 = tidal or 2 = wind)
NT	Number of turbines
RDIAM	Rotor diameter (m)
MDIAM	Monopile diameter (m)
LMON	Length of monopile in water column (m)
U_Cut	Cut in speed of rotor (m/s)
U_Des	Design speed of rotor (aka rated speed) (m/s)
CD	Coefficient of drag of monopile
CTo	Maximised coefficient of thrust of rotor
CPo	Maximised coefficient of power of rotor
P_Rated	Rated power of turbine (W)
RHO	Density of sea water (kg/m <sup>3</sup> )
XSOM	X-coordinate of quadrilateral
YSOM	Y-coordinate of quadrilateral

The variable TARR specifies how the drag from the support structure is treated. For TARR=1 the drag is treated as a seabed mounted tidal turbine where the support structure extends from the seabed to the hub height, whose length is defined by the variable LMON. If the tidal turbine is a floating turbine tethered to the seabed via a mooring cable, the variable CD is set to zero. The drag from a mooring line is considered negligible compared to that of a monopile or the thrust of the rotor. As a result, the calculation of drag from the support structure,  $F_D$ , is set to zero, i.e.:

$$F_D = \frac{1}{2} \rho C_D A_s U^2 = 0 \quad (3.23)$$

For TARR=2 the drag is treated as modelling a wind turbine monopile. As a wind turbine monopile is a surface piercing structure, the drag from the monopile extends through the entire water column. In this case the value of LMON in the text file is replaced by the value of the water depth, HN%R(I), which varies with time. As the total force of the wind turbine on the water column is comprised entirely of the support structure, the variable CT is set to zero, meaning the calculation of thrust from the rotor,  $F_T$ , is set to zero, i.e.:

$$F_T = \frac{1}{2} \rho C_T A_r U^2 = 0 \quad (3.24)$$

Whilst the subroutine was written with the capabilities to model wind turbines, it was never investigated as part of this study.

The rotor and support structure only apply a force over the frontal area exposed to incoming water flow. As such, the area of the rotor,  $A_r$ , and the area of the support structure,  $A_s$ , are calculated as:

$$A_s = MDIAM \times LMON \quad (3.25)$$

$$A_r = \pi \left( \frac{RDIAM}{2} \right)^2 \quad (3.26)$$

Within the subroutine the total drag, in the U and V directions, is calculated under the variable handle FUDRAG%R(I) and FVDRAG%R(I). These variables are called by other TELEMAC subroutines.

The subroutine also includes a power calculation. The power is calculated under the variable handle PRIVE%ADR(1)%P%R(I). The power calculation is outputted in Private Array 1 and is stored in the Selafin results file. The electrical power output is calculated as:

$$Power (kW) = \frac{1}{2} NT \rho A_r C_p U^3 \quad (3.27)$$

The final full code of the dragfo.f subroutine is shown in Appendix B.

### 3.4.3 Model Results

The idealised channel model was used to demonstrate the parameterisation of the tidal turbines and test which method for representing the tidal array provided

the most realistic representation. Figure 3-8 shows the velocity reduction due to the presence of the tidal array, as modelled as a) nine individual devices and b) the array modelled as a whole.

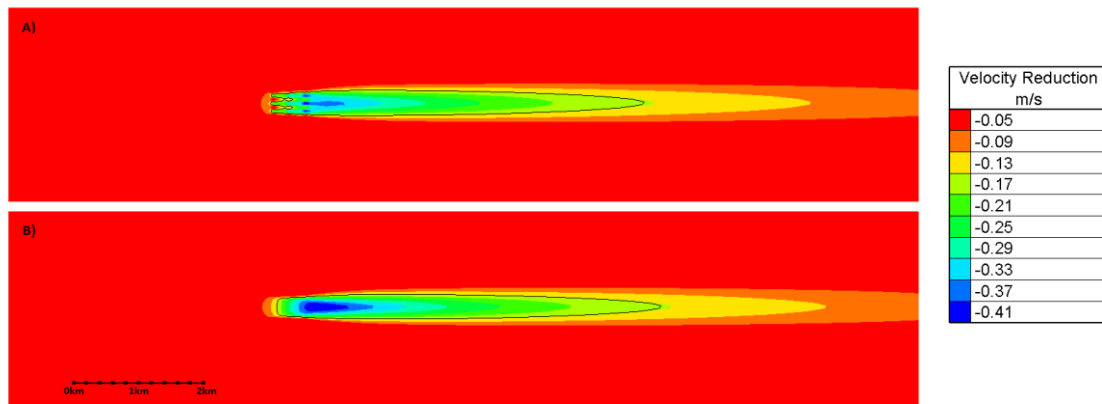


Figure 3-8: Velocity reduction with the tidal array represented as a) individual devices and b) the whole array. The black line represents where the flow speed has recovered to within 5% of the upstream velocity.

The results show that the two approaches to modelling tidal arrays yield similar results. Both the overall structure and magnitude of the wake is similar. The boundary of the wake is defined as the point where the flow velocity has returned to within 5% of the upstream velocity. However, the wake of the whole array is ~200m longer when compared to that of the individual turbines. The maximum reduction in flow speeds in case (a) is 0.37 m/s. In case (b) the velocity reduction is 0.4 m/s. The area over which this peak reduction is seen is much larger when the whole array is modelled as one area. Figure 3-9 shows the velocity profile down the centre line of the channel. It can be seen in the intra-array effects that the by-pass flow between the turbines allows for flow to recover more quickly. This provides a more realistic representation of the flow field through the array and matches tank testing by Myers & Bahaj (2012).



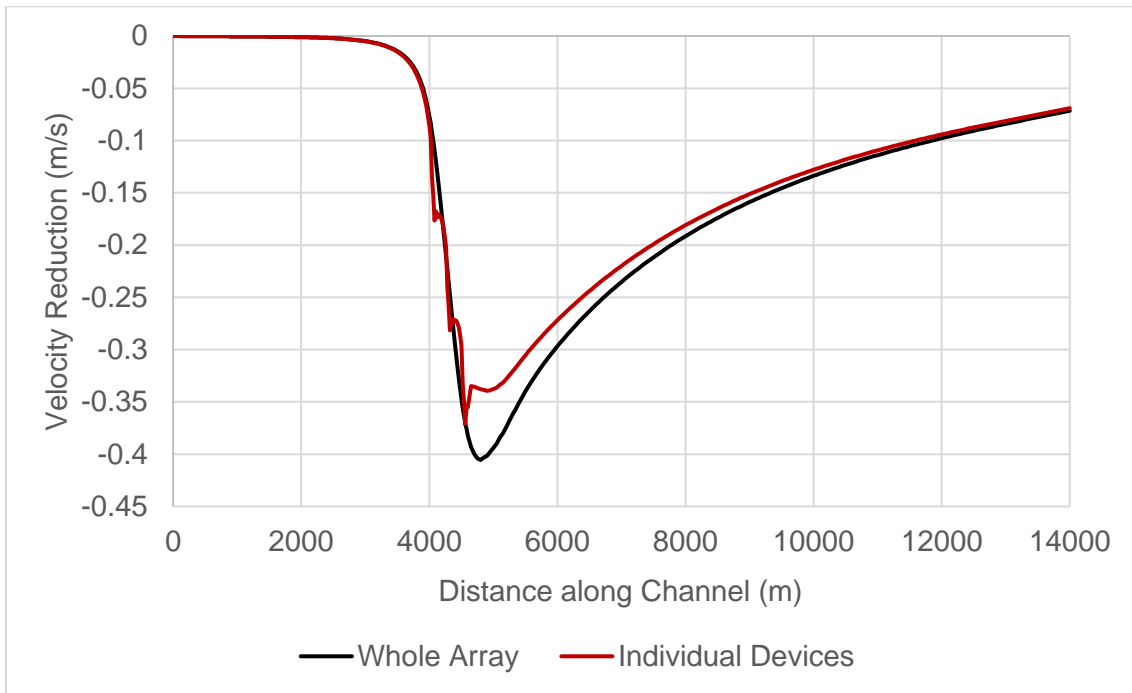


Figure 3-9: Velocity (m/s) reduction across tidal array, down centre line of channel (m).

Linear momentum actuator disc theory (LMADT) has been used to validate the parameterisation of the tidal turbine. LMADT was introduced by Betz (1920) to determine the limit of extractable power from a fluid, and is used in wind industry to benchmark the efficiency of wind turbines. For the application to a wind turbine, the volume of air is assumed infinite and unbounded. Due to the low density of air, the stream tube will expand freely when slowed. These assumptions do not hold when the fluid is water. Instead, Houlsby et al (2008) extended LMADT so that it could be applied to a tidal turbine in an open channel flow. Figure 3-10 shows geometry of flow Houlsby et al (2008) used to apply LMADT to an open channel flow.

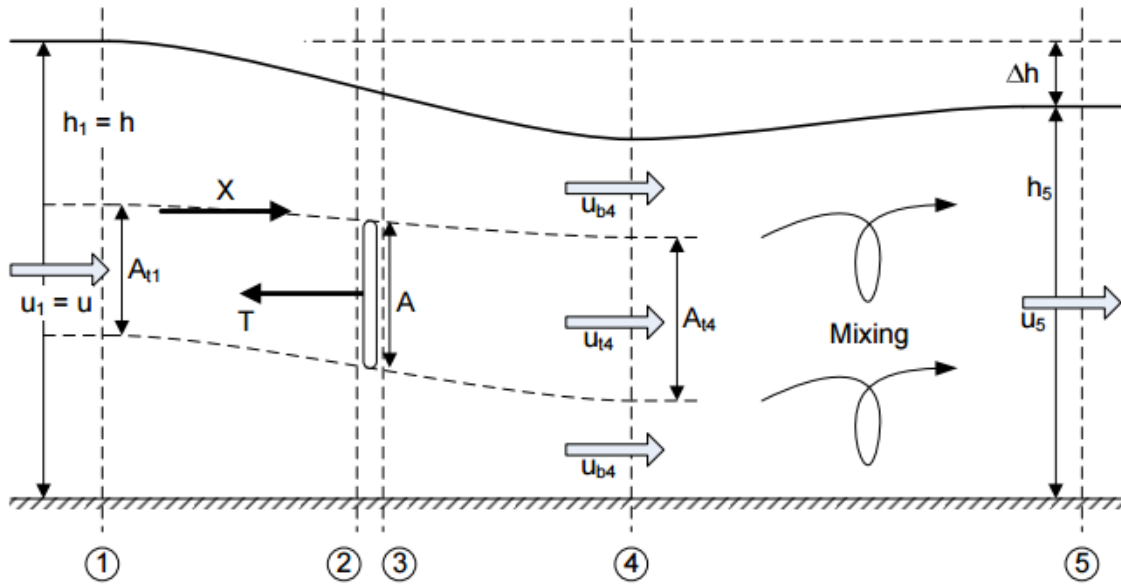


Figure 3-10: One dimensional linear momentum actuator disc theory in an open channel flow, originally shown in Houlsby et al, 2008.

Houlsby et al (2008) assumed that at locations 1, 4 and 5, shown in Figure 3-10, the pressure is treated as hydrostatic. The only pressure drop occurs across the rotor plane, resulting in a head drop. Using Houlsby et al (2008) application of LMADT in an open channel, the head drop  $\Delta h$  can be determined by solving:

$$\frac{1}{2} \left( \frac{\Delta h}{h} \right)^3 - \frac{3}{2} \left( \frac{\Delta h}{h} \right)^2 + \left( 1 - F_r^2 + \frac{C_T B F_r^2}{2} \right) \frac{\Delta h}{h} - \frac{C_T B F_r^2}{2} = 0 \quad (3.28)$$

where  $h$  is the channel depth,  $Fr$  is the Froude number,  $C_T$  is the thrust coefficient and  $B$  is the blockage ratio. Based on the parameters of the model, the expected head drop across the individual devices is 0.051m. The results in Figure 3-11 show the head drop across the three rows of devices.

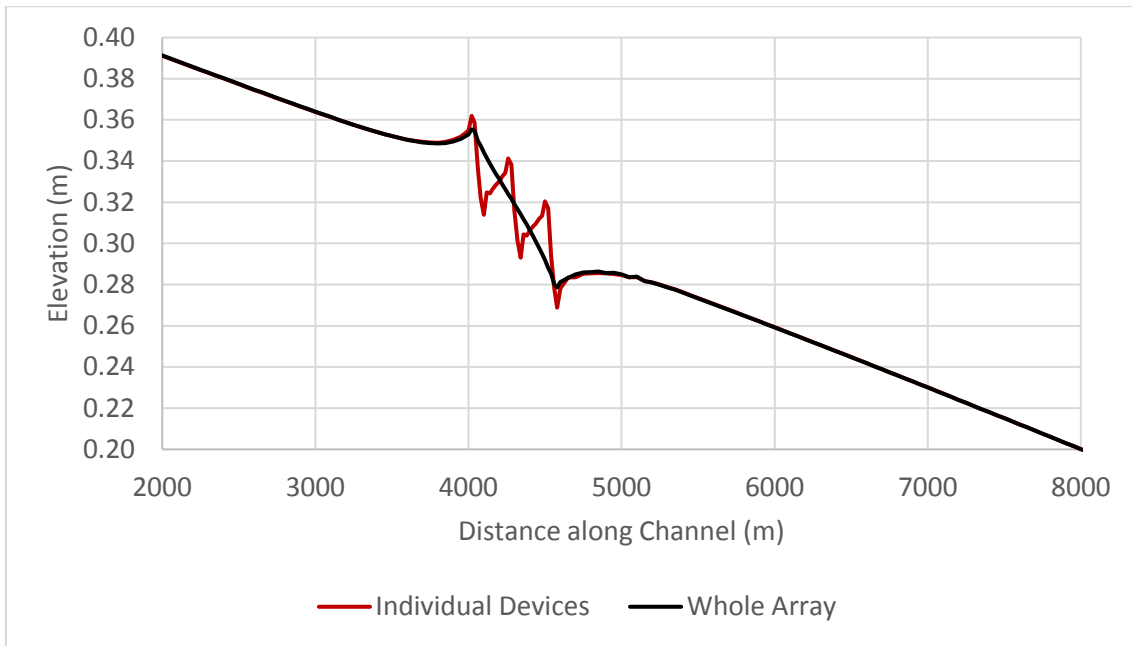


Figure 3-11: Free surface elevation (m) showing the head drop across tidal array, down centre line of channel (m).

It can be seen that there is head drop of 0.048m across the first row, a 0.048m drop across the second and a 0.051m drop across the last row. This shows a good relationship with theoretical values. However, this can only be applied to individual turbines or rows of devices. It cannot be applied to the whole array. The total head drop across the whole array is 7.3 cm compared to 9.4 cm after three devices, meaning the whole array is underestimating head reduction. Based on the results of the idealised channel model, the tidal turbines will be represented as individual devices for the remainder of this study.

### 3.5 Summary

The parameterisation of the influence of tidal turbines on the hydrodynamic flow has been tested in a depth averaged idealised channel model, using the hydrodynamic software package TELEMAC2D. The mesh is discretised as an unstructured mesh. To ensure a uniform force distribution, the area surrounding the turbine location is discretised with a regular mesh nested within the channel mesh. To provide a comparison a 10 MW array has been modelled as nine individual devices and also collectively as a single array. The performance of the parameterisation has been validated using linear momentum actuator disk theory. Modelling the array as nine individual devices has shown good agreement with theory, whilst modelling the whole array over-estimates the velocity reduction

and under predicts the head drop. As a result of this work, the parameterisation of tidal turbines using the Plew and Stevens (2013) method is adopted for the remainder of this study and the turbines will be represented as individual devices in areas within a regular mesh.

# Chapter 4

## Modelling the hydrodynamic and morphological impacts of a tidal stream development: Case Study of Ramsey Sound, UK

### 4.1 Introduction

The UK tidal stream industry has seen large growth in recent years (RenewableUK, 2015). The number of pre-commercial scale devices currently being tested at test facilities, such as the European Marine Energy Centre (EMEC) in Orkney, reflects this development. However, the ability to commercialise this technology remains a challenge. Even the booming UK wind industry still faces challenges. Numerous Round 3 offshore wind developments were halted on grounds of environmental impacts and the tidal industry is likely to prove no exception. Round 3 sites are third and latest set of lease sites designated by the UK Government that are permissible for development. They reflect the current state of the offshore wind industry, utilising the most state-of-the-art technology and best practices in the UK. The Argyll Array wind farm, near the Isle of Tiree in Scotland, was halted due to significant presence of basking

sharks, whose movements in the area required greater understanding (Scottish Power Renewables, 2013). Phase 2 of the London Array wind farm, situated near the mouth of the Thames Estuary in the Southern North Sea, was halted as it could not yet demonstrate that additional turbines would not affect the habitat of Red Throated Divers, a designated Special Protected Area (London Array, 2014). Despite numerous proposed array scale projects, some still fall to monetary barriers (reNEWS, 2014), and those that pass this barrier face an increasing challenge to show that their environmental impacts will be minimal. Unlike the wind industry, where physical effects of wind turbines have been catalogued through deployment of thousands of turbines, the tidal industry lacks these array-scale quantitative data. The MeyGen development in Orkney, which has started its Phase 1 of development consisting of eighty-six 1MW turbines, will be the first to provide such datasets. The first turbines are expected to be deployed by October 2016 (Meygen, 2015).

It is incorrect to say the likely impacts are unknown; it is more a case of understanding the scale of the impacts and their relative significance. Research studies have demonstrated how individual turbines and array scale developments will potentially alter the ecological environment (e.g. Shields et al., 2009; Shields et al., 2011; Miller et al., 2013). In summary, a tidal turbine decreases the near field current flow directly in its wake through energy extraction and the drag caused by the physical structure. The turbine may also affect the far field hydrodynamics, altering the spatial variability of turbulence. The likely consequence of this interaction is alteration to bed characteristics, sediment transport regimes and suspended sediment concentrations. As bed shear stress is proportional to the velocity squared, the seabed is sensitive to changes in the current flow. Environmental monitoring of the MCT SeaGen device, in Strangford Loch, concluded that it can “operate with no likely significant impacts on the marine environment” (Keenan et al., 2011). However, it is unlikely that the effects of a single device will be representative at array scale.

#### 4.1.1 Ramsey Sound

A number of sites around the UK are being considered for development, one of which is the Ramsey Sound, Southwest Wales, where flows are accelerated in a channel between Ramsey Island and the mainland. In 2011, Tidal Energy Ltd

(TEL) was given consent to test a prototype of their DeltaStream device in Ramsey Sound. Figure 4-1 shows the constructed prototype on the quayside prior to deployment. The prototype is full scale but only consists of a single 400 kW rotor mounted on the support structure. The triangular gravity base is 36m wide. The device was deployed for testing in December 2015 (Tidal Energy Ltd, 2015).



Figure 4-1: Constructed 400kW full scale prototype Tidal Energy Ltd DeltaStream device.

Following successful testing, TEL is intending to develop a 10MW demonstration array just north of the Sound at St David's Head. The 10MW array will consist of nine devices, each with three rotors mounted on the nine individual support structures, as shown in Figure 3-3. Figure 4-2 shows the boundaries of the lease sites overlaying the bathymetry. The complex bathymetry of Ramsey Sound includes a deep trench (~70m) running north-south, a rocky reef called the Bitches extending from Ramsey Island into the Sound and a semi-submerged rock pinnacle called Horse Rock, approximately 50m in diameter. To the west of Ramsey Island are islets known as the Bishop & Clerks. Within the St David's lease site, depths vary between 30-42m CD. The tidal range at the site varies by 5m with a peak spring velocities of 3m/s. Waves are predominantly from the south-west with wave heights of 4-5m. The seabed consists of bedrock, gravel and coarse sand (Tidal Energy Ltd, 2012).

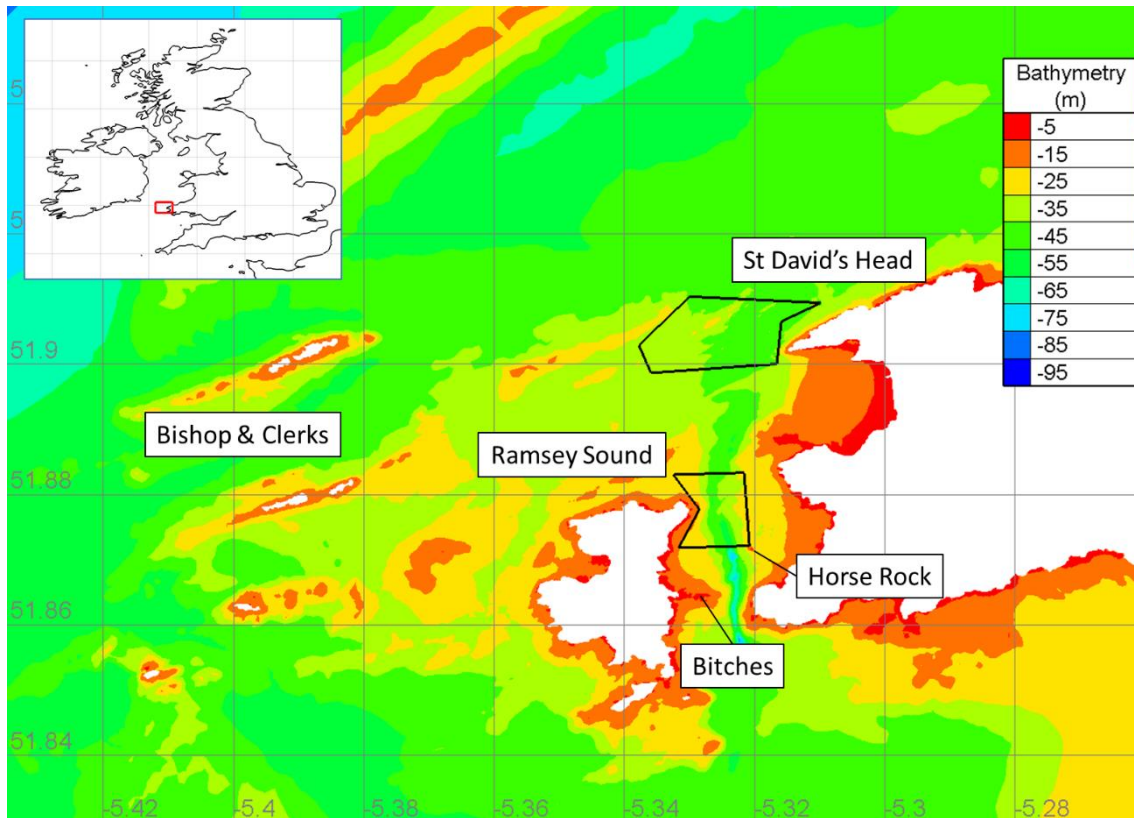


Figure 4-2: Location of initial test site (bottom) and 10MW lease site (top), in red overlaying bathymetry.

Previous work around tidal energy at Ramsey Sound has focused on characterisation of the wider resource through field measurements (Fairley et al., 2013). A detailed assessment of velocities through Ramsey Sound focused on the impact of Horse Rock and the likely environment the single prototype would experience (Evans et al., 2015). It showed that the local bathymetry significantly influences the local velocities causing a velocity reduction in the wake of Horse Rock. This introduces a source of turbulence and areas of vertical tidal flows resulting in a complex vertical velocity profile that may not be ideal for power production from a single tidal turbine in Ramsey Sound. Previous numerical models have included Ramsey Sound as part of a wider numerical model of the Irish Sea. In the Lewis et al. (2015) model the resolution is 278m at its finest meaning many of the islands and key bathymetric features are missing because they are smaller than the mesh elements. In Walkington & Burrows (2009) the tidal turbines neglect the drag effect of the support structure. A specific model of Ramsey Sound was presented by Fairley et al. (2011). However, the focus of the model was power potential and does not include any tidal turbines. There are presently no studies with sufficient resolution to model the dominant bathymetric



features or any studies looking at how the local hydrodynamics and morphodynamics will alter with the presence of tidal turbines at St David's Head.

This study investigates how a 10 MW tidal array, situated off St David's Head, influences local hydrodynamics using a high-resolution depth averaged numerical model. The aim is to determine the spatial extent of hydrodynamic change around Ramsey Sound and the potential morphological change.

## 4.2 Methodology

### 4.2.1 Numerical model

A high-resolution depth-averaged model of the Pembrokeshire coast was built using an unstructured triangular mesh, with the hydrodynamic software TELEMAC2D (v7p1). The model domain extends between 50.1°N – 53.2°N and 2.6°W – 7.6°W and is shown in Figure 4-3.

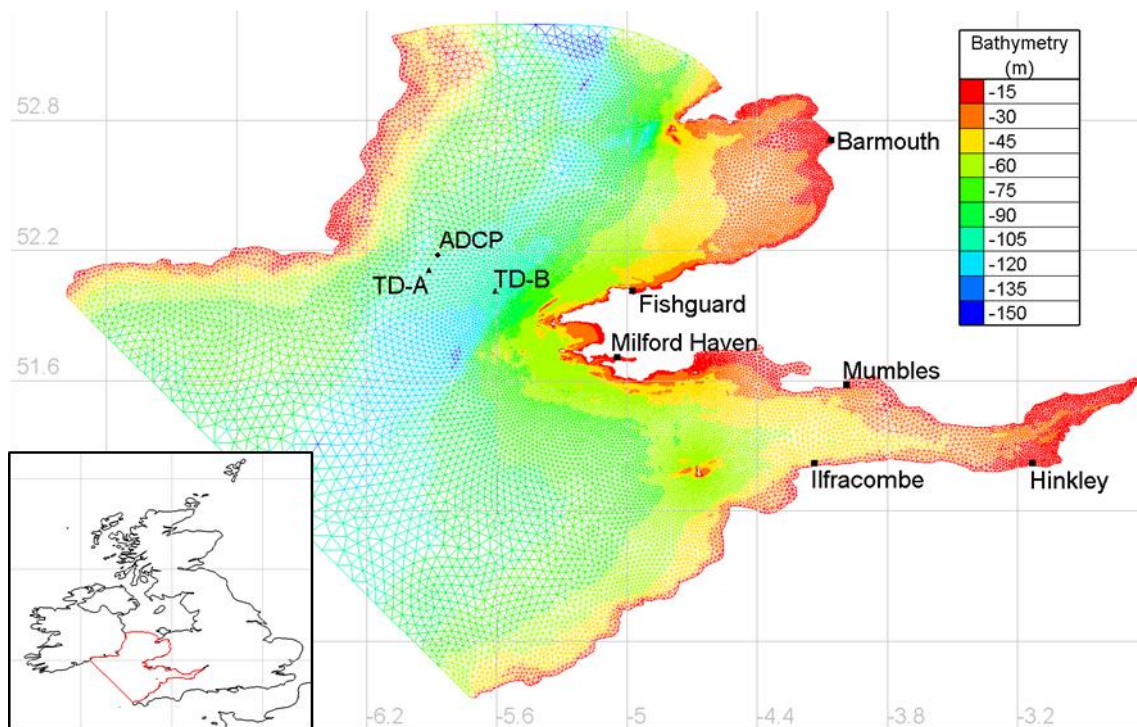


Figure 4-3: Model computational domain with the locations of six tide gauges, two tidal diamonds and one bottom mounted ADCP used for validation.

The unstructured mesh was discretized with 138,378 nodes and 271,676 elements. The mesh has a resolution of 10km around the open boundary, reducing to ~2km along the coastline. Along the Pembrokeshire coastline, the resolution increases to ~500m. In areas of interest, such as Ramsey Sound and

Stroma Sound, the resolution increases further to 50m. Around areas of key bathymetric influence within the Sound, such as Horse Rock and the Bitches, the resolution is refined further, to ~10m.

Bathymetry of the area was sourced from the Department for Environment, Food & Rural Affairs UKSeaMap 2010 (McBreen & JNCC, 2011) and was provided by the Centre for Environment, Fisheries and Aquaculture Sciences. The resolution of the bathymetry points from this dataset are 1 arc-second (~30m). However, as bathymetry strongly influences hydrodynamic characteristics through Ramsey Sound, a high resolution 2m and 4m bathymetry, from the UK Hydrographic Office, has also been applied around Ramsey Sound and the Bishop & Clerks.

The hydrodynamics are forced along the open boundaries using tidal constituents from the OSU TPXO European Shelf 1/30° regional model. The open boundaries are set far from the area of interest to reduce any dampening effect from the prescribed elevations. The Bristol Channel has been included due to its large range of tidal elevation and interaction with the Irish Sea due to the geometry of the channel and its quarter wave length resonance to the Atlantic tidal wave (Serhadlioglu, 2014). The model uses a k- $\epsilon$  turbulence model.

As discussed in Chapter 3, the Nikuradse law for bottom friction was used, with a constant value applied to the whole model domain. As the coefficient for bottom friction has a large impact on the magnitude of the modelled velocity field, it can be used to calibrate the model to give a better validation. A bottom friction coefficient  $k_s=0.01$  was initially chosen. However, after repeated runs, a value of  $k_s = 0.04$  was found to give the best validation, with the resulting validation shown in Section 4.3.

For the model run, a time step  $t_s = 1s$  was used. The Ramsey Sound model (138,378 nodes) was run on a single node with 16 processors, with an initial spin-up time of 5 days. After the spin-up period, the simulation was run for a model time  $t = 30$  days, taking approximately 1.5 days.

The TELEMAC steering file used for the Ramsey Sound case study is shown in Appendix D.

## 4.2.2 Modelling tidal turbines

The methodology used to represent the operation of the tidal turbines is presented by Plew & Stevens (2013), as outlined and discussed in Chapter 3. The turbines, used for this study, are based on the published figures of the TEL DeltaStream device (Tidal Energy Ltd, 2012). Each device consists of three 400kW rotors with a diameter of 15m. Each rotor reaches its rated power output at a current velocity of 2.25m/s. Based upon these parameters, the values for the constant power and thrust coefficients are  $C_{P0} = 0.29$  and  $C_{T0} = 0.8$ , and are used to create the power curve shown in Figure 3-4. A 10MW array contains 9 devices with 27 rotors. The hub height is 14m. It has been assumed that the rotor has a cut-in speed of 0.8m/s. For simplicity, the support structure has been modelled as a cylindrical monopile with a diameter of 2m and a drag coefficient  $C_D = 0.9$ .

Based on the findings in Chapter 3, a regular mesh using triangular elements is used in the area where turbines are modelled. The resolution of the regular mesh is 20m. The proposed 10 MW St David's Head tidal array consists of nine devices. Whilst details are yet to be finalised, the preferred option is to arrange the turbines in three rows of three situated to the east of the lease site due to the shallower depths (Tidal Energy Ltd, 2012). Figure 4-4 shows the location of each device with respect to the lease site boundary. The devices are situated in the shallowest depths east within the lease site.

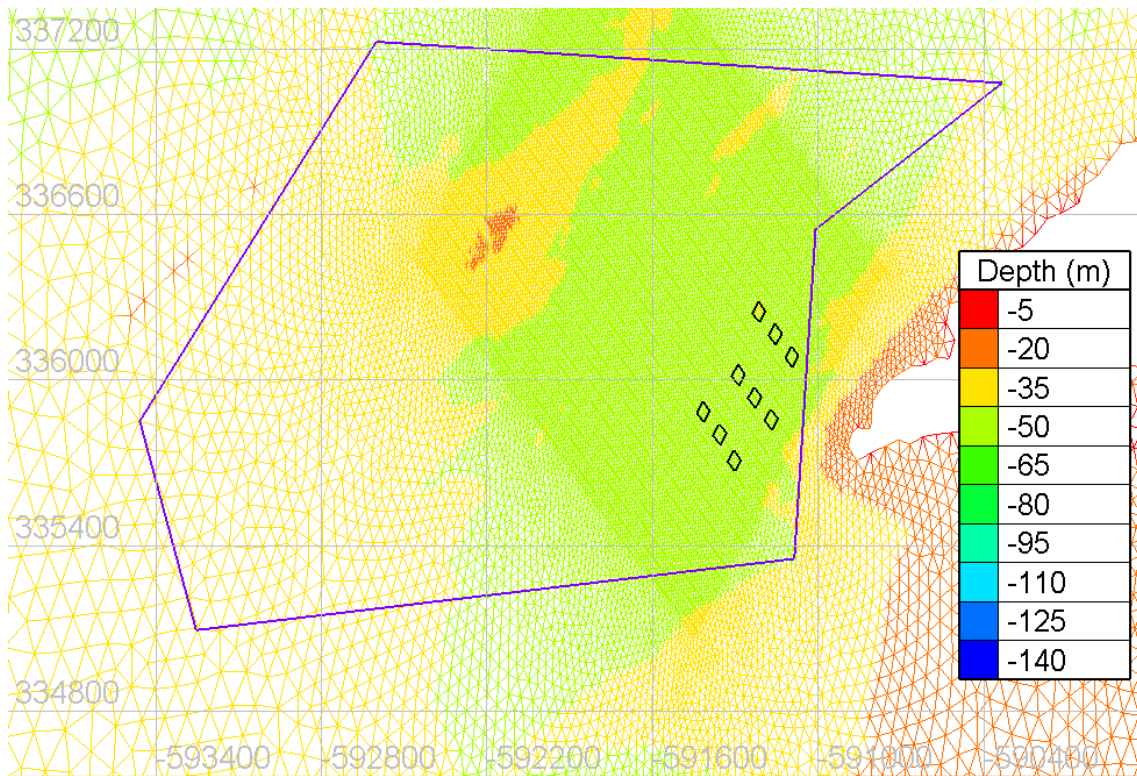


Figure 4-4: Array layout and location with respect to the lease site boundary (purple line), overlaying bathymetry.

### 4.3 Validation

Multiple sources of data have been used to provide a thorough validation of the model. Although the model is driven by prescribed elevations, meaning it is important to validate the elevations throughout the domain, the main influence of the tidal turbines is on the tidal velocities. It is also important to validate the tidal velocities alongside temporally concurrent tidal elevations. Validation data for tidal elevations are widely available. However, tidal velocity data is more limited. Bottom mounted acoustic doppler current profilers (ADCP) have become the standard for site investigations in the tidal industry as they provide direction and magnitude of velocities over the whole water column. Their downside is they only represent a single location and can be expensive to deploy. As a result, ADCP data are often closely guarded by tidal developers due to their sensitive commercial nature. Only one source of ADCP data could be acquired in the area of interest within the model domain, a boat mounted ADCP transect through Ramsey Sound. As such, tide gauge data used to validate the tidal elevations was sourced with a period of time encompassing the date and time of the transect. Tidal diamonds and a bottom mounted ADCP were also used to further

validate tidal velocities in other regions of the model. Along with tide gauge data, a harmonic analysis of the free surface was conducted to further validate tidal elevations throughout the model domain.

#### 4.3.1 Free Surface Elevations

Validation data have been obtained from the British Oceanographic Data Centre (BODC) for surface elevation at six tide gauges, whose locations are shown in Figure 4-3. The model was run for 30 days from 17/05/2012 00:00 to 16/06/2012 00:00. Comparisons of the modelled free surface elevation and observed tidal elevations, at Barmouth, Fishguard, Milford Haven, Mumbles, Ilfracombe and Hinkley, are shown in Figure 4-5.

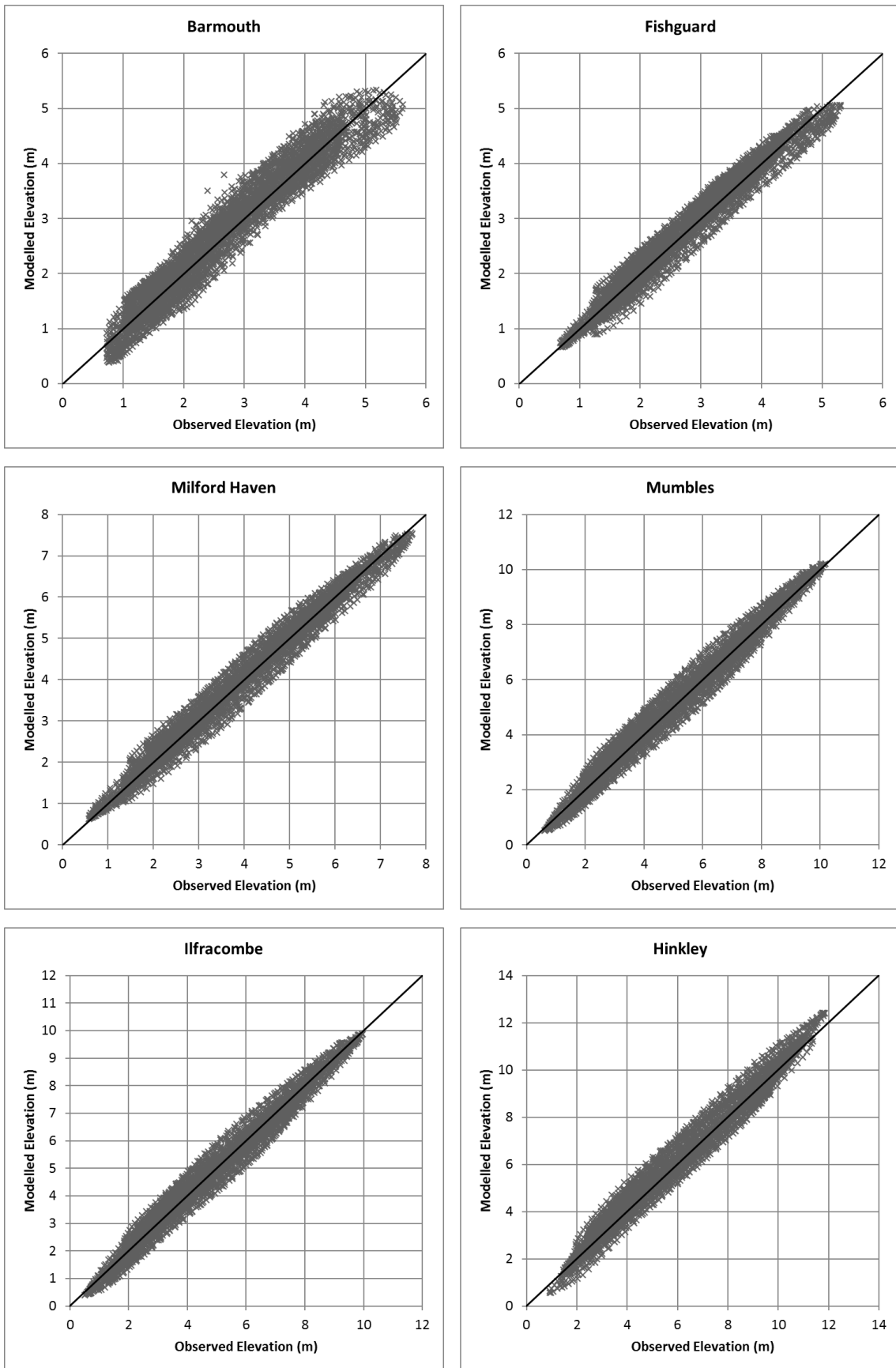


Figure 4-5: Comparison of modelled free surface elevation and observations from BODC tide gauges. Black line represents  $y=x$  relationship.

The scatter plots show good agreement for Fishguard, Milford Haven, Mumbles, Ilfracombe and Hinkley. A broader scattering is seen in Barmouth comparison due to a slight phase misalignment. This could be due to the Afon Mawddach estuary being clipped from the model to improve computation.

To validate the free surface elevations, three statistical quantities have been used: the coefficient of determination, the root mean squared error and the scatter index. The coefficient of determination,  $R^2$ , is the proportion of the variance explained by a linear regression model predicting the dependant variable from the independent variable as is defined as:

$$R^2 = 1 - \frac{\sum_i (y_i - \bar{y}_i)^2}{\sum_i (\hat{y}_i - \bar{y}_i)^2} \quad (4.1)$$

where  $y_i$  are the observed values,  $\bar{y}_i$  is the mean of the observed values and  $\hat{y}_i$  are the predicted values. The value of  $R^2$  ranges between 0 and 1, with 0 representing no correlation between predicted and observed values and 1 representing a perfect correlation. The root mean squared error (RMSE) is the standard deviation of error between the observed and predicted values and is defined as:

$$RMSE = \sqrt{\frac{1}{n} \sum_{i=1}^n (\hat{y}_i - y_i)^2} \quad (4.2)$$

where  $n$  is the total number of observations. The scatter index is RMSE normalised by the mean of the observations:

$$Scatter\ Index = \frac{RMSE}{\bar{y}_i} \times 100\% \quad (4.3)$$

The scatter index is widely used in the validation of wave models (van Nieuwkoop et al., 2013; Niclasen & Simonsen, 2007; Cox & Swail, 2001), meaning there is a wide source of literature for comparable values. However, there is no comparison for validating tide elevations. For the purpose of this study, a scatter index of less than 10% will be considered a good validation. Table 4-1 summarises the validation statistics of the six tide gauges.

Table 4-1: Validation statistics of the six tide gauges.

Tide Gauge	R <sup>2</sup>	RMSE (m)	Scatter Index (%)
Barmouth	0.940	0.296	10.99
Fishguard	0.967	0.196	7.18
Milford Haven	0.980	0.250	6.38
Mumbles	0.980	0.353	6.81
Ilfracombe	0.981	0.329	6.59
Hinkley	0.976	0.478	7.70

It can be seen from the validation statistics that model validates very well. The R<sup>2</sup> show a very strong correlation between the modelled and observed free surface, with an average of 0.971. It can be seen from the scatter index that all the tide gauges show good agreement, except for Barmouth, which is just outside the acceptable range.

## 4.3.2 Velocities

### 4.3.2.1 ADCP transect

The area of greatest interest within the model domain is St David's Head. The closest dataset that could be obtained for validation was a line transect through Ramsey Sound. Line transects, using a side mounted ADCP, were conducted to determine velocities within Ramsey Sound on behalf of the Low Carbon Research Institute Marine Consortium. Details of the survey methodology and results are published by Evans et al. (2015). The aim of the study was to investigate the influence of the rock pinnacle Horse Rock. As such, six transects in total were conducted, with three upstream of Horse Rock and three downstream. The transect obtained for validating this study was located approximately 400m north of Horse Rock and is shown in Figure 4-6.



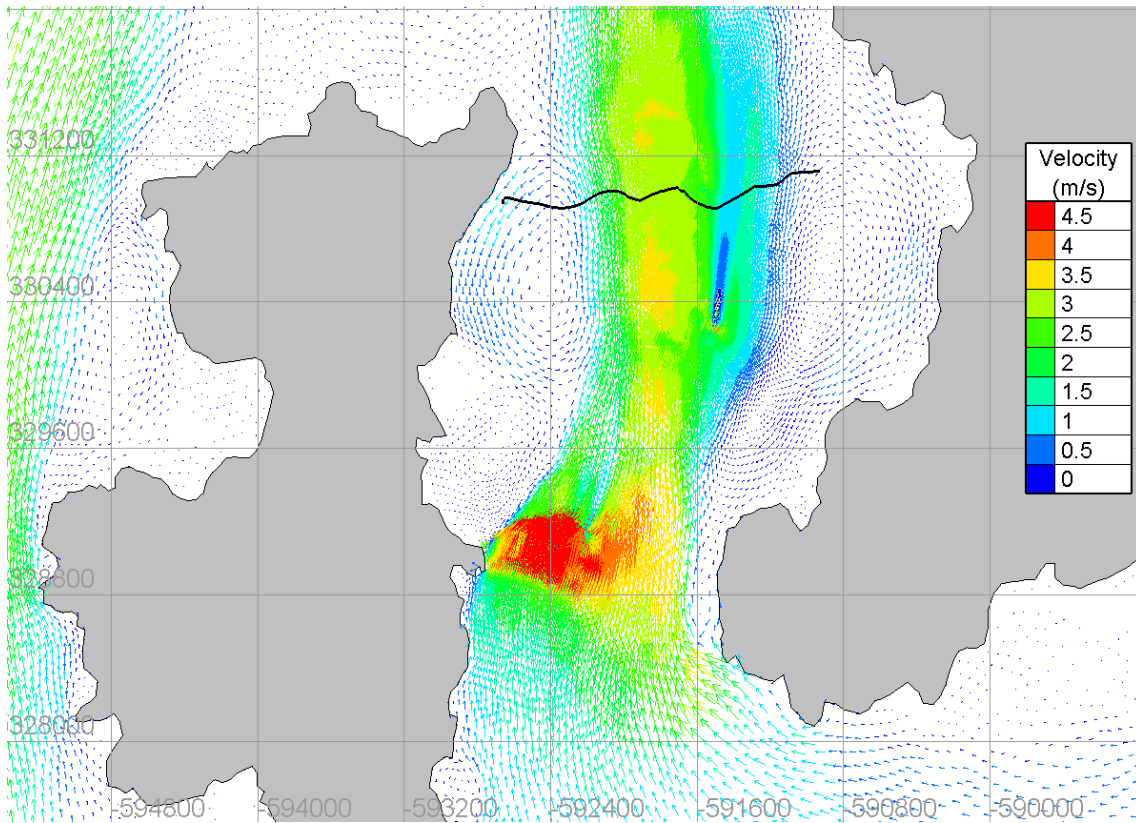


Figure 4-6: Location of ADCP transect with respect to the velocity modelled at the corresponding time step.

To compare the transect with the model results the ADCP record has been depth averaged. Figure 4-7 shows a comparison between the model and the transect.

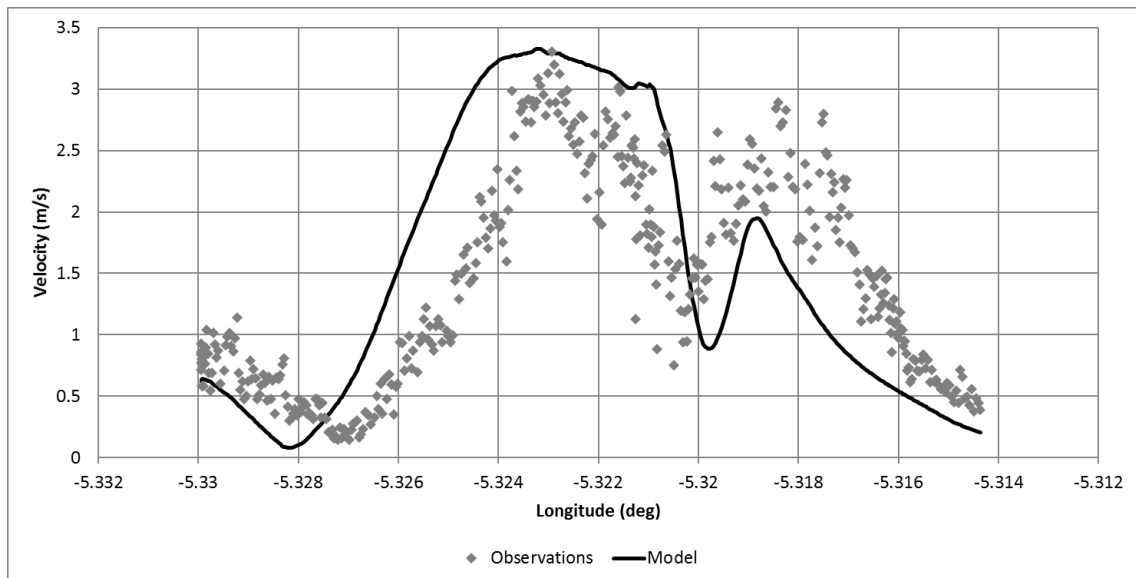


Figure 4-7: Line transect comparison of modelled and observed depth averaged tidal currents through Ramsey Sound.

The model does reproduce the peak velocity magnitude, of 3.3 m/s, through the centre of the Sound. Likewise, the velocity reduction in the wake of Horse Rock is visible, at the longitude  $-5.32^{\circ}$ . There are some discrepancies between the observed velocity profile and the model. The high velocities east of Horse Rock are under-predicted. It is expected that the model will not entirely match the ADCP transect. The 3D hydrodynamics through Ramsey Sound are strongly influenced by the local bathymetry meaning there are inherent limitations to a depth averaged model being able to accurately reproduce real 3D conditions. What is important for this study is the model reproduces the peak magnitude, which in this instance is correctly modelled.

#### 4.3.2.2 Bottom mounted ADCP

Along with the six tide gauges, the BODC provided a 30-day bottom mounted ADCP time series recorded between 17/05/2000 – 17/06/2000. The ADCP was located at  $52^{\circ}10.6N$   $5^{\circ}52.3W$  and is shown in Figure 4-3. The observed velocities have been depth averaged to compare against model results. Whilst the date of the ADCP record is the same month as the tide gauges and the model run, the ADCP was deployed two years earlier meaning a direct comparison of the time series cannot be achieved. However, the ADCP record length is sufficient to cover a full spring-neap cycle so a comparison of both the peak magnitude and direction is possible. Figure 4-8 shows the comparison of the observed and modelled depth averaged velocities at the location of the ADCP. It can be seen that the two time series show good agreement. The peak velocities for the ADCP is 1.43 m/s and 1.53 m/s for the flood and ebb respectively. The peak velocities from the model are 1.43 m/s and 1.58 m/s for the flood and ebb respectively.

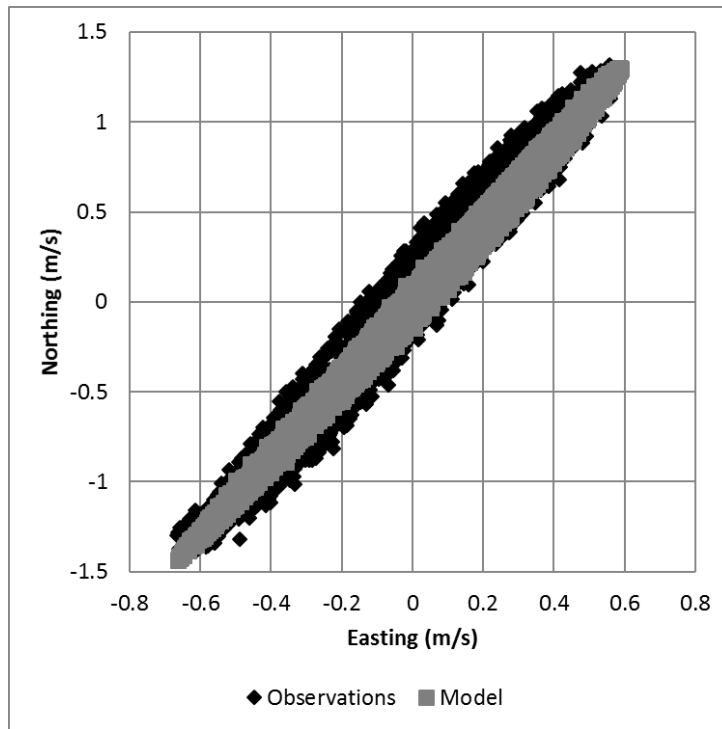


Figure 4-8: Comparison of observed and modelled depth averaged velocities situated at 52°10.6N 5°52.3W.

#### 4.3.2.3 Tidal diamonds

Velocities were further validated using tidal diamonds from United Kingdom Hydrographic Office (UKHO) Admiralty Chart 1121. The location of the two tidal diamonds are shown in Figure 4-3. Figure 4-9 shows the comparison between the modelled and observed tidal velocities and direction six hours either side of high water during a spring and neap cycle. High water is taken with respect to Milford Haven. The direction is that of the spring velocities.

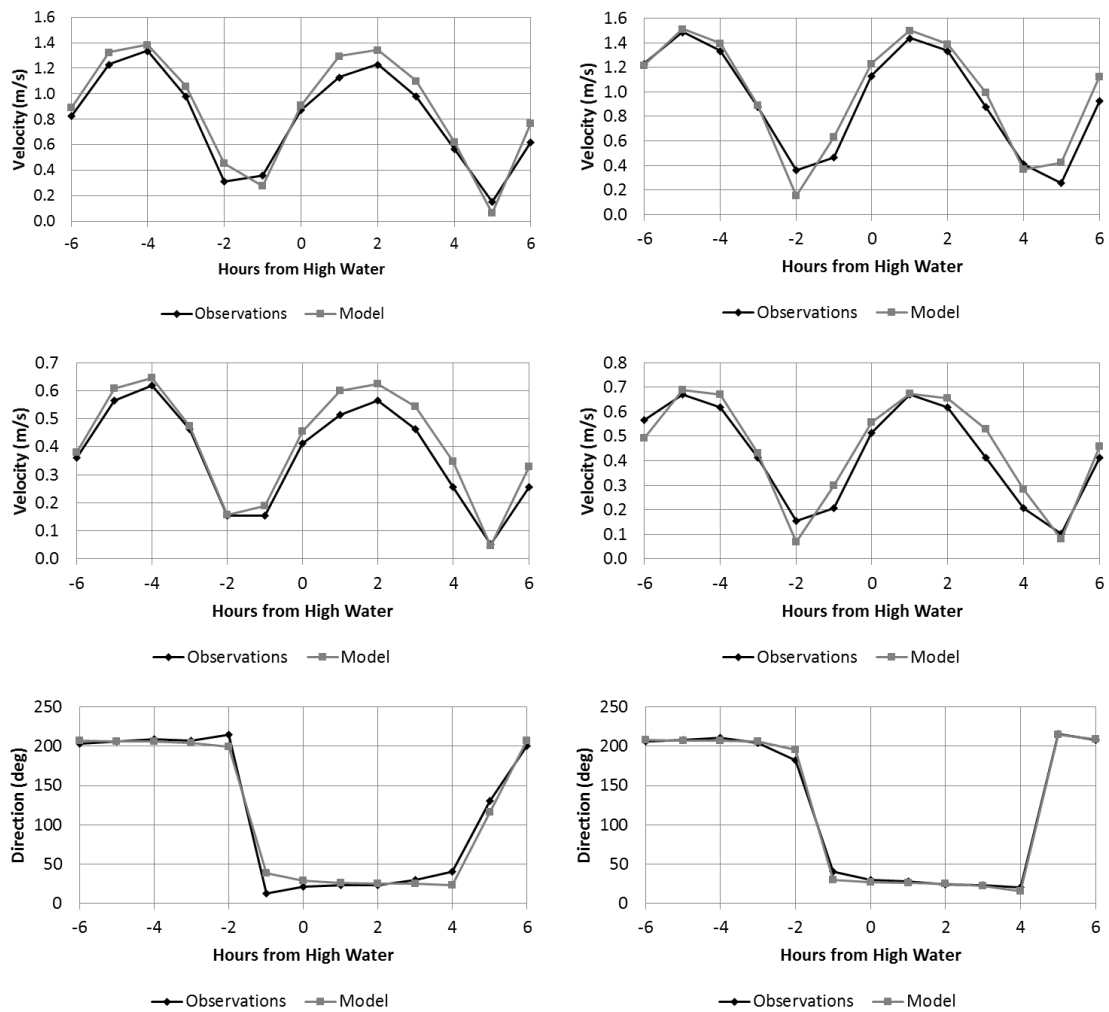


Figure 4-9: Comparison between modelled and observed velocities at spring (top), neap (middle) and direction of spring velocities (bottom) of two tidal diamonds from UKHO Admiralty Chart 1121 (a-left, b-right). High water is with respect to Milford Haven.

Results show good agreement between the model and the tidal diamonds. Table 4-2 shows the validation statistics of the tidal diamonds.

Table 4-2: Validation statistics of the tidal diamonds.

ADCP	Component	R <sup>2</sup>	RMSE	Scatter Index (%)
A	Direction	0.985	11.01 deg	9.42
	Spring	0.973	0.10 m/s	12.66
	Neap	0.976	0.05 m/s	14.25
B	Direction	0.997	5.17 deg	4.20
	Spring	0.945	0.12 m/s	12.57
	Neap	0.923	0.06 m/s	14.62

It can be seen from the coefficient of determination that there is a good correlation between the model and the observed tidal diamonds. The model does slightly over predict the tidal velocities, with an average percentage difference of 11.62% seen on the neap tide at tidal diamond 'A'. The quality of tidal diamond data is not always high (Bell & Carlin, 1998). Tidal diamond data is obtained over a twelve-hour period by a small boat with a current meter deployed to read off values at hourly intervals. Meteorological components are not removed from the readings. Due to the limited number of observations, tidal diamonds provide only a basic picture of the tidal conditions. Therefore, a very strong correlation between the model and the tidal diamonds is not necessarily desired.

### 4.3.3 Harmonic Analysis

The model was run for 30 days to provide a time series of sufficient length to permit a harmonic analysis which includes the dominant components. The dominant components are the M2 and S2 constituents. Table 4-3 and Table 4-4 show the comparison between harmonic constituents from the UKHO and the model for the M2 and S2 constituents at UK ports, whose locations are shown in Figure 4-10.

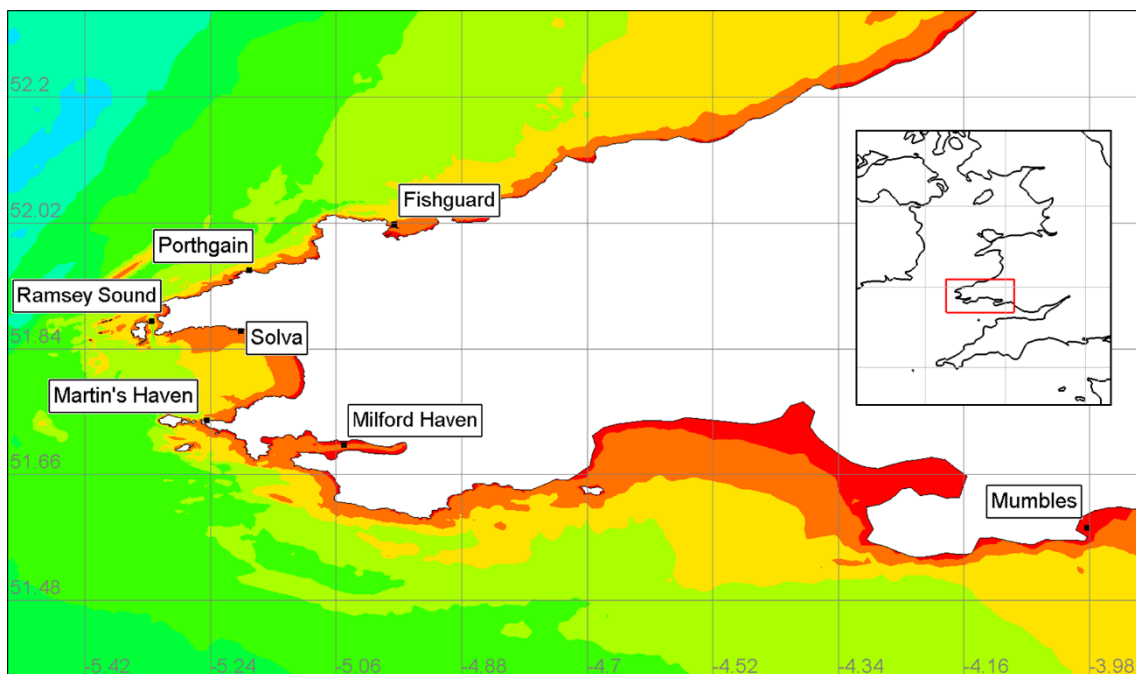


Figure 4-10: Location of the UK ports used for harmonic analysis.

Table 4-3: Comparison between observed and modelled M2 constituent

Port	M2					
	Observed	Model	Percentage	Observed	Model	Percentage
	Amplitude (m)	Amplitude (m)	Difference	Phase (deg)	Phase (deg)	Difference
Fishguard	1.35	1.34	-0.7%	207	206.9	-0.1%
Porthgain	1.33	1.39	4.5%	197	195.9	-0.6%
Ramsey Sound	1.46	1.47	0.7%	185	185.2	0.1%
Solva	1.89	1.89	0.0%	178	178.4	0.2%
Martin's Haven	1.84	1.86	1.1%	180	177.7	-1.3%
Milford Haven	2.22	2.22	-0.9%	173	171.9	-0.6%
Mumbles	3.18	3.19	0.3%	171	171.2	0.1%

Table 4-4: Comparison between observed and modelled S2 constituent

Port	S2					
	Observed	Model	Percentage	Observed	Model	Percentage
	Amplitude (m)	Amplitude (m)	Difference	Phase (deg)	Phase (deg)	Difference
Fishguard	0.53	0.51	-3.8	248	248.1	0.0
Porthgain	0.52	0.52	0.0	239	238.6	-0.2
Ramsey Sound	0.51	0.53	3.9	238	229.4	-3.6
Solva	0.75	0.68	-9.3	225	222.8	-1.0
Martin's Haven	0.68	0.67	-1.5	224	222.3	-0.8
Milford Haven	0.81	0.78	-3.7	217	216.8	-0.1
Mumbles	1.12	1.12	0.0	221	219.1	-0.9

Results of the harmonic analysis show that the M2 and S2 constituents are well validated for both amplitude and phase. The only discrepancy is with the S2 amplitude at Solva which is under-predicted. This could be due to the Solva inlet being clipped from the model domain to reduce computation run time. The validation results over the rest of the model domain show good agreement.

## 4.4 Results and Discussion

### 4.4.1 Array performance

The performance of the array has been assessed through the energy production. Results of the simulation show that over the spring-neap cycle the total output of the array is 2.15 GWh. This equates to 25.80 GWh per annum. The energy production is not uniform across the array. Figure 4-11 shows the array layout and the numbering convention of the devices. Devices 1, 2 and 3 represent row 1; devices 4, 5 and 6 represent row 2 and devices 7, 8 and 9 represent row 3.

Devices 1, 4 and 7 represent column 1; devices 2, 5 and 7 represent column 2 and devices 3, 6 and 9 represent column 3.

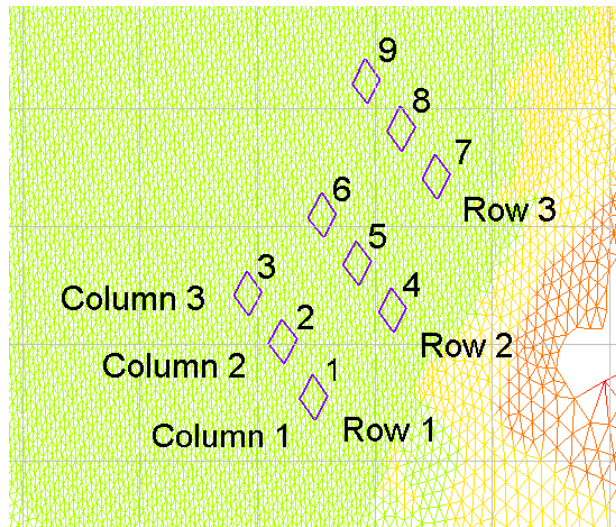


Figure 4-11: Device number convention.

Figure 4-12 shows the total energy production of each device with respect to their position within the array. It can be seen that some devices perform better than others.

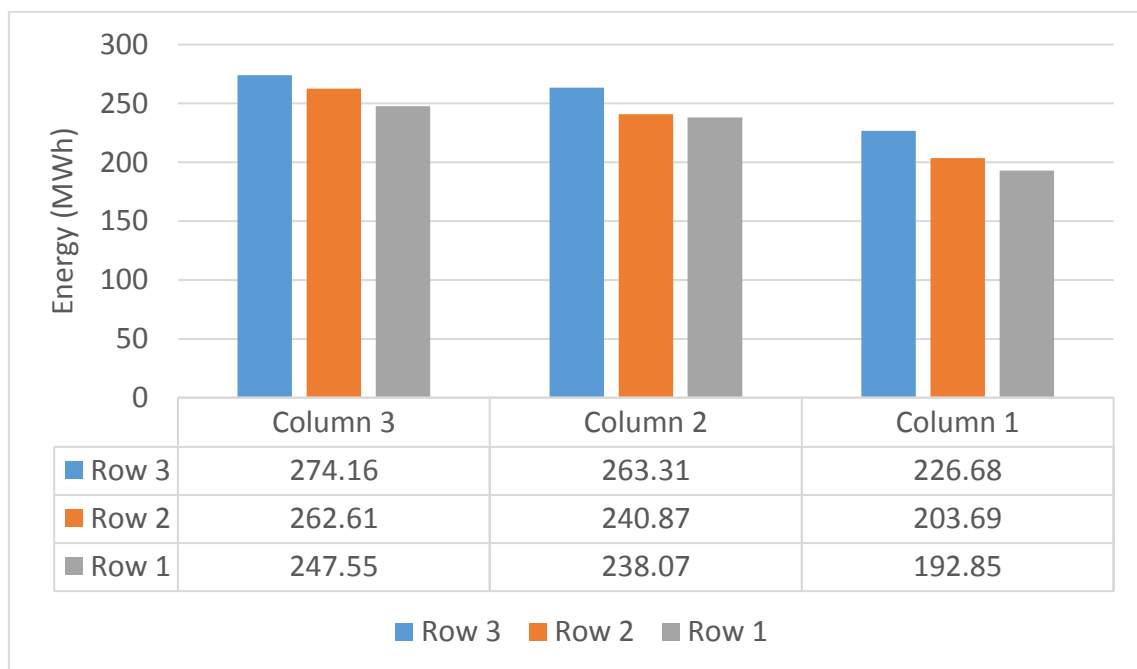


Figure 4-12: Total energy (MWh) produced over spring-neap cycle.

Figure 4-13 shows the power produced by Device 1 and 9 representing the smallest and largest producing devices, respectively.

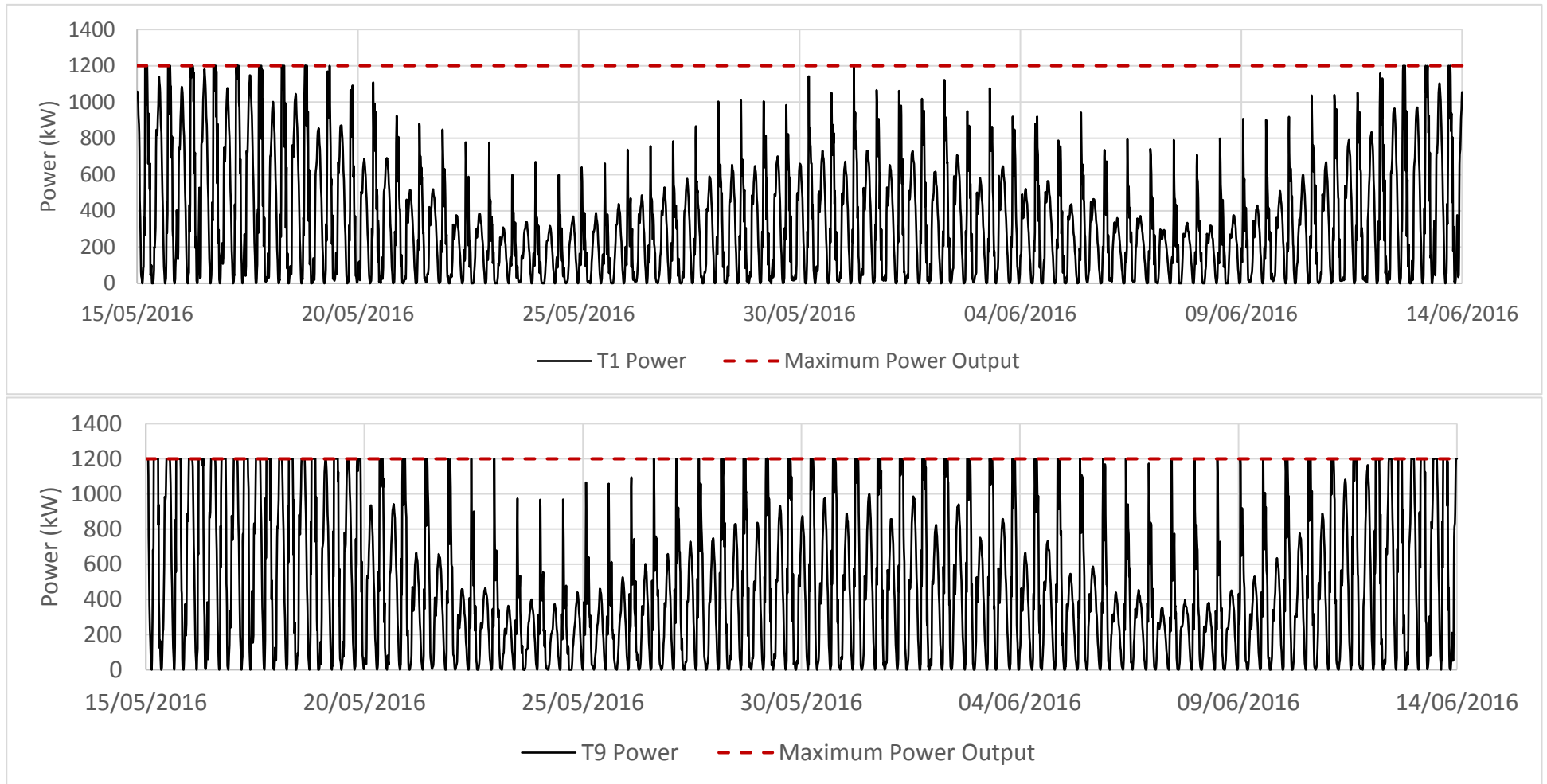


Figure 4-13: Power production from the Device 1 (top) and Device 9 (bottom) representing the smallest and largest producing devices, respectively, over the 30-day model run. Red dashed line represents the maximum instantaneous power production per device (1200 kW).



Device 9 reaches rated power regularly over the whole spring and neap cycles, whereas, Device 1 rarely reaches rated power. This is because the flow speed at this location rarely exceeds 2m/s, less than the rated speed. The strong tidal asymmetry between the flood and ebb cycle is clearly shown in the power output in Figure 4-13, with the ebb cycle producing a third less power than on the flood. The strong tidal asymmetry of the site is caused by the combination of the M2 tidal constituent and its higher harmonic the M4 constituent (Pingree & Griffiths, 1979).

#### 4.4.2 Influence of tidal array

The harmonic analysis used to validate the model was conducted on the reference run, without any turbines present. To assess the influence of the 10 MW tidal array, a harmonic analysis was conducted again, with the nine devices included. By comparing the two cases, it was possible to examine the spatial extent and magnitude of change to the principal M2 and S2 tidal constituents caused by the presence of the array. Figure 4-14 and Figure 4-15 show the changes to the M2 and S2 tidal velocity constituents, with the dashed lines representing contours of a 2% and 5% amplitude reduction.

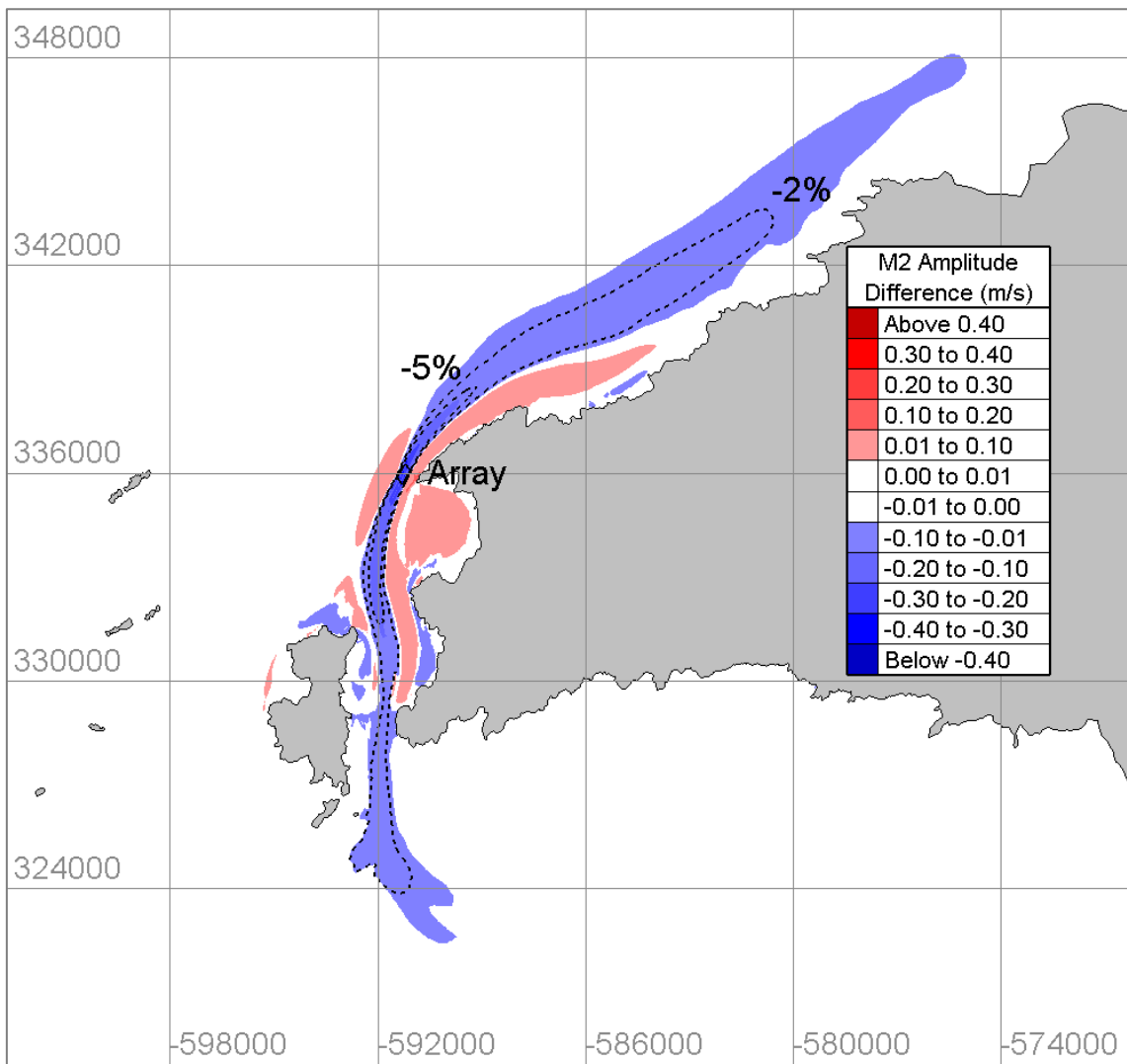


Figure 4-14: Changes to the M2 tidal velocity constituents. The dashed lines represent contours of a 2% and 5% amplitude reduction.

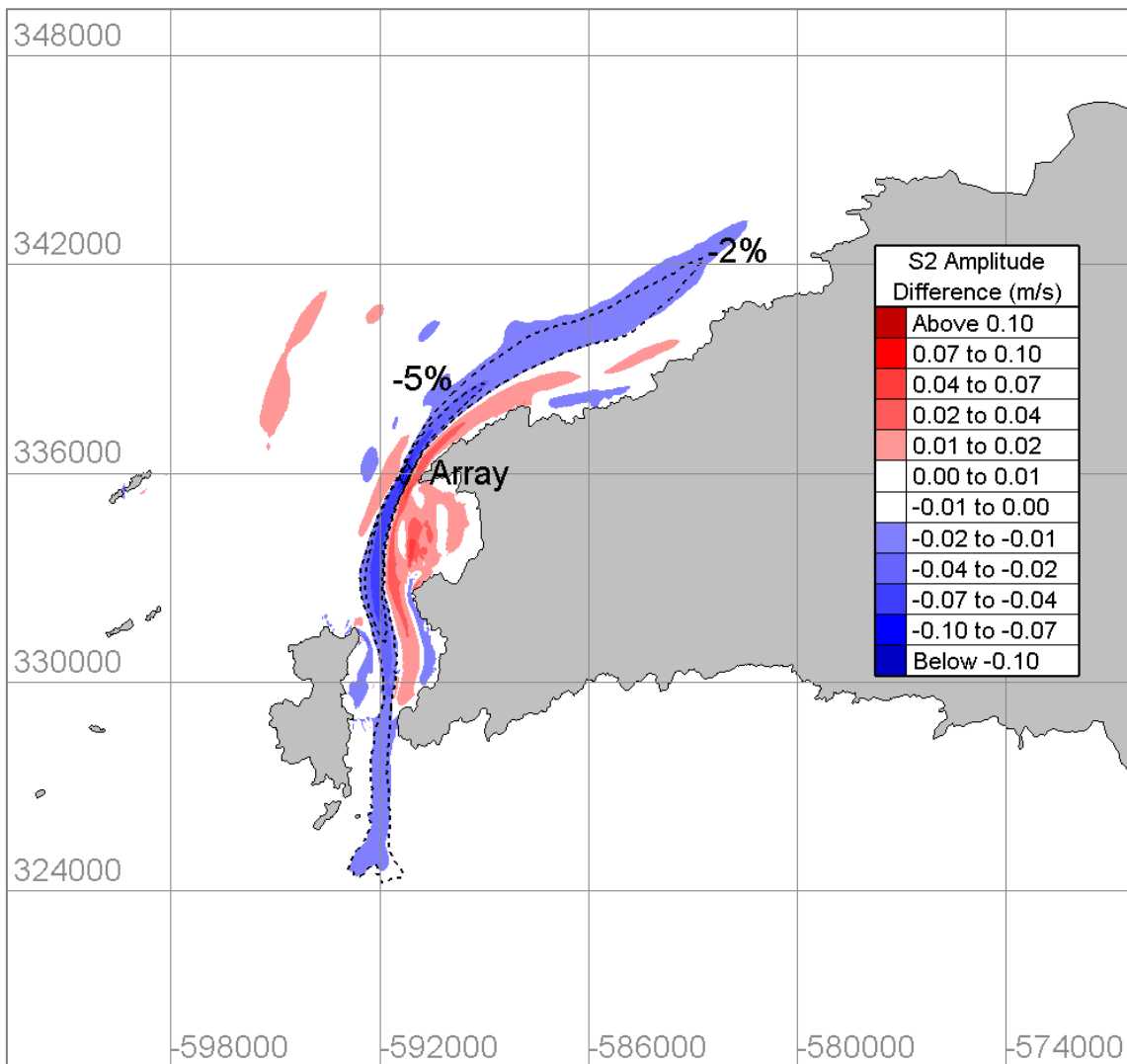


Figure 4-15: Changes to the S2 tidal velocity constituents. The dashed lines represent contours of a 2% and 5% amplitude reduction.

Using a 5% reduction contour, the reduction in the M2 amplitude in the wake of the array extends 3km north and 4.5km south. Using a 2% reduction contour, the influence of the array extends further to 13km north and 12km south. For the S2 amplitude, the wake extends 3.5km north and 5km south using a 5% reduction contour and extends 10.5km north and 12km south at 2%.

Results show that the largest reduction to the amplitude of the M2 tidal velocity constituent was at Device 9 with 0.41 m/s. This is equivalent to a 19.8% reduction. However, the largest percentage change occurred at Device 1 with a 0.36 m/s reduction, equivalent to 20.3%. For the S2 constituent, the largest percentage reduction also occurred at Device 1 with 18.9%. Table 4-5 summarises the amplitude and percentage differences at each device location.

Table 4-5: Changes to the M2 and S2 tidal velocity constituents at the location of the devices.

Device	M2 Velocity		S2 Velocity	
	Amplitude	Percentage	Amplitude	Percentage
	Difference (m/s)	Difference (%)	Difference (m/s)	Difference (%)
1	-0.36	-20.3	-0.09	-19.3
2	-0.36	-18.6	-0.09	-17.9
3	-0.35	-18.0	-0.10	-17.7
4	-0.23	-13.2	-0.05	-11.6
5	-0.33	-17.1	-0.09	-17.0
6	-0.37	-18.6	-0.10	-19.0
7	-0.30	-16.2	-0.07	-14.4
8	-0.36	-17.9	-0.09	-16.9
9	-0.41	-19.8	-0.11	-18.9

Black & Veatch (2005) used the term, ‘Significant Impact Factor’ (SIF), to quantify a percentage reduction in tidal velocity amplitude that could be extracted without significant economic or environmental impact. They suggest a value of 20%. The results gained in this study therefore, suggest that the size of the development is acceptable, with respect to the SIF, but the size of the development should not grow beyond 10MW without risking an impact larger than 20%. Determining the maximum size of array St David’s Head could accommodate without exceeding the 20% limit was beyond the scope of this study.

#### 4.4.3 Hydrodynamic far field effects

Ramsey Sound is a very turbulent environment due to its complex bathymetry. As a result, there are many sources of disturbance. The biggest source of disturbance is Ramsey Island itself, where the flow of water through the Sound re-joins the main flow around the west of the island. Robinson (1981) describes that when two separate streams of flow with different stagnation pressure or total head meet at a sharp headland it can lead to a discontinuity in velocity. This discontinuity is a vortex line that gradually diffuses into the surrounding water. It can be seen in the model that large eddy structures form off Ramsey Island on the flood cycle, propagating northwards along the coastline. Figure 4-16 shows a number of extracted streamlines (in red) that show the path of eddies as they propagate northwards.

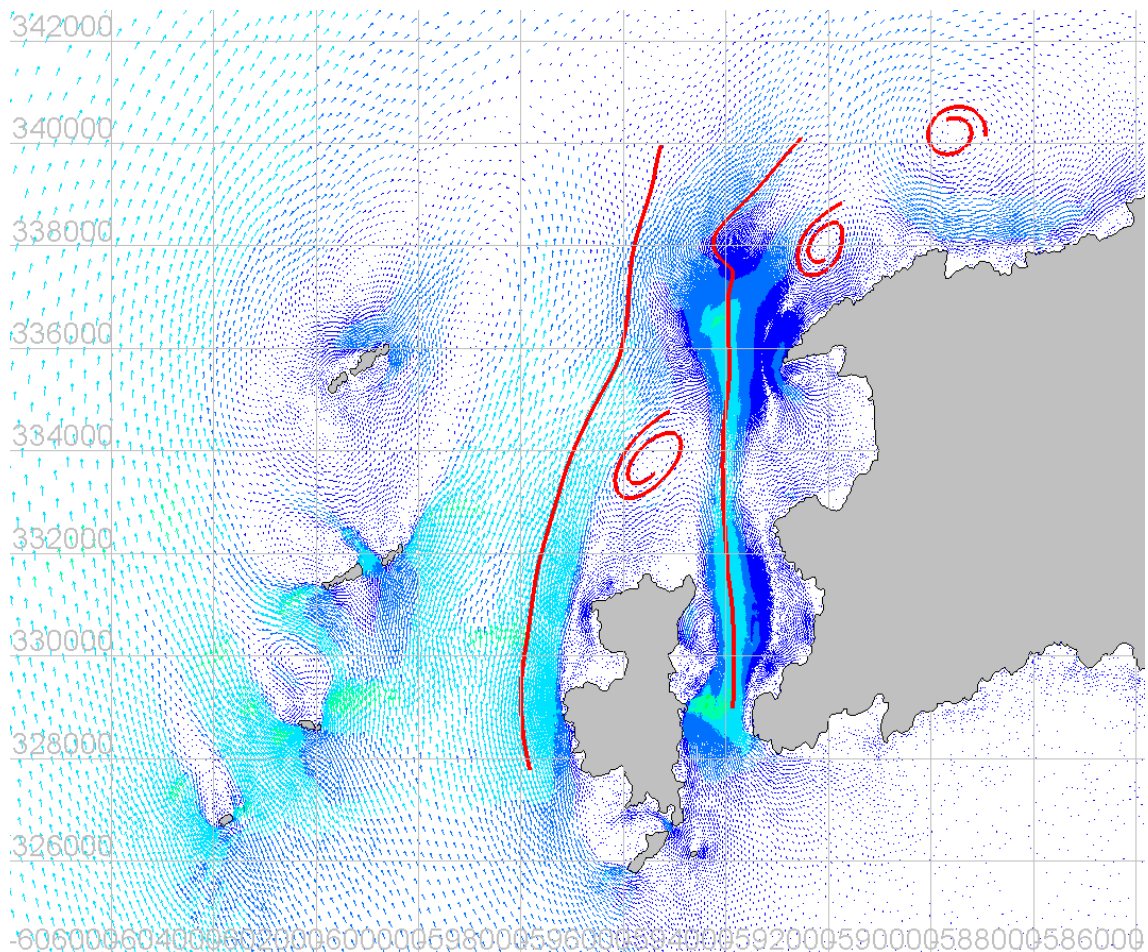


Figure 4-16: Extracted streamlines showing eddies propagating north during a flood tide.

When the influence of the tidal array is introduced, the wake of the array alters the production and propagation of the eddies, such that resulting change during the ebb flow influences the next cycle of eddy formation on the flood. This new disturbance then cyclically continues to alter the surrounding flow changing how other eddies propagate from other sources, such as the Bishop & Clerks, as shown in Figure 4-17. These disturbances can travel significant distances and can be used to characterise the far field effects. Figure 4-17 shows the difference in velocity between base case and turbine case over a single tidal cycle from low water to low water, overlaying the velocity vector field.

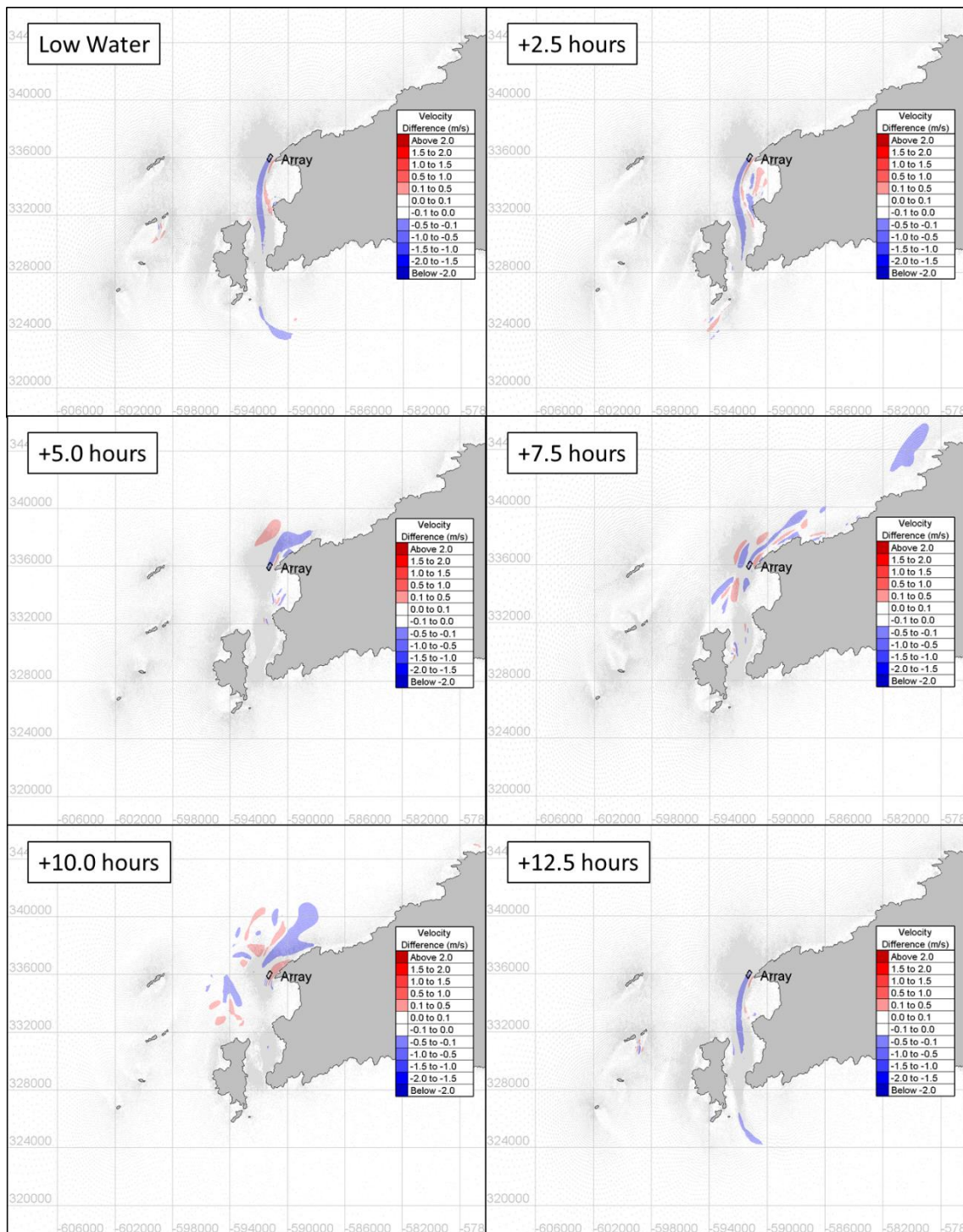


Figure 4-17: Difference in velocity (m/s) between base case and turbine case over a single tidal cycle from low water to low water.

It is important to note that the presence of the tidal array causes a small phase shift in the spatial and temporal production of the eddies that effects the surrounding area around Ramsey Sound. This is what leads to the large cyclic changes in the difference plots. However, the influence of the array and the resulting phase shift dissipates the further away from the location of the array and only lasts for a very short period. The phase difference does not get perpetually

worse throughout the model run. This means a zone of influence of the array can be calculated and used to determine the extent of the far field effects.

The zone of influence is calculated by the normalised range of difference. The range of difference is calculated by subtracting the magnitude of velocity at each node of the mesh of the turbine run from the magnitude of the velocity in the base case. This is done for each time step, producing a temporally and spatially varying difference between the two models. The range of difference is the difference between the maximum increase and decrease at each node over the whole model run. The range is then normalised to the maximum change to give a percentage figure. The range of difference does not represent the instantaneous velocity reduction due to the direct wake of the turbine array at any one time. Instead, it gives an indication of the total temporal and spatial extent of change. A value of 5% has been chosen to delineate the outer extent of the zone of influence, the same value chosen for determining the extent of the velocity wake of the tidal array in Section 3.4.3.

Figure 4-18 shows the range of difference caused by the 10MW array at St David's Head. It can be seen that the zone of influence of the tidal array extends 24km south west and 19km north east of the array.

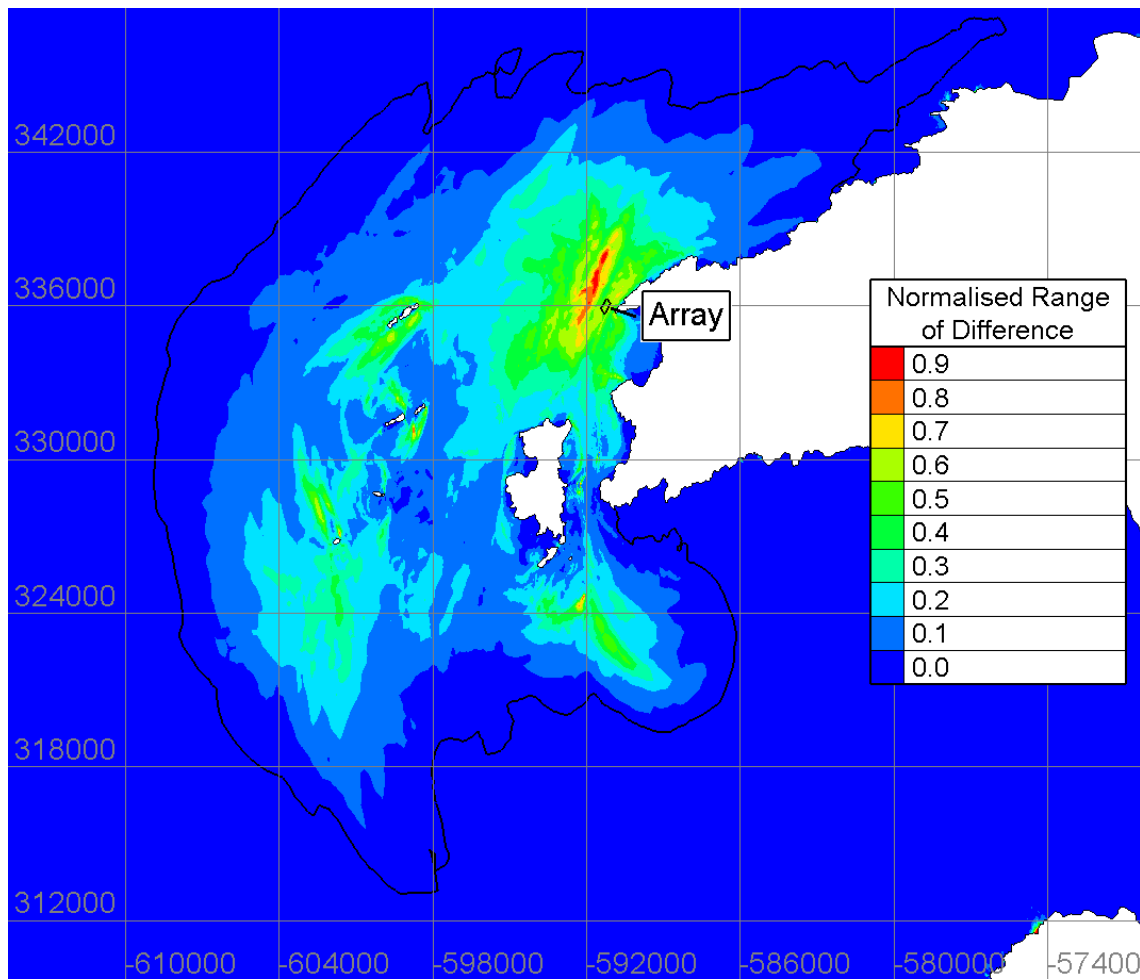


Figure 4-18: The zone of influence (black line), as characterised by the far field effects, of the 10 MW array at St David's Head.

#### 4.4.4 Morphological effects due to tidal velocities

The principal effects of a tidal turbine on the morphodynamics are alterations to bed characteristics, sediment transport regimes and suspended sediment concentrations. Where strong flows occur, sediments are re-suspended readily, deposition does not occur and the bed is often eroded down to hard strata with no laminae of overlying sediment. The wider area around Ramsey Sound is predominantly a mixture of sand and gravel, with a larger proportion of gravel. St Brides Bay consists of a mixture of fine sand and mud due to low tidal velocities that circulate just within the bay. Figure 4-19 shows the seabed sediments within the model domain based upon 1:250,000 digital sea-bed sediments map (DigSBS250), with the permission of the British Geological Survey.



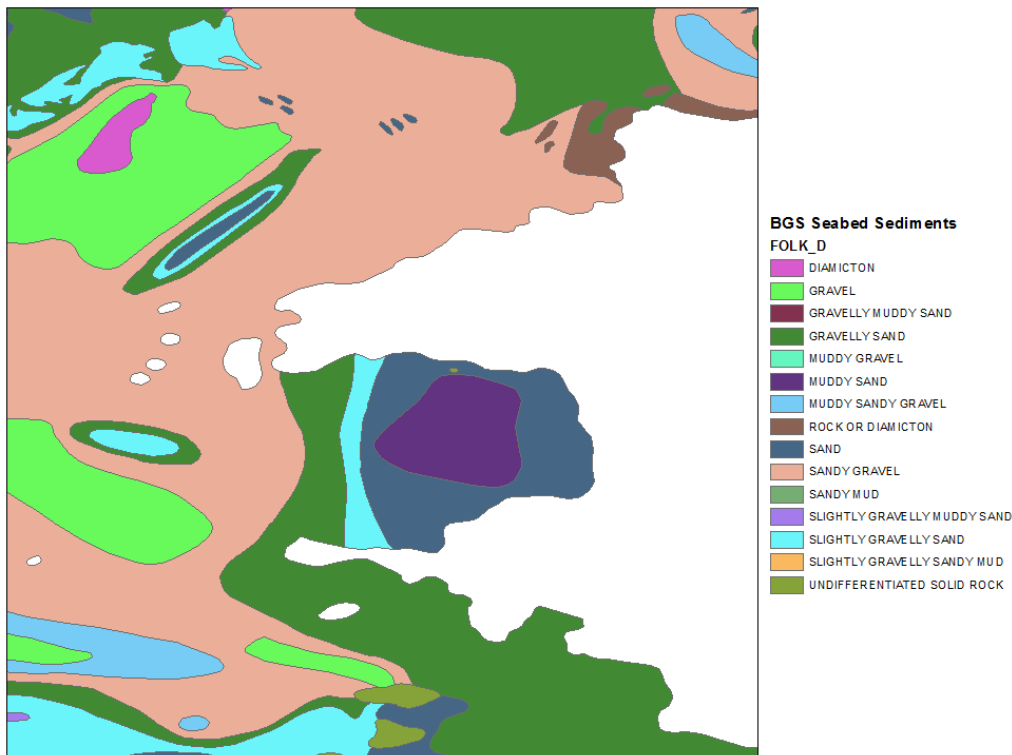


Figure 4-19: BGS Seabed Sediments using the Folk Classification. Reproduced with the permission of the British Geological Survey ©NERC. All rights Reserved.

The types of sediments found around Ramsey Sound suggests the area directly around a tidal array may not greatly change due to the absence of smaller sediments. Therefore, the far field effects shown in the model are potentially likely to have a greater impact on sediment dynamics in the more benign conditions away from the tidal array. It is important to note that this is a purely tidal hydrodynamic model with no atmospheric forcing or wave driven currents. The position and dispersion of eddies in this area would naturally vary if these additional interactions are included. A clearer indicator of potential impact is the change to bed shear stress as this is the parameter that drives the alterations to sediment dynamics. Bed shear stress is calculated as:

$$\tau = \rho C_d \|U\|U \quad (4.4)$$

where  $\rho$  is the density of seawater,  $C_d$  is the bottom drag coefficient and  $U$  is the velocity. For this study, a constant drag coefficient of 0.0025 was chosen representing a sand/gravel environment (Soulsby, 1997). This also matches the value used by Martin-Short et al (2015).

Figure 4-20 shows the change to the mean and maximum bed shear stress, respectively, over the 30-day simulation.

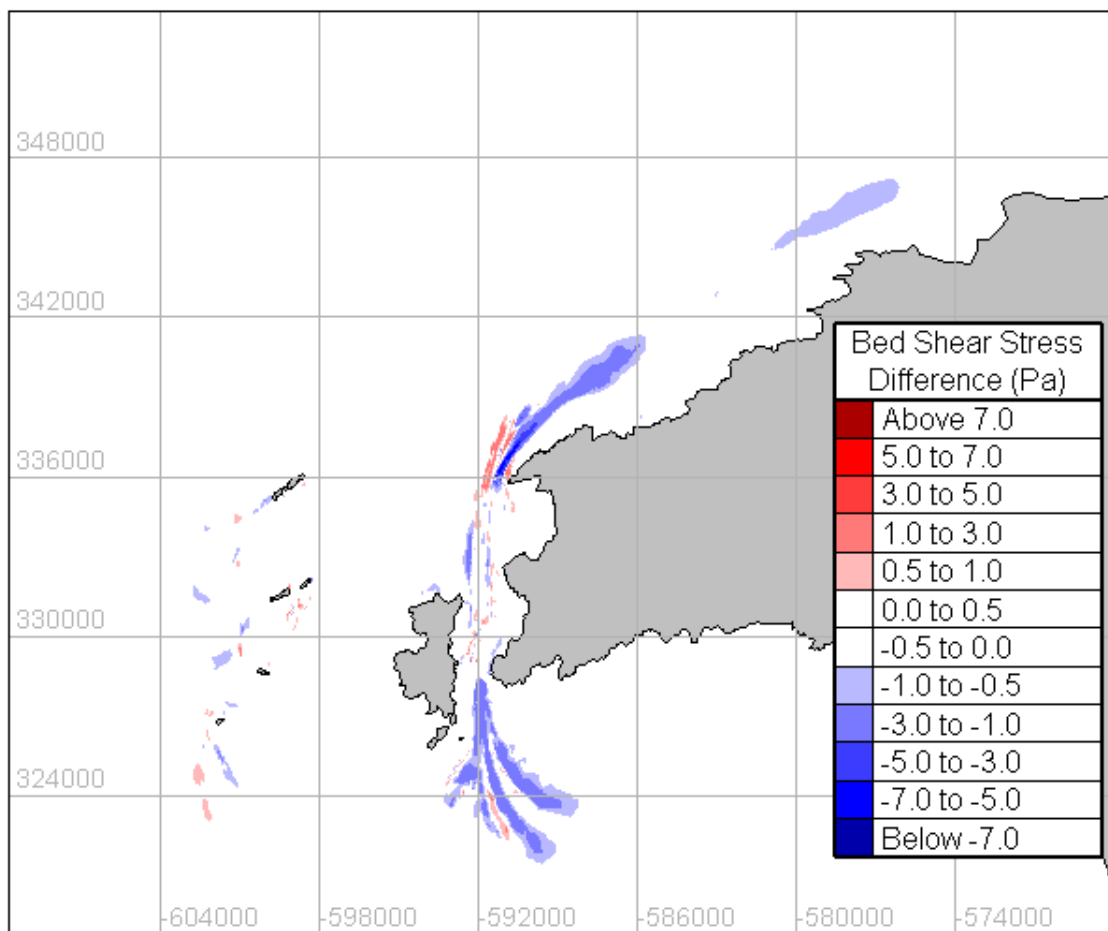
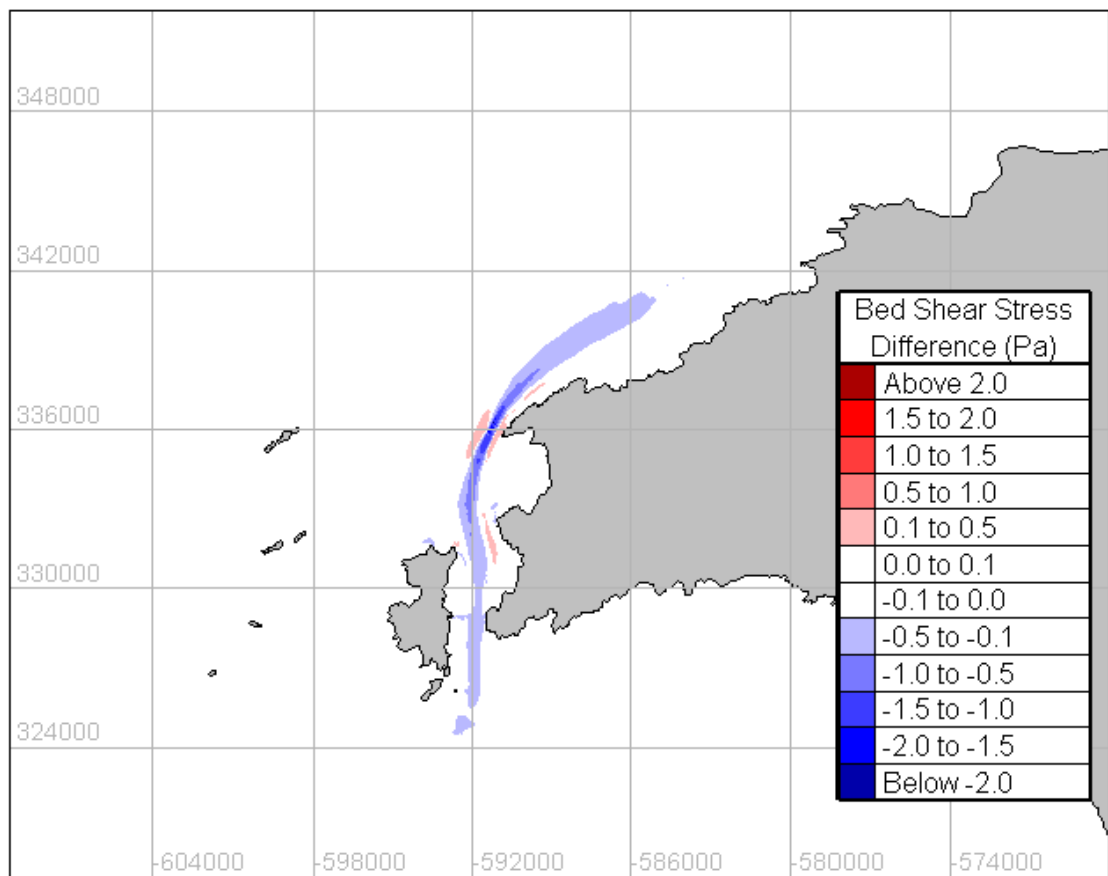


Figure 4-20: Change in mean (top) and maximum (bottom) bed shear stress.

The results show the spatial extent of the change due to the tidal array is more localised than Figure 4-18 suggests. The presence of the tidal array causes a local reduction in bed shear stress, with effects extending 16km from the site. Over the 30-day model run, the largest mean reduction is 2.3 Pa. The maximum reduction is 7.5 Pa. The resulting change in bed shear stress means that there will be an accumulation of sediment within the vicinity of the array where the bed shear stress has reduced. There will also be some scouring between the array and the mainland where the flow is accelerated by constriction due to the impedance of the array. Caution should be applied as the alterations to bed shear only show changes to skin friction. Further sediment modelling is required to determine the impact on bed feature evolutions and sediment transport.

A full sediment model, with bed evolution and suspended sediments, is difficult to achieve without appropriate sediment flux values at the boundary and sediment layers on the bed. However, Martin-Short et al. (2015) show that bed shear stress is a major controller of sediment movement making it possible to understand the sediment transport regime of the region and estimate the finest grain size that can be deposited. The threshold of motion for a particular grain size ( $d$ ) can be determined through the threshold shield parameter ( $\theta_c$ ):

$$\theta_c = \frac{\tau_{cr}}{g(\rho_s - \rho_f)d} \quad (4.5)$$

where  $\tau_{cr}$  is threshold shear stress,  $\rho_s$  is density of sediment and  $\rho_f$  is density of the fluid containing the sediment, in this case sea water. As there are insufficient data for the exact grain size distribution of the model domain, it is difficult to accurately calculate values of  $\theta_c$ . Instead, values for  $\tau_{cr}$  for a range of grain sizes have been taken from Martin-Short et al. (2015) and are shown in Table 4-6. These values were originally referenced by Berenbrock & Tranmer (2008).

Table 4-6: Mean threshold shear stress ( $\tau_{cr}$ ) conditions for the entrainment of various grain sizes (d) (from Berenbrock & Tranmer, 2008).

Sediment Class	Diameter (mm)	Threshold Shear Stress (Pa)	Critical velocity (m/s)
Coarse Gravel	16 - 32	12.2 - 26.0	2.16 - 3.19
Medium Gravel	8.0 - 16	5.7 - 12.2	1.49 - 2.16
Fine Gravel	2.0 - 8.0	1.26 - 5.70	0.70 - 1.49
Coarse Sand	0.5 - 2.0	0.27 - 1.26	0.325 - 0.7
Medium Sand	0.25 - 0.5	0.194 - 0.27	0.275 - 0.375

Figure 4-21 shows the predicted sediment distribution during the flood and ebb cycle of a peak spring tide. The colouration of each sediment class has been scaled to the values of  $\tau_{cr}$  in Table 4-6. The maps show broad agreement with the sediment mix detailed in the British Geological Survey (BGS) DigSBS250 map.

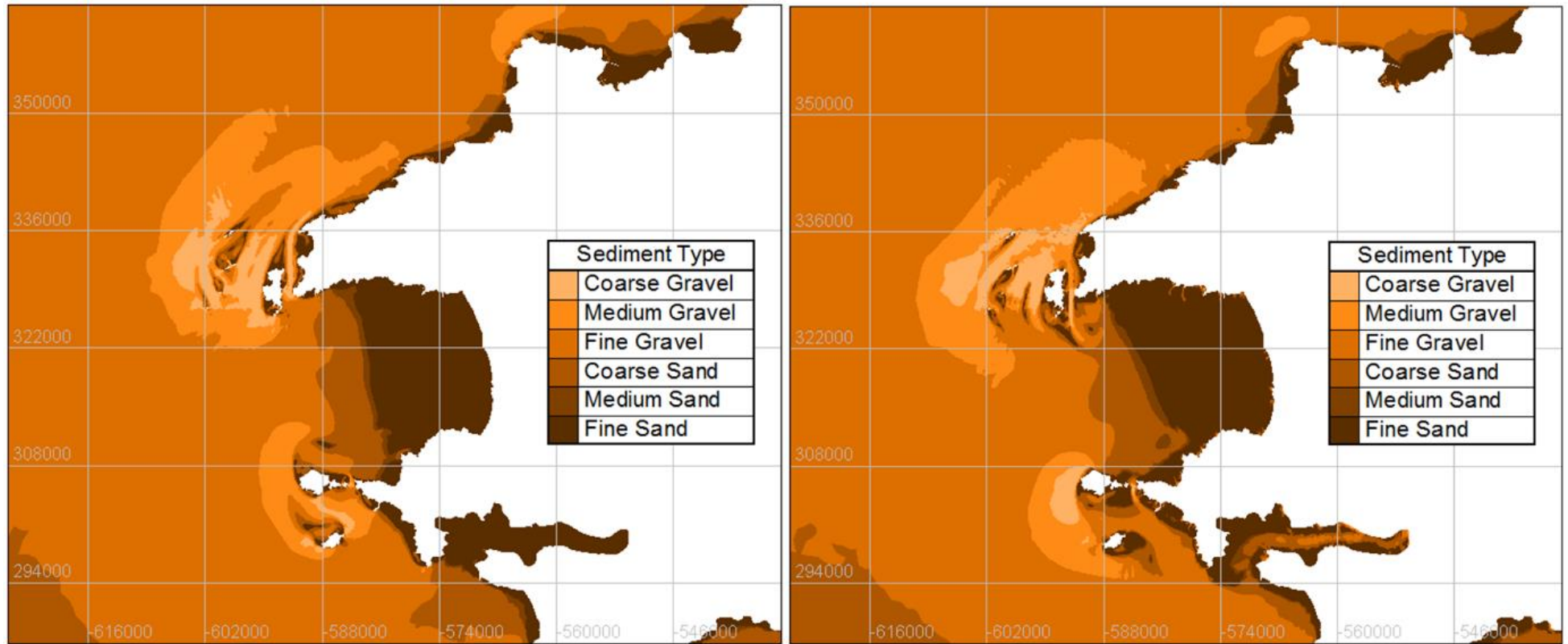


Figure 4-21: Predicted sediment maps during peak flood (left) and peak ebb (right).

There is a significant difference between the predicted sediment maps (Figure 4-21) during the flood and ebb suggesting any sediment accumulated over one half of the tidal cycle is likely to be transported over the next half. Figure 4-22 and Figure 4-23 show the changes to the sediment maps during a peak flood and ebb with and without the tidal array.

Due to the size of the tidal array, the changes to sediment transport are subtle. During the flood, there is a greater accumulation of medium gravel within the array and 1 km downstream in its wake. During the ebb, there is an increased accumulation of fine gravel 3 km downstream of the array at the northern entrance of Ramsey Sound as well as coarse sand north of Ramsey Island. As flow speeds through St David's Head and the Bishop's & Clerks exceed 2m/s, as well as speeds exceeding 3m/s in Ramsey Sound, any sediment smaller than coarse gravel is unlikely to stay within this region for long. Any sediment fed into the area from the north or south is likely to be transported through the region within a few tidal cycles. Therefore, the largest impact the tidal array will have is as a barrier to the net transport of sediment. The width of fine gravel accumulation adjacent to the coastline at St David's Head is larger during both the flood and ebb cycle. The discussion of the results is qualitative in nature as the maps do not allow for quantifiable changes to sediment transport to be assessed, hence, caution should be applied when interpreting the impacts from these sediment maps.

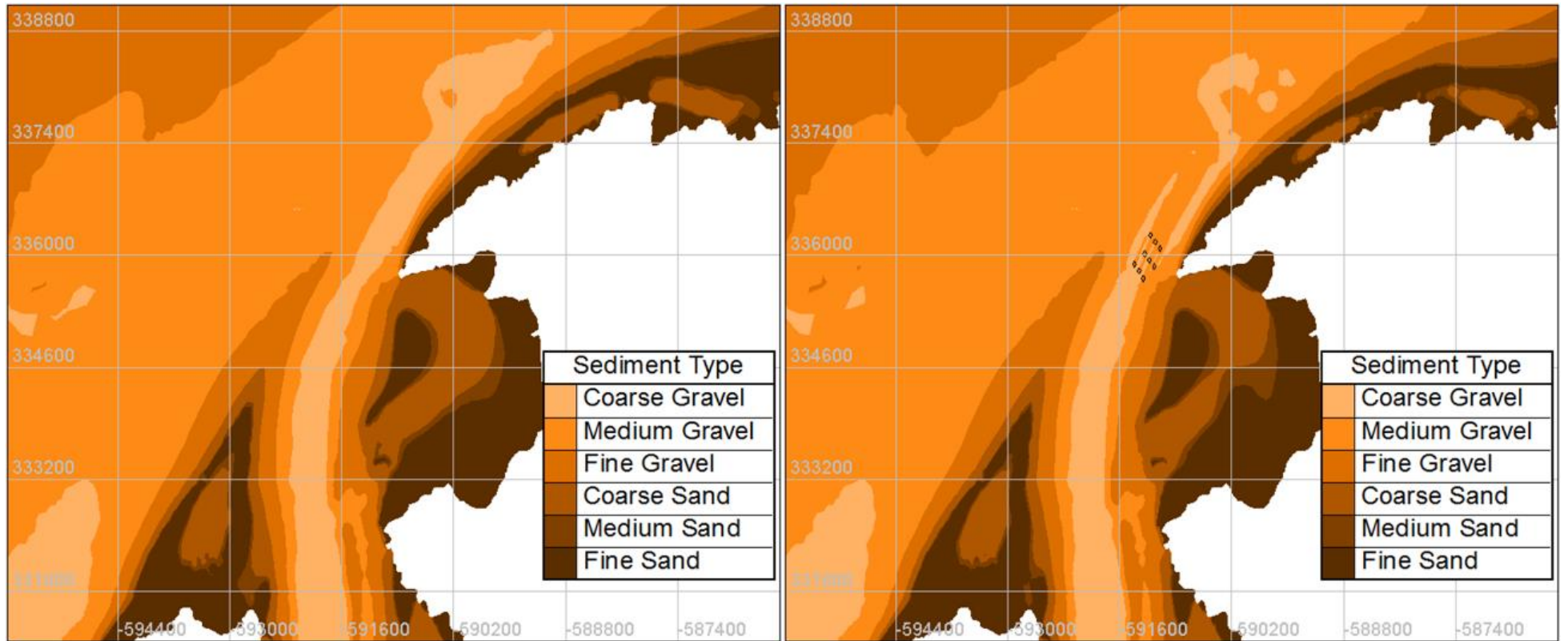


Figure 4-22: Predicted sediment maps during peak flood with no turbines (left) and 9 devices (right).

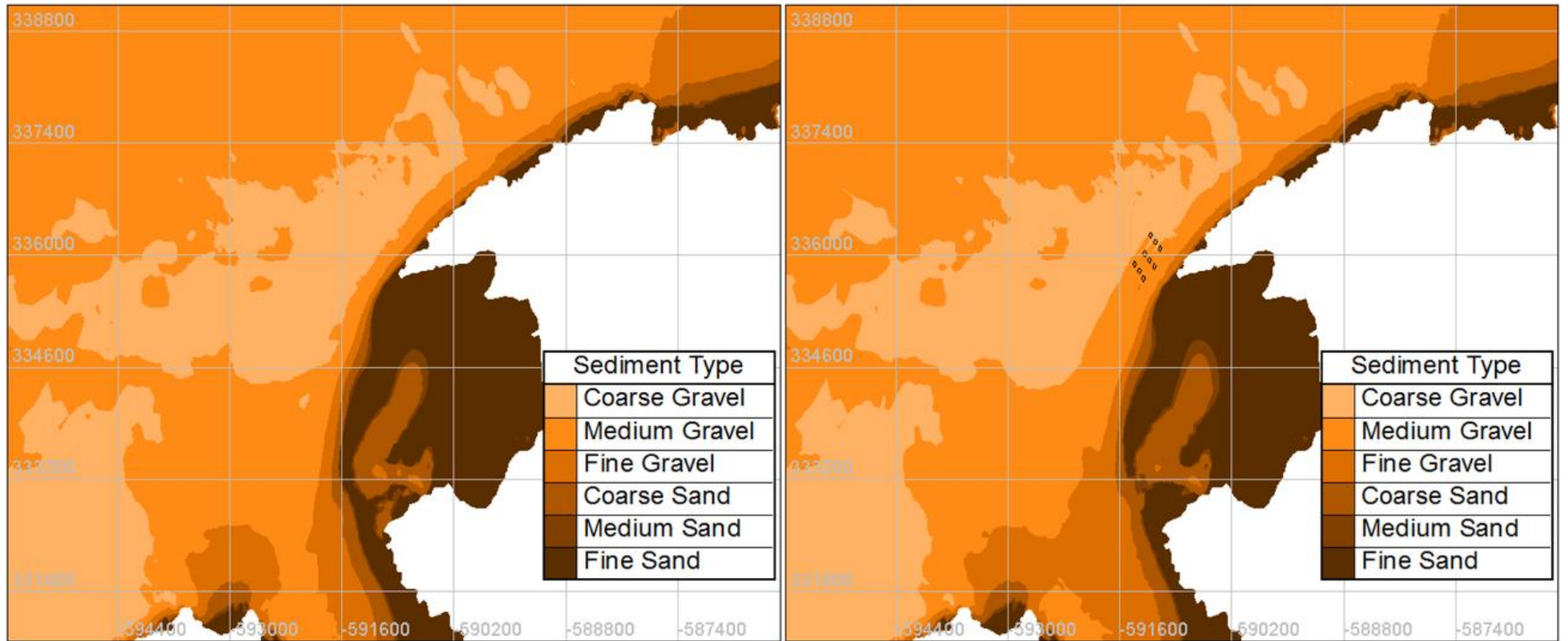


Figure 4-23: Predicted sediment maps during peak ebb with no turbines (left) and 9 devices (right).



#### 4.4.5 Morphological effect due to waves

Morphological conditions are not driven by tidal currents alone but also by wave interactions. In sufficiently shallow waters, waves can induce an orbital velocity at the seabed that can result in the motion of sediment. Soulsby (1997) defines 'sufficiently shallow' when depths meet the following condition:

$$h < 0.1gT^2 \quad (4.6)$$

where  $h$  is depth,  $g$  is gravity and  $T$  is wave period. In shallow waters, the wave skin friction shear stress with an orbital wave velocity  $U_w$  can be many times larger than that produced by an equal depth averaged tidal current (Soulsby, 1997). Therefore, it is important to determine whether the change in bed shear stress, as a result of the presence of the tidal turbine, is greater than the background variation in wave induced bed shear stress. If the bed shear stress due to waves is larger, then the resulting impact of the tidal turbines will be greatly reduced.

Wave skin friction bed shear stress is calculated as:

$$\tau_w = \frac{1}{2}\rho f_w U_w^2 \quad (4.7)$$

where  $\rho$  is density,  $f_w$  wave friction factor and  $U_w$  is the near bed wave orbital velocity. Using Soulsby's exponential approximation (Soulsby, 2006) the near bed wave orbital velocity is calculated as:

$$U_w = \left(\frac{H_s}{2}\right) \left(\frac{g}{h}\right)^2 \exp\left\{-\left[\left(\frac{4.41}{T}\right) \left(\frac{h}{g}\right)^{\frac{1}{2}}\right]^{2.45}\right\} \quad (4.8)$$

where  $H_s$  is significant wave height,  $h$  is depth,  $T$  is period and  $g$  is gravity. Using Soulby's formula (Soulsby, 1997) the wave friction factor is calculated as:

$$f_w = 1.39 \left(\frac{A}{z_0}\right)^{-0.52} \quad (4.9)$$

where  $A$  is orbital amplitude of wave motion at the bed and  $z_0$  is roughness length. A value of  $z_0=0.3\text{mm}$  has been used representing a sand/gravel bed (Soulsby, 1997). The orbital amplitude of wave motion at the bed is calculated as:

$$A = \frac{U_w T}{2\pi} \quad (4.10)$$

In order to determine the wave induced bed shear stress a numerical model was created using the wave propagation component TOMAWAC. Using a finite element mesh, TOMAWAC solves a steady state spectro-angular density wave action. To reduce the computation run time, the model domain was reduced in size. The model domain extends between 51.2°N - 51.4°N and 4.8°W - 5.9°W and is shown in Figure 4-24. The unstructured mesh was discretized with 152,716 nodes and 300,948 elements. The model domain uses the same bathymetry and coastline as that shown in Figure 4-3.

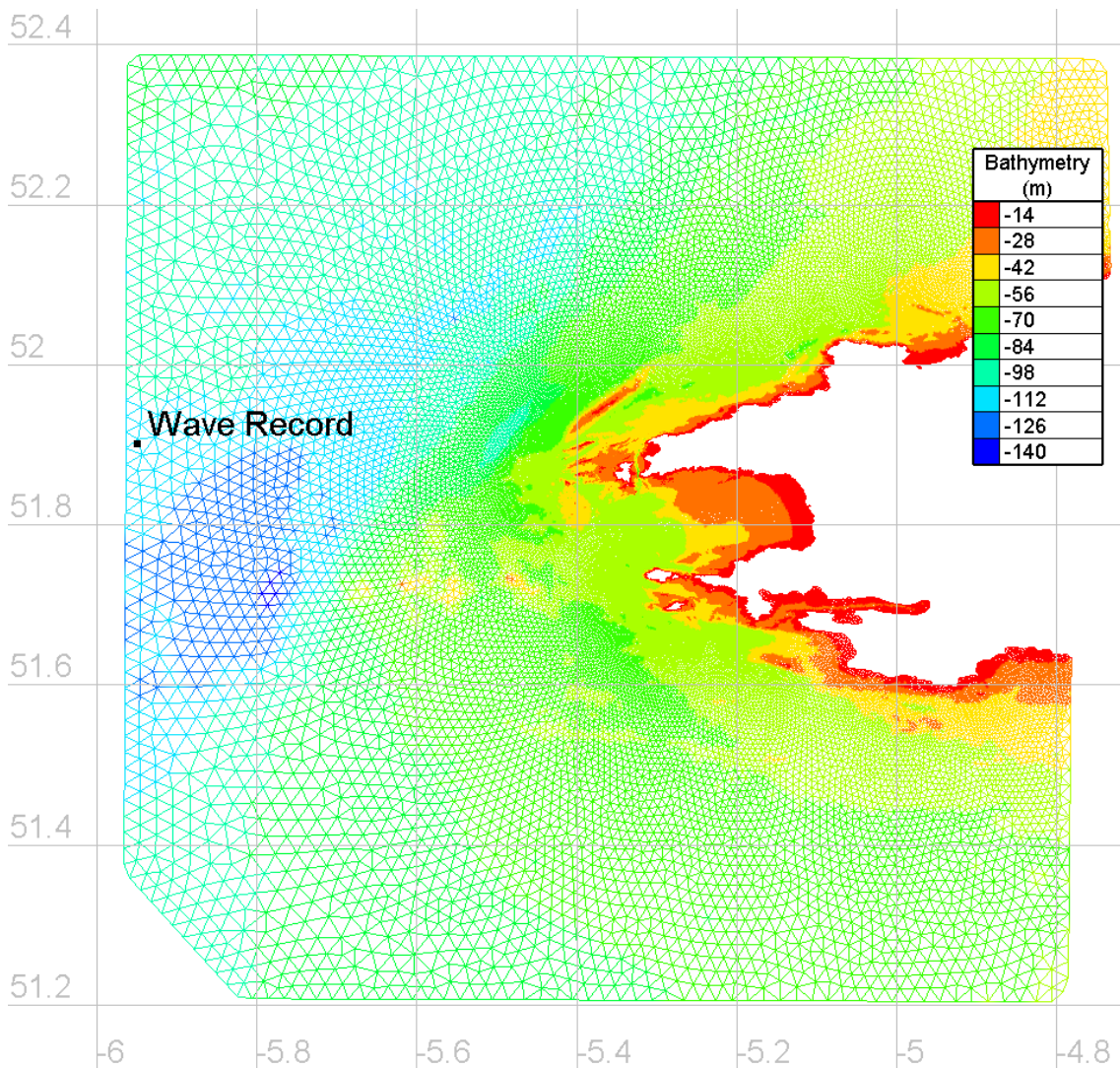


Figure 4-24: TOMAWAC model computational mesh. The black dot represents the location of the wave record used to determine the model boundary conditions.

To determine the boundary conditions for the wave model, a year-long wave record between 01/01/2000 to 01/01/2001 was obtained from the UK Meteorological Office’s Wave-Watch 3 hindcast model. The location of the wave

record is shown in relation to the model domain in Figure 4-24. Figure 4-25 shows the significant wave height over the entire wave record.

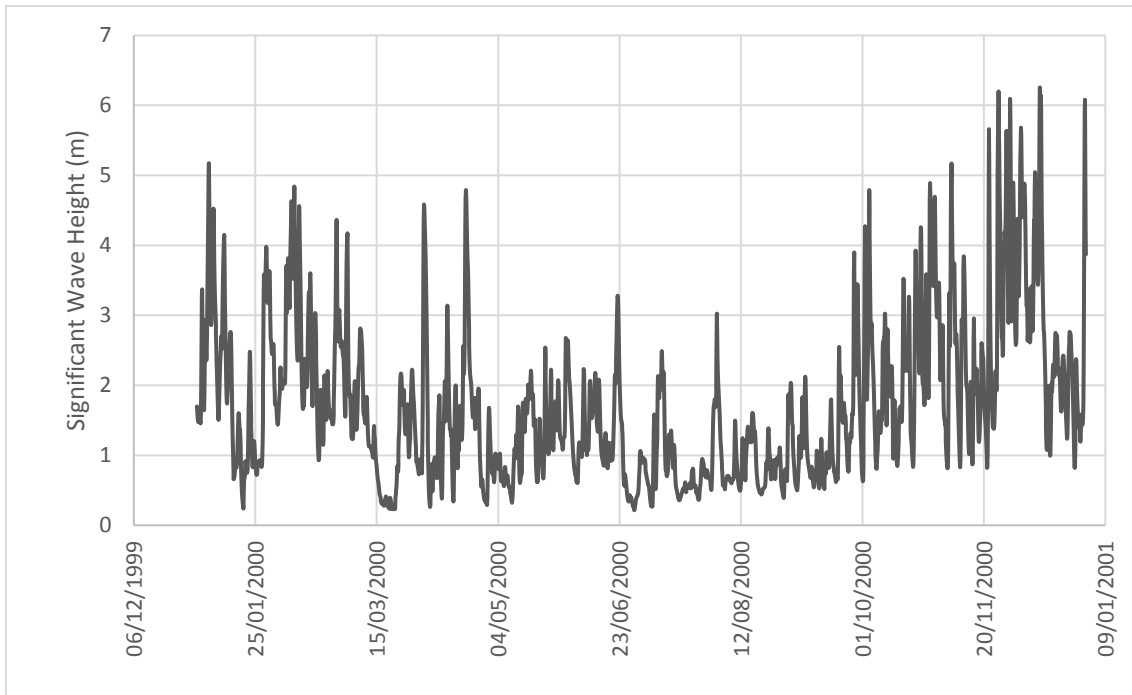


Figure 4-25: Significant wave height from Met Office WW3 hindcast model between 01/01/2000 to 31/12/2000.

Analysis of the wave record shows the largest wave was 6.2m with a period of 10.0 seconds, corresponding to a winter storm event in December. The predominant wave direction was from the south-west. In TOMAWAC's coordinate reference system, that represents a wave direction of  $65^\circ$ . As the storm event represents a worst-case scenario, it was chosen as the boundary condition for the model. The model was run on a single node with 16 processors for a model time of 10 hours, allowing the model to reach a steady state, taking approximately 3 hours. Figure 4-26 shows the propagation of significant wave height and the corresponding bed shear stress.

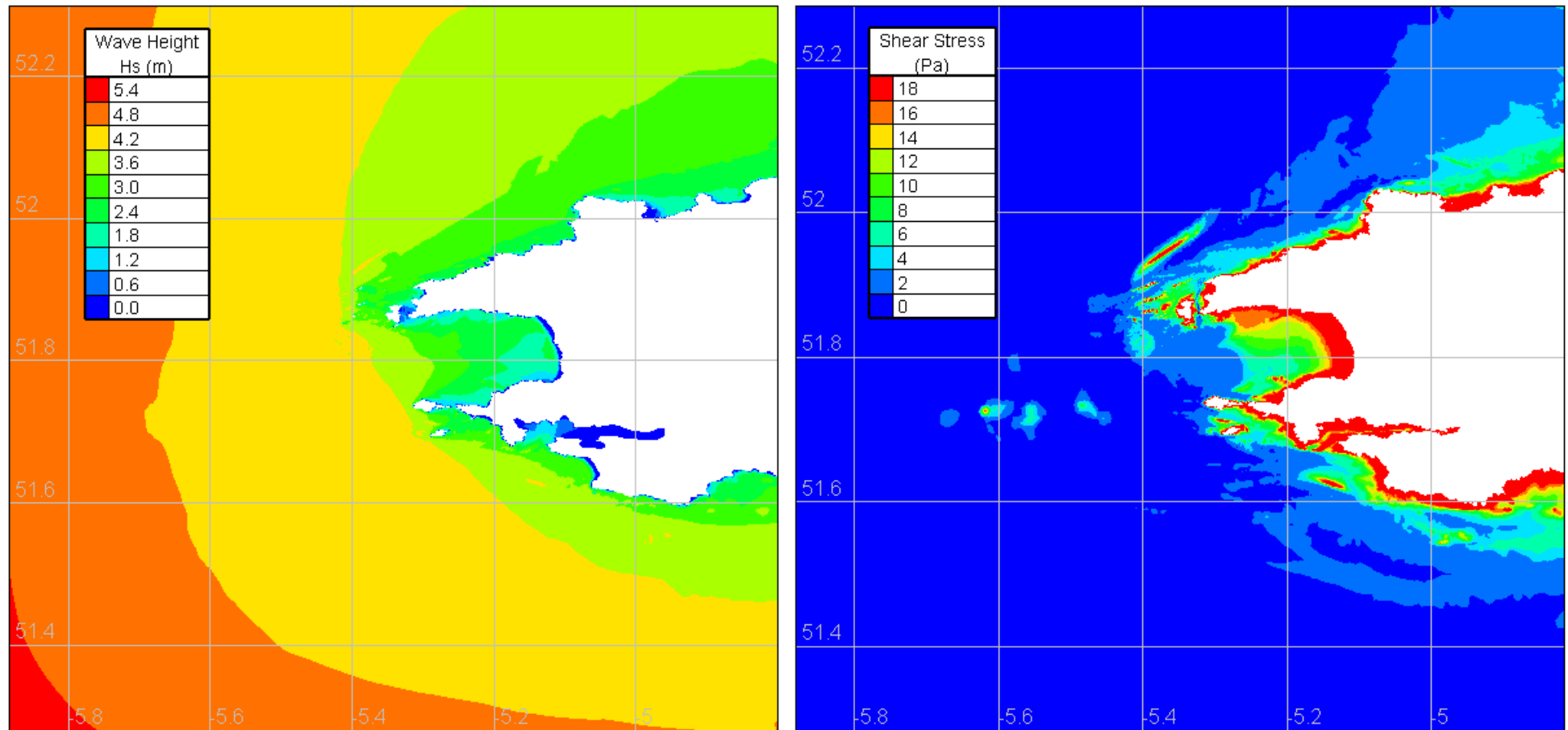


Figure 4-26: Modelled wave height (left) and the resulting bed shear stress (right).

Under the modelled conditions the wave induced bed shear stress, in the vicinity of the array, is 4.4 Pa. The maximum bed shear stress due to tidal currents is 22.6 Pa. Even with the reduction in bed shear stress due to the presence of the tidal turbines, the maximum bed shear stress is approximately four times larger than the peak wave-induced bed shear stress. Due to the strong tidal velocities, the area is predominantly tidal-dominated. Figure 4-27 shows the spatial extent of where either tidal currents or waves are the dominate bed shear stress. The black contour represents the extent of the reduction in maximum bed shear stress due to the presence of the tidal turbines, as seen in

Figure 4-20. It is clear that the extent of the change in bed shear stress is still within the area dominated by tidal flows. Despite the reduction in bed shear stress, the tidal turbines will have a clear impact that will not be masked by wave interaction. As a result, bed shear stress due to waves will be ignored.

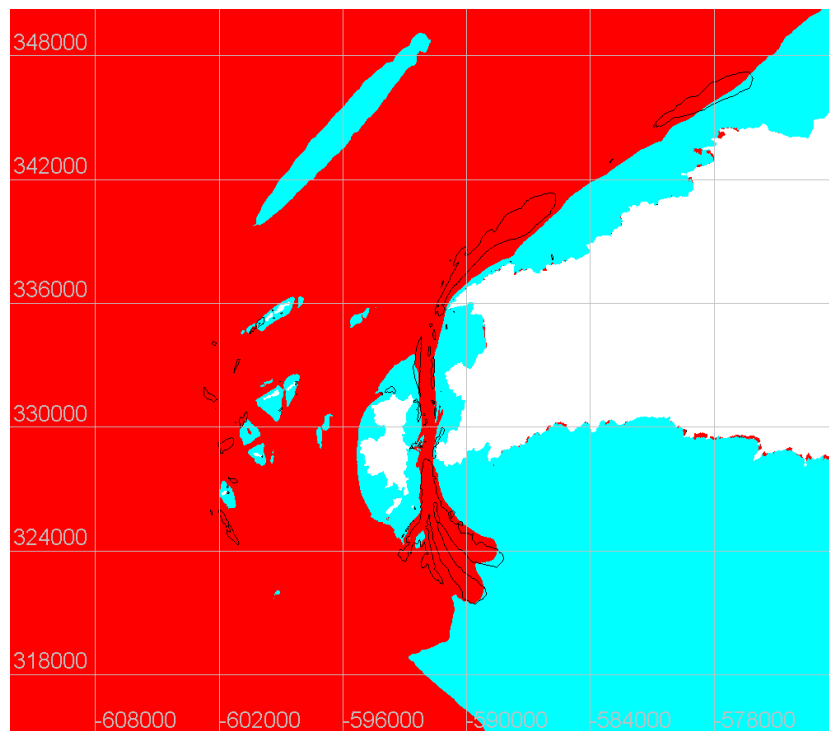


Figure 4-27: Bed shear stress dominance due to tidal velocities (red) and waves (blue). The black contour represents the extent of the reduction in maximum bed shear stress due to the presence of the tidal turbines.

The bed shear stress due to tidal currents and waves have been calculated using two separate models. The two models could be coupled to give an improved assessment of the total bed shear stress as the presence of waves can reduce the bed shear stress due to tidal currents. However, Guillou et al (2016) showed

the available mean spring tidal stream potential during extreme wave conditions only reduced by 12%. Taking this into account, the maximum bed shear stress found in the tidally dominated area would still be significantly larger than the contribution due to the waves. As such, a couple wave and tidal model is not necessary.

## 4.5 Summary

A high resolution depth averaged hydrodynamic model has been used to simulate the impact of a 10MW tidal array at Ramsey Sound. The model results show there is a strong disparity between the flood and ebb tide with local bathymetric effects leading to significant differences between the power output of each device. Over the 30-day model run, the tidal array will produce 2.15 GWh, equating to 25.80 GWh per annum. The tidal array impacts the local hydrodynamics by reducing the amplitude of the M2 and S2 tidal constituents by 20% and 19% respectively. Far field effects are seen as far as 24km from the site through changes to eddy propagation. Investigations of tidal arrays are particularly site specific and no generic value of impact can be made. If a tidal array is sited such that it does not influence areas of vorticity generation, then impacts can be greatly reduced. However, the sites of interest around the UK are typically in turbulent environments. The results show the need for high resolution modelling, at an appropriate scale, to enable the complex features of the environment to be correctly resolved.

However, changes to eddy propagation only provide a short-term view. The model is purely hydrodynamic with no atmospheric forcing or wave driven currents. The position and dispersion of eddies in this area would naturally vary if these additional interactions are included. Therefore, the influence on bed shear stress can provide a better insight into the longer-term impact on morphodynamics. The influence of the array on bed shear stress is more localised and extends to within 12km of the tidal site. Tidal arrays can alter complex hydrodynamic processes and lead to far field effects greater than just the direct wake of the turbines. These alterations could drive significant changes in bed characteristics and sediment dynamics. Results show the tidal array will lead to localised sediment accumulation and will act as a barrier to sediment transport.

# Chapter 5

## Cumulative Impact Assessment of Tidal Energy in the Irish Sea

### 5.1 Introduction

The development of tidal stream energy extraction technology and the establishment of a tidal stream industry has seen considerable growth in the past two decades (Neill et al., 2017). As tidal energy extraction is only just starting to take the first steps toward commercial viability, strategic planning of the marine environment is needed to maximise its full potential (RenewableUK, 2015). Many of the optimum sites for tidal resource are clustered in a select number of locations, and it is not efficient or in the best interest of the industry to consider each project in isolation. Cumulative impact assessments should be conducted, but have only recently been considered (Fairley et al., 2015). Wilson, Bourban & Couch (2012) investigated the interaction between tidal barrages and tidal turbines across the UK and its effect on the European continental shelf. The results provided several conclusions. Large scale extraction of tidal current energy was shown to have severe near-field effects if extraction is not limited and would require close management between nearby projects to limit environmental and economic impacts. Similarly, large scale deployment of tidal range

technologies would have unacceptable levels of change. Furthermore, in the most extreme future scenario (55GW of tidal range and 38 GW of tidal stream) would have impacts on countries outside of the UK across the continental shelf. However, it was found that deployment of tidal barrages and tidal stream did not interact.

Whilst a lot of focus has been given to modelling the Pentland Firth (Martin-Short et al., 2015; Draper et al., 2014; Woolf, 2013), it is not the only site being developed within the UK, the Irish Sea has a number of proposed developments. The Irish Sea is well studied through observations (Robinson, 1979; George, 1980) and numerical modelling (Pingree and Griffith, 1987; Davies and Jones, 1992; Young, Aldridge and Brown, 2000). Depths in the Irish Sea range from intertidal mud flats to ~140m in the central Irish Sea, to the extreme of 250m in the North Channel. There are two amphidromic systems in the Irish Sea, one found on the east coast of Ireland and the other to the north of Northern Ireland. Tidal ranges in the east Irish Sea are the largest in the UK, with ranges more than 9m at Workington and 12m at Hinkley. Large tidal velocities (>2m/s) can be found in several locations in the Irish Sea, notably around Pembrokeshire, Anglesey and Northern Ireland.

Several studies have been conducted assessing these locations for the available tidal energy resource and the suitability for tidal stream extraction (Robins et al., 2015; Lewis et al., 2015; Neil et al., 2014). However, these studies do not include the presence of tidal stream devices, nor the interaction of devices or arrays of devices with one another. Robins et al (2015) investigate how the ratio of the  $M_2$  and  $S_2$  harmonics can affect the annual practical power and estimating the spatially distribution of a tidal stream capacity factor. Lewis et al (2015) investigate the total annual mean tidal resource of the Irish Sea within the constraints of 1<sup>st</sup> generation devices (velocities > 2.5m/s and depths between 25-50m) and show that the total potential resource could be larger if devices could be deployed in water depths greater than 50m. Neil et al. (2014) investigate the phasing of tidal sites around the European shelf for power generation, but conclude there is minimal phase diversity between sites for power generation.

As well as the discussed resource assessments, studies have been conducted in the Irish Sea including the presence of tidal turbines. Robins et al (2014) assessed the impact of tidal-stream arrays in relation to the natural variability of



sedimentary processes at Anglesey, but only included a single tidal array of increasing capacity. Hashemi et al. (2015b) investigated the influence of waves on tidal resource at Anglesey, showing that extreme wave-current interactions can reduce the tidal resource by 20%. Walkington & Burrows (2009) conducted an assessment of tidal stream power in the Irish Sea with the influence of tidal turbines included. However, the hydrodynamic effect of the tidal array at each of the four locations was considered in isolation. Furthermore, the tidal turbines were represented as a constant drag term, neglecting the operation of the turbine and the drag due to the support structure, leading to an under-representation of the total force and influence exerted by the turbine.

At the time of this study, there were eight existing and proposed tidal projects within the Irish Sea, totalling 264 MW. These include: Ramsey Sound (10 MW), Anglesey (10 MW), Strangford Loch (1.2 MW), Mull of Kintyre (3 MW), Torr Head (100 MW), Fair Head (100 MW), Sound of Islay (10 MW) and West of Islay (30 MW) (see Figure 5-1). The size of these arrays represent the actual proposed installed capacities of the site developers and not the maximum theoretical capacities of the sites. Ramsey Sound is the same project as discussed in detail in Chapter 4. The 10 MW Anglesey tidal project is situated 1km from the Anglesey coastline, North Wales, with depths across the site between 20-40m and a tidal range of 4.9m. Modelling estimates the annual mean wave height at the site to be between 1.2m and 1.6m. The peak spring velocities are greater than 3m/s. The seabed is comprised of exposed bedrock with patches of coarse sand (PMSS Ltd, 2006).

The single Seagen-S turbine at Strangford Lough is located within the centre of the Strangford Lough Narrows, in Northern Ireland. Depths in the narrows vary between 30-60m, with a tidal range of 3.3m. As the entrance to the Narrows are sheltered from the predominant swell waves from the Atlantic, the site only experiences small wind driven waves. Tidal currents at the site peak in excess of 4.5m/s. The seabed is comprised of exposed rock and coarse sediment (Savidge et al., 2014).

The Mull of Kintyre tidal site is situated 1km south-west from the coast of the Kintyre peninsula, Scotland. Depths at the site vary between 35-40m, with a tidal range of 0.71m. The site experiences waves predominately from the Atlantic to

the west, with extreme waves of 12m. Tidal velocities at the site approach 4m/s. The seabed consists of gravelly sand and rocky substrate (Nautricity, 2013).

The Torr Head tidal array is situated less than 1km from Torr Head point, Northern Ireland. Depths at the site vary between 30-110m, with a tidal range of 1.4m. Waves at the site rarely exceed 2m. The maximum spring currents reach up to 4m/s. The seabed consists of exposed rock, boulders and coarse gravel (Tidal Ventures, 2015).

The Fair Head tidal array is situated less than 1km from the Northern Ireland coastline and is 5km to the north-west of the Torr Head tidal array. Depths at the site vary between 25-130m, with a tidal range of 1.5m. The site is in lee of Ratlin Island and is sheltered from the Atlantic swells from the west. The annual average significant wave height is 1.2m. The mean spring tide reaches more than 4m/s. The seabed consists of exposed rock and coarse gravel (McGrath, 2013).

The Sound of Islay tidal array is situated in the sound between Isles of Islay and Jura, Scotland. The turbines are intended to be deployed in depths below 48m. The tidal range within the sound is 1.7m, with currents reaching 2.8m/s. The site is sheltered by the land mass of Islay, meaning the maximum wave height is 1.2m. The seabed consists of coarse gravel and a rocky substrate (Scottish Power Renewables, 2010).

The West of Islay tidal array is situated 8km to the south west of the Isle of Islay, Scotland. Depths at the site vary between 25-50m, with a tidal range of 2.1m. Waves are predominant from the west, with waves exceed 3-4m for 10% of the year. The seabed consists of exposed bedrock, cobbles and boulders (DP Marine Energy Ltd, 2013)

Since this work has been undertaken, funding for the Anglesey project was removed and the project stalled. However, for the purpose of this analysis, it has been included. This chapter will investigate the cumulative impact of tidal energy in the Irish Sea to examine the extent to which the projects interact with each other. For this study, only tidal stream developments have been considered; tidal barrages were not included.

## 5.2 Irish Sea Model

### 5.2.1 Model Domain

A high-resolution depth-averaged model of the Irish Sea was built using an unstructured triangular mesh, with the hydrodynamic software TELEMAC2D (v7p1). The model domain extends between 50.14°N – 56.72°N and 2.38°W – 7.73°W and is shown in Figure 5-1.

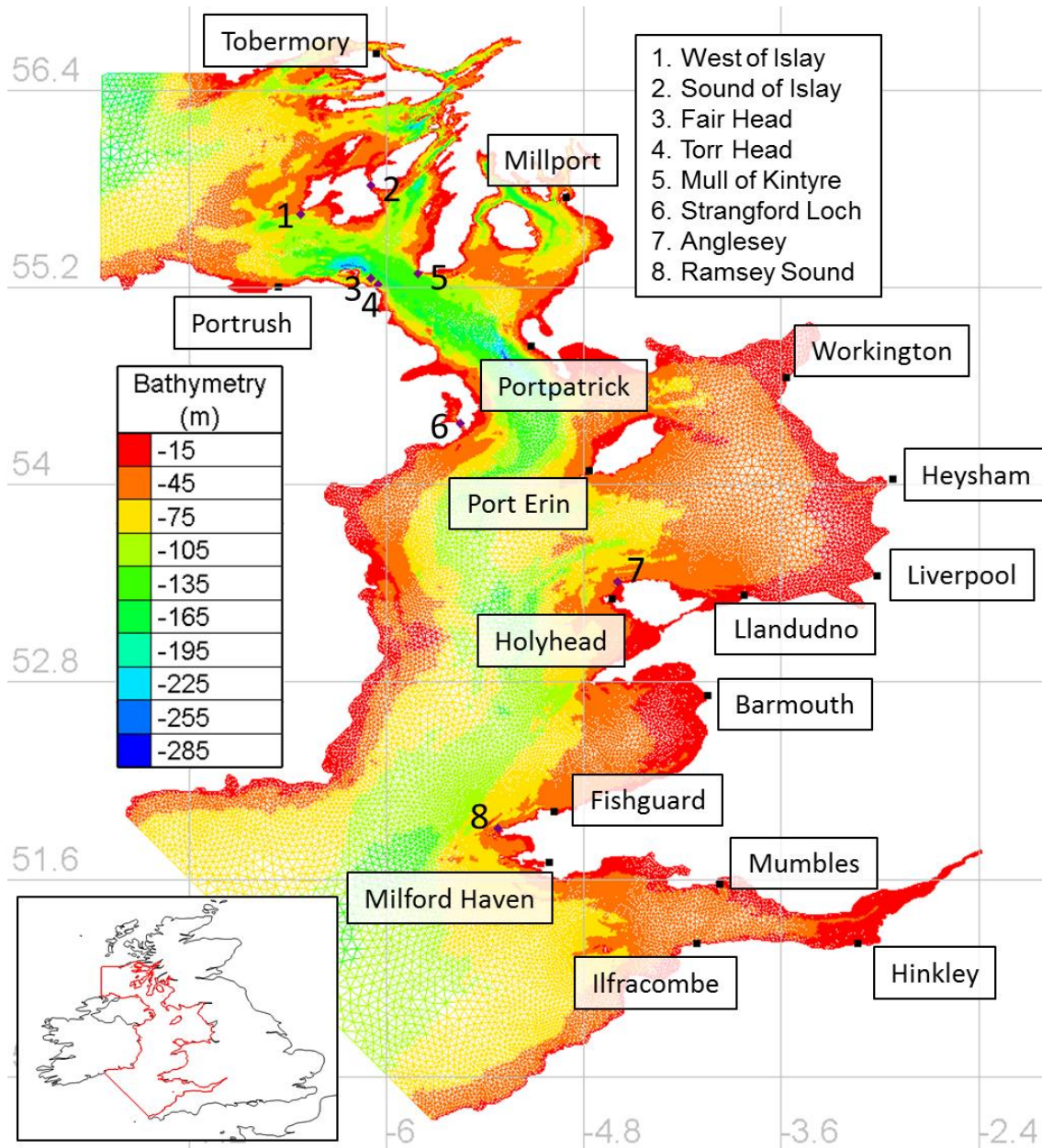


Figure 5-1: Irish Sea model domain showing the locations of the tidal arrays (purple diamonds) and tide gauge locations (black squares) used for validation.

The unstructured mesh was discretized with 304,916 nodes and 594,109 elements. The mesh has a resolution of 15 km around the open boundary,

reducing to 1km along the coastline. Based on the results presented in Chapter 3, a regular mesh using triangular elements is used in the area where turbines are modelled. The resolution of the regular mesh in the turbine regions is 20m.

Bathymetry of the area was sourced from the Department for Environment, Food & Rural Affairs UKSeaMap 2010 (McBreen & JNCC, 2011) and was provided by the Centre for Environment, Fisheries and Aquaculture Sciences. The resolution of the bathymetry points from this dataset are 1 arc-second (~30m). However, as bathymetry strongly influences hydrodynamic characteristics through Ramsey Sound, a high resolution 2m and 4m resolution bathymetry, from the UK Hydrographic Office (UKHO), has also been applied around Ramsey Sound, Fair Head, Torr Head and the Sound of Islay.

The hydrodynamics are forced along the open boundaries using tidal constituents from the OSU TPXO European Shelf 1/30° regional model. The open boundaries are set far from the area of interest to reduce any dampening effect from the prescribed elevations. The model uses a k- $\epsilon$  turbulence model. The Nikuradse law for bottom friction was used, with a constant value of  $k_s = 0.04$  applied to the whole model domain.

For the model run, a time step  $t_s = 1s$  was used. The Irish Sea model (304,916 nodes) was run on a single node with 16 processors, with an initial spin-up time of 5 days. After the spin-up period, the simulation was run for a model time  $t = 30$  days, taking approximately 3 days.

The TELEMAC steering file used for the Irish Sea case study is shown in Appendix E.

### 5.2.2 Modelling tidal turbines

The methodology used to represent the operation of the tidal turbines is presented by Plew & Stevens (2013), as outlined and discussed in Chapter 3. Over the eight tidal developments, five different tidal technologies have been proposed. Ramsey Sound will use Delta Stream devices; Strangford Loch, Anglesea, West of Islay and Fair Head will use Atlantis Resource's MCT SeaGen-S; Torr Head will use Openhydro; Sound of Islay will use Hammerfest and Mull of Kintyre will use Nautricity. Figure 5-2 illustrates the five different designs of tidal technology.

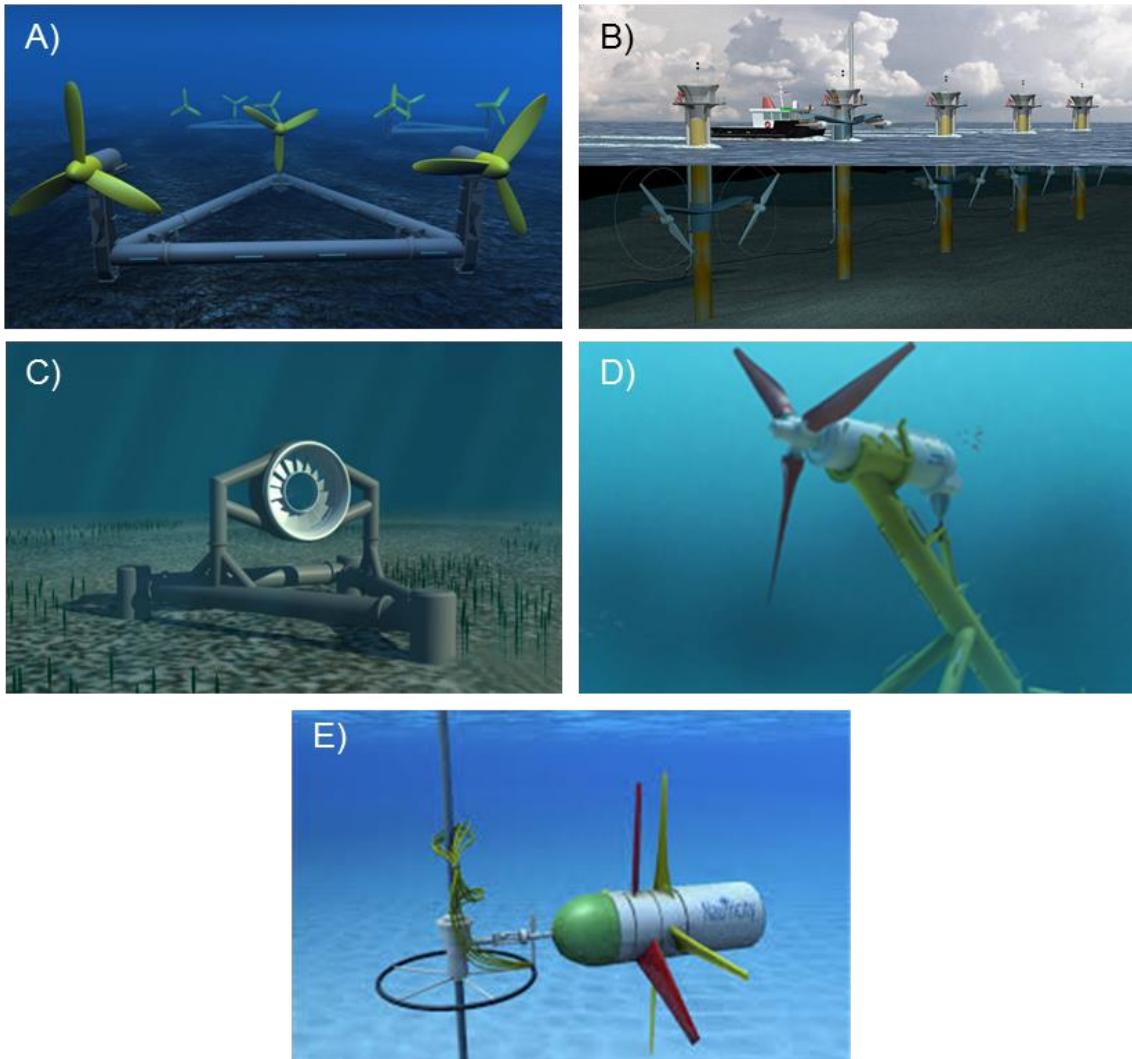


Figure 5-2: Tidal turbine technologies: a) DeltaStream, b) SeaGen-S, c) Openhydro, d) Hammerfest and e) Nautricity. Figure 1a copyright of TEL Ltd, sourced: [www.tidalenergyLtd.com](http://www.tidalenergyLtd.com). Figure 1b copyright of Marine Current Turbines, sourced: [www.marineturbines.com](http://www.marineturbines.com). Figure 1c copyright of Openhydro, sourced: [www.openhydro.com](http://www.openhydro.com). Figure 1d copyright of Andritz, sourced: [www.andritz.com](http://www.andritz.com). Figure 1e copyright of Cameron Johnstone, sourced: [www.globalmarinerenewables.com](http://www.globalmarinerenewables.com).

For all the projects, each device is modelled individually. Furthermore, each technology type is parameterised differently in the model. The turbine parameters for each device can be found in Table 5-1. As the SeaGen-S, Nautricity and Delta Stream device have multiple rotors, the total force of these devices is combined into one device. For simplicity, all the support structures have been assumed to be single cylindrical monopiles, with the exception of Openhydro and Nautricity. Openhydro has two monopiles and Nautricity is a tethered floating turbine. The drag coefficient for the cylindrical monopile was  $C_D=0.9$ . The drag of the tether has been ignored due to its negligible drag force.

Table 5-1: Characteristics of the five device technologies used to parameterise the turbines in the model, using the Plew & Stevens (2013) method.

Device	Rated Power (MW)	Rotor Diameter (m)	Hub Height (m)	Monopile Diameter (m)	$U_c$ (m/s)	$U_D$ (m/s)	$C_{T0}$	$C_{P0}$
Delta stream	1.2	18	15	2	0.8	2.25	0.81	0.27
SeaGen-S	2	20	15	2	0.8	2.5	0.8	0.41
Openhydro	2	16	16	2	0.8	3.5	0.8	0.45
Hammerfest	1	23	22	2	0.8	2.5	0.7	0.33
Nautricity	0.5	14	12	0	0.8	2.5	0.8	0.41

## 5.3 Validation

### 5.3.1 Free surface elevations

Validation data has been obtained from the British Oceanographic Data Centre (BODC) for surface elevation at sixteen tide gauges, whose locations are shown in Figure 5-1. The model was run for 30 days from 17/05/2012 00:00 to 16/06/2012 00:00. Comparisons of the modelled free surface elevation and observed tidal elevations, at each tide gauge is shown in Figure 5-3 & Figure 5-4.

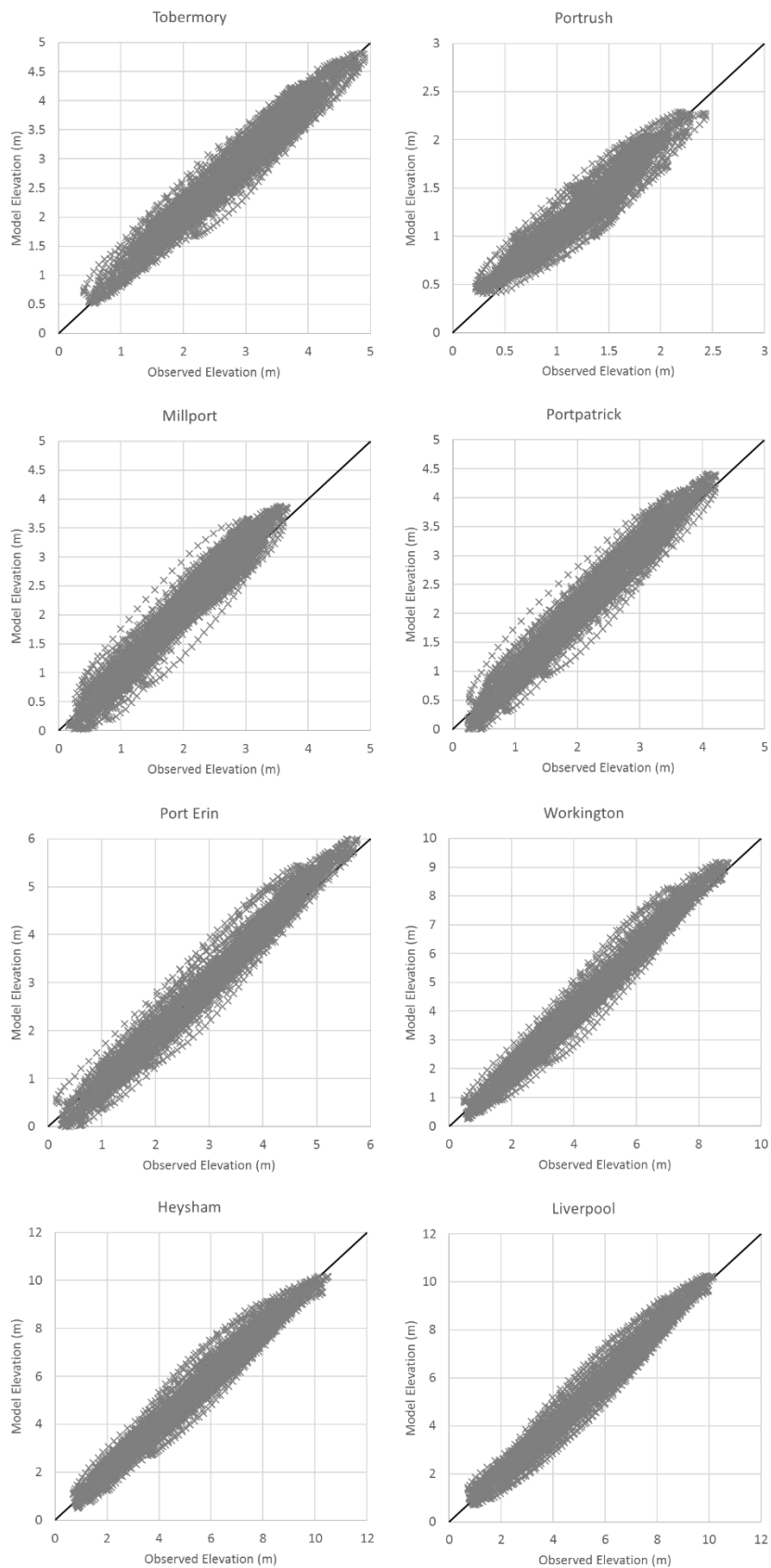


Figure 5-3: Comparison of observed and modelled free surface elevation. The black line represents a  $y=x$  relationship with the dashed line representing a regression line of best fit.

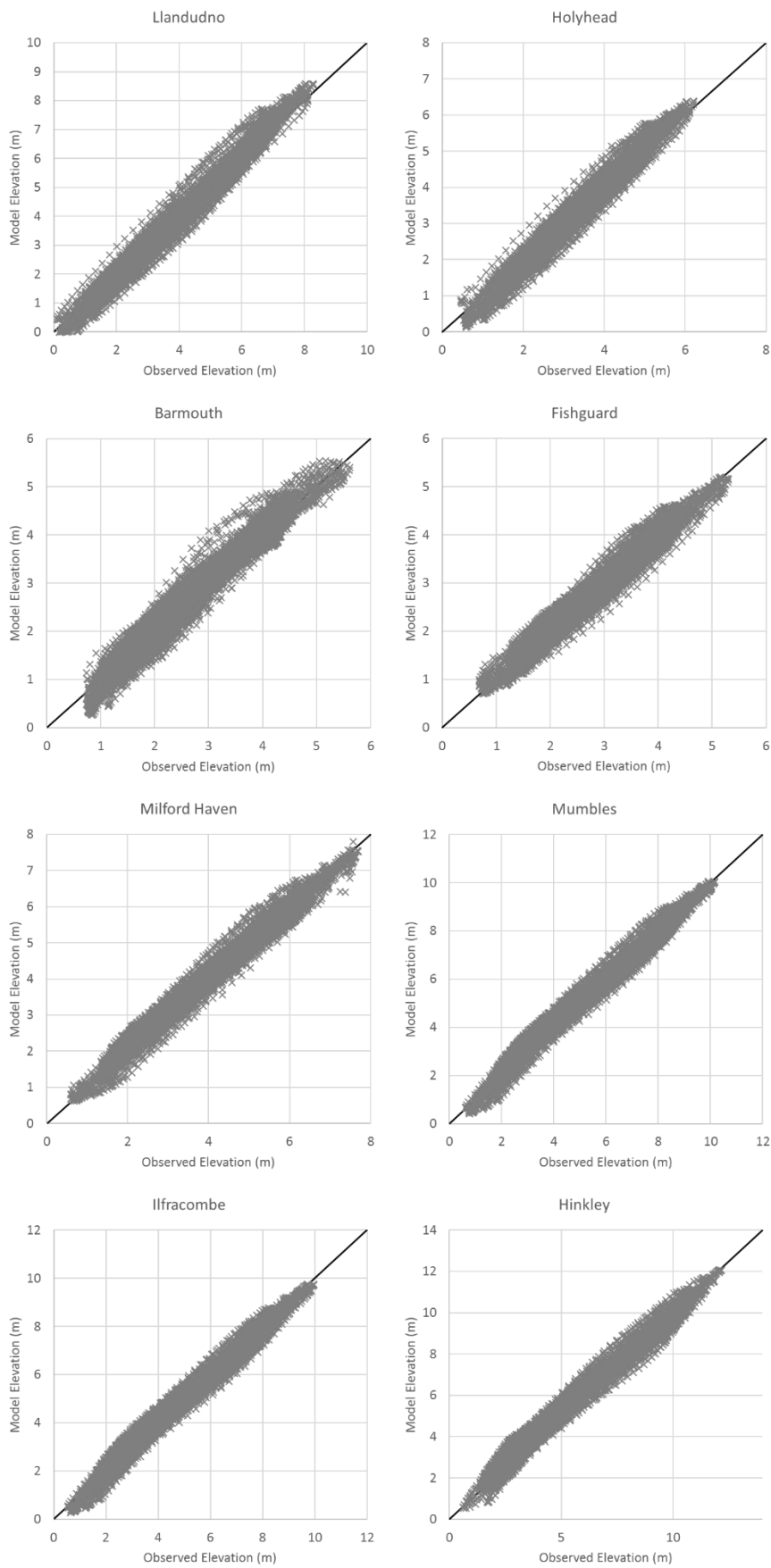


Figure 5-4: Comparison of observed and modelled free surface elevation. The black line represents a  $y=x$  relationship with the dashed line representing a regression line of best fit.



The results in Figure 5-3 & Figure 5-4 show the validation between modelled and observed values shows are in close agreement at the tide gauges in the southern half of the model (Fishguard, Milford Haven, Mumbles, Ilfracombe and Hinkley) which includes the Severn Estuary. Tide gauges in the central Irish Sea, such as Barmouth, Millport, Portpatrick and Port Erin show a larger scattering due to a phase misalignment. This could be due to features, (River Clyde, Afon Mawddach and Lough Foyle), being clipped from the model to improve computational efficiency. Portrush shows some disagreement, however, this may more be due to errors in the tide gauge rather than the model, as a number of erroneous records were removed from the tide gauge data.

The coefficient of determination, the root mean squared error and the scatter index, as calculated by Equations 4-1, 4-2 & 4-3, shown in Section 4.3.1, have been used to assess the comparison between the observed and modelled free surface elevations. Table 5-2 summarises the validation statistics of the sixteen tide gauges.

Table 5-2: Validation statistics of the 16 tide gauges.

Tide Gauge	R <sup>2</sup>	RMSE (m)	Scatter Index (%)
Tobermory	0.965	0.200	7.54
Portrush	0.901	0.149	5.64
Millport	0.950	0.260	9.83
Portpatrick	0.969	0.235	8.88
Port Erin	0.974	0.301	11.35
Workington	0.977	0.381	14.38
Heysham	0.974	0.407	15.36
Liverpool	0.974	0.403	15.19
Llandudno	0.976	0.387	14.58
Holyhead	0.968	0.308	11.63
Barmouth	0.948	0.287	10.82
Fishguard	0.952	0.236	8.89
Milford Haven	0.974	0.280	10.56
Mumbles	0.978	0.368	13.87
Ilfracombe	0.977	0.363	13.67
Hinkley	0.975	0.506	19.07

The coefficient of determination shows that there is a good correlation between the observed and modelled free surface. However, the RMSE and scatter index

indicate a poorer correlation. As the free surface varies about the mean sea level, the difference between the mean of the observed and the predicted will always be small. The difference between time series are more likely to be due to uncertainty in the location of the tide gauges than an error in the model (Gunn & Stock-Williams, 2013).

Figure 5-5 shows the maximum tidal range of the 30-day model run. It shows the model is correctly representing the known features of the Irish Sea. The model is reproducing the amphidromic points of the east coast of Ireland and north of Northern Ireland, and compares well with the co-tidal charts of Young, Aldridge and Brown (2000), shown in Figure 5-6.

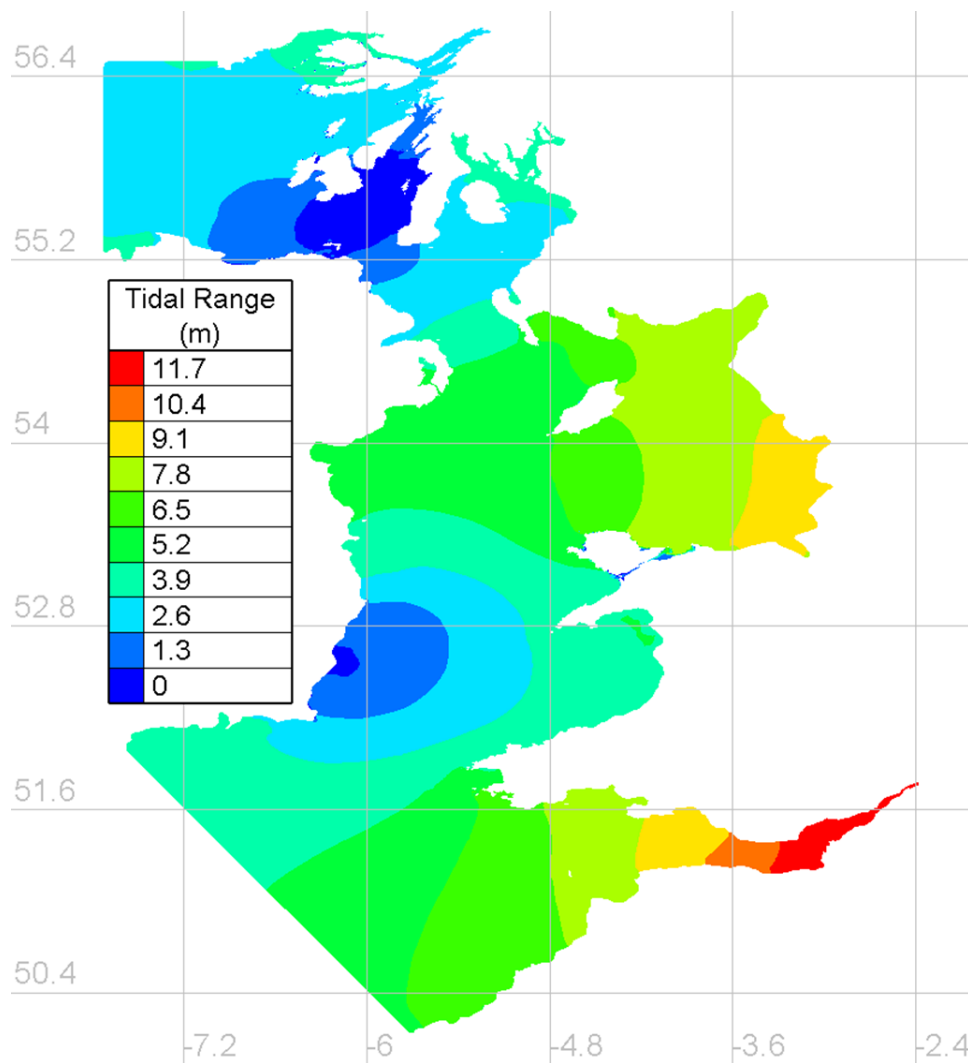


Figure 5-5: Maximum tidal range of the free surface elevations from the 30-day model base case.

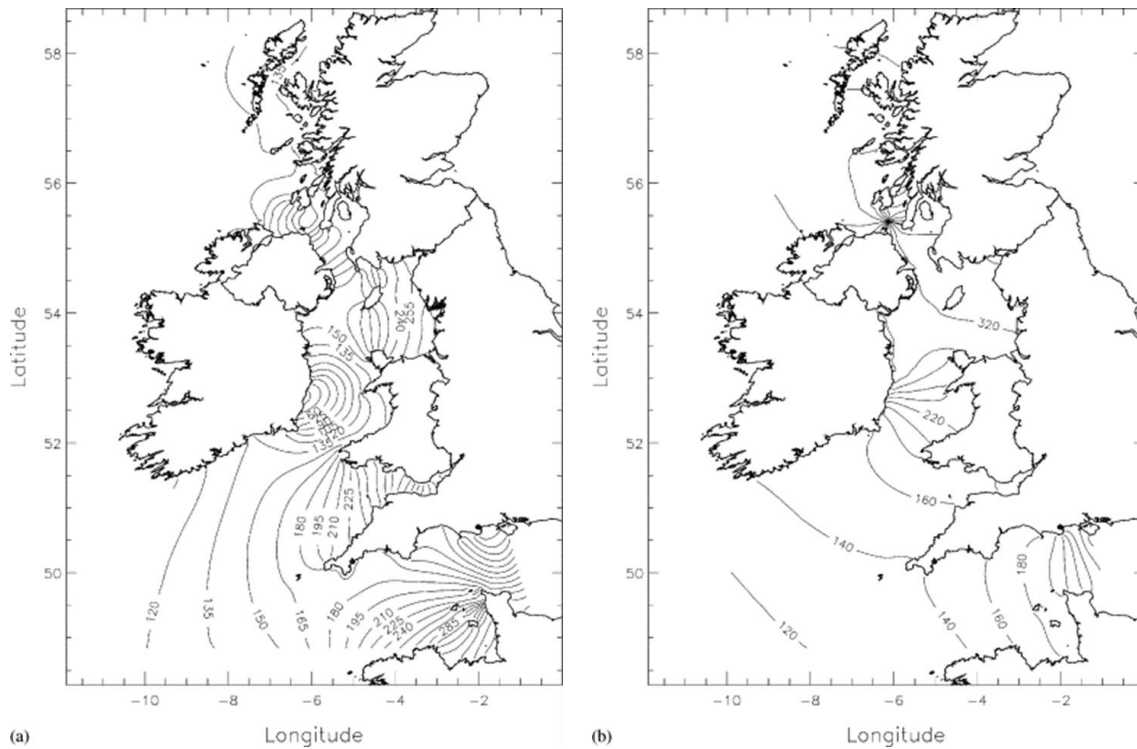


Figure 5-6: Co-tidal charts of the amplitude (left) and the phase (right) of the M2 tidal constituent. Originally shown in Young, Aldridge and Brown (2000).

### 5.3.2 Harmonic Analysis

The model was run for 30 days to provide a time series of sufficient length to permit a harmonic analysis which includes the dominant components. The dominant components are the M2 and S2 constituents. Table 5-3 and Table 5-4 show the comparison between harmonic constituents from the UKHO and the model for the M2 and S2 constituents. Figure 5-7 plots the comparison between the modelled and observed M2 & S2 constituent amplitude.

Table 5-3: Comparison between observed and modelled M2 constituent.

	M2					
	Observed Amplitude (m)	Model Amplitude (m)	Percentage Difference (%)	Observed Phase (deg)	Model Phase (deg)	Percentage Difference (%)
Tide Gauge						
Tobermory	1.27	1.29	1.6	175.0	168.1	-1.9
Port Ellen	0.15	0.17	13.3	50.3	52.2	0.5
Portrush	0.54	0.50	-7.4	201.0	203.9	0.8
Millport	1.12	1.30	16.1	341.0	341.3	0.1
Portpatrick	1.33	1.54	15.8	331.0	330.8	-0.1
Port Erin	1.88	2.08	10.7	322.7	321.2	-0.4
Workington	2.70	3.00	11.2	333.7	330.5	-0.9
Heysham	3.18	3.24	1.9	325.0	321.7	-0.9
Liverpool	3.08	3.16	2.6	315.2	318.6	1.0
Llandudno	2.65	2.96	11.8	310.1	310.3	0.1
Holyhead	1.80	2.03	12.8	292.0	294.3	0.6
Barmouth	1.47	1.52	3.4	244.0	241.5	-0.7
Fishguard	1.37	1.32	-3.6	208.0	212.2	1.2
Milford Haven	2.22	2.19	-1.4	173.0	172.6	-0.1
Mumbles	3.18	3.10	-2.5	171.0	171.6	0.2
Ilfracombe	3.07	3.03	-1.3	163.0	162.3	-0.2
Hinkley	3.80	3.90	2.6	185.0	181.5	-1.0

Table 5-4: Comparison between observed and modelled S2 constituents.

	S2					
	Observed Amplitude (m)	Model Amplitude (m)	Percentage Difference (%)	Observed Phase (deg)	Model Phase (deg)	Percentage Difference (%)
Tide Gauge						
Tobermory	0.52	0.54	3.8	211.0	204.4	-1.8
Port Ellen	0.16	0.13	-18.8	141.0	143.9	0.8
Portrush	0.23	0.22	-4.3	216.0	212.7	-0.9
Millport	0.30	0.34	13.3	33.0	31.9	-0.3
Portpatrick	0.37	0.43	15.8	16.0	15.0	-0.3
Port Erin	0.56	0.63	12.3	2.9	1.3	-0.4
Workington	0.86	0.95	11.0	17.3	13.6	-1.0
Heysham	1.03	1.04	1.0	8.0	4.1	-1.1
Liverpool	1.00	0.99	-1.0	359.2	361.7	0.7
Llandudno	0.86	0.95	10.2	352.7	351.5	-0.3
Holyhead	0.59	0.65	11.0	329.0	332.3	0.9
Barmouth	0.53	0.57	7.5	283.0	279.8	-0.9
Fishguard	0.54	0.50	-7.4	249.0	253.2	1.2
Milford Haven	0.81	0.78	-3.7	218.0	217.0	-0.3
Mumbles	1.12	1.10	-1.8	221.0	218.2	-0.8
Ilfracombe	1.12	1.08	-3.6	209.0	208.3	-0.2
Hinkley	1.42	1.37	-3.5	237.0	232.5	-1.3

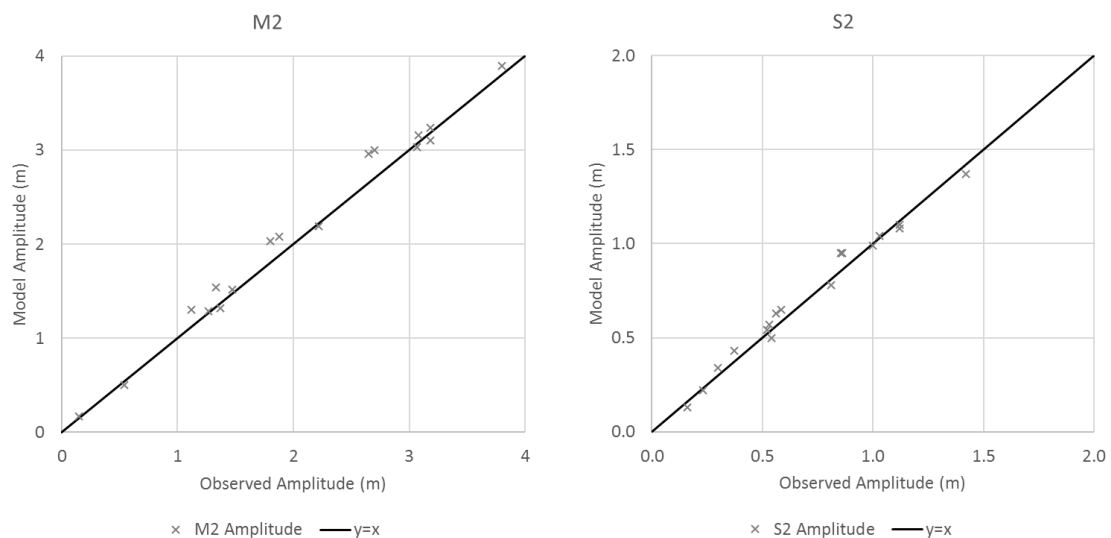


Figure 5-7: Comparison between modelled and observed M2 (left) and S2 (right) tidal constituent.

Analysis of the harmonics reveals agreement between the model and observations in the northern and southern parts of the model domain. In the central Irish Sea, the model over-predicts the elevations, on average, by 13%.

Pingree & Griffith (1979) found a similar effect in their model of the Irish Sea. Whilst they found an improvement by increasing the drag coefficient in this region they could not remove all the discrepancies due to errors caused by a depth-averaged model. However, the validation of this model is comparable to other studies of the Irish Sea (Robins et al., 2015; Lewis et al., 2015). Table 5-5 summarises the model validation compared against Robins et al (2015) and Lewis et al. (2015). Compared to the tide gauges the scatter index is smaller and within acceptable ranges, 7.44% and 6.93% for the M2 and S2 respectively.

Table 5-5: Comparison of model validation with similar studies.

	Haverson (2016)		Robins et al (2015)		Lewis (2015)	
RMSE	Amplitude	Phase	Amplitude	Phase	Amplitude	Phase
	(m)	(deg)	(m)	(deg)	(m)	(deg)
M <sub>2</sub>	15	3	15	12	13	6
S <sub>2</sub>	5	3	5	10	8	14

Along with tidal elevations, a harmonic analysis was performed on the tidal currents. Currents have been validated against published tidal current ellipse data from 31 offshore current meters (Young et al., 2000; Jones, 1983). Figure 5-8 plots the comparison between the modelled and observed M2 & S2 constituent amplitude for tidal currents.

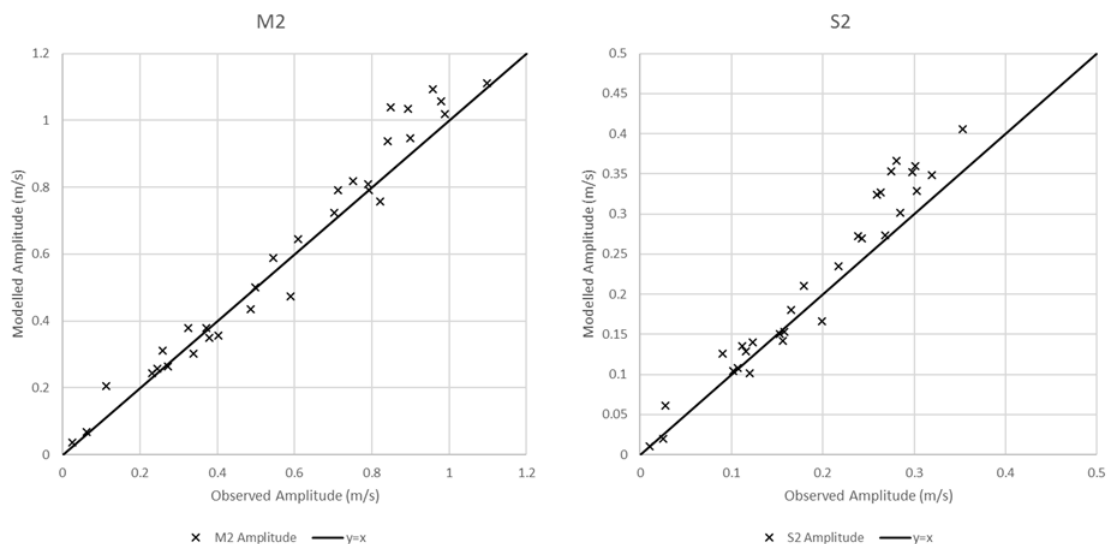


Figure 5-8: Comparison between modelled and observed M2 (left) and S2 (right) tidal constituents for tidal velocities.

Analysis of the harmonics reveals agreement between the model and observations. It can be seen that the model does slightly over-estimate the

currents, with a bias towards the model of 3.4 cm/s for M2 and 2.4 cm/s for S2. However, the validation of this model is comparable to other studies of the Irish Sea (Robins et al., 2015; Lewis et al., 2015). **Error! Reference source not found.** Table 5-6 summarises the model validation compared against Robins et al (2015) and Lewis et al. (2015) with this study.

Table 5-6: Comparison of model validation of tidal currents with similar studies.

RMSE	Present Study Amplitude (cm/s)	Robins et al (2015) Amplitude (cm/s)	Lewis (2015) Amplitude (cm/s)
M <sub>2</sub>	6.7	4.6	8
S <sub>2</sub>	3.7	1.6	2

### 5.3.3 Results

To determine if any of the tidal projects were interacting with each other, their zones of influence were calculated using the range of difference. Figure 5-9 shows the cumulative range of difference for the eight developments.

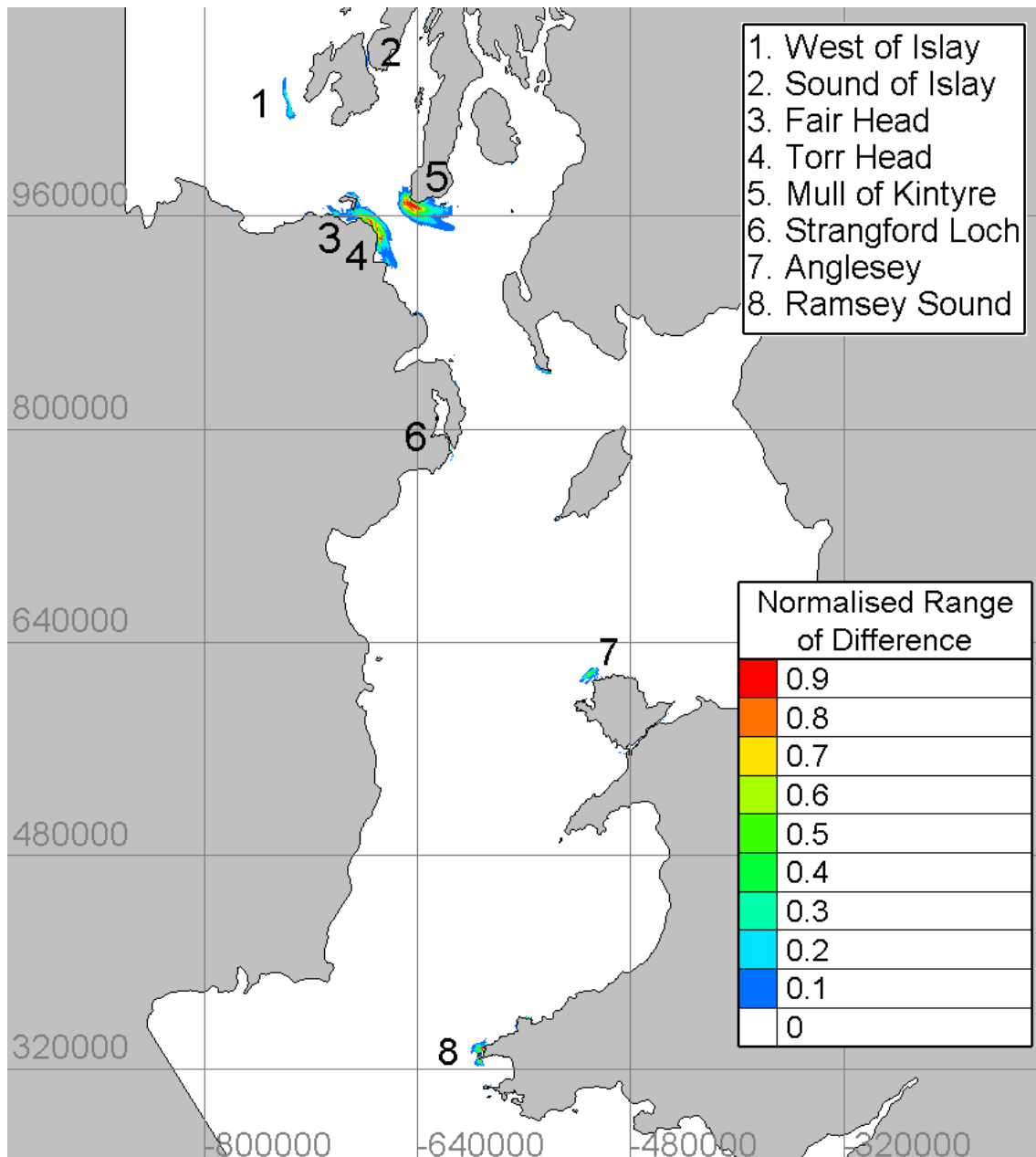


Figure 5-9: The cumulative zones of influence for all 8 tidal projects, calculated using the range of difference.

The range of difference from Ramsey Sound (10MW), the Anglesea Skerries (10MW), Stangford Loch (1.2MW), West of Islay (30MW) and the Sound of Islay (10MW) are sufficiently small that their zones of influence do not overlap. However, Fair Head and Torr Head do overlap. The zone of influence for Mull of Kintyre is large given the scale of project (3MW), especially when compared to Fair Head (100MW) and Torr Head (100MW). Fair Head and Torr Head may be influencing the Mull of Kintyre as well. As the model domain is computationally expensive to run, a smaller model domain encompassing these three projects was created to investigate the interaction.



## 5.4 Northern Ireland Model

### 5.4.1 Model Domain

The Northern Ireland model uses the same structure as the full Irish Sea model but only covers the smaller area of interest. It uses the same coastline and bathymetry as the previous model. The model domain extends between 54.80°N – 56.02°N and 4.62°W – 7.04°W and is shown in Figure 5-10. The unstructured mesh was discretized with 137,086 nodes and 270,088 elements. A regular mesh using triangular elements is used in the area where turbines are modelled. The resolution of the regular mesh is 20m. For the model run, a time step  $t_s = 1s$  was used. The Northern Ireland model (137,086 nodes) was run on a single node with 16 processors, with an initial spin-up time of 5 days. After the spin-up period, the simulation was run for a model time  $t = 30$  days, taking approximately 1 days. The model was run over the same period of time as the Irish Sea model.

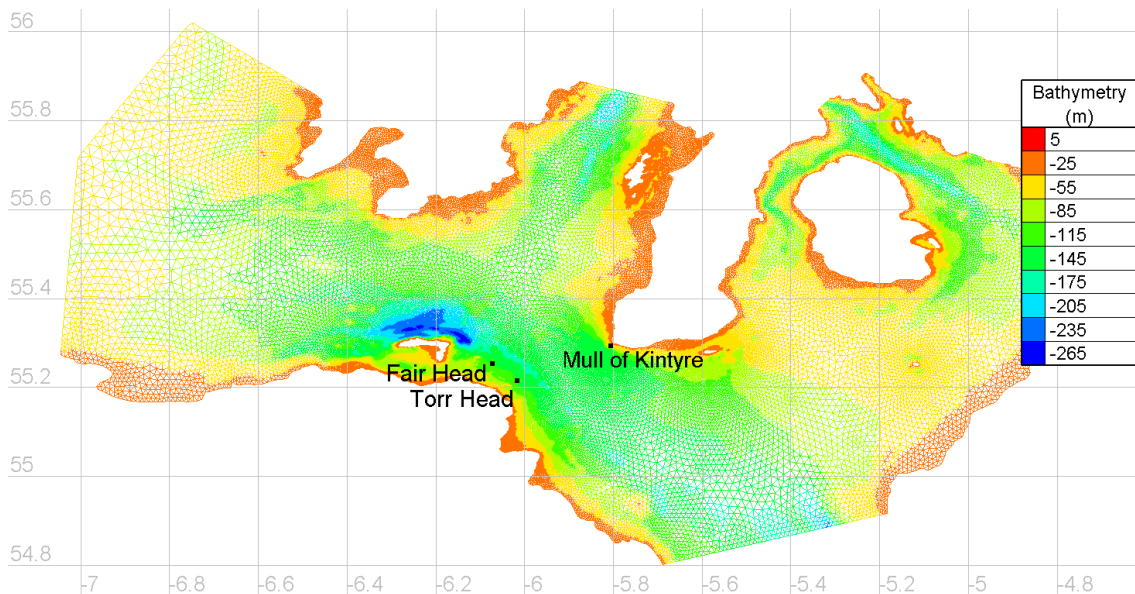


Figure 5-10: Northern Ireland model domain. Locations of the tidal arrays are indicated in black dots.

Using the parameterisation found in Table 5-1, Fair Head is modelled as fifty Seagen-S devices, Torr Head has fifty Openhydro devices and Mull of Kintyre as six Nautricity devices. The turbines at Fair Head were laid out uniformly as five rows of ten devices with a device spacing of ten rotor diameters downstream of each other and a lateral spacing of two and half rotor diameters (EMEC, 2009).

Torr Head is a deeper site with depths reaching 100m within the lease boundary. Based upon the indicative layout of Openhydro devices during Phase 1 of the Brims Tidal Array, a 60m depth limitation was applied along with the device separation limits (Openhydro, 2016). The turbines at the Mull of Kintyre were laid out as a single line of six devices. The layout of the individual devices of each project is shown in Figure 5-11 and Figure 5-12.

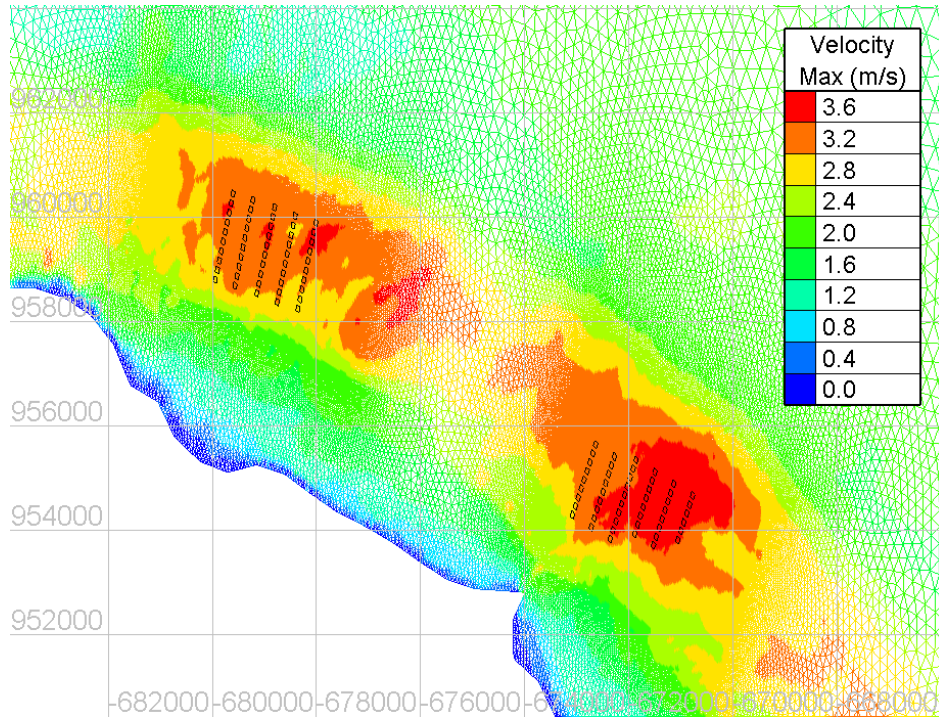


Figure 5-11: Array layout of Fair Head (left) and Torr Head (right) overlaying peak spring velocity.

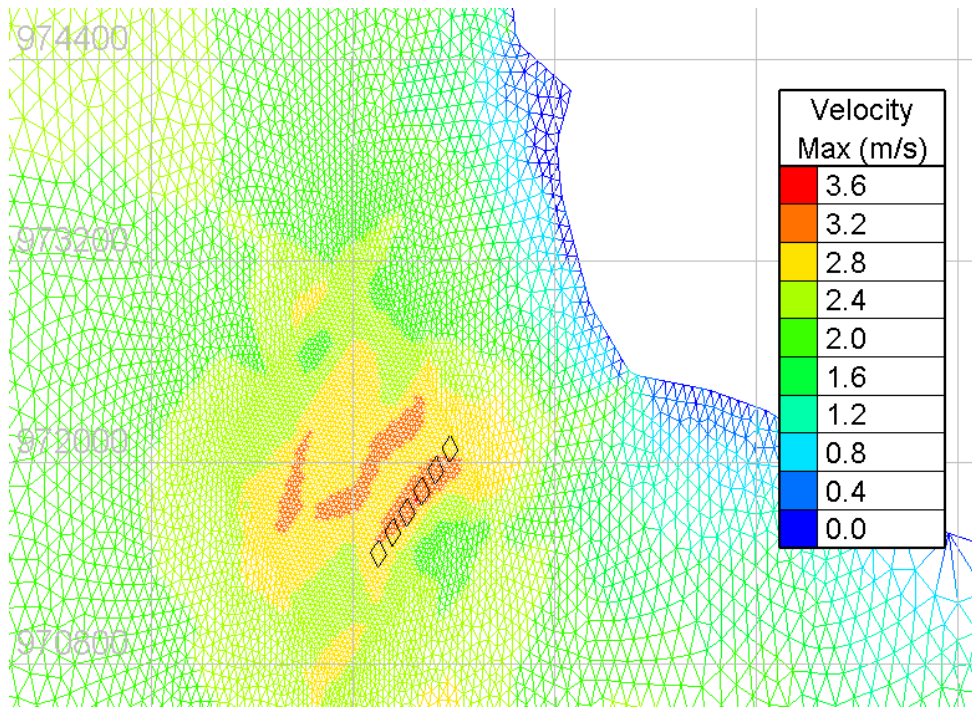


Figure 5-12: Array layout of Mull of Kintyre overlaying peak spring velocity.

To investigate the interaction between the three projects the model was run as eight cases. The first case is the base case with no turbines. The seven remaining combinations included each project individually, two of the projects and finally all three projects. Table 5-7 shows the numbering of the project combinations.

Table 5-7: The eight combinations of Fair Head Torr Head and Mull of Kintyre used to investigate their interaction.

Case	Fair Head	Torr Head	Mull of Kintyre
1	-	-	-
2	X	-	-
3	-	X	-
4	-	-	X
5	X	X	-
6	X	-	X
7	-	X	X
8	X	X	X

#### 5.4.2 Validation

Only one tide gauge, Portrush, falls within the Northern Ireland model. Figure 5-13 shows a scatter plot of the model time series against the tide gauge. The smaller model validates better than the Irish model. It has an  $R^2$  value of 0.962,

a RMSE of 8.3cm and a scatter index of 6.88%. This suggests that the problem with validation of the Irish Sea model lies within an inaccurate transfer of energy from within the central region of the Irish Sea.

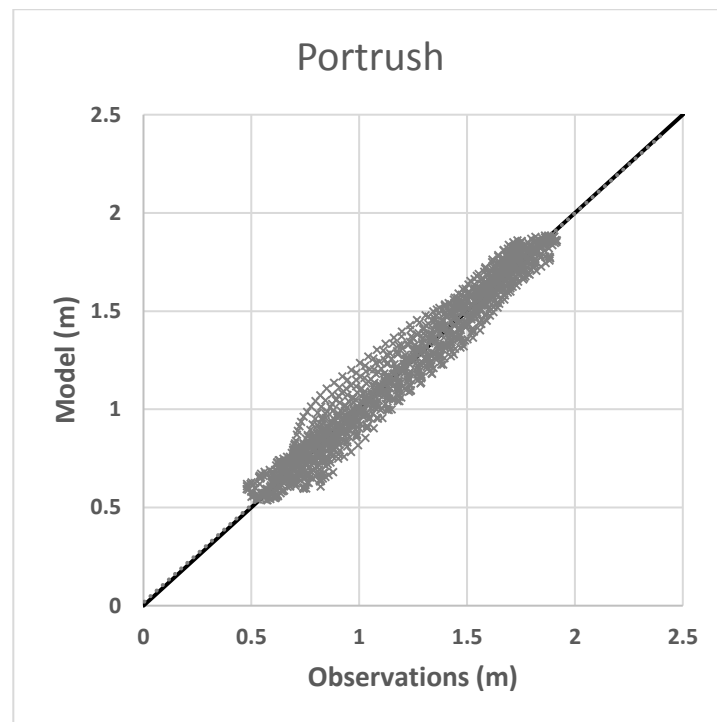


Figure 5-13: Comparison of observed and modelled free surface elevation. The black line represents a  $y=x$  relationship with the dashed line representing a regression line of best fit.

The model base case was run for 30 days to allow enough time to include a sufficient number of harmonic components in the analysis. Harmonic constituents at ten locations were extracted from the TPXO database to validate the model. The location of those ten points are shown in Figure 5-14, along with the location of two tidal current observations.

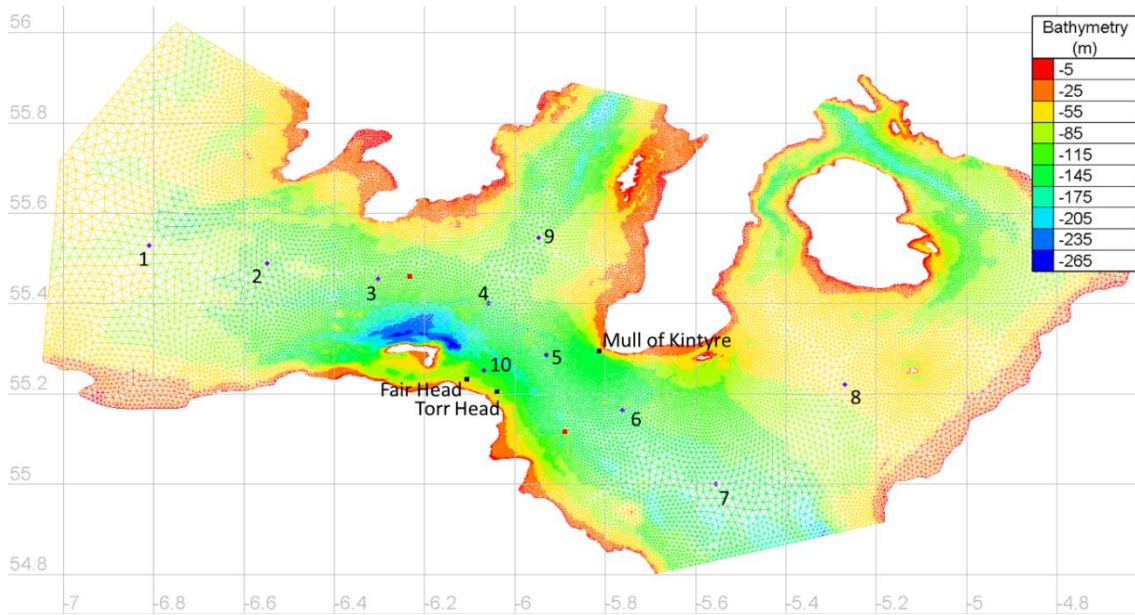


Figure 5-14: Location of harmonic constituents extracted from TPXO database used for validation in purple diamonds and current observations in red squares.

Table 5-8 & Table 5-9 show the comparison between harmonic constituents from the TPXO database and the model for the M2 and S2 constituents. Figure 5-15 shows the comparison between the modelled and observed M2 and S2 constituent amplitude.

Table 5-8: Comparison between observed and modelled M2 constituent.

Location	M2					
	Observed Amplitude (m)	Model Amplitude (m)	Difference (m)	Observed Phase (deg)	Model Phase (deg)	Difference (deg)
1	0.64	0.61	-0.03	164.2	164.0	-0.1
2	0.40	0.36	-0.04	158.1	154.9	-3.2
3	0.13	0.08	-0.06	137.9	145.4	7.5
4	0.11	0.18	0.07	344.9	338.3	-6.6
5	0.38	0.41	0.03	332.3	330.2	-2.2
6	0.74	0.72	-0.02	331.7	329.0	-2.7
7	0.98	0.99	0.01	327.8	326.5	-1.2
8	1.02	1.03	0.01	338.9	337.6	-1.3
9	0.18	0.22	0.04	28.5	15.0	-13.6
10	0.33	0.36	0.02	300.8	301.7	0.9

Table 5-9: Comparison between observed and modelled S2 constituent.

Location	S2					
	Observed Amplitude (m)	Model Amplitude (m)	Difference (m)	Observed Phase (deg)	Model Phase (deg)	Difference (deg)
1	0.30	0.26	-0.03	194.9	194.4	-0.5
2	0.22	0.19	-0.03	189.3	185.0	-4.3
3	0.12	0.10	-0.02	178.2	176.5	-1.7
4	0.05	0.04	-0.01	161.0	133.1	-27.8
5	0.05	0.06	0.01	28.4	29.9	1.6
6	0.17	0.15	-0.02	15.5	16.6	1.1
7	0.25	0.24	-0.01	9.4	10.3	0.9
8	0.27	0.26	0.00	22.2	24.1	1.9
9	0.08	0.08	0.00	136.3	121.4	-14.9
10	0.04	0.04	-0.01	306.4	314.4	8.0

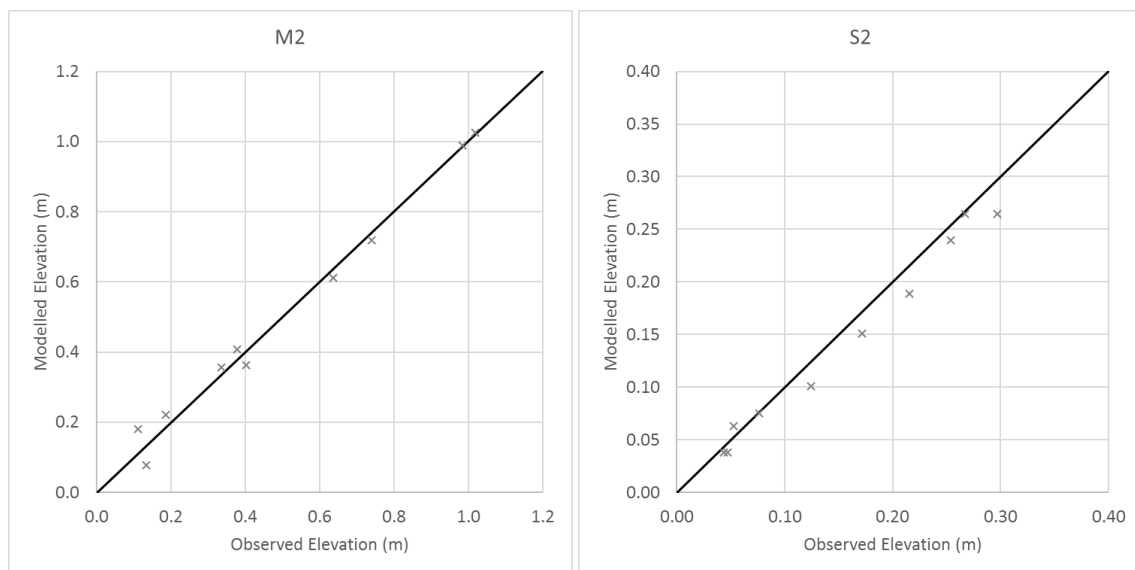


Figure 5-15: Comparison between modelled and observed M2 (left) and S2 (right) tidal constituent.

Results show the Northern Ireland model validates better than the Irish Sea domain. The RMSE of the M2 and S2 amplitude is 4cm and 2cm, respectively, with a scatter index of 7.55% and 3.62%. However, this may be due to the model being validated using harmonics from the same database that drives the model. As the Irish Sea model was validated against tide gauge data, the harmonics from the Northern Ireland model were also compared against the harmonics of the Irish Sea model at the 10 locations, and is shown in Figure 5-16. The M2 amplitude of

the Northern Ireland model is on average 4cm smaller than the Irish Sea model. The S2 amplitude is on average 2cm smaller. The Irish Sea model was found to be slightly over predicting the amplitude of the M2 and S2 constituent, meaning that the smaller amplitudes in the Northern Ireland model show an improvement. As the model shows close agreement to both the TPXO database and the Irish Sea model, the validation of Northern Ireland model will be considered adequate.

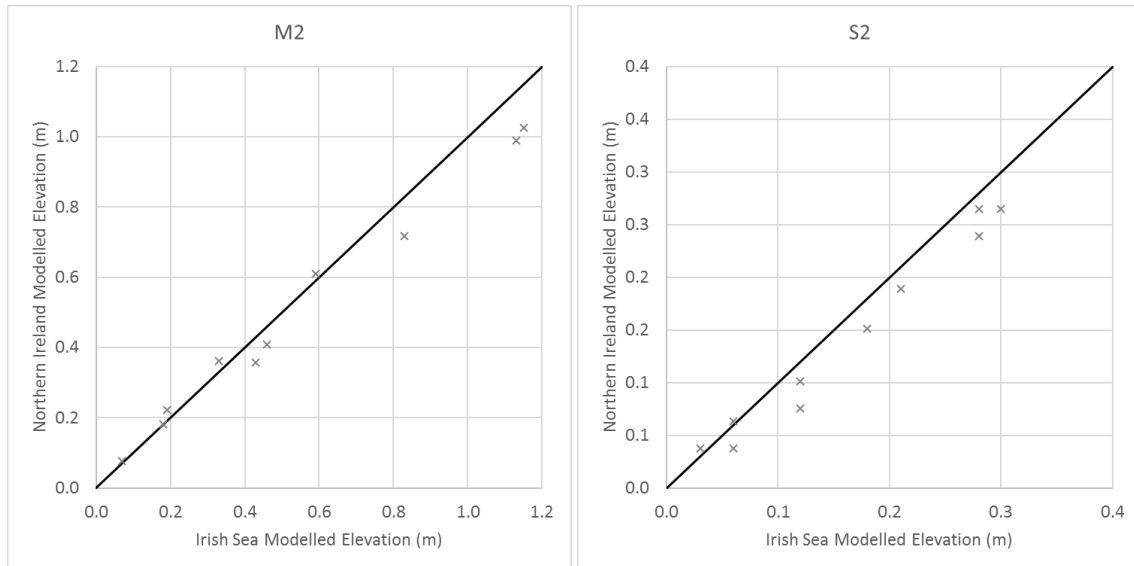


Figure 5-16: Comparison between Northern Ireland and Irish Sea modelled M2 (left) and S2 (right) tidal constituent.

Figure 5-17 shows the maximum tidal range of the 30-day model run. It can be seen that the model is reproducing the known amphidromic point north of Northern Ireland and compares well with Figure 5-6.



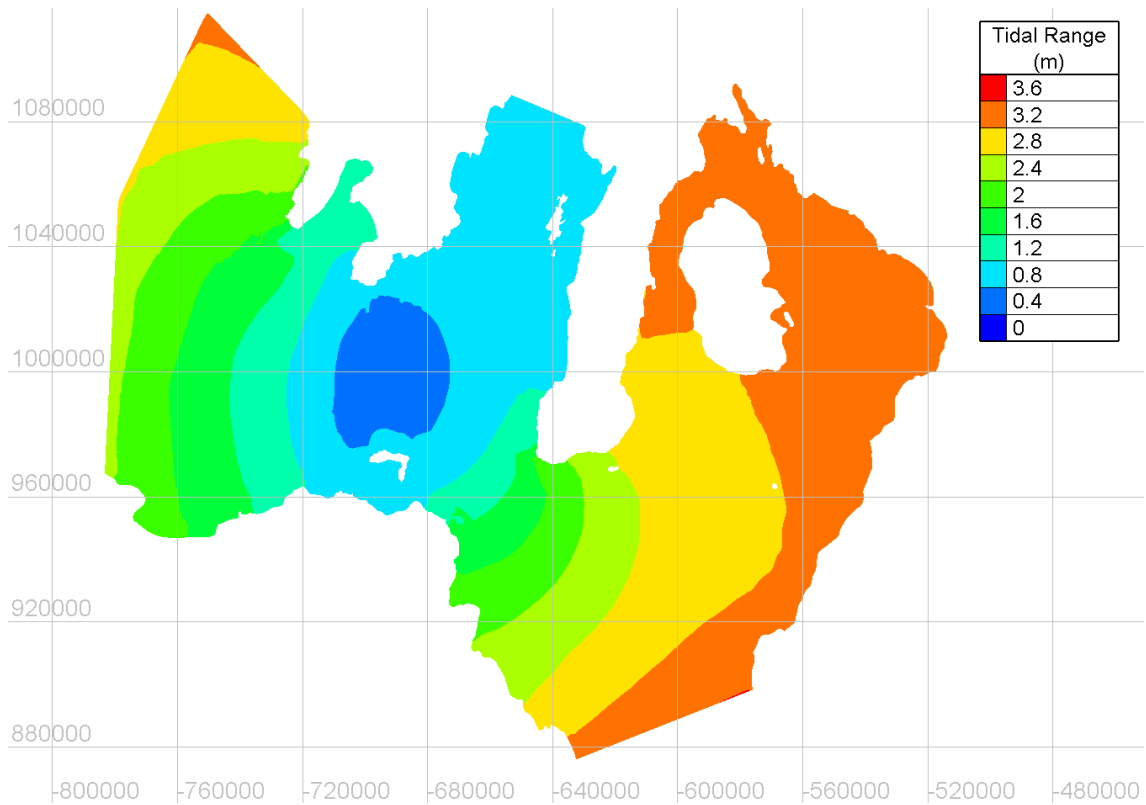


Figure 5-17: Maximum tidal range of the free surface elevations from the 30-day model base case.

As insufficient points from the previous harmonic analysis of tidal currents lie within the smaller model domain, current observations were obtained from the BODC. The two validation points lie to the east and west of the sites of interest and are shown in Figure 5-14. The first observation point was located at 55.46°N and 6.2333°W and recorded tidal velocities between 13-09-1994 16:25 and 29-10-1994 08:35, with a ten-minute interval. The second observation point was located 55.1167°N and 5.8883°W and recorded tidal velocities between 08-05-1995 12:15 and 08-06-1995 08:35, with a ten-minute interval. As the period of observation does not match the period of the model, a direct comparison cannot be made. However, it can be seen in Figure 5-18, that both the shape and magnitude of the tidal velocities are in good agreement.



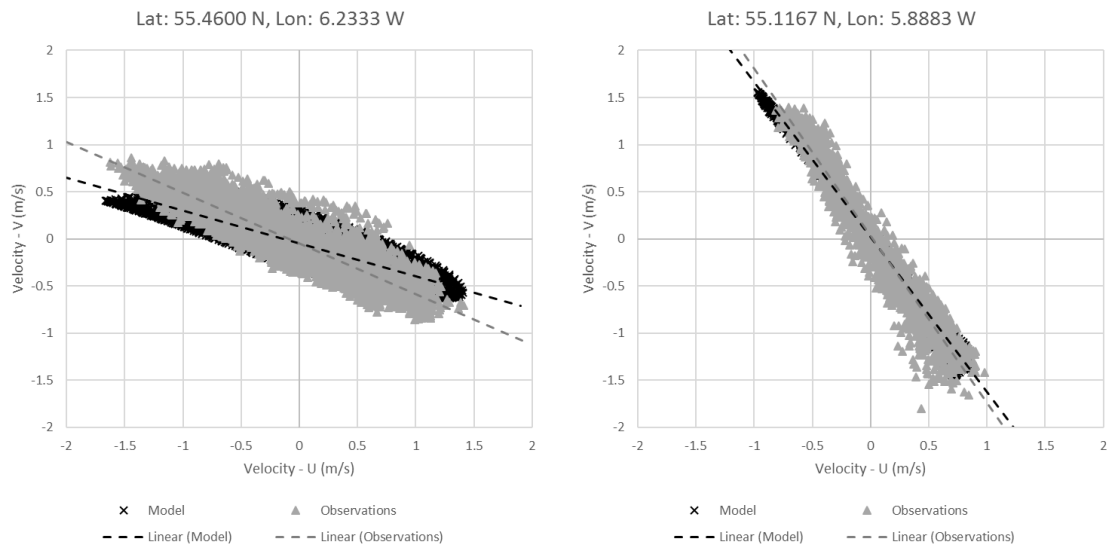


Figure 5-18: Comparison between modelled and observed tidal velocities at 55.46°N, 6.2333°W and 55.1167°N, 5.8883°W.

## 5.5 Results

The base case was run for 30 days to allow for a harmonic analysis for validating the model. The model runs containing the tidal turbines were limited to 10 days and encompass the periods of peak spring and neap tidal velocity. Figure 5-19 shows the range of difference for case 8, with all three projects within the Northern Ireland model.

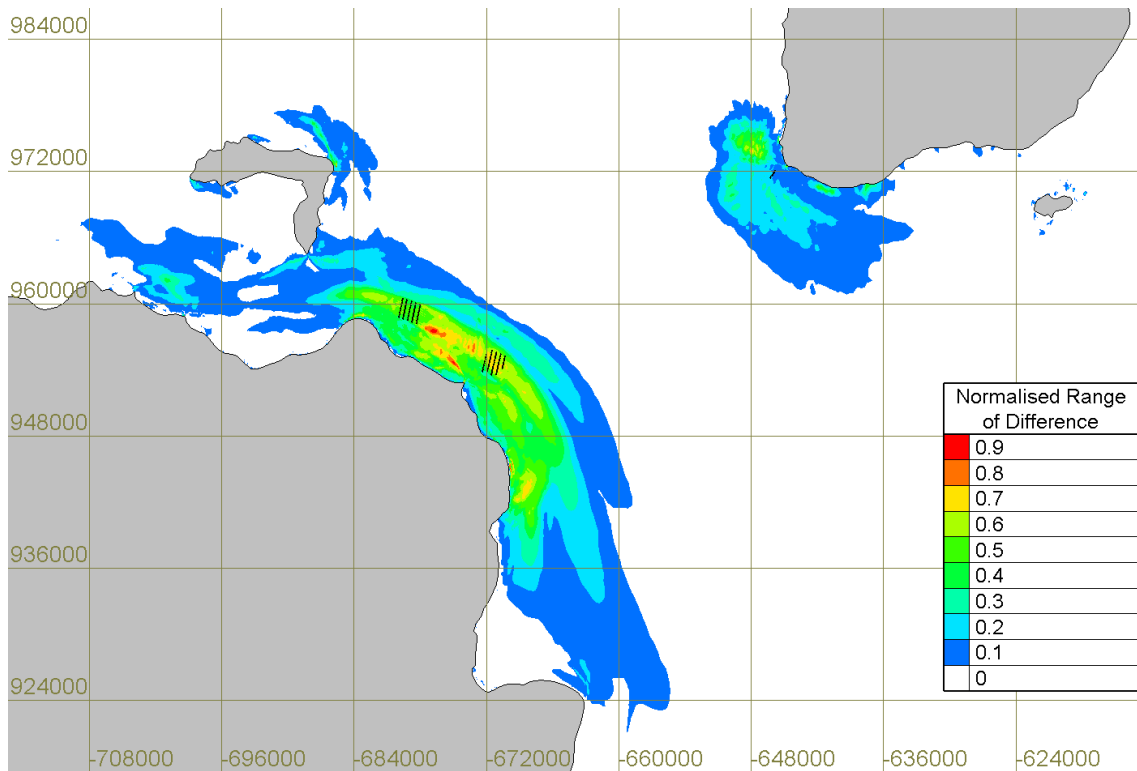


Figure 5-19: Range of difference for case 8 (all three projects). Black outlines represent turbine locations.

The zone of influence around Fair Head and Torr Head extends to a range of approximately 75km. In comparison, the zone of influence around Mull of Kintyre is approximately 20km. This is larger than expected given Mull of Kintyre is using relatively small 500kW devices. The presence of Fair Head and Torr Head systems running together lead to impact off the Mull of Kintyre coastline, regardless of the presence of the 3MW tidal development, as seen in Figure 5-20, Figure 5-21 and Figure 5-22.

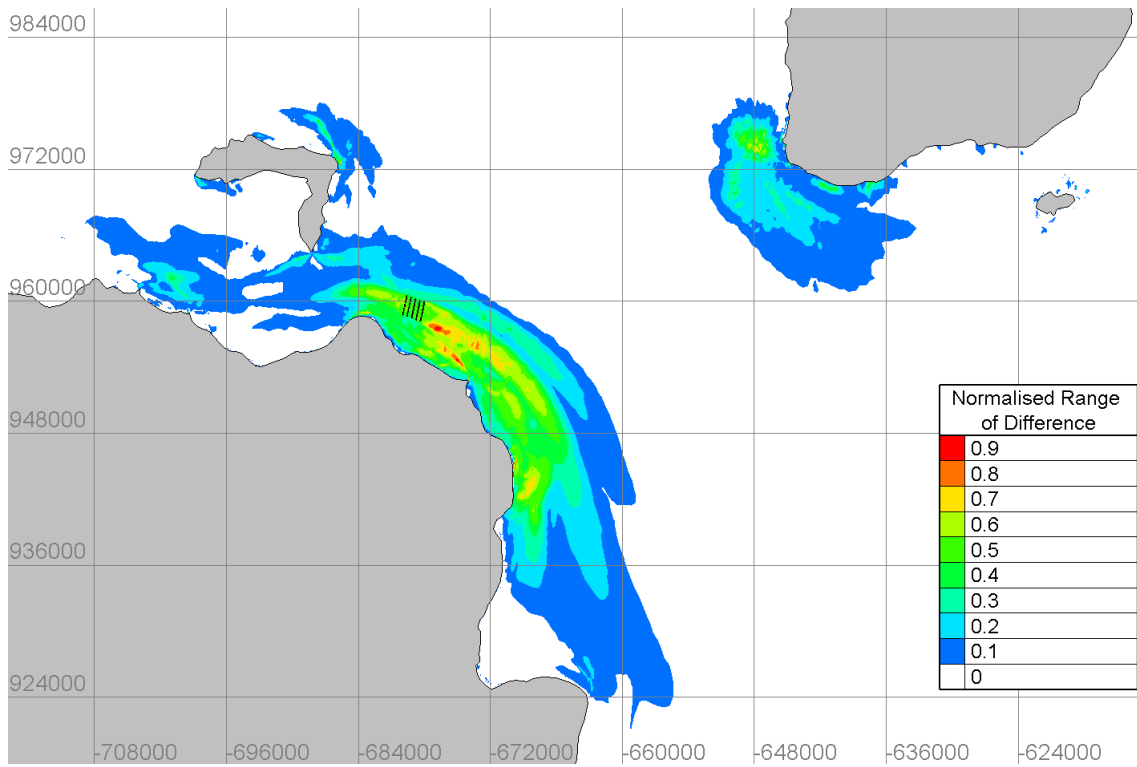


Figure 5-20: Zone of influence for case 2, only Fair Head.

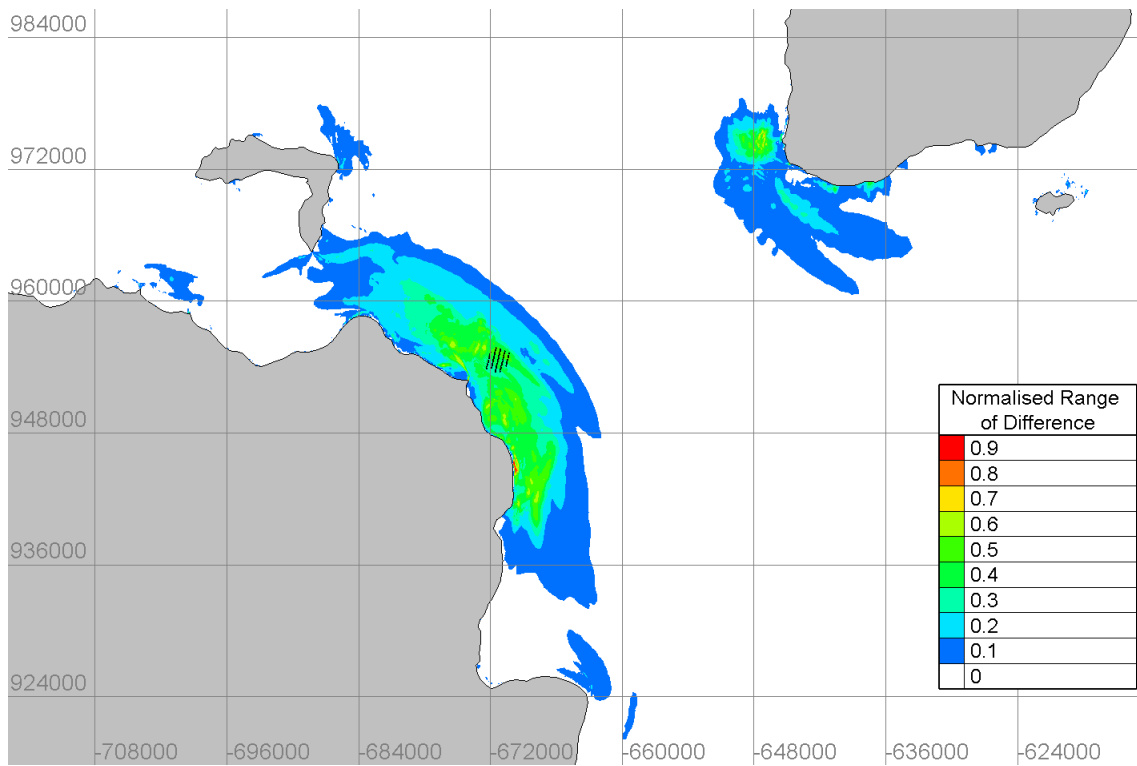


Figure 5-21: Zone of influence of case 3, only Torr Head.

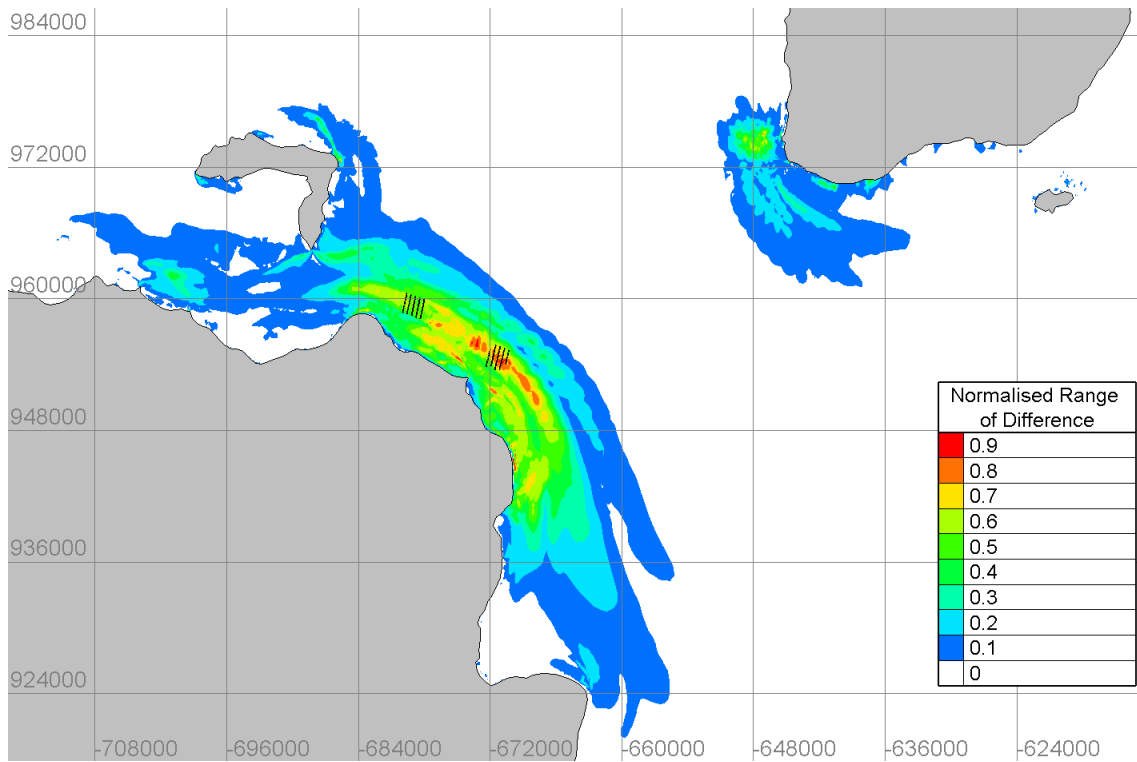


Figure 5-22: Zone of influence of case 5, Fair Head and Torr Head.

Figure 5-20 and Figure 5-21 indicate that Fair Head is having a larger impact than Torr Head and the spatial extent of change due to Fair Head alone is similar to the spatial extent where all three projects are modelled together, shown in Figure 5-19. The true influence of Fair Head can be seen more clearly from the energy production. Table 5-10 shows the total energy produced over the 10-day period. Table 5-11 shows the percentage difference in energy production.

Table 5-10: Energy production of each tidal project for all 8 test cases.

Case	Fair Head (MWh)	Torr Head (MWh)	Mull of Kintyre (MWh)
1	-	-	-
2	4942.0	-	-
3	-	4179.4	-
4	-	-	423.2
5	4828.6	3470.9	-
6	4934.7	-	423.6
7	-	4155.4	423.4
8	4817.1	3464.8	423.6

Table 5-11: Percentage change in energy production for cases 5 – 8.

Case	% Difference		
	Fair Head	Torr Head	Mull of Kintyre
5	-2.29	-16.95	-
6	-0.15	-	0.09
7	-	-0.57	0.05
8	-2.53	-17.10	0.09

From the energy production it can be seen that the interaction between Mull of Kintyre and the other projects is an order of magnitude smaller than the interaction between Fair Head and Torr Head. The Mull of Kintyre project benefits in all cases with the inclusion of Fair Head and Torr Head. Torr Head loses the most energy in this study. The total energy production at Fair Head is reduced by over 2% due to Torr Head, whereas, Torr Head itself loses 17% due to the presence of Fair Head. This caused by a large tidal asymmetry between the flood and the ebb tide. The flood (west to east) is considerably stronger than the ebb (east to west) and can clearly be seen in the power production. Figure 5-23 shows the total instantaneous power production for Fair Head and Torr Head for cases 2, 3 and 5 (both arrays operating separately and operating concurrently).

When both arrays operate separately, the power production is approximately 4-5 times larger on the flood tide than the ebb tide. As Fair Head is situated to the west of Torr Head, the tidal asymmetry means that Fair Head has a larger detrimental effect on Torr Head. During the flood tide, Fair Head extracts energy from the flow reducing the peak velocities at Torr Head such that the power production at Torr Head is reduced to approximately two thirds the power output as if it was operating in isolation. Whereas, during an ebb tide when the flow is slower, the presence of Torr Head only reduces the power output at Fair Head by 20%. Despite both arrays having an installed capacity of 100 MW, when operated in isolation Fair Head never exceeds 40 MW on the ebb and Torr Head never exceeds 30 MW. Furthermore, due to the intra-array effects, the total maximum power output is 97.8 MW for Fair Head and 93.8MW for Torr Head. When the two sites are operated concurrently, the maximum power during the flood tide is 98.1MW for Fair Head and 64.5 MW. This represents a 31% reduction in peak power output.

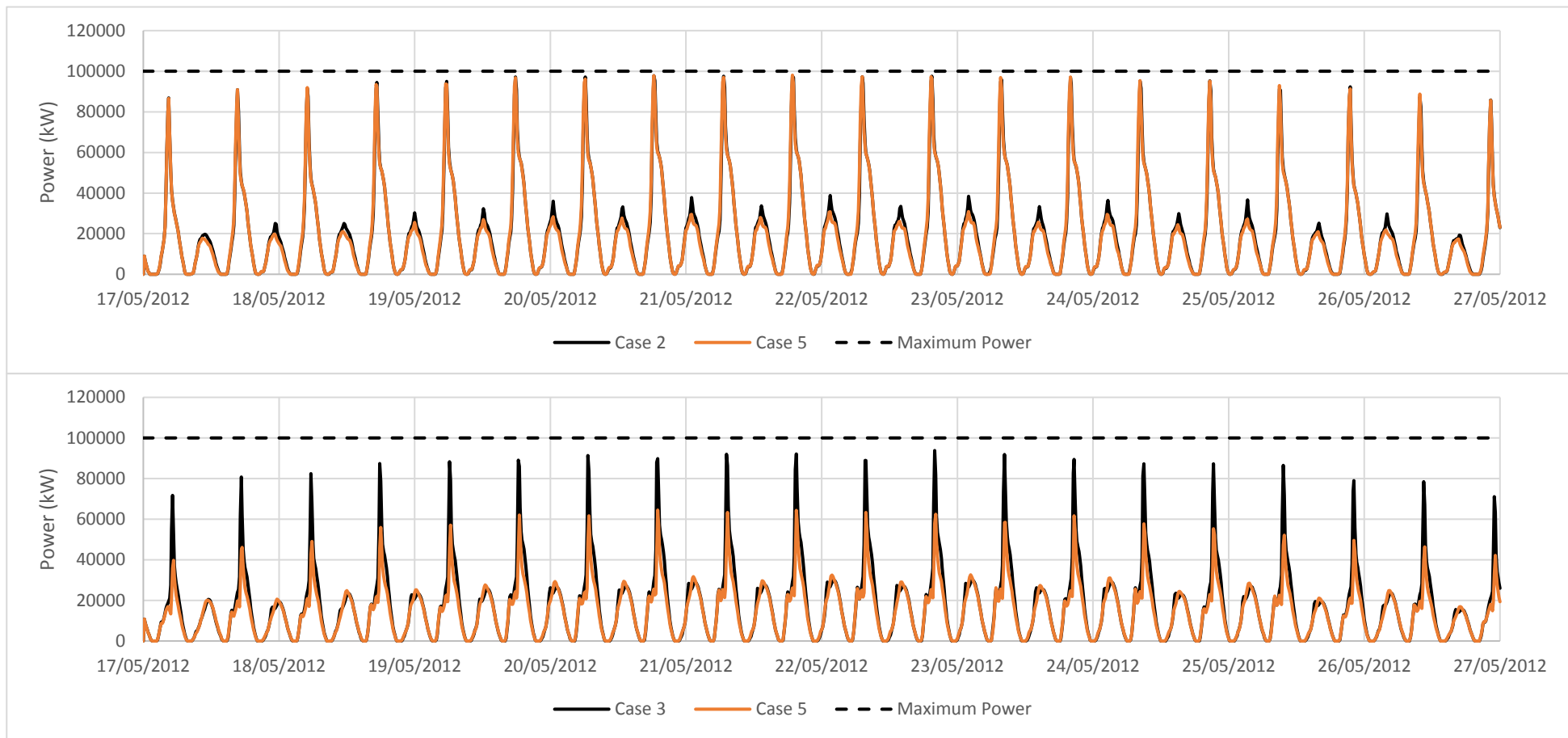


Figure 5-23: Total power production for Fair Head (top) and Torr Head (bottom). The solid black line represents the power production from each array separately (case 2) and the solid orange represents both Fair Head and Torr Head operating concurrently (case 5). The dash black line represents the maximum total power output of each array.

## 5.6 Bed Shear Stress

Maximising the power output within in the constraint of the Levelised Cost of Energy of a tidal project is considered best single outcome for optimising the cumulative deployment of tidal stream energy extraction (Wilson et al., 2012). But, it should also be considered in partnership with the constraint of minimising the environmental impact. The economic viability of tidal energy is not considered within the remit of this study. However, it is clear that with a 17% reduction in energy production, if deployed alongside Fair Head, Torr Head would lose a considerable amount of revenue. However, if Torr Head could still operate commercially despite the presence of Fair Head then there are environmental positives. Comparing Figure 5-19, Figure 5-20 and Figure 5-22, the spatial extent of change is similar. If Fair Head is built, then the additional impact of Torr Head is reduced. The alteration in bed shear stress provides a more intuitive proxy to environmental change. Using Equation 4-4, in Section 4.4.4, the maximum and mean change in bed shear stress has been calculated. Figure 5-24 and Figure 5-25 show the maximum and mean change in bed shear stress for case 8 (all three projects).

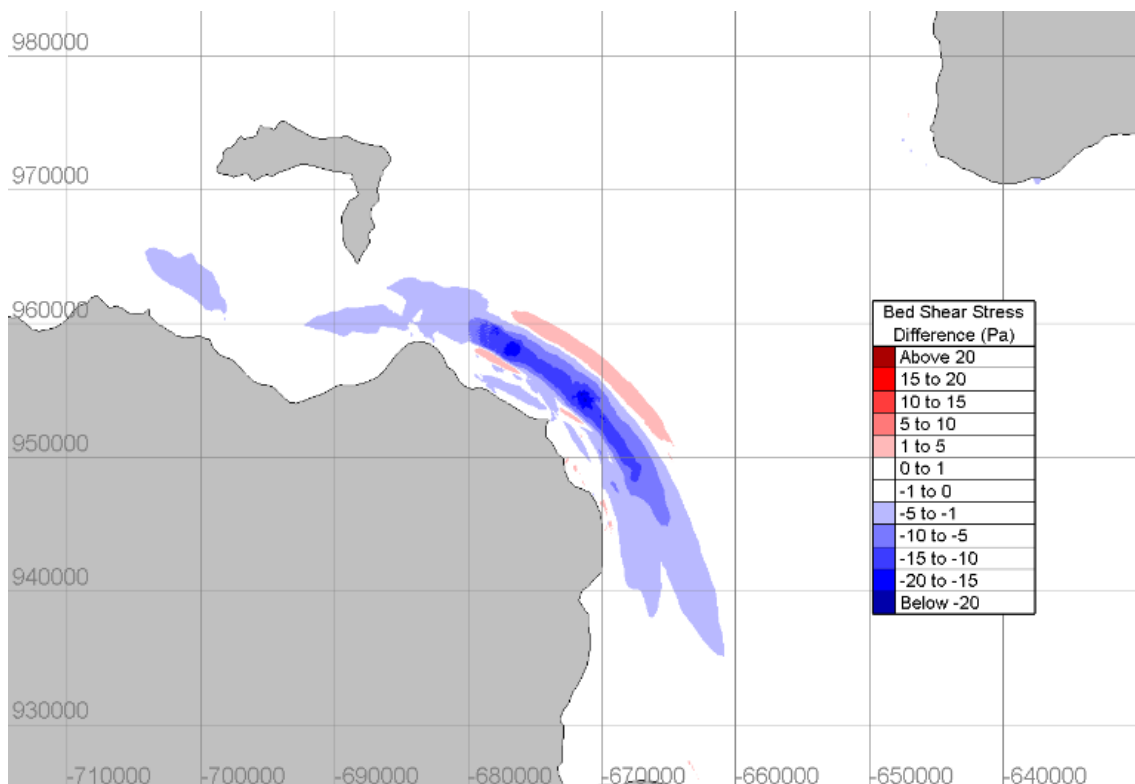


Figure 5-24: Variation in maximum bed shear stress for case 8.

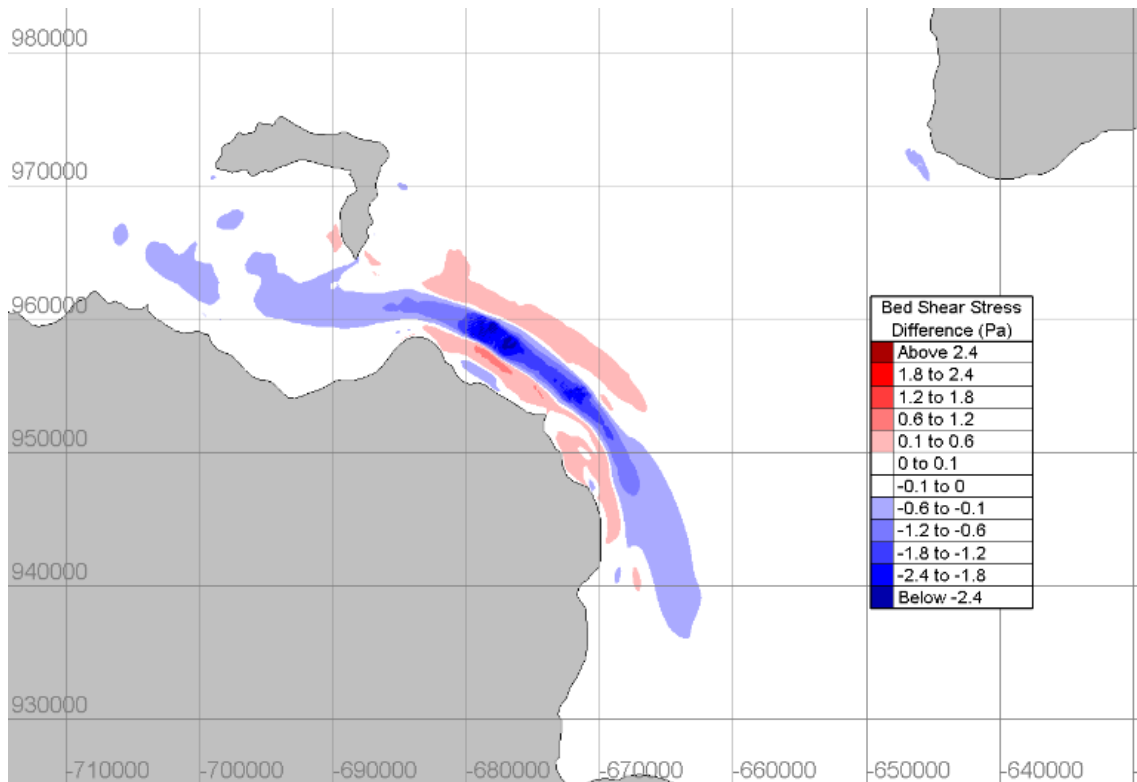


Figure 5-25: Variation in mean bed shear stress for case 8.

Case 8 represents the worst case scenario with all three projects present. Whilst a change could be seen in Figure 5-19 around the Mull of Kintyre, the impact on the mean and maximum bed shear stress is minimal. The major change is limited to the vicinity of Fair Head and Torr Head. For case 8, the peak reduction in maximum bed shear stress is 23.2 Pa. The peak reduction in mean bed shear stress is 2.6 Pa. These values are similar to changes seen in the Pentland Firth, as modelled by Martin-Short et al. (2015). When only Fair Head is present the peak reduction in maximum and mean bed shear stress is 17.5 Pa and 2.4 Pa respectively. Figure 5-26 and Figure 5-27 show the maximum and mean change in bed shear stress for case 2. The black contour represents the extent of change for case 8, as shown in Figure 5-24 and Figure 5-25.



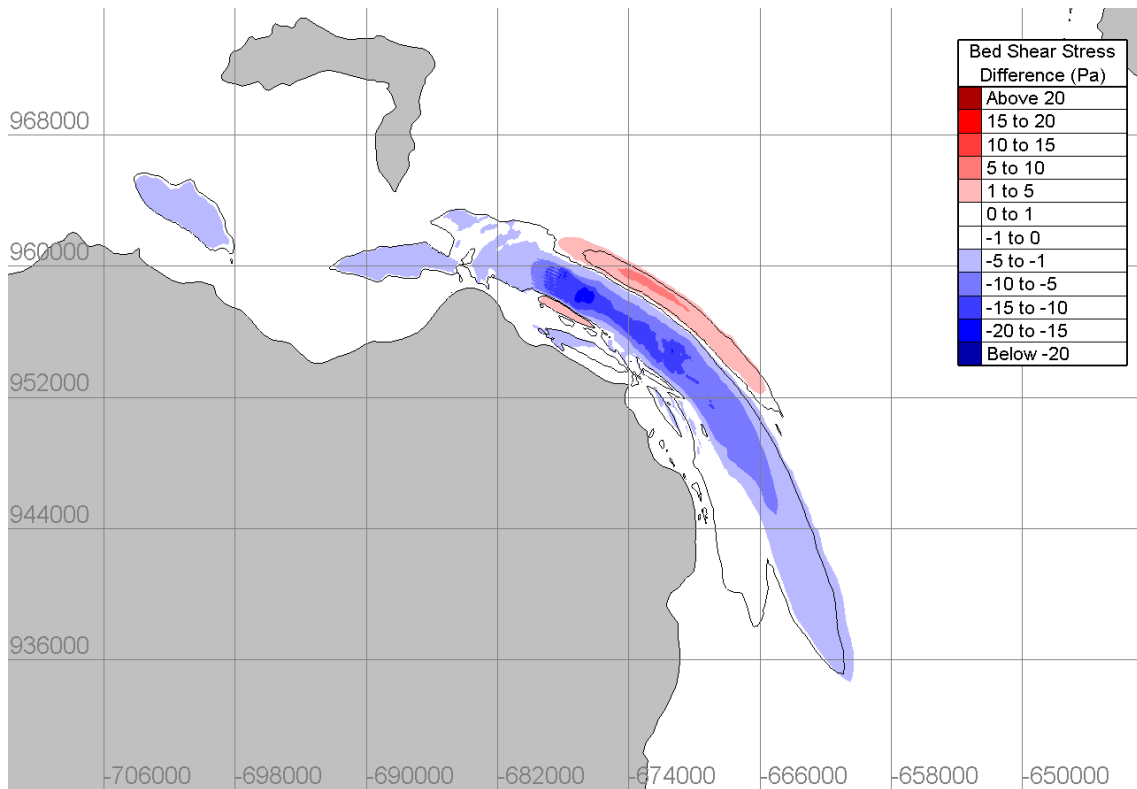


Figure 5-26: Variation in maximum bed shear stress for case 2. The black contour represents the spatial extent of change for case 8.

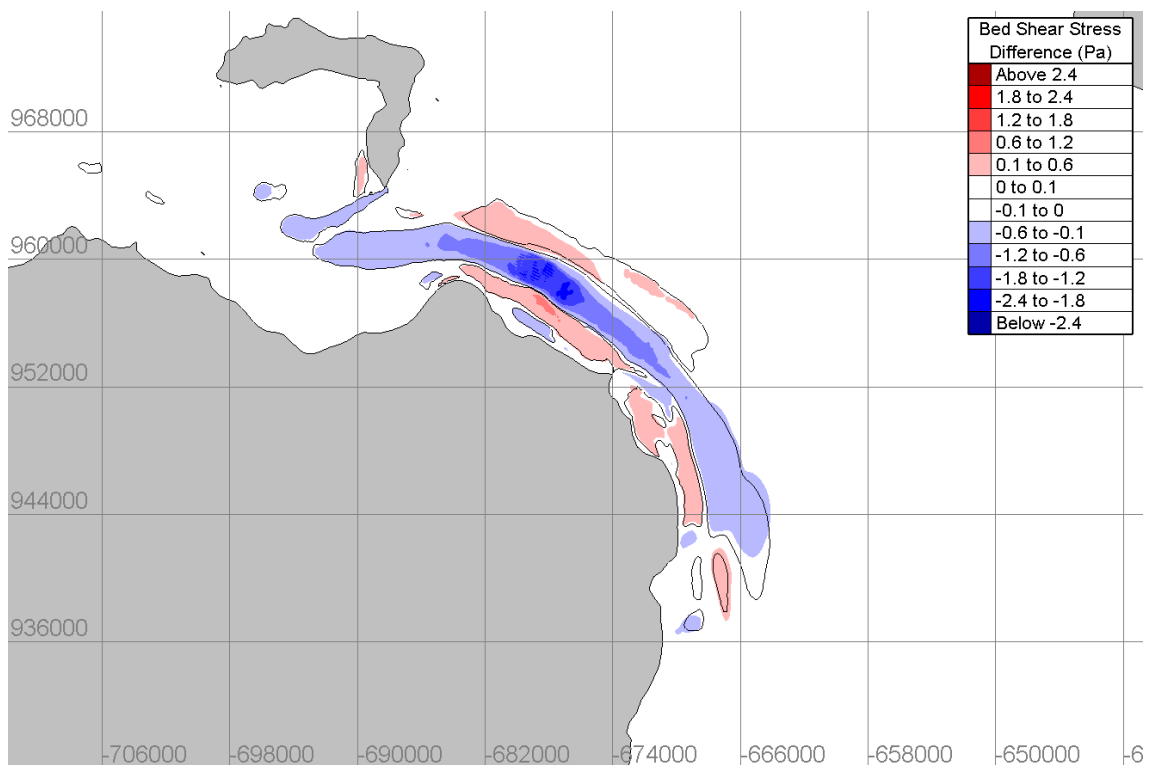


Figure 5-27: Variation in mean bed shear stress for case 2. The black contour represents the spatial extent of change for case 8.

The spatial extent between case 2 and case 8 is very similar. In both cases sediment would accumulate within the vicinity of the arrays with areas of erosion either side. The turbines are located in areas that are void of any fine sediment and are mainly gravel or exposed bed rock (Tidal Ventures, 2015). The magnitude of change would result in medium gravel accumulating in an area of coarse gravel so the impact is likely to be minimal. This change would occur within the Torr Head site with or without the presence of Torr Head if Fair Head was present. Sand is present between the coastline and the tidal turbines and the resulting increase in bed shear stress would likely cause erosion in this area. However, the magnitude of bed shear stress increase is similar in both case 2 and 8. The maximum increase in bed shear stress for case 7 is 4.5 Pa. For case 2 it is 4.0 Pa. The mean increase in both cases is 0.7 Pa. Whilst the seabed around Fair Head and Torr Head is mainly gravel, 40 km to the west is the Skerries and Causeway Special Area of Conservation (SAC). One of the primary designations of the SAC was the protection of sandbanks. It has been shown that tidal stream devices can influence the maintenance of sandbanks (Neill et al., 2012). In this case study, the effect should be minimal. The net transport of sediment to the SAC is from the west (Pingree and Griffith, 1979) and the large tidal asymmetry means any accumulation within the vicinity of the tidal array should transport eastwards. However, the only way to be certain is to use the methodology shown in Robins et al. (2014), which can determine the array size that would not cause an impact above natural variation in sediment transport.

There is a clear interaction between Fair Head and Torr Head. This is due to their proximity and installed capacity. Likewise, with the lack of interaction with the other six sites. The installed capacity of the other sites is significantly smaller than Fair Head and Torr Head. Thus, their zone of influence is much smaller. Although, not investigated, the interaction between Ramsey Sound, Anglesey and Fair/Torr Head, would likely be minimal if their rated capacity were all equal. This is due to distances between the sites. It is approximately 175km between Ramsey Sound and Anglesey and 225km between Anglesey and Fair/Torr Head. The risk of interaction to these sites will be when more intermediary sites are developed. The risk of interaction between other forms of energy extraction in the Irish Sea, i.e. offshore wind and tidal barrages, will be of little risk. The reduction in tidal velocities due to wind turbine monopile structures is negligible (Zhang et al.,

2009). There is no interaction between tidal stream devices and tidal barrages in the Irish Sea (Wilson et al, 2012). Whilst the deployment of tidal stream extraction remains small, ~10MW, the risk of interaction within the Irish Sea is small. As the industry grows and the technology matures, allowing sites with lower peak velocities to be exploited, the risk of interaction will grow. Other tidal sites, such as in the Pentland Firth, where there are four proposed projects geographically within 20km of each other, the potential for interaction is significantly higher.

## 5.7 Summary

A cumulative impact assessment of eight tidal stream developments, totaling 264 MW, in the Irish Sea has been undertaken using a high-resolution depth-averaged hydrodynamic model. Results show that five of the eight tidal projects run quite independently of each other. However, projects at Fair Head, Torr Head and Mull of Kintyre lie within each other's zone of influence. Due to the computational expense of running the model, a second smaller model was developed which included only these three projects.

Results of the second model show that the Mull of Kintyre project had very little impact on the energy production at Fair Head and Torr Head. Energy production slightly increased (+0.09%) at the Mull of Kintyre with the presence of the other two projects. For the two remaining projects, Fair Head had a greater impact on Torr Head than the other way. Torr Head reduces energy production at Fair Head by 2%, whereas Fair Head reduces energy production by 17% at Torr Head. On closer examination, this is due to the tidal asymmetry at the site. The flood (west-east) is stronger than the ebb. As Fair Head lies to the west of Torr Head, the impact is greater. Despite both arrays having an installed capacity of 100 MW, the maximum power during the flood tide is 98.1MW for Fair Head and 64.5 MW for Torr Head. Due to the intra-array effects, the total maximum power output is 97.8 MW for Fair Head and 93.8MW for Torr Head, when operated separately. This represents a 31% reduction in peak power output at Torr Head. Whilst the economics may allow Fair Head to operate commercially with a slight reduction in energy production, a further detailed analysis would be required to determine if Torr Head remains economically viable. However, if Torr Head can still operate commercially in the presence of Fair Head, then the additional environmental impact of Torr Head, such as the change in bed shear stress, is small.

Within the Irish Sea, very few tidal projects investigated are geographically within close proximity of each other, meaning their interaction is limited. Whilst the deployment of tidal stream extraction remains small, ~10MW, the risk of interaction within the Irish Sea is small. As the industry grows and the technology matures, allowing sites with lower peak velocities to be exploited, the risk of interaction to these sites will grow when more intermediary sites are developed.

# Chapter 6

## Modelling the Benthic Environment

### 6.1 Introduction

The purpose of this chapter is to outline what the benthic environment is and why changes to habitats should be assessed. It will discuss the role of species distribution modelling, using the software package MaxEnt (Phillips et al, 2006) and how it can be used for the assessing the impact of tidal turbines on the benthic environment. Continuing the numerical modelling of tidal turbines in Chapter 4, the application site chosen for investigation is the 10 MW tidal array at St David's Head, Pembrokeshire. This chapter outlines the different species chosen for the species distribution modelling. It discusses the setup of the MaxEnt model, describing the background variables used to develop the model. After the assessment of the models performance, it presents the results of the case study and then discusses their impact.

### 6.2 Benthic Environment

#### 6.2.1 Defining Benthic Environment

The term 'benthic environment' is used here to express both the physical benthic zone and habitat, along with the species that inhabit this zone, referred to as benthos. The benthic zone is the bottom surface layer, penetrating into the

subsurface of the seabed. In contrast, the rest of the entire water column from the seabed to the surface is known as the pelagic zone (Costello, 2009). The benthic zone is comprised of a range of physical substrates including mud, sand, gravel and rocky outcrops. This substrate composition is influenced by hydrodynamic conditions such as water depth, tidal currents and wave exposure. It is this close relationship between the benthic substrate, hydrodynamics and the benthos that dictates where different species are found. Due to the high spatial variability in the types of habitats found in coastal regions, marine biodiversity tends to be higher in the benthic zone than the pelagic zone (Gray, 1997). The suitability of one habitat to a particular species does not necessarily translate to another. Each benthic species will populate a niche, regardless of anthropogenic stresses, providing it can tolerate its environment (Burd et al., 2008).

### 6.2.2 Role of Benthos in the Food Web

Traditionally, the benthic zone has been seen as the bottom layer of the food web system, with the top layers feeding down to the bottom. However, the coastal and ocean linkages between the benthic and pelagic systems are much more complex and often misunderstood (Rolet et al., 2015), leading to continual study (Denderen et al, 2016; Zheng et al., 2015).

A simplified representation of the food web is shown in Figure 6-1. The pelagic zone is represented by the following species: fish, phytoplankton, zooplankton. Detritus and dissolved nutrients are also found in the water column. The benthic zone is comprised of the benthos and the sediment stored on the seabed. Phytoplankton are microscopic plants and zooplankton are microscopic animals. However, not all zooplankton are microscopic. Jelly fish are examples of larger zooplankton species. Detritus is debris in the water column produced by either sediment erosion or organic material produced by decomposing organisms. Oceans take up atmospheric gases such as nitrogen and carbon dioxide, dissolving them into the water column, through phytoplankton. The dissolved nutrients are taken up by the phytoplankton, which in turn are taken up by the zooplankton. The fish take up the zooplankton and benthos, releasing detritus.

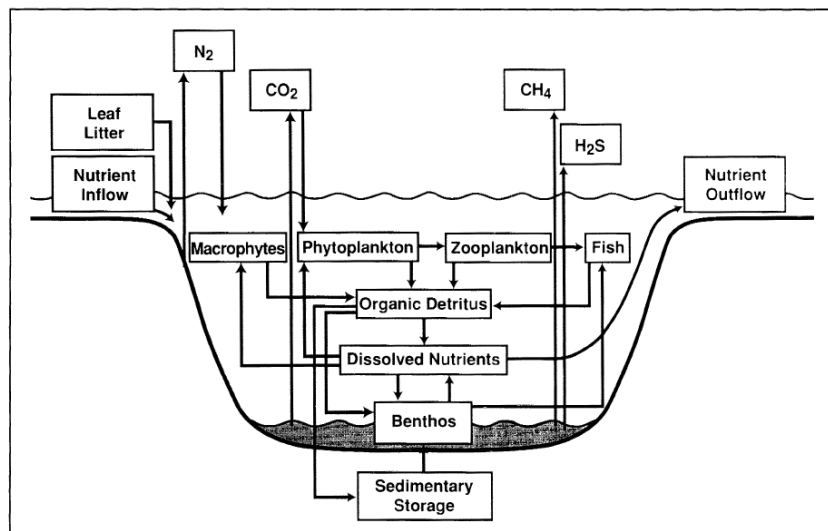


Figure 6-1: Role of benthos in cycling nutrients. Figure originally from Covich et al (1999).

The benthos plays an important role in the food web by processing and transforming nutrients in the system. The benthos consumes the detritus and dissolved nutrients combining it with the sediment. But it also releases nutrients back into the system along with gases, such as nitrogen and carbon dioxide. Not only do the benthos act as a filter, cleaning the water column, it acts as a buffer. It controls the exchange nutrients stored in the sediments and the water column stopping an excessive build-up of nutrients leading to eutrophication (McGlathery et al., 2007).

Eutrophication is the process whereby excessive nutrients can lead to an increased production of phytoplankton and algae blooms and a reduction of dissolved oxygen in the water column, although, harmful algae blooms can occur naturally (Berdalet et al., 2015). These excessive nutrients can have negative impacts on the ecosystem. Anthropogenic sources, such as agriculture, industrial activities and coastal populations, have increased the supply of nitrogen and phosphorus in coastal regions (Ferreria et al., 2011). There are two distinct forms of harmful algae blooms: high and low biomass (Davidson et al., 2014). When high biomass blooms occur, it can lead to a reduction of dissolved oxygen when the bloom sinks within the water column and is decomposed on the seabed. This can lead to a reduction in biodiversity in areas affected (Khan & Mohammad, 2013). Low biomass harmful algae blooms are much smaller in concentration but produce biotoxins that are harmful to both humans and fauna. These toxins are concentrated in benthic species, such as shellfish, and can lead to poisoning of the benthos, risking exposure to humans (Backer & McGillicuddy, 2006). As such,

benthic species are commonly used as bio-indicators to assess the health of the ecosystem from contamination (Stein et al., 1992; Coccioni, 2000; Frontalini & Coccioni, 2011).

### 6.2.3 Anthropogenic Impact on the Benthic Environment

Many benthic species are either sessile (non-mobile) or semi-sessile. Due to high site fidelity they are easy to examine spatially and temporally meaning they are ideal subjects for studying the impacts of disturbances (Arntz et al, 1999). The presence of species in the benthic environment is influenced by climatic conditions and available resources meaning its distribution will spatially vary over time. Despite this, it does remain relatively consistent. However, it varies considerably under pressures from anthropogenic sources (Frid, 2011). The impact of commercial fishing on the benthic environment is well studied (Auster et al., 1996; Ball et al., 2000; Collie et al., 1997; Engel, 1998; Sparks-McConkey & Watling, 2001). Impacts of heavy trawling include, but are not limited to, removal of physical habitat, decreased biomass and alteration of the types and numbers of species found. However, benthic communities have been shown to recover from anthropogenic changes (Retière, 1994; Borja et al., 2010; Whiles & Wallace, 1995). An example is the 240 MW La Rance tidal barrage which has been operational since 1966. Due to its construction and operation the La Rance basin saw significant changes in tidal range, water salinity and sediment transport, causing a radical shift in the ecosystem. However, after 10 years of recolonization, the environmental system is considered balanced and rich in species (Retière, 1994; Kirby and Retière, 2009).

Not all disturbances are necessarily bad. Small-scale disturbances can create patchiness in resources leading to a greater diversity within a community (Thrush & Dayton, 2002). This in turn is important in creating a fully functioning ecosystem. Many species fill a niche within a system, obtaining resources in different ways. Whilst different species adapt to take on different functions, the relative importance of different species will vary within the system (Covich et al, 1999). The loss of an individual species due to a disturbance may not impact the system providing its function is fulfilled by another species. Depending on the scale of the disturbance, neighbouring species may quickly repopulate the area.



The construction phase of marine renewables will clearly have an impact on the benthic environment through physical disturbance to the seabed, but in the long term it may provide benefits. Beam trawling through offshore wind farms is prohibited, creating protected areas. These ‘no fish’ zones may become important in allowing sensitive species to recover. It has been recorded that species abundance has increased within an offshore wind farm off the Belgian coast (Coates et al., 2016). Furthermore, the introduction of hard substrates, i.e. steel and concrete monopiles, creates new habitats and can lead to reef effects increasing biodiversity (Andersson et al., 2009).

Hydrodynamic modelling in the previous chapters have shown that tidal turbines do have an influence on hydrodynamics, which in turn will alter the morphodynamics. The main impact of a tidal turbine is the reduction in current velocity which in turn reduces bed shear stress. Bed shear stress is the prime driver of sediment transport meaning any change will result in a change in the sediment class distribution. This could lead to sediment erosion and accumulation leading to a change in the habitat substrate. As sites of high tidal flow can produce large concentrations of suspended sediments (Robins et al., 2014), a reduction in current velocity will lead to an increase in the settling of suspended sediments. As many benthic species are sessile they are at a greater risk of burial. Not all species are able to recover from being buried (Hinchey et al, 2006).

#### 6.2.4 Habitat Mapping

In the context of classifying the marine environment, habitat mapping is the process of spatially mapping the different physical habitats on the seabed. Typically, this is carried out by remote acoustic sensing and validated using physical grab samples and drop down cameras. However, a habitat is more than just its physical environment. A more robust definition is provided by Kostylev et al. (2001) whereby a habitat is *“a spatially defined area where the physical, chemical, and biological environment is distinctly different from the surrounding environment”*. This combination of physical and biological components, referred to as abiotic and biotic respectively, are used to classify habitat biotopes.

Habitat mapping has become an integral part of the marine spatial planning process. Marine spatial planning is the process of bringing together all interested

stakeholders in the marine environment to ensure it is used and managed sustainably. The use of habitat maps allows for spatial planning (Ezhova et al, 2012), fish stock assessments (Getsiv-Clemons et al., 2011) and the creation of marine protected areas (MPA) (Allee et al., 2011). In 2012, the Scottish Government conducted public consultations to develop a marine spatial plan in Scottish waters. One of the results was the production of data layers that provide assistance to developers in site selection for wave and tidal energy sites (Scottish Government, 2016).

To assist the process of habitat mapping, standard habitat classification systems are widely used around the world. For example: The Coastal/Marine Ecological Classification Standard (CMECS) in the USA (Madden and Grossman, 2007), the Integrated Australian Classification Scheme (Last et al., 2010) and Global Open Ocean and Deep Sea-habitats Classification (Agnostini et al., 2008). In the UK, the EUNIS habitat classification is used. The European Nature Information System (EUNIS) was developed by the European Environment Agency for use on the European continental shelf (EUNIS, n.d). There are several levels to the hierarchy of the EUNIS classification. Level 1 distinguishes between the terrestrial and marine environment. Level 2 defines eight broad scale habitats. The level 3 further subdivides the Level 2 habitats based on sediment type. Level 4 subdivides based on the biotope. Levels 5 and 6 are finer subdivides with increasing finer biotopic detail. Figure 6-2 shows an example breakdown of the EUNIS classification.

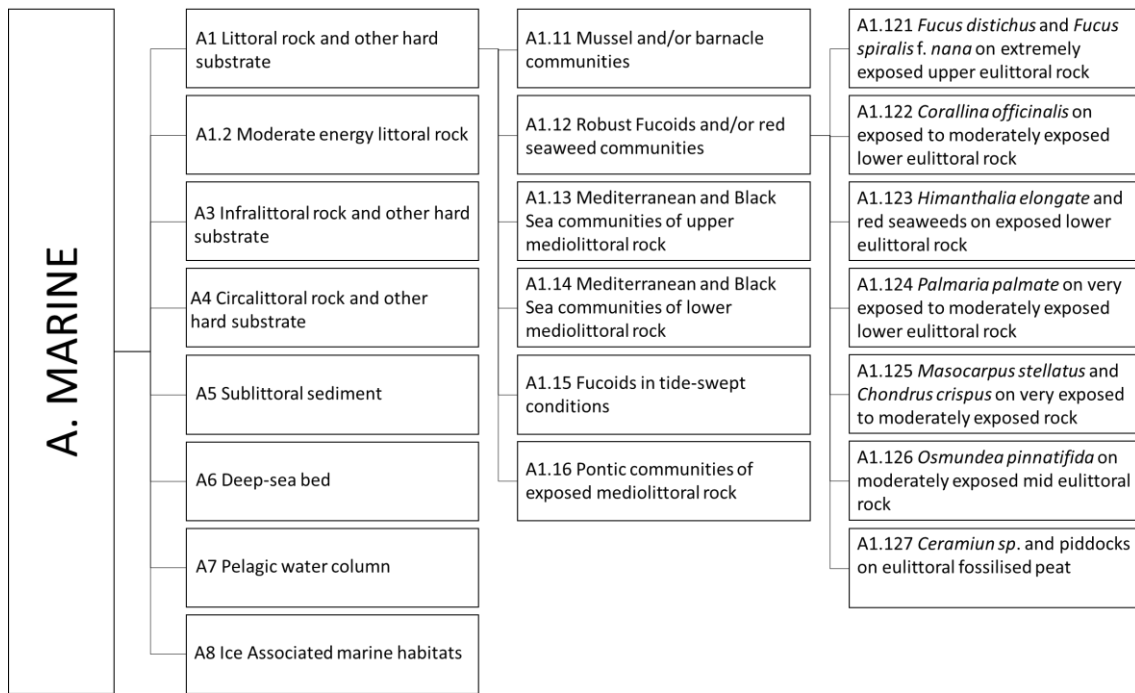


Figure 6-2: Example breakdown of the EUNIS Habitat Classification

Level 3 habitat maps of the entire UK shelf are available (see [www.emodnet-seabedhabitats.eu/webgis](http://www.emodnet-seabedhabitats.eu/webgis)), largely down to the ability to create geological maps through the use of remote acoustic sensing. Multi-beam acoustic sensors allow for collection of large swathes of bathymetric data. Backscatter data from the multi-beam gives the ability to further determine the type of sediment (Simons and Snellen, 2009). Level 4 maps are much harder to produce than level 3 because of the lack of ability to remote sense the biotic component of the habitat. This data is collected through physical grab samples or in situ observations through divers and drop down cameras (Anderson et al., 2007; Eleftheriou, 2013; Mallet and Pelletier, 2014). It is difficult to create Marine Conservation Zones (MCZs) that target a specific species for conservation because of the effort to physically locate them. But by understanding the type of habitat and community they are associated with it is easier to create areas that protect the habitat rather than a specific species (Friedlander et al., 2003).

The problem then with assessing the impact of tidal turbines on the benthic environment through the use of habitat maps is that they are too broad. It is possible to map the change in habitat as a result of the presence of tidal turbines but the problem then lies in inferring the change to benthos. As “*different species can occupy the same ecological niche in different occurrences of the same habitat*” (Harris and Baker, 2012) it requires detailed understanding of which

species are actually present and their preferred habitat. Furthermore, benthic species can have a range of tolerances to the type of habitat, meaning that a change in physical habitat may not result in a change of species occurrence. An alternative method for assessing the impact is to use species distribution modelling.

### 6.2.5 Species Distribution Modelling

The use of species distribution modelling allows for the prediction of occurrence for a particular species. A species distribution model works by using two types of data: the geolocation of an observed occurrence of a species and background conditions found at that location of occurrence (Elith and Leathwick, 2009). The background conditions could be anything that is variable that influences the likelihood of occurrence, such as depth, temperature, current speed etc. The model then determines a relationship between the observations and the background conditions at the location of the observations. From this relationship, a prediction is made on the likelihood that that species may occur within the rest of the model domain.

There are a number of different models used for species distribution modelling, but they fall into two main types based on their observation data: presence-absence models and presence-only models. Presence-absence data is the result of a systematic sampling regime whereby a species presence is recorded but also importantly where it is not present (Elith et al, 2006). This provides a much clearer indication of the distribution of a species. However, most observation datasets do not include absence data, meaning methodologies that require presence-only data are increasingly being used (Reiss et al, 2011; Huang et al, 2011; Elith et al, 2006).

There are three main techniques for species distribution modelling: environmental envelope, regression and machine learning (Elith et al, 2006). An envelope model calculates bioclimatic envelopes for each predictor variable. The model then predicts the suitability of a site providing all the variables are within their envelopes for that point. An example environmental envelope model is BIOCLIM (Busby, 1991). A similar model is DOMAIN, which uses proximity in environmental space to calculate its envelopes (Carpenter et al, 1993). Both BIOCLIM and DOMAIN are examples of presence only models. Regression

based techniques such as the use of a Generalized Linear Model (GLM) uses parametric terms to fit linear functions between predictor and response variables (Hastie and Tibshirani, 1990). A variation on this is the Generalized Additive Model (GAM), which uses non-parametric terms to fit nonlinear functions (Zaniewski et al., 2002). Both GLMs and GAMs are examples of presence-absence models. Machine learning uses algorithms that learn from their input data in order to make predictions without following strict programming. Two examples are Genetic Algorithm for Rule set Production (GARP) (Stockwell, 1999) and MaxEnt (Phillips et al, 2006). Both GARP and MaxEnt are examples of presence-only models.

All of these techniques are widely used. As such, their comparative performances have been comprehensively assessed. Reiss et al. (2011) compared nine different species distribution models, Huang et al. (2011) compared fifteen models and Elith et al. (2006) compared sixteen models. Based on model evaluation measurements, such as receiver operating characteristic curve and kappa, all three studies conclude that MaxEnt is the best performing model.

### 6.2.6 Species Distribution Modelling using MaxEnt

MaxEnt is a freely available and widely used machine learning software package for species distribution modelling, with over 1000 published applications between 2006 and 2013 (Merow et al., 2013). It has been applied in both the terrestrial (e.g. West et al., 2016) and marine environment (e.g. Breen et al., 2017) to model fauna species distributions, the distribution of flora species (e.g. Yang et al., 2013), the distribution of infectious diseases (e.g. Lawrence et al., 2016) and used to assess current and future habitat suitability (e.g. Remya et.al., 2015). The following description is a summary of how MaxEnt works, provided in detail by Phillips et al. (2006) and further by Elith et al. (2011).

MaxEnt is a presence only model that estimates the species distribution of a target species. MaxEnt is short for the principle of Maximum Entropy. Jaynes (1957) describes the best approach to approximating an unknown probability distribution, subject to constraints, is that the distribution should have maximum entropy. Maximum entropy means a distribution that is closest to uniform. MaxEnt requires three inputs to make a prediction: the geographic region of interest, locations of known observations and background predictor variables, such as

depth, temperature, salinity etc. For a geographic region of interest, the space,  $X$ , is discretised into a finite set of grid cells. In this space, a set of points  $x_1, \dots, x_m$  represent the point locations of where a species is known to occur within an unknown distribution,  $\pi$ .

The aim of MaxEnt is to predict a species distribution,  $\hat{\pi}$ , from the point observations subject to environmental constraints, that approximates to the unknown distribution,  $\pi$ . In constructing the predicted distribution, the model is constrained with a number of background predicted variables, or features  $f_1, \dots, f_n$  where  $f_j : X \rightarrow \mathbb{R}$ . Whilst unconstrained, it can be expected that  $\hat{\pi}$  does not represent  $\pi$ . Whereas, for a given function,  $f : X \rightarrow \mathbb{R}$ , it is expected that the empirical average,  $\tilde{\pi}[f]$ , or expectation, is close the true expectation,  $\pi[f]$ . Therefore, the aim is to seek an approximate distribution,  $\hat{\pi}$ , where the expectation of all the features,  $f_j$ , is equal to the empirical average,  $\tilde{\pi}[f]$ , for each feature. In practical terms, the model is supplied with training data of known observations of the target species and the background variables found at those locations. From those observation points the model has an observed probability distribution of each background variable. The model then limits its prediction whereby for each feature the mean of the probability distribution at the locations of the predicted species distribution equals the mean of the observed features probability distribution.

As there are many possible distributions that can satisfy the constraints of the features, the maximum entropy principle is to choose the one that is closest to uniform. The entropy of  $\hat{\pi}$  on  $X$  is defined as:

$$H(\hat{\pi}) = - \sum_{x \in X} \hat{\pi}(x) \ln \hat{\pi}(x) \quad (6.1)$$

Della Pietra and Lafferty (1997) showed that the maximum entropy distribution is equal to a Gibbs probability distribution in the form:

$$q_{\lambda}(x) = \frac{e^{\lambda \cdot f(x)}}{Z_{\lambda}} \quad (6.2)$$

Where  $\lambda$  is the weight of the feature,  $f$  is the vector of all  $n$  features and  $Z_{\lambda}$  is a normalizing constant that means  $q_{\lambda}$  sums to 1. To find a distribution of maximum entropy, MaxEnt uses a sequential update algorithm that modifies one weight,  $\lambda_j$ , at a time. For each sequence of update, the feature,  $f_j$ , is updated to maximise

the relative entropy,  $RE(\tilde{\pi}[f_j] \parallel q_\lambda[f_j])$ . Next, the weight of the feature is updated by  $\lambda_j \leftarrow \lambda_j + \alpha$  where:

$$\alpha = \ln \left( \frac{\tilde{\pi}[f_j](1-q_\lambda[f_j])}{(1-\tilde{\pi}[f_j])q_\lambda[f_j]} \right) \quad (6.3)$$

By aiming to predict a distribution whereby  $\hat{\pi}[f_j] = \tilde{\pi}[f_j]$ , there is a risk the model could become overfitted to the input data. Instead, the constraints are softened using a L1 regularization such that:

$$|\hat{\pi}[f_j] - \tilde{\pi}[f_j]| \leq \beta_j \quad (6.4)$$

where  $\beta_j$  is the regularization parameter and is approximated to:

$$\beta_j \approx \frac{\sigma[f_j]}{\sqrt{m}} \quad (6.5)$$

Where  $\sigma[f_j]$  is the standard deviation of  $f_j$  under  $\pi$  and  $m$  is the total number of observations.

To assess the performance of species distribution models, the receiver operating characteristic (ROC) curves are widely used (Reiss et al., 2011; Huang et al., 2011; Elith et al., 2006). The ROC curve is created by plotting ‘sensitivity’ against ‘1-specificity’. Sensitivity is the fraction of all positive instances, or observations, whereas, specificity is the fraction of all negative instances, or absences. The area under the ROC curve, known as AUC, is then used to assess the model performance. Phillips & Dudík (2008) explains that the AUC is a measure of how good a model is at distinguishing between a randomly chosen presence site and sites of absence. The problem with a presence-only model is there are no absences to which to calculate specificity. Instead, MaxEnt uses a pseudo-absence to distinguish presence from random instead of presence from absence. It does this by assigning each pixel representing the observed species as a presence and then assigning every other pixel in the model domain as background. The model then predicts the species distribution without knowing how the pixels are labelled. The ROC is then plotted by taking a sample of the positive occurrences and a random sample of the background pixels. From this, the ROC can be plotted. The AUC of a perfect model is 1. For a random model the AUC is 0.5. Figure 6-3 shows an example ROC curve. The red line shows the

curve of a hypothetical trained model; the black line represents a random model. The closer the red line tends towards the top left corner the better the model is at discerning between suitable and unsuitable habitats.

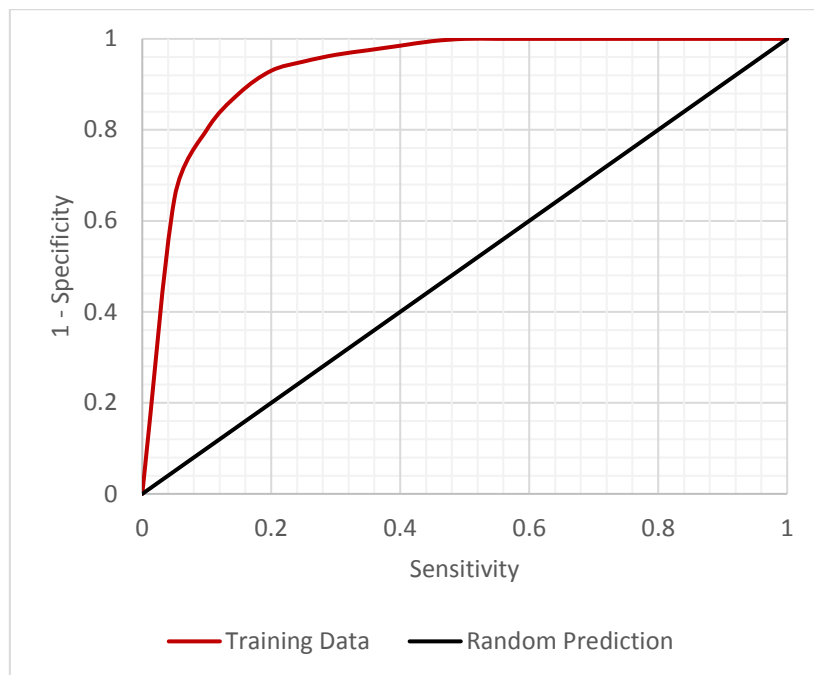


Figure 6-3: A hypothetical ROC curve of a trained model (red) and a random model (black). The closer the red line tends towards the top left corner the better the model is at discerning between suitable and unsuitable habitats.

One of the advantages of MaxEnt is that it is generative rather than discriminative. This means the model is learning based on a joint probability distribution rather than a conditional probability distribution. The result is a model that can use limited training data. In comparing MaxEnt to a GARP model, Philips et al. (2006) splits the observations such that 70% are used to train the model and the remaining 30% to testing the results.

There are two potential pitfalls to be aware of with species distribution modelling. The first is sampling bias. The disadvantage with desk studies using publicly available data is there is no control on sampling effort (Reddy and Dávalos, 2003). Previous surveys may be interested in a specific area meaning observations are tightly focused in a spatial context. Furthermore, the surveyors may be geographically restricted to where they can sample. This may lead the model becoming biased. This can be minimised providing there is sufficient spatial coverage in the model training data. The second potential pitfall is that the background environmental variables used in the model may not fully represent



an ecological niche for each species (Philips et al., 2006). However, by drawing on previous studies, it is possible to omit variables that are not fully representative. Harris and Baker (2012) collated a synthesis of lessons learned from 57 case studies in habitat mapping. In their review they found that water depth was the most suitable predictor for benthic communities. This was followed by substrate/sediment type, acoustic backscatter, wave-current and grain size. Water property predictors, such as temperature, salinity and seabed slope, were less useful as predictors.

At the time of this research the only other study into the effects of tidal turbines on the benthic environment using MaxEnt was Bell et al. (2011). The study investigated the resulting change in bed shear stress due to tidal turbines and its effect on bryozoans in Scottish waters. The study was limited due to the resolution being ten times coarser and the change in bed shear stress was introduced as a uniform 10% and 50% reduction across the array site. The influence and operation of the tidal turbines was not modelled directly. However, the work provides useful information on predictor variables. In the study Bell et al. (2011) used depth, sediment type, maximum and minimum bed temperature, maximum difference in surface and near bed temperature, maximum and minimum salinity, maximum difference in surface and near bed salinity, maximum near bed shear stress, spring tide current shear stress and annual mean significant wave height. Although, salinity was later omitted due to its uniformity in the model domain.

## 6.3 Modelling the Benthic Environment with MaxEnt

### 6.3.1 Benthic Species

The 10 MW tidal array at St David's is situated off the Pembrokeshire coast, in South-West Wales. The location of the tidal array means it falls within the Pembrokeshire Special Area of Conservation (SAC) (Joint Nature Conservation Committee (a), n.d.). Furthermore, 30 km to the south is the Skomer Marine Nature Reserve. The Pembrokeshire SAC was primarily designated for protection of the following Annex I habitats: Estuaries (Milford Haven), large shallow bays (St Brides bay) and reefs with a specific mention of *Zostera angustifolia*, commonly known as eelgrass. These habitats are dominated by hydroids, bryozoans, soft corals, cnidarians, sponges, ascidians and crustaceans (Joint

Nature Conservation Committee (a), n.d.). Benthic species that are representative of the Annex I habitats have been focussed upon in order to determine the impact of the tidal array.

For this study, the two main criteria for selecting a species for modelling are that they are sessile and there are sufficient observations for modelling. The minimum number of observation for training the model is 100 (Callaway, 2015, pers. Comm., 28 August). Observation data were provided by SeaSearch and Natural Resources Wales and accessed through the National Biodiversity Network Gateway (NBN, n.d.).

The following nine species were selected as they provide a representation of the Pembrokeshire SAC communities and there are sufficient observations for modelling:

- *Alcyonium digitatum*
- *Axinella dissimilis*
- *Bugula turbinata*
- *Dendrodoa grossularia*
- *Eunicella verrucosa*
- *Flustra foliacea*
- *Nemertesia ramosa*
- *Pachymatisma johnstonia*
- *Raspailia ramosa*

*Eunicella verrucosa* was specifically chosen as it is a biodiversity action plan species (Joint Nature Conservation Committee (b), n.d.). Crustaceans have not been included as they are mobile and capable of recovering from smothering. Molluscs, such as *Mytilus edulis*, are very abundant in the area but have not been included because of their abundance and they also exhibit a low response to change in suspended sediments and flow rate (Tyler-Walters, 2008). Despite the SAC designation stating it supports “*extensive beds of narrow-leaved eelgrass Zostera angustifolia*” it was recorded only once within the observation data therefore, it was not included in the modelling.

A description of the individual species phyla is provided by Synderman & Wiseman (1996) and is summarised here after. *Axinella dissimilis*, *Pachymatisma*

*johnstonia* and *Raspailia ramosa* are examples of sponges. A sponge is a porous bodied invertebrate that absorbs nutrients out of the water. *Alcyonium digitatum* and *Eunicella verrucosa* are cnidarians. Cnidarians are invertebrates that form compact colonies of individual polyps, such as corals. They feed on nutrients that pass over them. *Bugula turbinata* and *Flustra foliacea* are bryozoans. Bryozoans are colonies of mossy invertebrates that are filter feeders. *Dendrodoa grossularia* is an ascidian. Ascidians are more commonly known as sea squirts who feed by drawing water into their sac-like body, expelling it through a second hole. *Nemertesia ramosa* is a hydroid. A hydroid is a colony of cells that branch out in a stem like fashion and are often mistaken as plants. Figure 6-4 shows photographic examples of the species chosen for modelling.

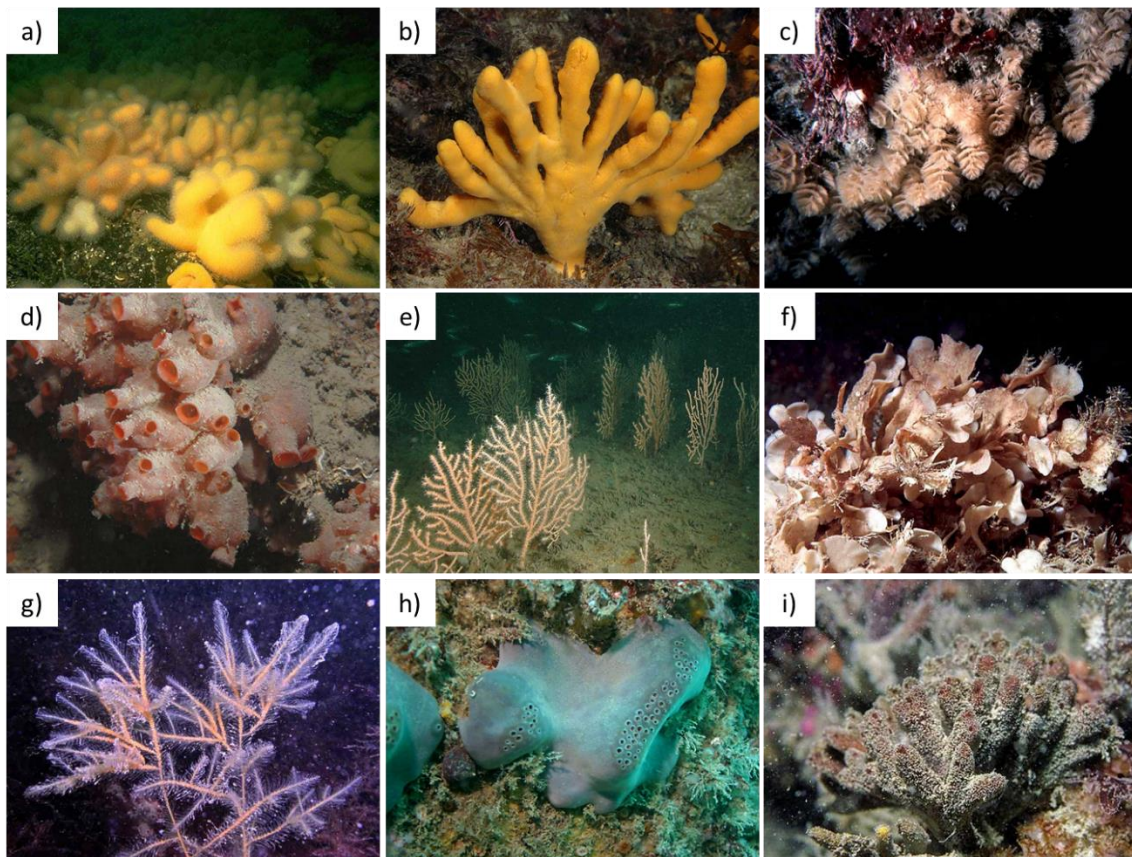


Figure 6-4: The nine benthic species chosen for modelling: a) *Alcyonium digitatum*, b) *Axinella dissimilis*, c) *Bugula turbinata*, d) *Dendrodoa grossularia*, e) *Eunicella verucosa*, f) *Flustra foliacea*, g) *Nemertesia ramosa*, h) *Pachymatisma johnstonia* and i) *Raspailia ramosa*.

Figure 6-4-a is copyright of Sue Scott, Figure 6-4-b, c, d, e of Keith Hiscock, Figure 6-4-g of Paul Newland and Figure 6-4-h of Sue Daly. All are accessed from the Marine Life Network website, [www.marlin.ac.uk](http://www.marlin.ac.uk). Figure 6-4-i is copyright

of Bernard E. Picton and Christine C. Morrow, accessed from Encyclopaedia of Marine Life of Britain and Ireland, <http://www.habitas.org.uk/marinelife/>.

### 6.3.2 MaxEnt Model Set-up

The extent of influence exerted by the tidal turbines on the hydrodynamic conditions is a localised effect and smaller than the model domain used for Ramsey Sound. The MaxEnt model domain considers the areas where the impacts are greatest and extends between 51.6° - 52.1° N latitude and 5.0° - 5.5° W longitude. MaxEnt computes on a regular grid with a spatial resolution of the square grid of 0.0001° (~ 11.13m x 6.89m).

The primary dataset MaxEnt needs to function are the species observations, as these are used to train the model. Based on Philips (2006) the observations were split such that 70% are used to train the model and the remaining 30% to test the results. The subset of observations used for testing were chosen at random and visually checked to ensure they provided a full spatial range within the model domain. Table 6-1 shows the number of total observations for each species. The data was split into a training and testing dataset with a ratio of 70:30, respectively.

Table 6-1: Breakdown of the total number of observations of the nine modelled species into training and testing sets.

Species	Total	Training	Testing
Alcyonium digitatum	699	489	210
Axinella dissimilis	376	263	113
Bugula turbinata	182	127	55
Dendrodoa grossularia	245	172	73
Eunicella verucosa	145	102	43
Flustra foliacea	175	123	52
Nemertesia ramosa	345	242	103
Pachymatisma johnstonia	664	465	199
Raspailia ramosa	241	169	72

To assess the impact of the 10 MW tidal array at St David's Head, MaxEnt runs a reference base case where the model is trained on the observations and background conditions without the influence of the tidal array. MaxEnt is then rerun with the background conditions altered due to the presence of the tidal array but using the feature constraints trained in the reference case. The predicted

species distribution can change depending on the split of observation points used for training. Therefore, the MaxEnt model is repeated 10 times, using bootstrapping replication, to assess whether the change due to the turbines is statistically significant compared to the variation in the background distribution. Bootstrapping replication is whereby the training data is selected by sampling with replacement from the presence observations, with the total number of training points equalling the total number of presence observations.

Along with the observations, MaxEnt requires the background environmental data throughout the model domain. There are a number of predictor variables that could represent the physical processes that are likely to determine the marine habitat. Based on Bell et al. (2011) and the lessons learnt from Harris and Baker (2012) the following environmental background variables have been chosen as predictors for the MaxEnt model:

- Depth
- Mean bed shear stress
- Maximum bed shear stress
- Mean annual significant wave height
- Mean summer suspended particulate matter
- Mean winter suspended particulate matter
- Grainsize
- Gravel fraction
- Sand fraction
- Mud fraction

Bell et al (2011) also used salinity as a predictor but finally omitted salinity due to its uniformity within the model domain. Salinity values were sourced from the European Marine Ecosystem Observatory data portal (EMECO, n.d.) around Pembrokeshire and were also found to be uniform throughout the model domain. Therefore, salinity have also been omitted. Bell et al (2011) has used sediment type as a predictor. In this study the sediment type has been parameterised into grainsize and the composition fraction of gravel, sand and mud.

Depth, bed shear stress and wave height were taken from the hydrodynamic model results of Ramsey Sound, as shown in Chapter 4. Observation data for mean summer and winter suspended particulate matter were obtained from the

MyOcean data portal (Copernicus, n.d.). The summer period represents the lowest level of suspended particulate matter and was defined as June through to August. The winter period represents the highest levels and was defined as December through to February. Grainsize and sediment fractions are predicted variables. The methodology for determining these parameters are detailed in the following sections. The background conditions used in the MaxEnt model that were altered by the presence of the tidal turbines were mean and maximum bed shear stress and grainsize.

### 6.3.3 Predicting Grainsize Distribution

The grainsize was calculated using the method shown in Soulsby (1997) to determine threshold of motion and hence the minimum grainsize that would settle under the mean bed shear stress conditions. The threshold bed shear stress,  $\tau_{cr}$ , is calculated as:

$$\tau_{cr} = \theta_{cr} g (\rho_s - \rho) d \quad (6.6)$$

where  $\theta_{cr}$  is the threshold Shields parameter,  $g$  is gravity,  $\rho_s$  is density of sediment,  $\rho$  is density of water and  $d$  is grain diameter. The threshold Shields parameter,  $\theta_{cr}$ , is calculated as:

$$\theta_{cr} = \frac{0.3}{1+1.2D_*} + 0.055[1 - \exp(-0.020D_*)] \quad (6.7)$$

where  $D_*$  is the dimensionless grainsize, calculated as:

$$D_* = \left[ \frac{g(s-1)}{\nu^2} \right]^{\frac{1}{3}} d \quad (6.8)$$

where the kinematic viscosity of water  $\nu = 1.36 \times 10^{-6} \text{m}^2/\text{s}$  and  $s = \frac{\rho_s}{\rho}$ . For the calculations  $g = 9.81 \text{m/s}^2$ , the density of sediment is taken as that of quartz  $\rho_s = 2650 \text{kg/m}^3$  and the density of sea water  $\rho = 1027 \text{kg/m}^3$ .

Using Equations 6.1 – 6.3, the threshold of motion was calculated for each grainsize between 0.001mm and 35mm, at an interval of 0.001mm. The predicted grainsize distribution was then determined by finding the smallest grainsize diameter whose threshold of motion did not exceed the mean bed shear stress calculated from the Ramsey Sound study, in Chapter 3. Figure 6-5 shows the resulting predicted grainsize distribution.

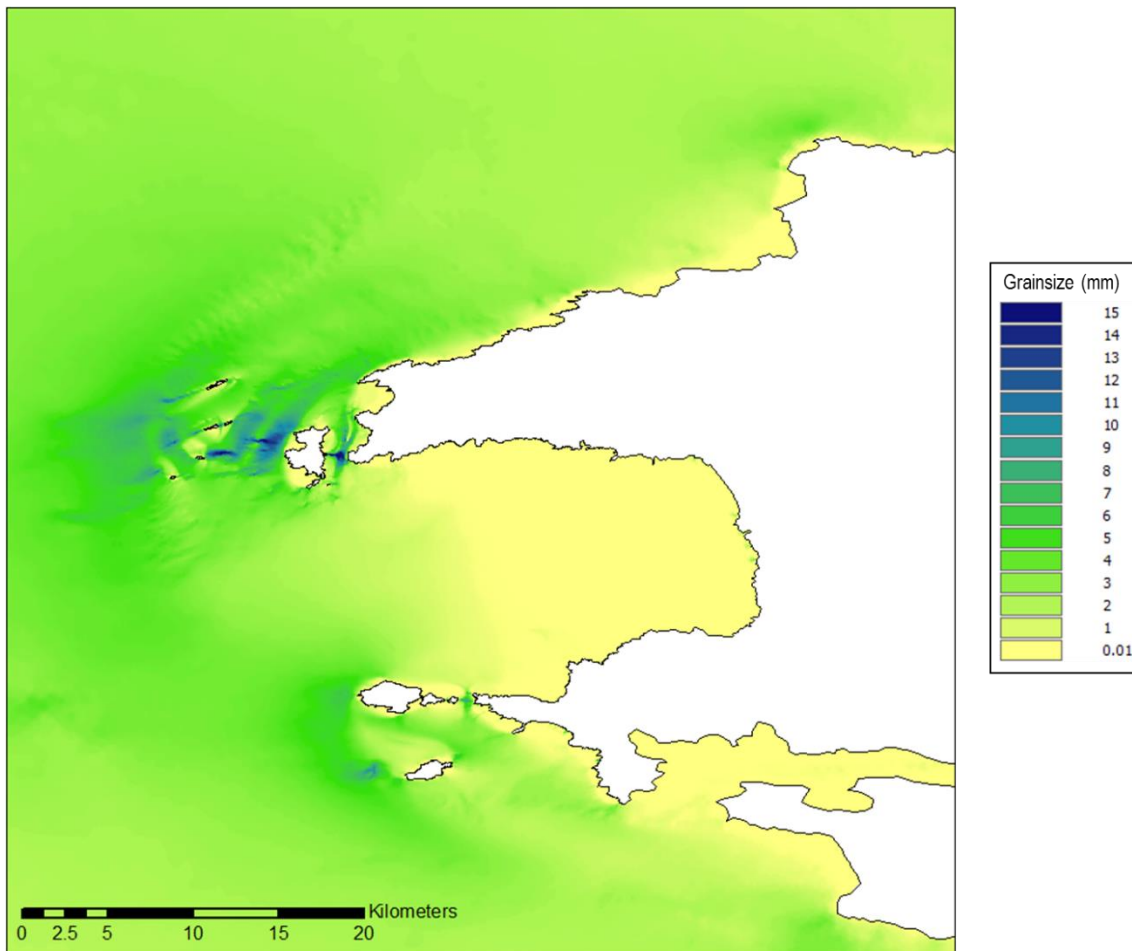


Figure 6-5: Predicted grainsize, determine by the smallest grainsize whose threshold of motion does not exceed the mean bed shear conditions.

### 6.3.4 Predicting Sediment Fraction Distribution

Sediment type fraction distribution falls into three main categories based on grainsize diameter. The categories are mud, sand and gravel. Throughout this study sediment classes will be referred to with respect to the scale defined by the British Geological Survey (BGS). The BGS scale defines the sediment classes as follows:

- Mud: 0.001 – 0.0625 mm
- Sand: 0.0625 – 2 mm
- Gravel: 2 – 25 mm

Grainsizes larger than 25mm are considered as boulders. Sediment is rarely uniformly one grain size but made up of a distribution of grainsizes. Instead, sediment is often referred to by the notation  $d_{50}$ .  $d_{50}$  represents the diameter whereby 50% of the grains by mass are smaller. Sediments are then classified according to their mixture of mud, sand and gravel. A commonly used

classification is the Folk triangle based on the classification of Folk (1954). Sediment is classified on the triangle by its percentage gravel fraction and the ratio of sand to mud. Figure 6-6 shows the simplified Folk classification as adapted from Long (2006).

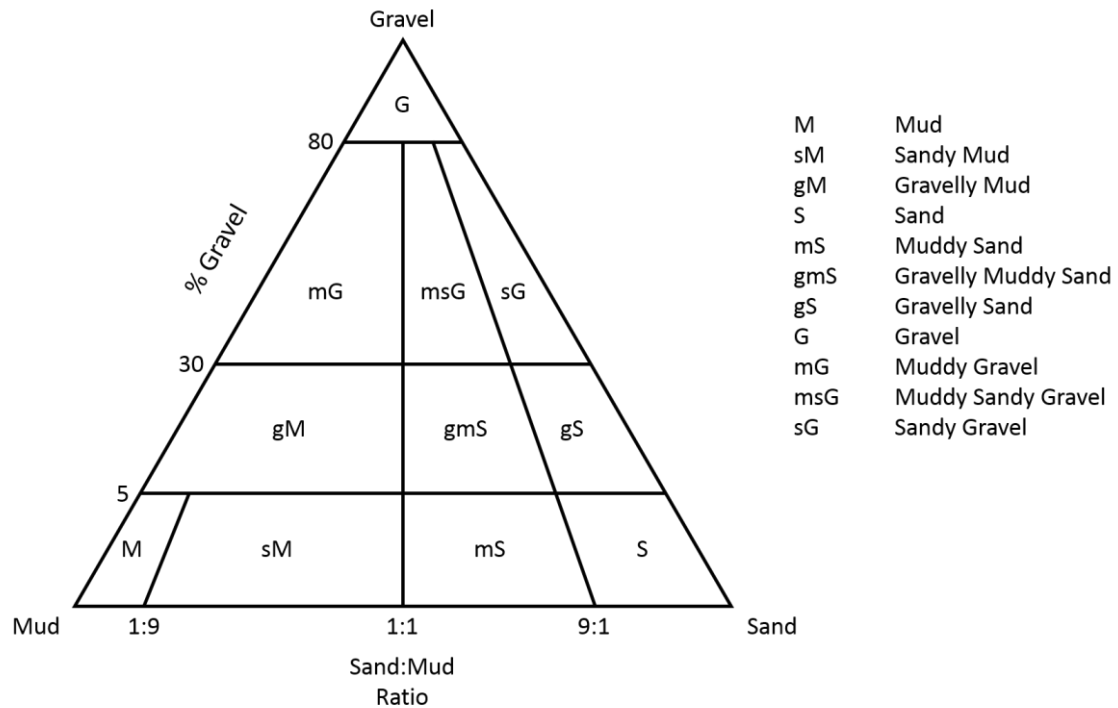


Figure 6-6: Simplified Folk classification based on the classification of Folk (1954). Sediments are classified according the fractions of mud, sand and gravel. Figure adapted from Long (2006).

MaxEnt is capable of assimilating data either categorically, such as sand, mud, gravel, or in a continuous form, such as numerical values ranging 0 – 1. Grainsize and sediment fraction are significant properties for predicting benthic community structures and is preferable to use them in the continuous form (Coggan et al., 2012). Observation data of sediment composition is obtained from the seabed through physical grab samples meaning its spatial coverage is limited. As with species distribution modelling, the spatial distribution of sediment fractions can be modelled from a sample of known observations. Spatial distribution of sediment composition has been predicted using a Random Forest algorithm as shown in Stephens & Diesing (2015).

A Random Forest algorithm is a statistical classification method using decision trees (Breiman, 2001). Decision trees are widely used because of their ability to characterise complex interactions between predictor variables (Cutler et al., 2007). In common with how MaxEnt works, the Random Forest is supplied with



the geolocation observation data and a set of background environmental variables at coincident locations. In a traditional decision tree rules are developed from classified observations in order to predict new observations. Decision trees are split, or grown, by partitioning the data into groups of similar classes (background variables). The tree continues to grow until the sub-divisions no longer produce variation in the sub-groups. A Random Forest works by applying hundreds of (user defined) trees using a subset of the sample data, typically two thirds, for each tree. The Random Forest then makes a prediction based on all the trees. Observations that are not used in the sub-samples are called out-of-bag observations (OOB). As the OOBs have not been used to grow the trees, they can be used as a means of cross-validation to assess the accuracy of the model. Providing enough trees are grown, this can provide a reliable measure of model performance (Liaw & Weiner, 2002).

Sediment is characterised as a fraction of gravel, sand and mud whose total must equal 100%. The components are not considered independently from each other. Aitchison (1986) recommends transforming the three variables into two continuous unconstrained response variables using an additive log-ratio (alr). For this study, the sediment fractions have been transformed into a sand and mud additive log-scale, using Equation 6.9 and 6.10. It does not matter which variable forms the denominator (Lark et al., 2012).

$$alr_m = \log\left(\frac{mud}{gravel}\right) = \log(mud) - \log(gravel) \quad (6.9)$$

$$alr_s = \log\left(\frac{sand}{gravel}\right) = \log(sand) - \log(gravel) \quad (6.10)$$

Observations of sediment fractions were obtained from the BGS Offshore GeoIndex portal (British Geological Survey, n.d.). Within the model domain, there were 406 observations. As with MaxEnt, the observations were split with 70% used to train the Random Forest model and 30% to validate. As  $\log(0)$  cannot be computed, for the purpose of the calculation, any observations with a zero value are replaced with the value 0.005%.

The Random Forest algorithm has been implemented in ArcGIS using the Marine Geospatial Ecology Toolbox 0.8a60 ([mgel.env.duke.edu/mget](http://mgel.env.duke.edu/mget)). The number of trees used was 1000 with 2 variables available for each splitting. The

environmental background variables used included: depth, mean & maximum velocity, annual mean significant wave height (Hs), mean summer & winter suspended particulate matter (SPM) and grainsize.

Figure 6-7– Figure 6-9 show the spatial prediction of gravel, sand and mud fraction, respectively.

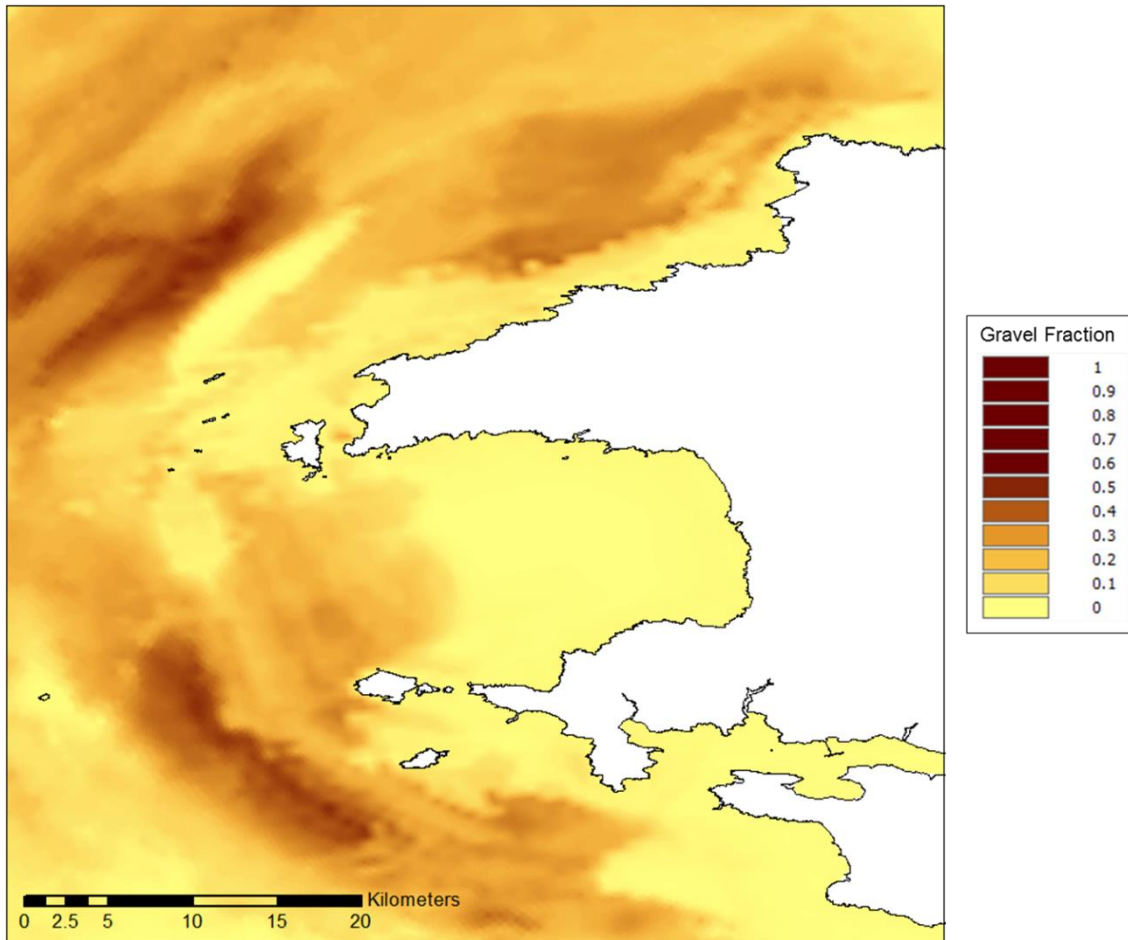


Figure 6-7: Predicted gravel fraction distribution from BGS observations using Random Forest algorithm.

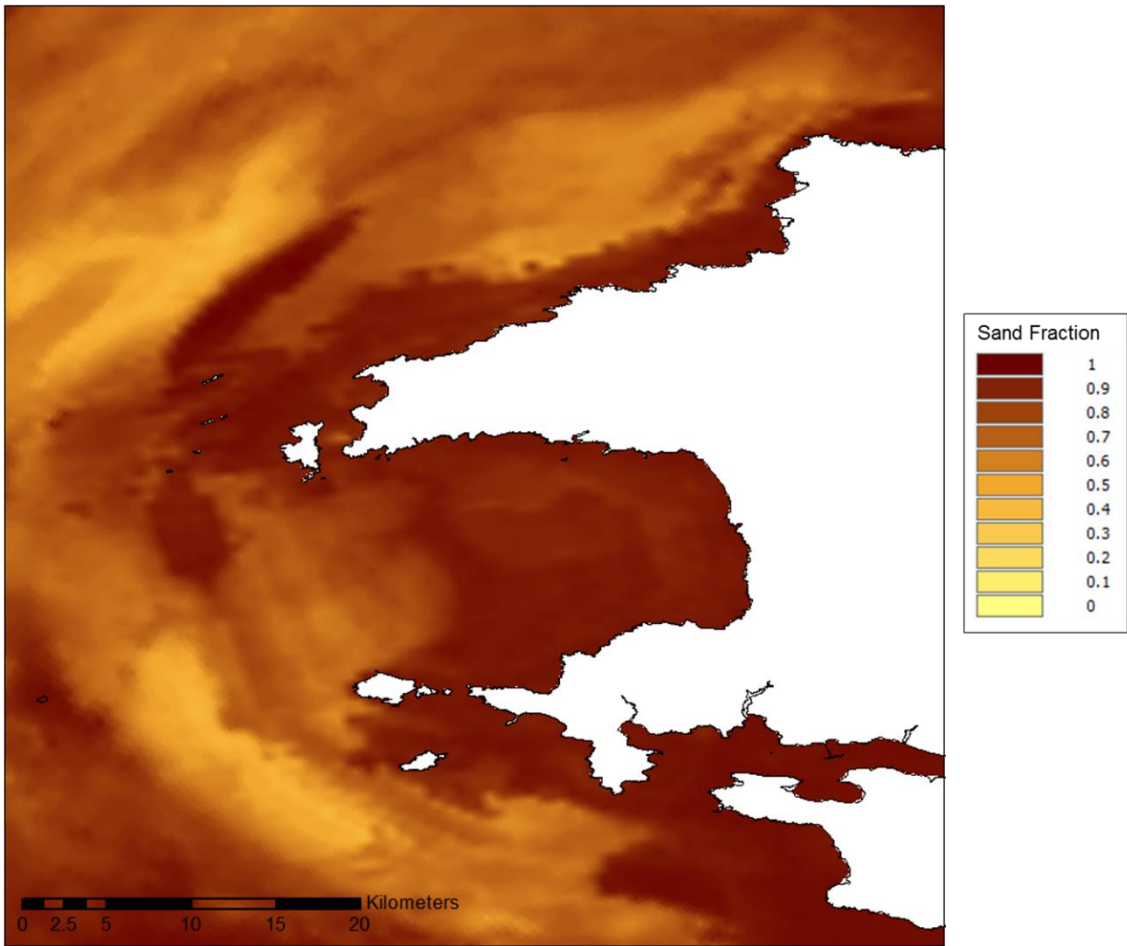


Figure 6-8: Predicted sand fraction distribution from BGS observations using Random Forest algorithm.

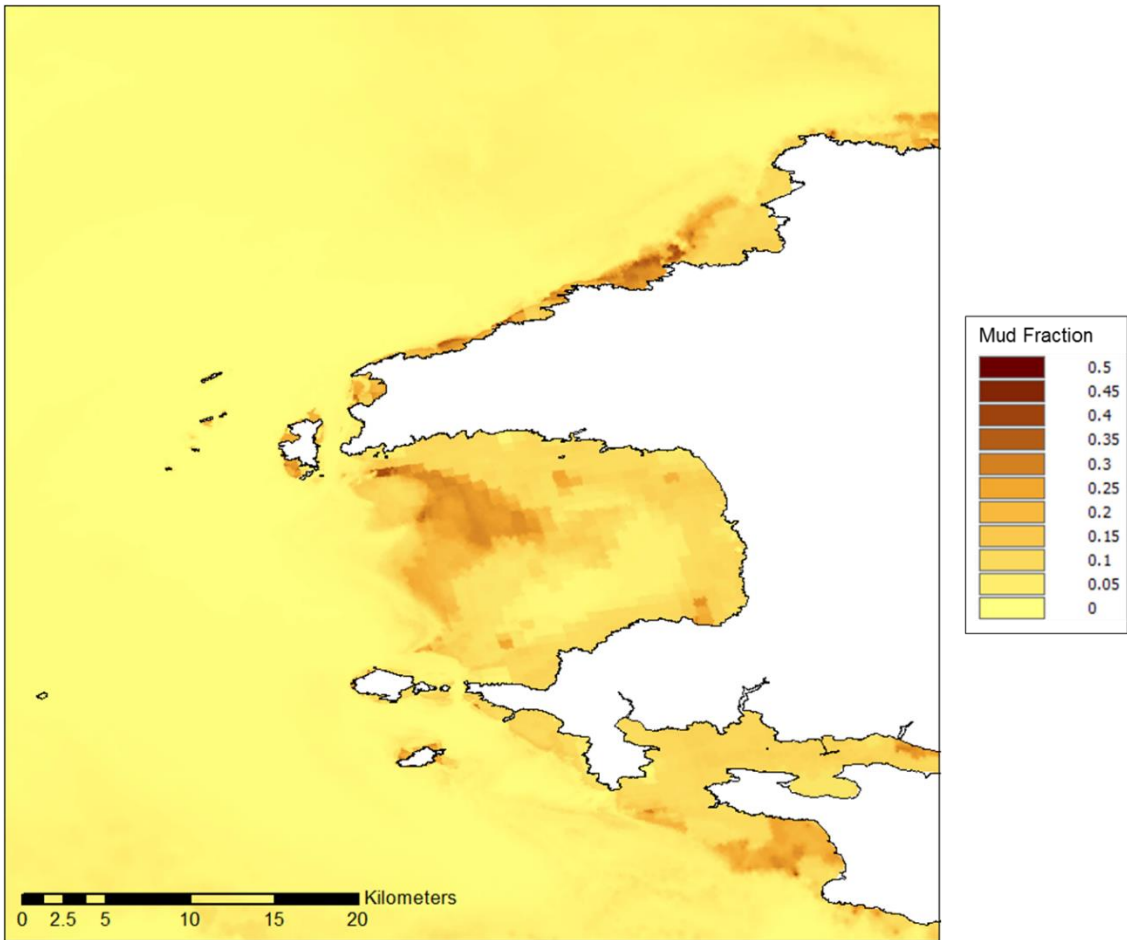


Figure 6-9: Predicted mud fraction distribution from BGS observations using Random Forest algorithm.

The Random Forest analysis performs a cross-validation using the OOB observations to test the model performance. Along with the cross-validation, an assessment of the model has been performed using subset of the observations for testing. The Random Forest assesses the model performance using the ‘variance explained’ which is a measure of how well a model predicts the variation of a given data set. This is calculated by first calculating the mean of the squared prediction error (MSE):

$$MSE_{\hat{y}} = \frac{1}{n} \sum_{i=1}^n (y_i - \hat{y}_i)^2 \quad (6.11)$$

where  $y$  are the observations and  $\hat{y}$  are the predicted values. The variance explained is then calculated by taking the ratio of the MSE to the variance ( $\sigma^2$ ) of the observed values:

$$1 - \frac{MSE_{\hat{y}}}{\sigma_y^2} \quad (6.12)$$

Table 6-2 summarises the cross-validation of the Random Forest model and the validation against the test dataset.

Table 6-2: Validation of Random Forest model and test data

	alr <sub>m</sub>	alr <sub>s</sub>
MSE (cross-validation)	1.46	1.15
% Variance explained (cross-validation)	56.1	54.7
MSE (test set)	1.54	1.05
% Variance explained (test set)	45.3	58.5
Spearman rank correlation index	0.68	0.76

It can be seen from the cross-validation variance explained, in Table 6-2, that the variables used to predict the spatial extent of the sediment fractions did not account for all the variance within the observed training data. When comparing the variance explained between cross-validation and test-set, the values imply that the model is not over-fitted to the training data. Overfitting is a problem in machine learning where a model is more complex than necessary and the variables are fitting to random noise in the data rather than learning the general trend (Hawkins, 2004). The Spearman rank coefficient index shows that despite the poor variance explained there is a correlation between predicted sediment fractions and observations. Stephens & Diesing (2015) also achieved Spearman coefficients values of this order.

The availability of additional variables would improve this prediction. For example, a back-scatter index from multibeam acoustic surveys would improve performance significantly. However, there was insufficient spatial coverage within the model domain to be useful. Figure 6-10 and Figure 6-11 show the correlation between the predicted and observed additive log ratios and mud and sand, respectively. The solid black line denotes a  $y=x$  relationship with the dashed line representing the 95% prediction intervals.

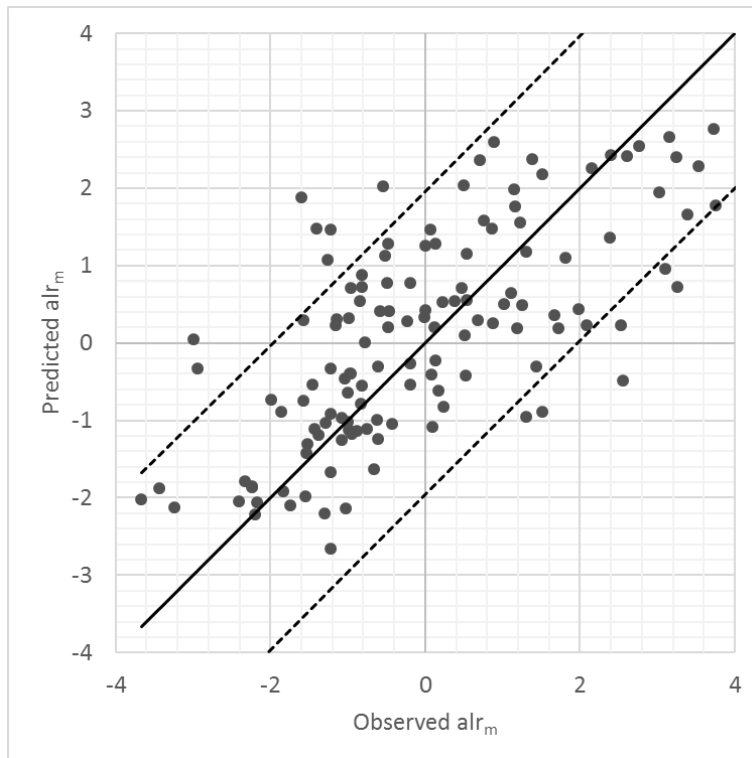


Figure 6-10: Comparison of observed and predicted additive log ratio of mud. The solid black line denotes a  $y=x$  relationship with the dashed lines representing the 95% prediction intervals.

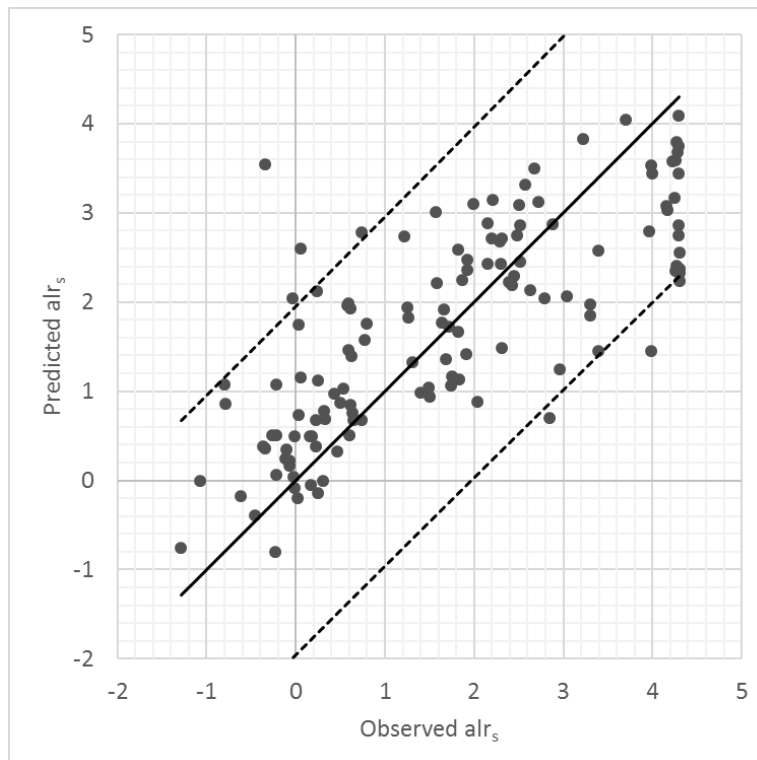


Figure 6-11: Comparison of observed and predicted additive log ratio of sand. The solid black line denotes a  $y=x$  relationship with the dashed lines representing the 95% prediction intervals.

So that the sediment fractions can be used in the Random Forest model, the additive log ratios, as defined by Equation 6.9 & 6.10, were converted back into their constituent fractions by the following equations:

$$\text{sand fraction} = \frac{e^{alr_s}}{(1+e^{alr_s}+e^{alr_m})} \quad (6.13)$$

$$\text{mud fraction} = \frac{e^{alr_m}}{(1+e^{alr_s}+e^{alr_m})} \quad (6.14)$$

$$\text{gravel fraction} = 1 - \text{sand} - \text{mud} \quad (6.15)$$

To give a more intuitive understanding of how the model performed, Figure 6-12 – Figure 6-14 show scatter plots of the predicted sediment fractions versus observations. The solid black line denotes a  $y=x$  relationship with the dashed line representing a line of best fit to the data.

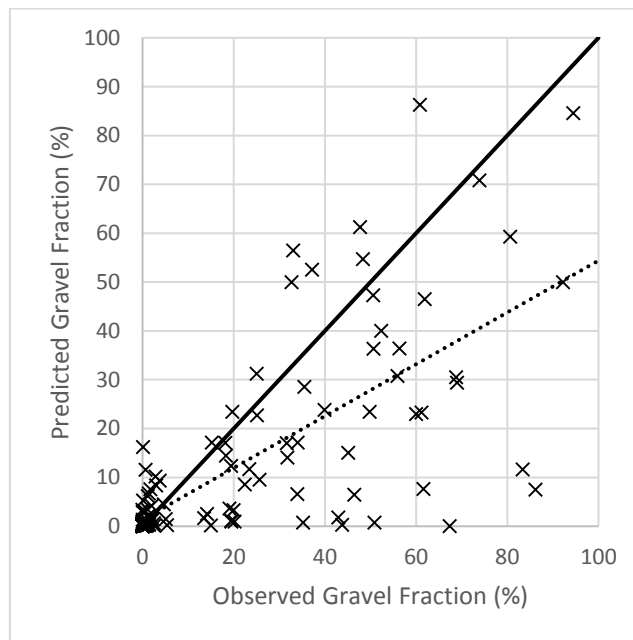


Figure 6-12: Comparison of observed and predicted gravel fraction. The solid black line denotes a  $y=x$  relationship with the dashed line representing a regression line of best fit.

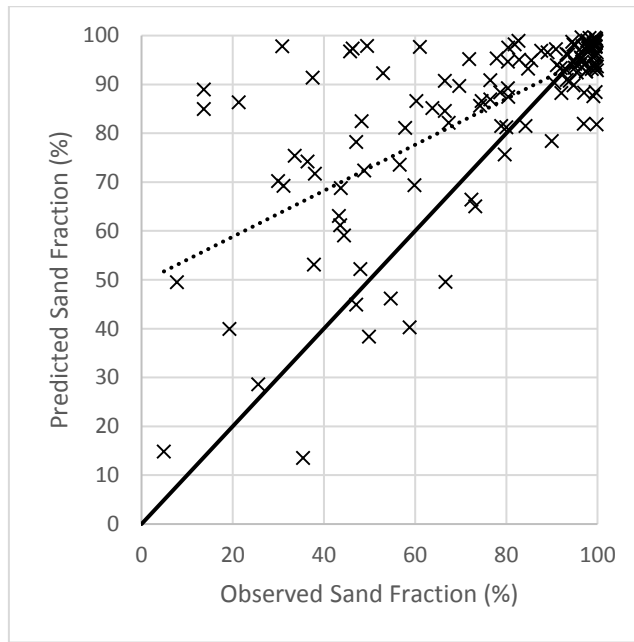


Figure 6-13: Comparison of observed and predicted sand fraction. The solid black line denotes a  $y=x$  relationship with the dashed line representing a regression line of best fit.

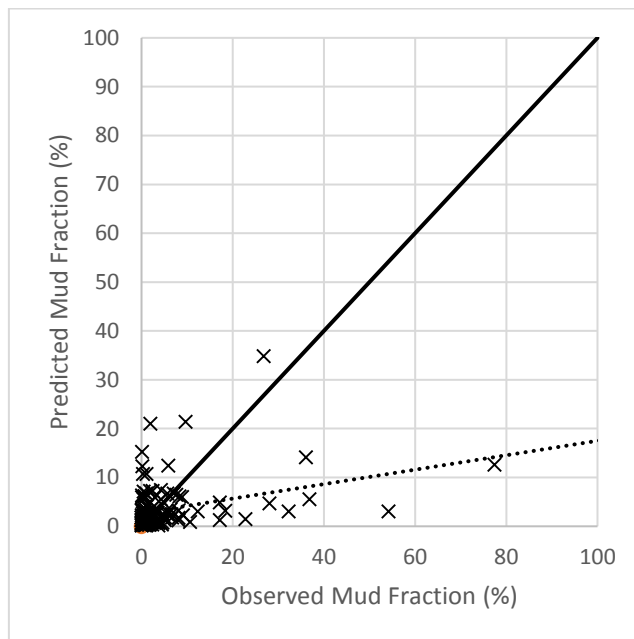


Figure 6-14: Comparison of observed and predicted mud fraction. The solid black line denotes a  $y=x$  relationship with the dashed line representing a regression line of best fit.

The results show that the model is biased towards sand, under predicting gravel and mud. This is a result of the bias towards sand observations in the Random Forest training dataset. Figure 6-15 shows a histogram of the observed sediment fractions. The region is dominated by sand, with 46.7% of the observations having a sand fraction in excess of 90%. This value increases to 47.1% if the whole



observation dataset is included. This is why the model does not perform as well as it can, in terms of variance explained, but still provides a reasonable correlation between prediction and observation. It is over predicting sand in a region dominated by sand. Stephens & Diesing (2015) see a similar bias in their study.

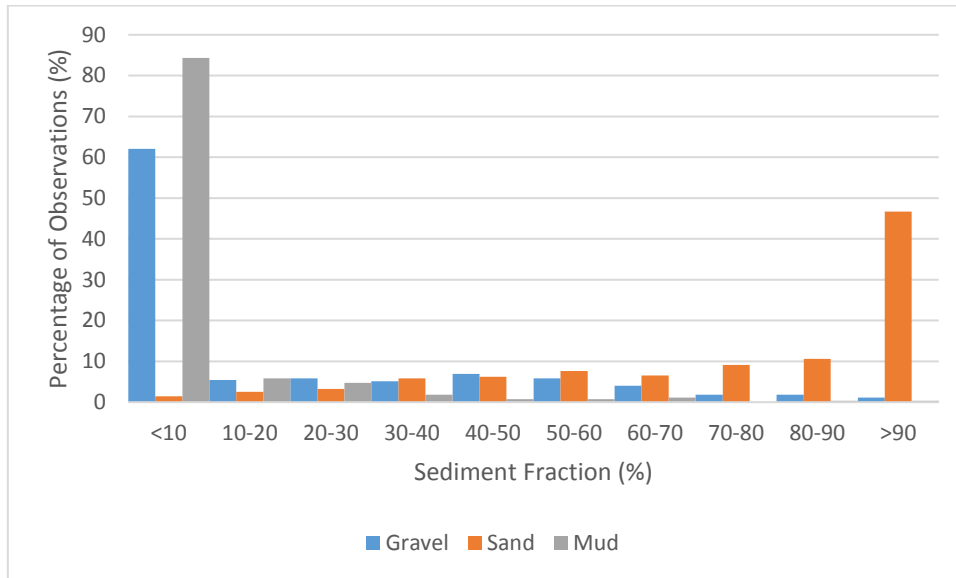


Figure 6-15: Histogram of gravel, sand and mud fraction of the BGS Observations.

Quantitatively, the model could perform better. Qualitatively, the model distinguished the main sediment regional classifications when compared to BGS seabed sediment maps. Figure 6-16 shows the seabed sediments within the model domain based upon 1:250,000 digital sea-bed sediments map (DigSBS250), with the permission of the British Geological Survey (originally shown in Figure 4-19).

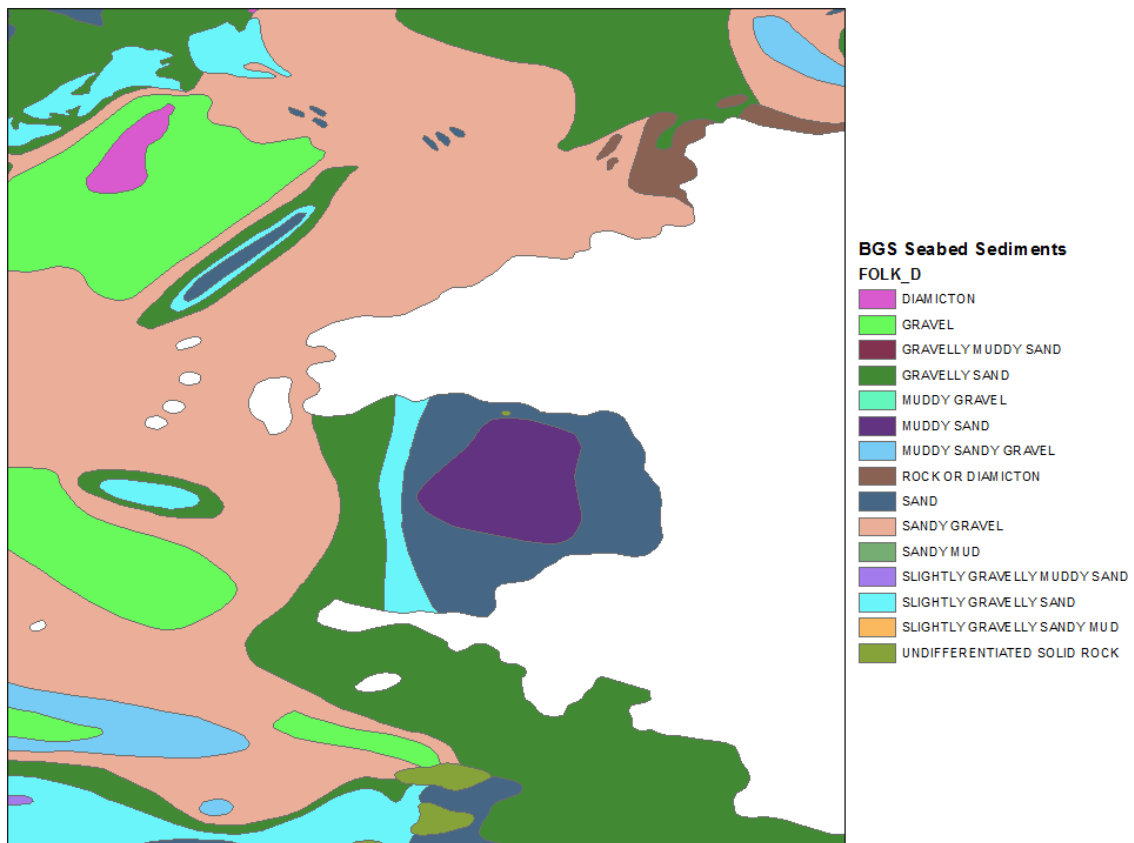


Figure 6-16: BGS Seabed Sediments using the Folk Classification. Reproduced with the permission of the British Geological Survey ©NERC. All rights Reserved.

When comparing the predicted sediment composition distributions with Figure 6-16, it is evident that the model predicts a high concentration of mud in St Brides Bay, the sand bank north of Ramsey Sound and the gravel regions north and south of the Bitches. A method to reduce the bias towards sand would be to increase the proportion of higher gravel and mud fraction samples. However, in the absence of a more extensive and expensive sediment survey of the region, publicly available and legacy datasets are the only options for a desk based approaches. Therefore, the predicted sediment fractions were used in the MaxEnt model.

## 6.4 MaxEnt Results and Validation

### 6.4.1 Validation

The area under the curve (AUC) method was used to assess the performance of the model's reference case. For illustration, Figure 6-17 shows the mean ROC for the 10 replications of *Pachymatisma johnstonia* as the red line with the blue area representing +/- one standard deviation from the mean. The black line

shows the ROC of a random model. The closer the red line tends towards the top left of the graph the better the model is at discerning between suitable and unsuitable habitats. For a random model the AUC is 0.5. A perfect model would have a value of 1. The other eight ROC curves are shown in Figure 6-18. Table 6-3 summarises the mean AUC for each of the nine species modelled along with the standard deviation of the 10 replicants. In comparison, Bell et al (2011) saw AUC values between 0.86 to 0.96, with an average of 0.93.

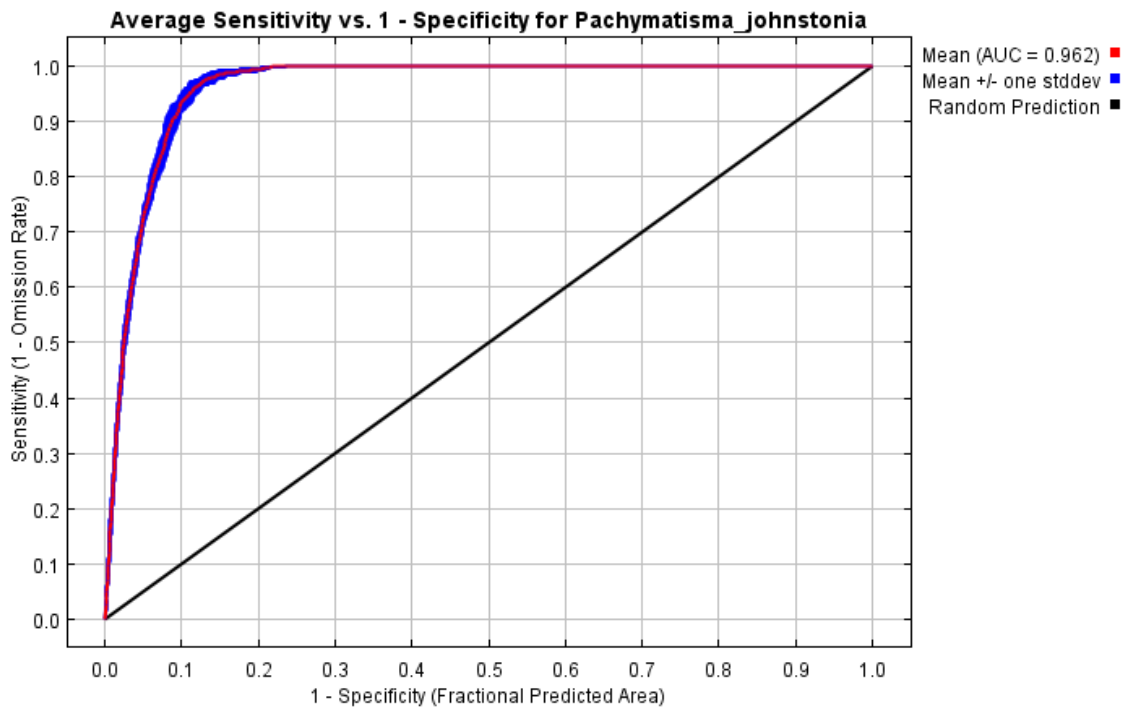


Figure 6-17: Response operating characteristic curves for *Pachymatisma johnstonia*.

Table 6-3: Average area under curve of all replicants of all species.

Species	Average Area	
	Under Curve	Standard Deviation
<i>Alcyonium digitatum</i>	0.962	0.002
<i>Axinella dissimilis</i>	0.971	0.001
<i>Bugula turbinata</i>	0.960	0.005
<i>Dendrodoa grossularia</i>	0.973	0.003
<i>Eunicella verucosa</i>	0.973	0.004
<i>Flustra foliacea</i>	0.962	0.004
<i>Nemertesia ramosa</i>	0.963	0.004
<i>Pachymatisma johnstonia</i>	0.962	0.002
<i>Raspailia ramosa</i>	0.968	0.003
<b>Average</b>	<b>0.966</b>	<b>0.003</b>

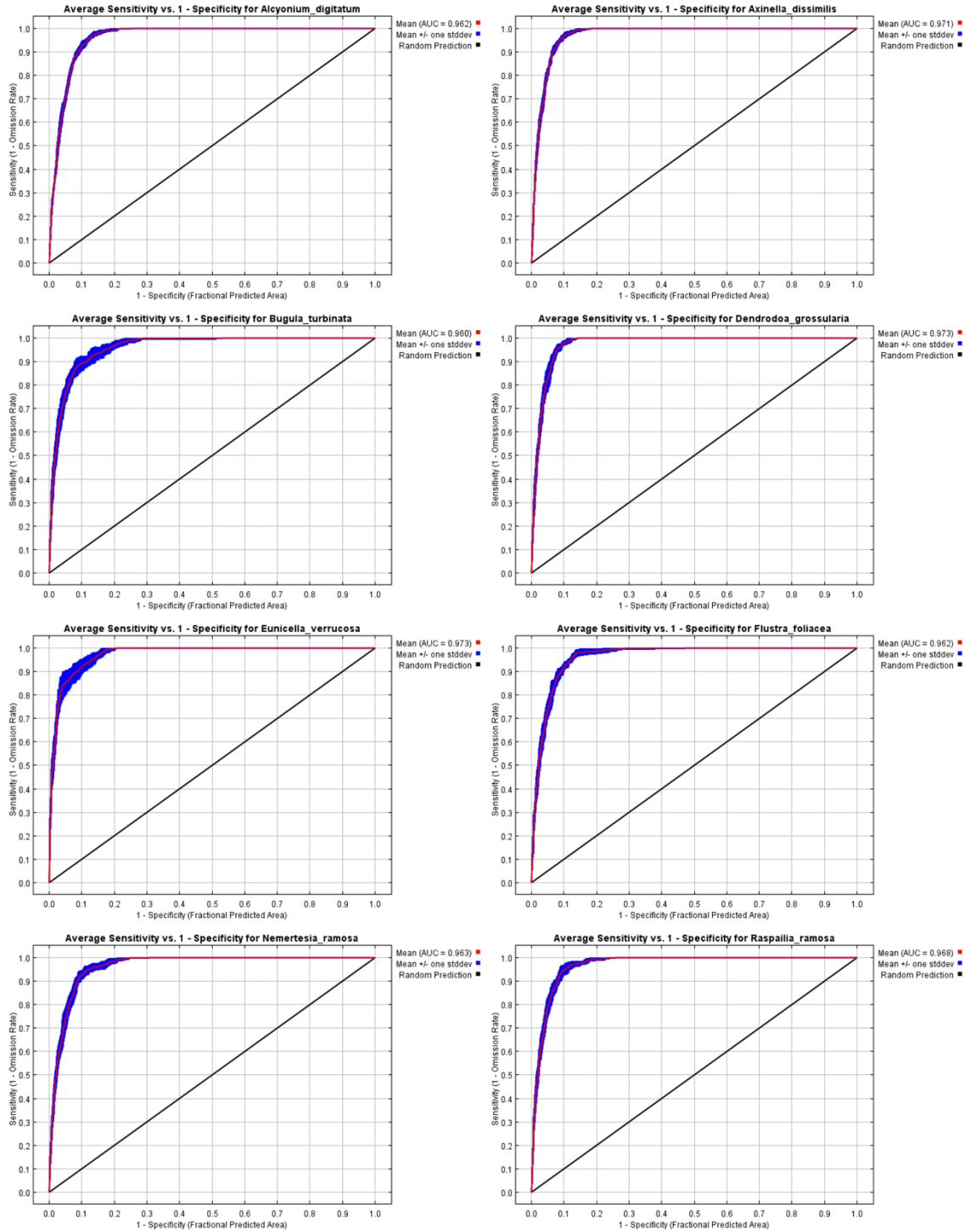


Figure 6-18: Response operating characteristic curve for *Alcyonium digitatum*, *Axinella dissimilis*, *Bugula turbinata*, *Dendrodoa grossularia*, *Eunicella verrucosa*, *Flustra foliacea*, *Nemertesia ramosa*, *Pachymatisma johnstonia*, *Raspailia ramosa*.

## 6.4.2 Results

For illustration, Figure 6-19 shows the mean predicted spatial distribution of the 10 replications of *Axinella dissimilis*, without the tidal turbines present. The white spots represent all the training observations.

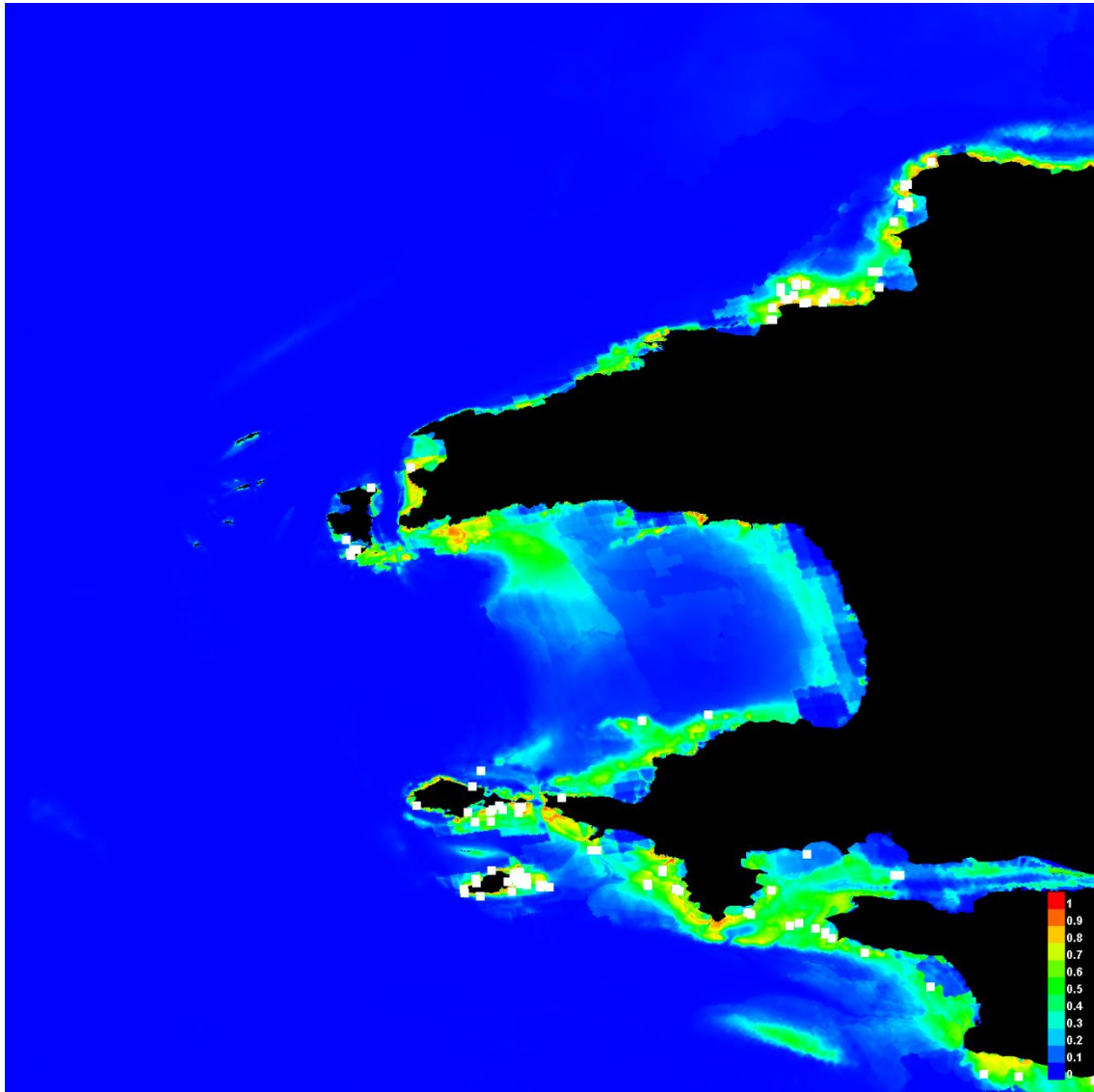


Figure 6-19: MaxEnt prediction of *Axinella dissimilis*

MaxEnt provides a probability of a species presence, a range from zero to one. A species is present when the probability is one and absent when zero with a range between. Specific presence/absence is more useful than a probability, meaning the MaxEnt results needed to be transformed. Lui et al (2005) assessed twelve methods for selecting thresholds of occurrence in the species distribution predictions. The average probability/suitability approach (Cramer, 2003) has been used in this study as it is simple, effective and just as good as the more complicated approaches (Lui et al, 2005). The method works by taking the mean

of the predicted probability at the locations of the observation set aside for testing. This value is then applied as the threshold value such that any occurrence of predicted probability above this threshold is treated as present. Table 6-4 shows the threshold values calculated for each replicant for each species. As the distribution is different for each replicant, the replicants are combined with the pixel value of each distribution equal to one. The distribution is then scaled between 0 and 10 to give a confidence of the distribution, whereby 0 means the species was absent in all ten replicants and 10 meaning the species was present in all ten. Figure 6-20 – Figure 6-28 shows the presence/absence prediction for each species without the tidal turbines present.

Table 6-4: Threshold values used to determine presence/absence.

Species	Replicant										Average	St Dev
	0	1	2	3	4	5	6	7	8	9		
<i>Alcyonium digitatum</i>	0.481	0.471	0.483	0.487	0.461	0.475	0.476	0.455	0.473	0.469	0.473	0.009
<i>Axinella dissimilis</i>	0.504	0.472	0.480	0.465	0.471	0.451	0.467	0.467	0.465	0.469	0.471	0.013
<i>Bugula turbinata</i>	0.561	0.574	0.604	0.602	0.610	0.573	0.511	0.579	0.571	0.538	0.572	0.029
<i>Dendrodoa grossularia</i>	0.492	0.535	0.493	0.476	0.445	0.469	0.436	0.467	0.504	0.506	0.482	0.028
<i>Eunicella verucosa</i>	0.553	0.614	0.544	0.606	0.484	0.532	0.514	0.483	0.549	0.511	0.539	0.042
<i>Flustra foliacea</i>	0.464	0.404	0.451	0.457	0.479	0.454	0.458	0.422	0.487	0.502	0.458	0.028
<i>Nemertesia ramosa</i>	0.498	0.477	0.512	0.523	0.496	0.434	0.515	0.479	0.555	0.491	0.498	0.030
<i>Pachymatisma johnstonia</i>	0.472	0.472	0.455	0.501	0.448	0.476	0.484	0.465	0.460	0.488	0.472	0.015
<i>Raspailia ramosa</i>	0.540	0.520	0.465	0.528	0.514	0.536	0.542	0.522	0.501	0.532	0.520	0.022

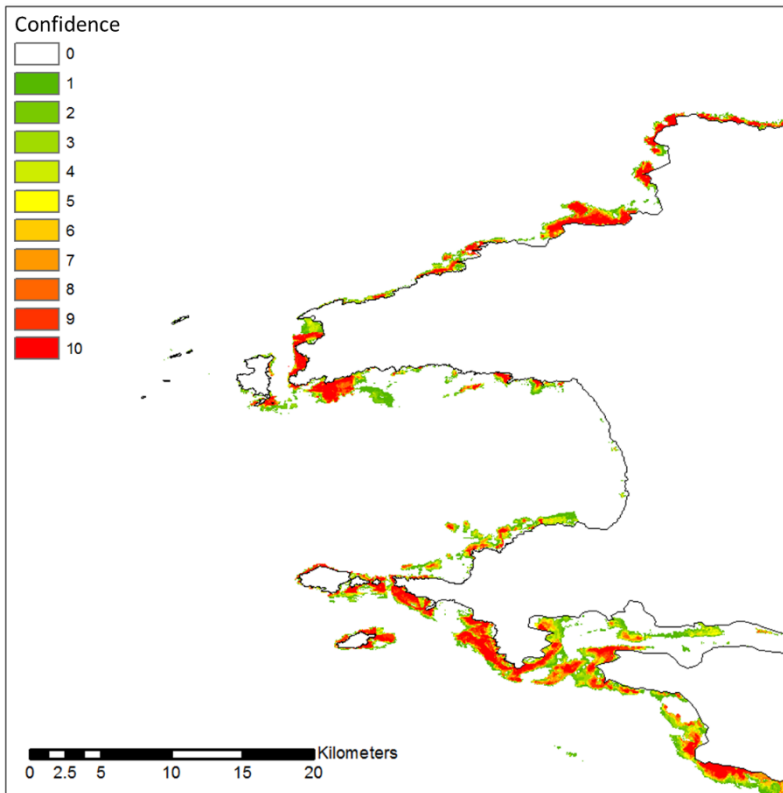


Figure 6-20: Combined predicted spatial distribution of *Axinella dissimilis*, with a confidence score of 0 (absent in all 10 predictions) to 10 (present in all 10 predictions).

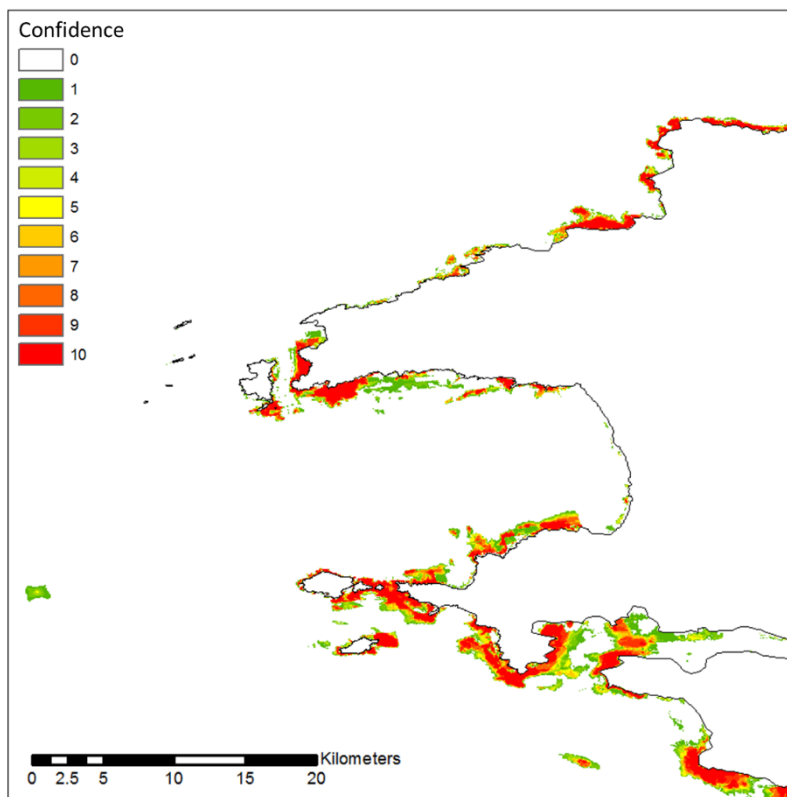


Figure 6-21: Combined predicted spatial distribution of *Alcyonium digitatum*, with a confidence score of 0 (absent in all 10 predictions) to 10 (present in all 10 predictions).



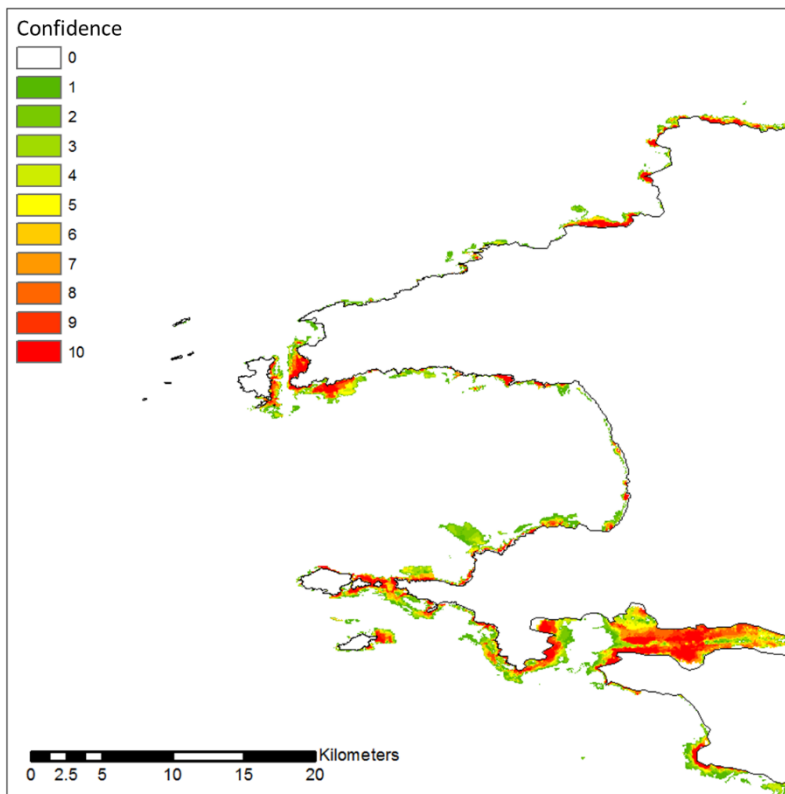


Figure 6-22: Combines predicted spatial distribution of *Bugula turbinata*, with a confidence score of 0 (absent in all 10 predictions) to 10 (present in all 10 predictions).

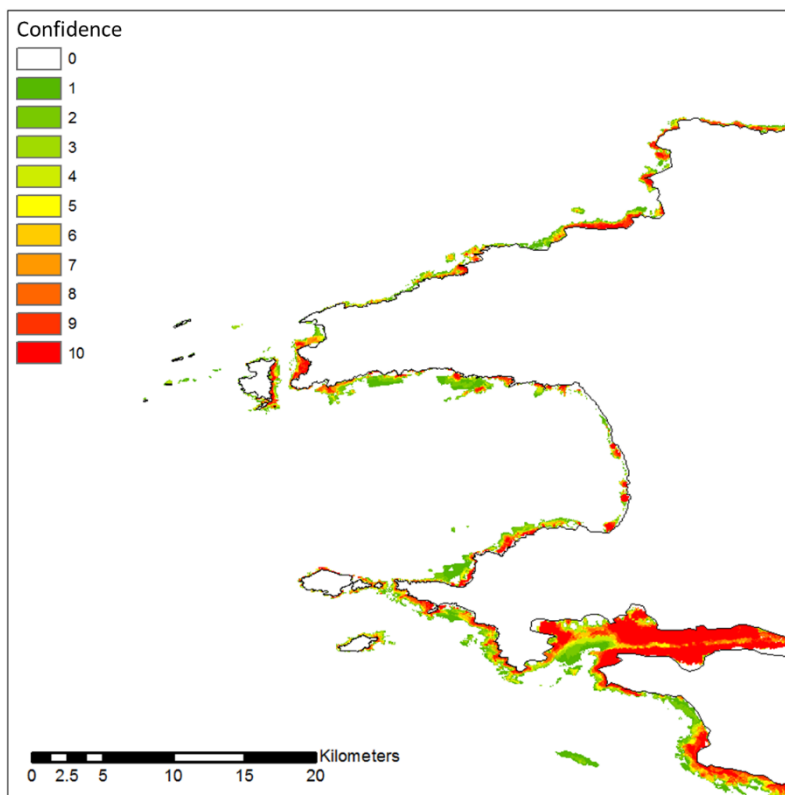


Figure 6-23: Combined predicted spatial distribution of *Dendrodoa grossularia*, with a confidence score of 0 (absent in all 10 predictions) to 10 (present in all 10 predictions).

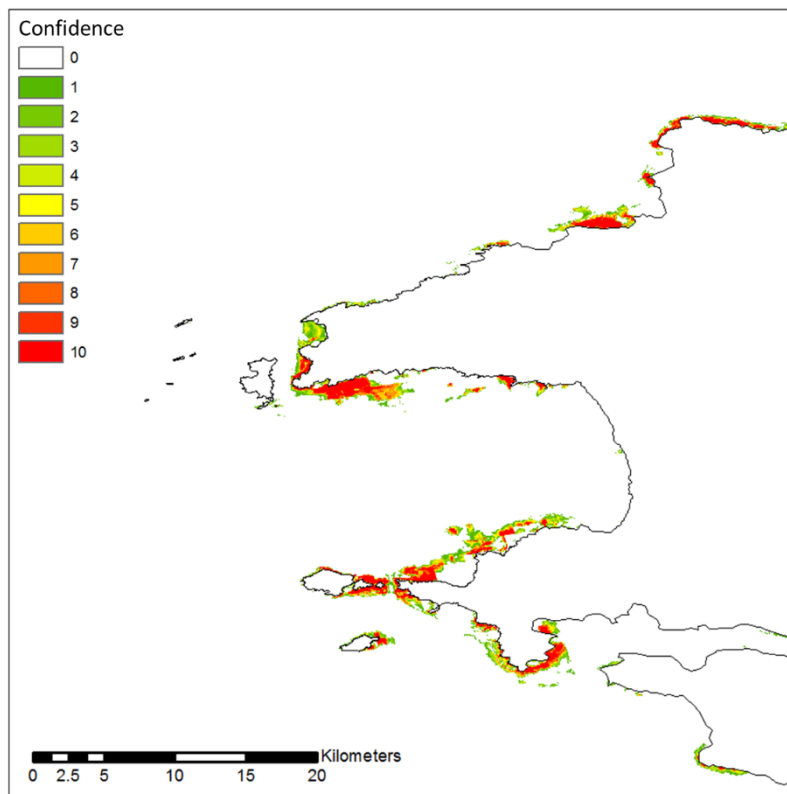


Figure 6-24: Combined predicted spatial distribution of *Eunicella verucosa*, with a confidence score of 0 (absent in all 10 predictions) to 10 (present in all 10 predictions).

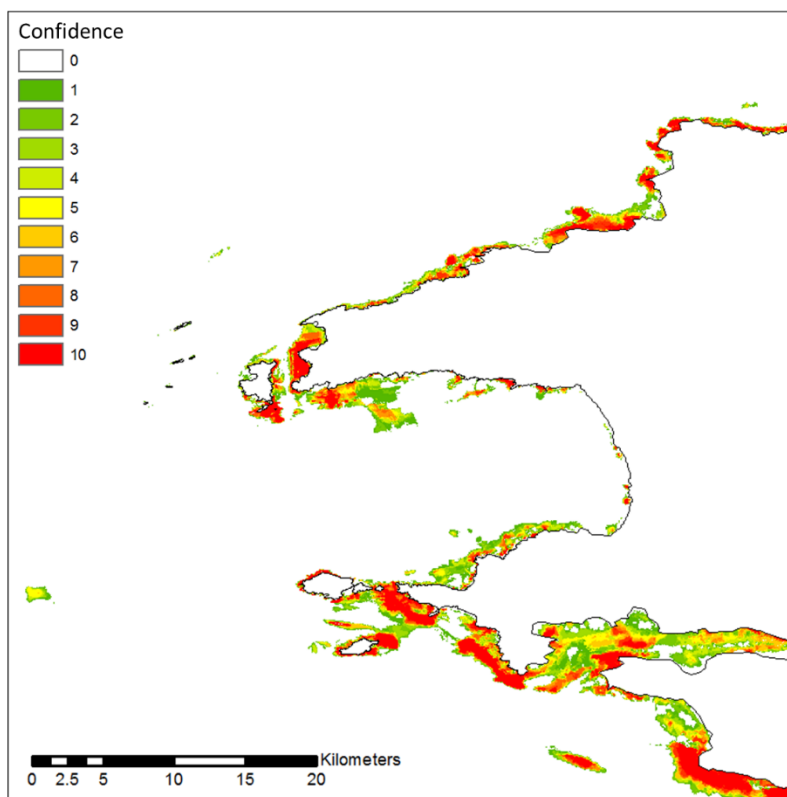


Figure 6-25: Combined predicted spatial distribution of *Flustra foliacea*, with a confidence score of 0 (absent in all 10 predictions) to 10 (present in all 10 predictions).

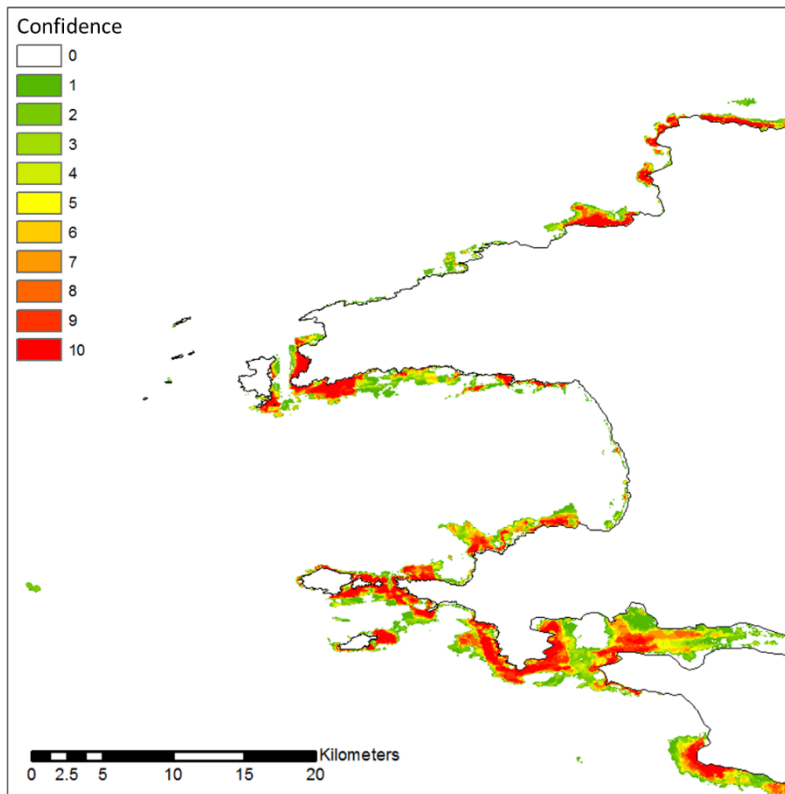


Figure 6-26: Combined predicted spatial distribution of *Nemertesia ramosa*, with a confidence score of 0 (absent in all 10 predictions) to 10 (present in all 10 predictions).

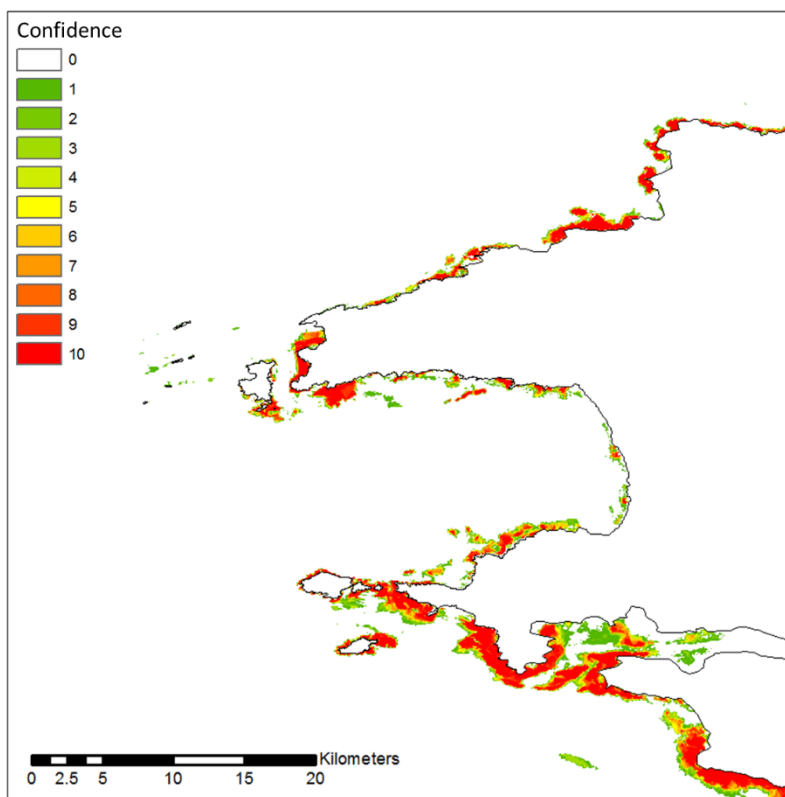


Figure 6-27: Combined predicted spatial distribution of *Pachymatisma johnstonia*, with a confidence score of 0 (absent in all 10 predictions) to 10 (present in all 10 predictions).

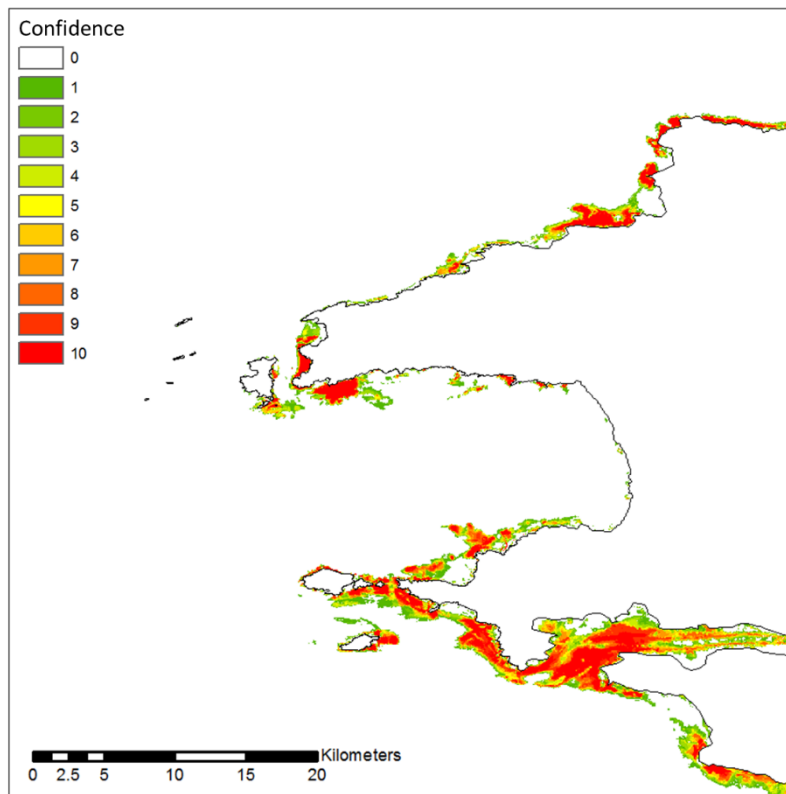


Figure 6-28: Combined predicted spatial distribution of *Raspailia ramosa*, with a confidence score of 0 (absent in all 10 predictions) to 10 (present in all 10 predictions).

To determine the effect of deploying the turbines, the MaxEnt model was run with the background variables from a reference model run without the influence of the tidal turbines and again with the turbines in place. By transforming the predicted probabilities to presence/absence, it was possible to provide a comparison between the two cases by producing plots of areas of habitat that were lost and created. By habitat lost it is meant that the area is no longer suitable for that particular species. Figure 6-29 shows the predicted habitat lost and created for *Axinella dissimilis*.

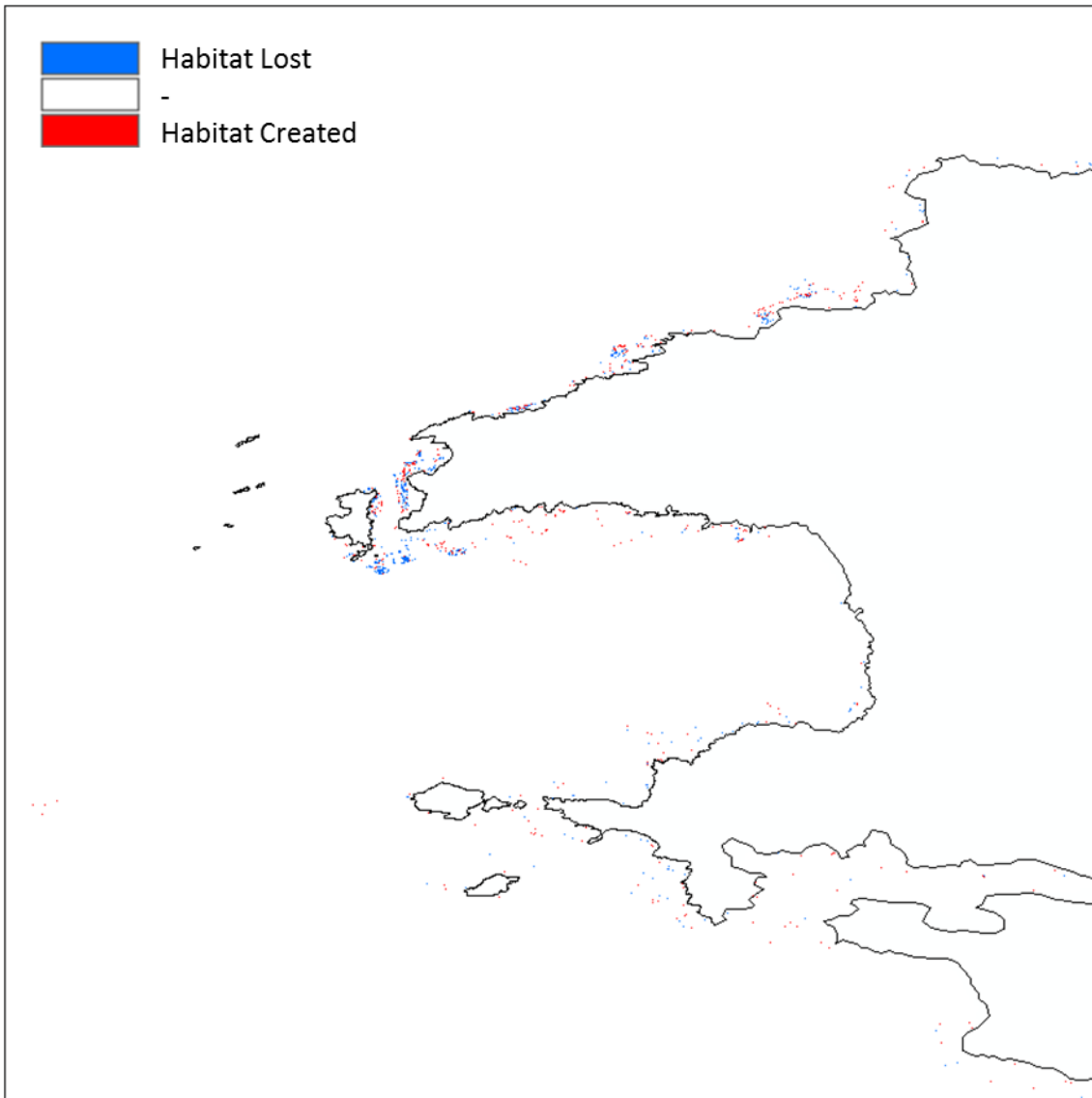


Figure 6-29: Combined predicted habitat lost (blue) and created (red) of *Alcyonium digitatum* due to the presence of a 10 MW tidal array at St David's Head.

To quantify the change in habitat, the percentage difference in habitat lost and the net change in habitat were calculated. However, due to the large model domain, these values were negligible. A more practical approach was to limit the calculation to a smaller area. The principal background variable to change, under the influence of the turbines, was bed shear stress. As such, the calculation was limited to the spatial extent of the change in bed shear stress, as shown in Figure 6-30.

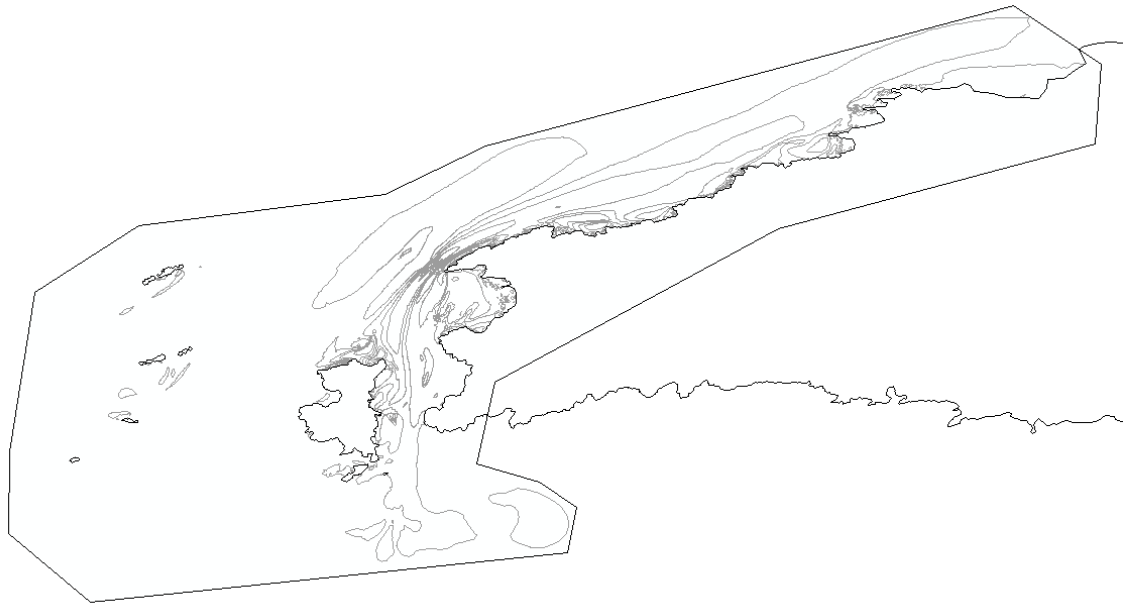


Figure 6-30: Zonal boundary of bed shear stress change

Figure 6-31 is box and whisker plot of the total predicted habitat within the zone of bed shear change for the ten replicants. Figure 6-32 and Figure 6-33 are is box and whisker plots of habitat lost and created due to the presence of the tidal array. Table 6-5 summarises the average habitat change for each species.

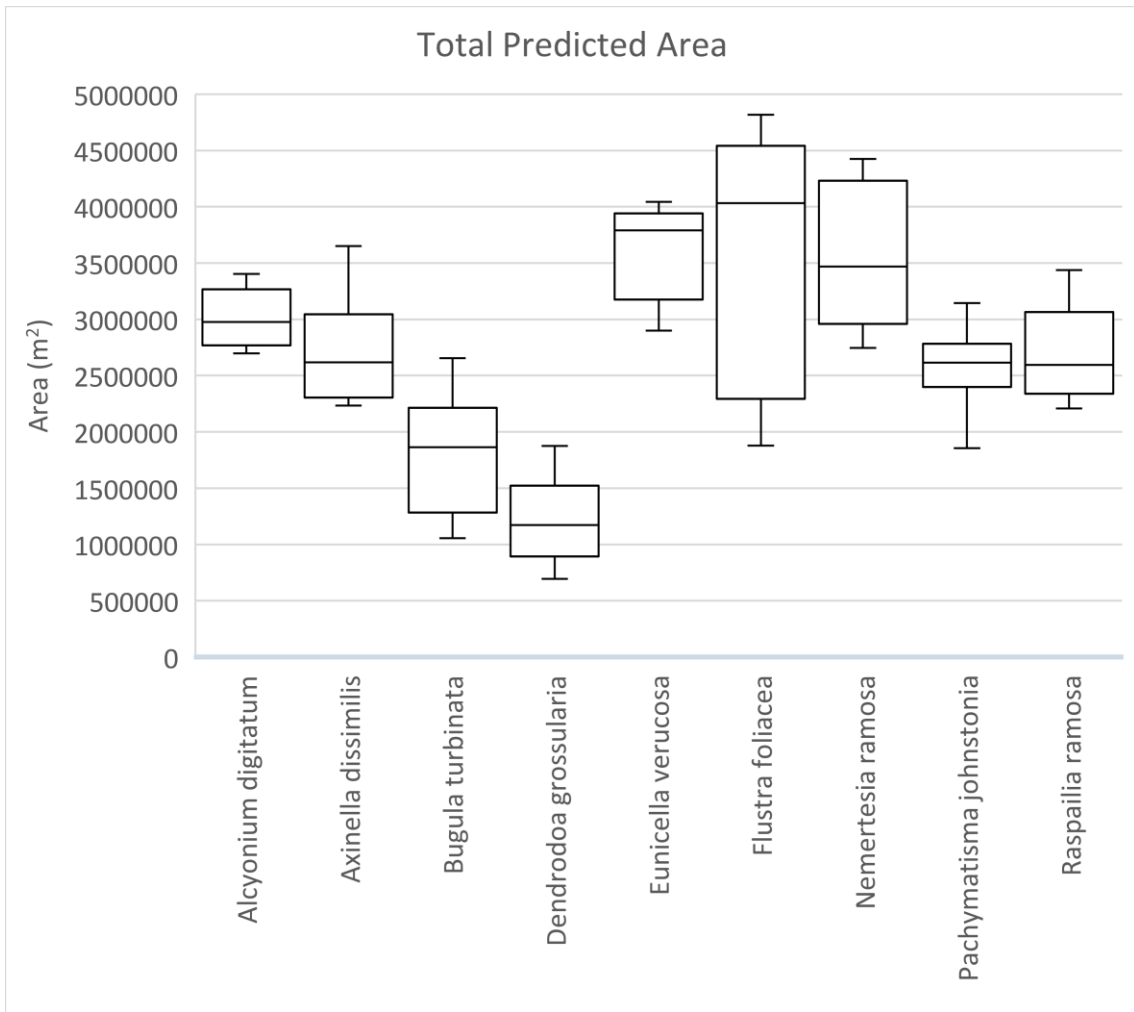


Figure 6-31: Box and whisker plots of the total area of predicted spatial distribution from the ten replicants for each species.

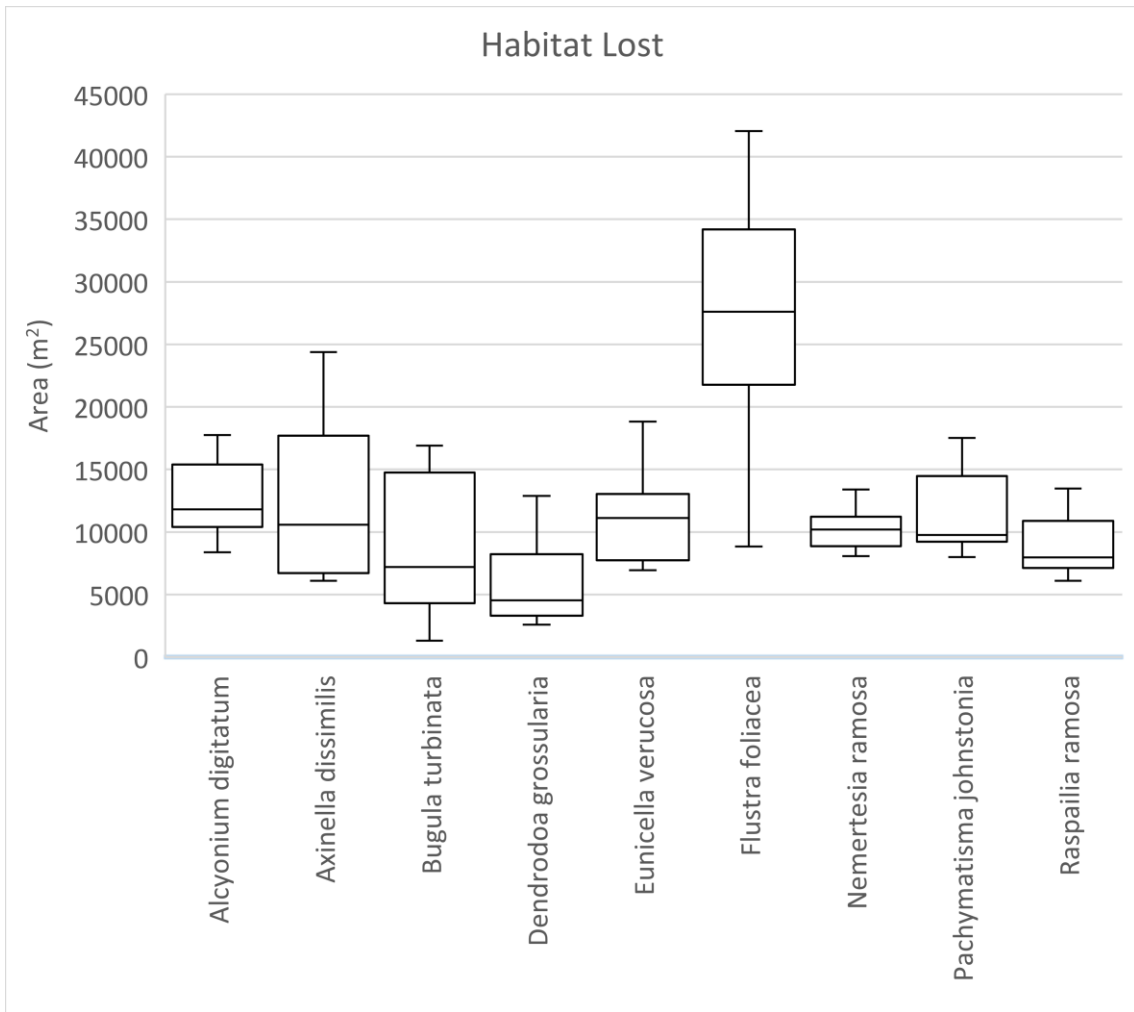


Figure 6-32: Box and whisker plots of the area of habitat lost due to the tidal stream array from the ten replicants for each species.



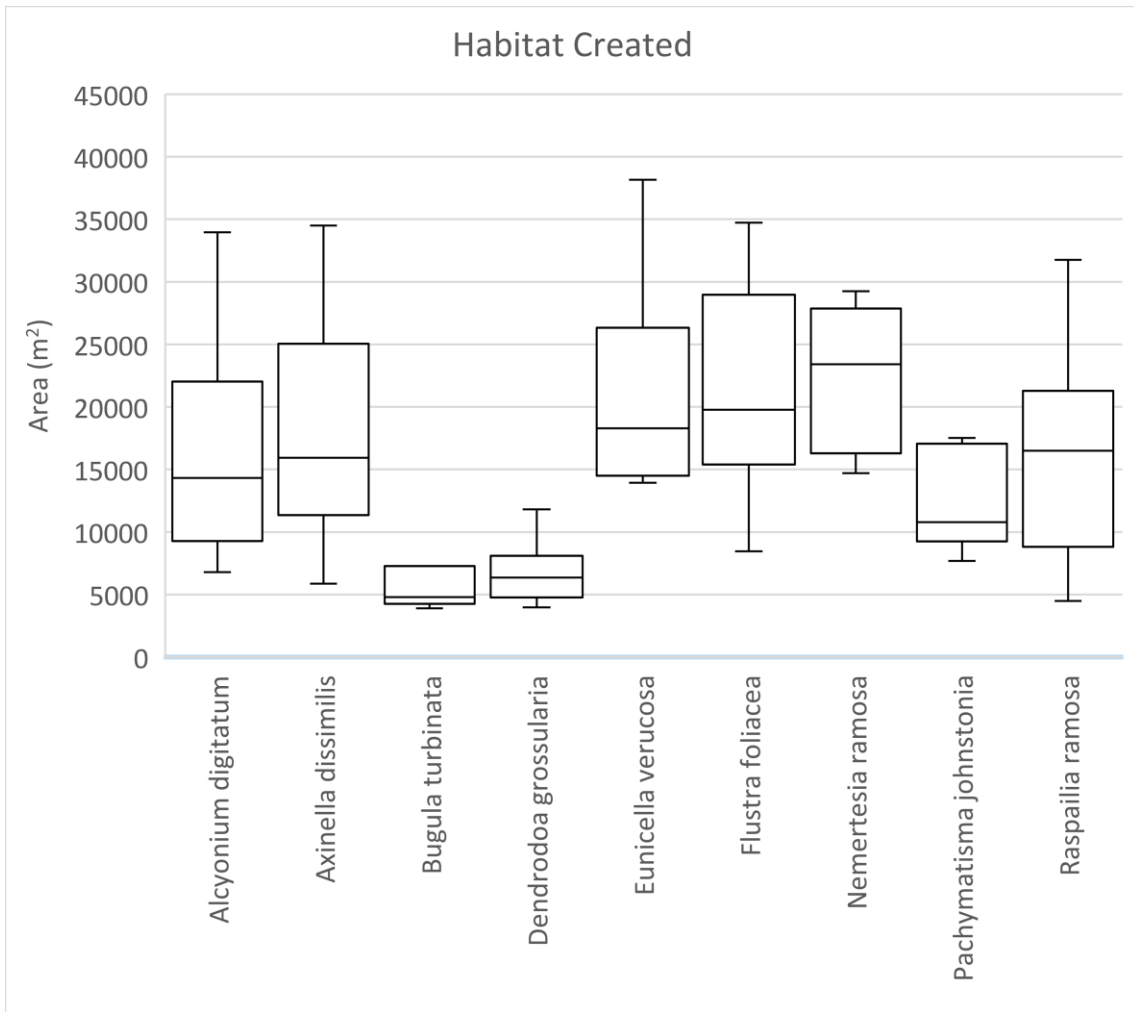


Figure 6-33: Box and whisker plots of the area of habitat created due to the tidal stream array from the ten replicants for each species.

Table 6-5: Summary of the average change in habitat for all ten replicants.

Species	Area Lost (m <sup>2</sup> )	Standard Deviation (m <sup>2</sup> )	Area Lost (%)	Standard Deviation (%)	Area Created (m <sup>2</sup> )	Standard Deviation (m <sup>2</sup> )	Area Created (%)	Standard Deviation (%)
<i>Alcyonium digitatum</i>	12399	2958	0.405	0.106	16717	8261	0.518	0.196
<i>Axinella dissimilis</i>	12483	5993	0.483	0.278	18187	9061	0.656	0.271
<i>Bugula turbinata</i>	8507	5190	0.451	0.220	6854	4616	0.394	0.235
<i>Dendrodoa grossularia</i>	5948	3455	0.482	0.204	8073	5527	0.732	0.641
<i>Eunicella verucosa</i>	11226	3413	0.313	0.095	20632	7294	0.566	0.168
<i>Flustra foliacea</i>	27913	9221	0.882	0.498	23252	12221	0.648	0.255
<i>Nemertesia ramosa</i>	9802	2469	0.287	0.086	27722	19231	0.773	0.481
<i>Pachymatisma johnstonia</i>	11569	3087	0.444	0.080	13663	7418	0.523	0.232
<i>Raspailia ramosa</i>	8911	2267	0.334	0.084	16511	7757	0.599	0.245

Table 6-5 indicates that the tidal array at St David's Head does not have a large negative effect. The largest average loss was experienced by *Flustra foliacea* at 0.882%. To assess whether the change caused by the tidal array is statistically significant, a Student's t-test was performed. For a Student's t-test there are two hypotheses: the null hypothesis that states there is no difference between the total predicted area and the change in habitat, and the alternative hypothesis that states there is a difference (Nickerson, 2000). The chosen threshold for significance is 0.05, whereby the probability of observing the difference between the two datasets by chance is 5% (Nakagawa and Cuthill, 2007). Therefore, for the results to be significant, a p-value of less than 0.05 is required. The p-value is found by determining a t-score and the number of degrees of freedom of the two datasets. The t-score,  $t$ , is calculated by:

$$t = \frac{(\mu_1 - \mu_2)}{s_d} \quad (6.16)$$

where  $\mu_1$  and  $\mu_2$  are the means of the two datasets and  $s_d$  is the variance between the two datasets, as calculated by:

$$s_d = \sqrt{\left(\frac{s_1^2}{N_1} + \frac{s_2^2}{N_2}\right)} \quad (6.17)$$

where  $s_1$  and  $s_2$  are the standard deviation of the two datasets and  $N_1$  and  $N_2$  are the number of samples in each dataset. To assess the statistical significance of change, the two datasets used will be the total area predicted in the base case and the total area +/- the habitat created/lost. The number of degrees of freedom is equal to the total number of samples of both groups minus two. As the MaxEnt model was replicated ten times, the number of degrees of freedom is 18. Table 6-6 summaries the t-score for the habitat lost and created for each of the nine species.

Table 6-6: T-Score for the habitat lost and created for a species.

Species	T-Score	
	Habitat Lost	Habitat Created
<i>Alcyonium digitatum</i>	0.050	0.068
<i>Axinella dissimilis</i>	0.065	0.094
<i>Bugula turbinata</i>	0.037	0.030
<i>Dendrodoa grossularia</i>	0.038	0.051
<i>Eunicella verucosa</i>	0.065	0.120
<i>Flustra foliacea</i>	0.058	0.048
<i>Nemertesia ramosa</i>	0.036	0.101
<i>Pachymatisma johnstonia</i>	0.080	0.093
<i>Raspailia ramosa</i>	0.051	0.093

Based on the calculated t-scores and 18 degrees of freedom, the p-value for all nine species falls between 0.25 and 0.5, which is larger than the threshold of significance. Therefore, the alternative hypothesis is rejected and it can be said that the change caused by 10 MW tidal array at St David's Head does not significantly change the benthic environment. For the array to cause a statistically significant change to the predicted distribution, the t-score would need to be larger than 1.734, which equates approximately to a 17% change in the area.

When considered in isolation, the spatial extent of the impact on each species is limited. However, when considering cumulatively, it gives a broader picture. Figure 6-34 shows the combined change in habitat for the ten replicants of all nine species modelled.

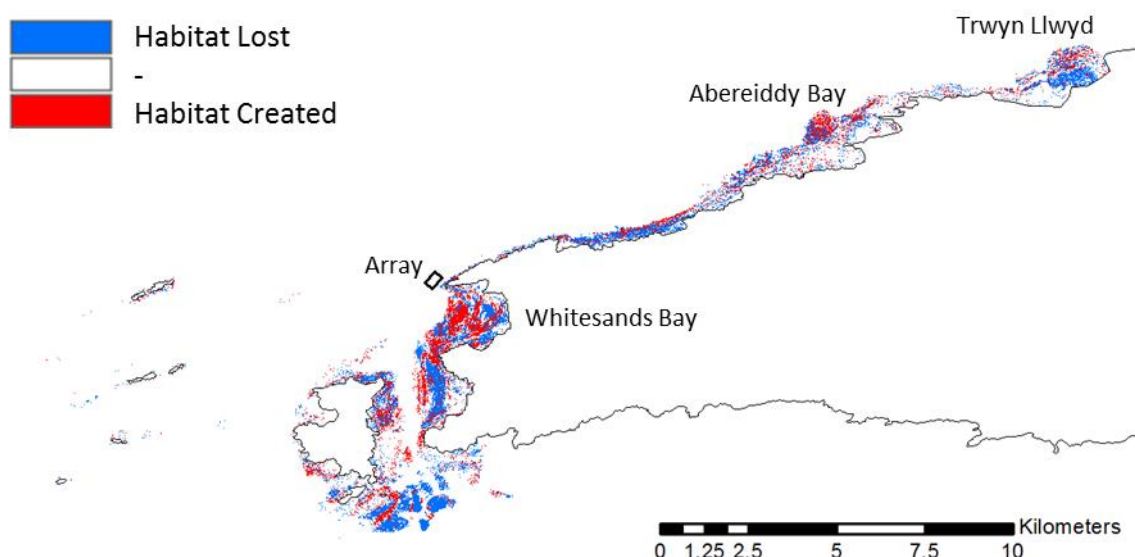


Figure 6-34: Combined changes in habitat of all replicants and species.

Unlike the impact on the bed shear stress, which was greatly affected in the direct wake and vicinity of the array, it is evident from Figure 6-34 that the main impact of the tidal turbines on the benthic habitat occurs further away. The impact is primarily seen in the edges of Ramsey Sound, Abereidddy Bay, Whitesands Bay, Trwyn Llwyd and amongst the coves along the north Pembrokeshire coast. The changes extend approximately 20km north of the tidal array.

## 6.5 Discussion

The results of this case study show the relative value this type of integrated modelling can provide to developers and its importance to the regulators. This approach has highlighted a number of key observations:

1. The far field impacts extend further than the direct wake of the tidal array.
2. The results provide insight into potential sites for environmental monitoring.
3. For this site, the tidal turbines have a limited impact on the benthic environment.
4. The impacts are dependent upon sediment type at the location being considered.

In this study it was expected that the impact of the tidal turbines would not occur at the location of the tidal array. It is clear from Figure 6-20 – Figure 6-28 that none of the indicator species were present within the vicinity of the tidal array. It

is a relatively exposed site with strong tidal currents meaning anything that does live there, most likely crustaceans and molluscs, are already adapted to living under extreme conditions (Warwick and Uncles, 1980). Where the tidal turbines are likely to impact is further away where sediment and nutrients are transported into more benign locations, such as bays and inlets. Figures of combined impacts, such as Figure 6-34, provide valuable insight of where the greatest potential impact will occur. As physical environmental monitoring is expensive, this type of modelling approach can be used to maximise its effectiveness by informing the selection of monitoring sites (Van der Meer, 1997).

It is known that the key impact of a tidal turbine is its physical presence reducing the velocity of the water. This in turn alters bed shear stress and hence sediment transport patterns around the turbine. The change in sediment transport is the dominant factor in driving change to the benthic habitat. There are two mechanisms for a species being removed. The first is the gradual change in sediment grainsize to the point the habitat becomes unsuitable. The second is the burial of a species from settling of suspended sediments. It was intended to model this in MaxEnt through the three variables: bed shear stress, grainsize and suspended particulate matter. Chapter 4 showed a clear impact from the tidal array on bed shear stress and the change in mean and maximum values were included in the model. In this Chapter, grainsize distribution was determined. Whilst the change in grainsize was included in the model, its impact on the results were subtle. The results showed the grainsize in the vicinity of the tidal array would reduce but never enough to change the category of the sediment type. Hence the sediment distribution did not radically alter. As for the last variable, suspended sediments, because there were no post installation observations or model predictions the suspended particulate matter was the one variable that could not be altered. Whilst the inclusion of a suspended sediments prediction would make for an improved model, it is believed in this instance the results would not widely change. Robins et al (2014) investigated the impact of tidal stream arrays in relation to the natural variability of sedimentary processes. In their case study, they found that up to 50MW of tidal energy could be extracted without causing alterations to sediment transport that were larger than the natural variation around Anglesey. As only 10MW are being deployed within the St David's Head case study, it can be reasoned that the impact on suspended

sediments will be less. Therefore, if the changes would not cause an impact greater than the natural variation, then the result of not including the variation in suspended sediments within MaxEnt are minimal.

On the subject of natural variation, due to the small change in habitat suitability it may be impossible to discern a change in actual field observations. In Chapter 4 it was concluded that the spatial variation in bed shear stress was in a location that was tidally dominated, hence the contribution due to waves was ignored. However, the spatial extent of the habitat variation extends into areas where the bed shear stress is dominated by waves. As such, the small variation in bed shear stress due to the tidal array in places like Abereid Bay will be masked by the natural variation due to wave interaction. As such, the impact due to the tidal array will be potentially less than predicted.

## 6.6 Summary

This chapter presents the results of an impact assessment of the 10 MW tidal array at St David's Head on the benthic environment. This has been achieved through the use of the species distribution modelling software MaxEnt. It has been shown that tidal turbines will influence local hydrodynamics which are a driver for morphodynamics and can lead to change in the benthic habitat. Nine sessile species were identified for inclusion in the model which represent hydroids, bryozoans, soft corals, sponges and ascidians commonly found on reefs within the Pembrokeshire Special Area of Conservation and the Skomer Marine Nature Reserve.

The impact of the tidal turbines was determined by the change in the total area of each species with and without the presence of the tidal turbines, with the model replicated ten times. Results showed that whilst the presence of the tidal turbines resulted in a loss of habitat for each species (0.28-0.88%), it also created areas of new suitable habitat (0.39-0.77%). However, the change was small and was found not to be statistically significant compared to the total area of predicted distribution. The spatial extent of habitat change extends beyond the direct hydrodynamic wake of the tidal turbines and into areas where other factors, such as bed shear stress due to waves, are more dominant. As such, the change in habitat driven by the tidal turbines may be masked by natural variation. Therefore, in this location, tidal turbines will not adversely affect the benthic environment.

Whilst there are limitations to the application of this type of modelling can achieve, it can provide some useful insights. For example, evaluation of cumulative impact can provide an insight into where the greatest potential impact will occur and allow a more subjective approach to site selection and the design of physical monitoring programmes.



# Chapter 7

## Discussion & Conclusions

### 7.1 Introduction

The marine environment has intrinsic value beyond the monetary (World Health Organisation, 2005). Whilst marine renewable energy can play an important role in tackling climate change and global warming, it needs to be sited sensitively so as not to hinder an already stressed environment (Moffitt et al., 2015). The benthic habitat plays an important role in the ecosystem where a diverse range of species fulfil many different ecological niches and roles. Whilst they can adapt and even thrive with small changes (Thrush and Dayton, 2002), dramatic disturbances can have fatal consequences (Sparks-McConkey and Watling, 2001; Hinchley et al., 2006). The principal aim of this study was to investigate the interaction between tidal turbines and the benthic environment. This was achieved through a variety of modelling techniques, fulfilling the research objectives as outlined in Section 1.3.

### 7.2 Modelling Tidal Turbines

As the physical interaction of the tidal turbines with the hydrodynamics is the primary driver of change, it is important that this is correctly implemented. A tidal turbine causes change in momentum in two phases: thrust force produced by the

rotor due to energy extraction and a drag force caused by the supporting structure. It is important to include the structural drag otherwise the impact would not be sufficiently representative as it would underestimate the impact of the tidal turbine, especially at velocities higher than the turbine's rated output.

Implementing tidal turbines into hydrodynamic models, such as TELEMAC, is not a new technique (see Neill et al., 2012; Plew and Stevens, 2013 Thiebot et al., 2015). However, one of the key features that differentiates how the tidal turbines have been implemented in this study is the ability to model tidal turbines in multiple areas with different types of turbine technology. This gives the model greater flexibility and makes it more adaptable to different studies.

The advantage of using an unstructured mesh for hydrodynamic modelling is it allows complex coastlines to be more accurately represented by providing a varying resolution in these areas particularly. The disadvantage, with respect to modelling tidal turbines, is that it results in mesh elements with different areas meaning the force of the tidal array is not uniformly distributed. To ensure a uniform force distribution the area surrounding the turbine location was discretised with a regular mesh nested within the unstructured mesh. This was important as it meant the impact of each turbine was identical and any variation was due to the interaction with the hydrodynamic conditions and not the parameterisation.

The role of the idealised channel model was to test not only the parameterisation of a tidal turbine but also how best to represent tidal arrays. Studies typically represent the influence of a tidal array as a single area (e.g. Draper et al., 2014; Thiebot et al., 2015). The alternative, tested in this study, was to represent individual devices. Representing a tidal array as a single area is a misrepresentation as it does not include the intra-array effects and leads to an over-estimation. This was confirmed by the results of the idealised channel model. The parameterisation of a tidal turbine was successfully implemented into the model using the depth averaged hydrodynamic modelling software TELEMAC2D. The performance of the parameterisation was validated using linear momentum actuator disk theory (Houlsby et al., 2008). Results showed that modelling the array as individual devices exhibited good agreement with theory, whilst modelling the whole array over-estimates the velocity reduction and under predicts the head drop. Based on the results of this study it is recommended to

model the individual devices within a tidal array and not represent the total influence of the array as a single area.

### 7.3 Modelling the hydrodynamic morphological impacts of a tidal stream development in Ramsey Sound

A high-resolution depth averaged hydrodynamic model has been used to simulate the impact of the proposed 10MW tidal array at Ramsey Sound. The model was validated against a range of sources of data. Although the model did not exactly reproduce the profile of the ADCP transect through Ramsey Sound, the model did reproduce the peak velocity magnitude. It highlights the potential limitation of using depth averaged models to accurately reproduce real 3D conditions. Despite this, the model showed good agreement with the tide gauges, tidal diamonds, a bottom mounted ADCP and harmonic analysis.

The model represents a significant improvement in model resolution over previous models of the Pembrokeshire area allowing for the complex features of the environment to be resolved. Previous models (Fairley et al., 2011) have made assessments of the potential power of the site but do not include the presence of tidal turbines or a detailed assessment of power production. The model used in this study is the first to implement individual tidal turbines and investigate their hydrodynamic influence.

Harmonic analysis of the model results showed the 10MW tidal array reduced the amplitude of the M2 and S2 tidal constituents by 20% and 19%, respectively in the location of the array. Whilst the wake effect of the array extends 13km from the site, far field effects were seen as far as 20km due to alterations in eddy propagation. It is important to stress that the investigation into the impacts of tidal turbines are particularly site specific and no generic value of impact can be made. Ramsey Sound represents a challenging environment, not just for modelling but also for the operators of a tidal array. The complex nature of the surrounding bathymetry means it is an area of high eddy generation. Results showed that the presence of the tidal array altered these natural processes leading to effects further afield than the direct wake of the array.

Plots of the range of difference can provide useful insights for developers and regulators as they provide a clear zone of influence which is considerably larger

than the direct wake effect of the array. The model is purely hydrodynamic with no atmospheric forcing or wave driven currents. The position and dispersion of eddies in this area would naturally vary if these additional interactions are included, meaning the zone of influence may change. The formation and dissipation of the eddies only last for a tidal cycle, meaning any changes to eddy propagation only provides a short-term view. The influence on parameters, such as bed shear stress, can provide a better insight into the longer-term impact on sediment dynamics.

Whilst this study does not include a full morphodynamic model, it is the first study to investigate the impact of tidal turbines on morphological processes around Pembrokeshire. There are currently no other published studies meaning the results fill a gap in understanding in processes around Pembrokeshire, even if the results are qualitative in nature.

The principal impact of the tidal array is to act as a barrier to sediment transport by causing sediment to accumulate in the wake of the array. During the flood, there is a greater accumulation of medium gravel within the array at St David's Head and 1 km downstream in its wake. During the ebb, there is an increased accumulation of fine gravel 3 km downstream of the array at the northern entrance of Ramsey Sound as well as coarse sand north of Ramsey Island. As flow velocities through St David's Head and the Bishop's & Clerks exceed 2m/s, as well as speeds exceeding 3m/s in Ramsey Sound, any sediment smaller than coarse gravel was previously unlikely to stay within this region for long. As a result of the tidal turbines, finer sediment is accumulating in areas previously void of that sediment class. The implication of this is that the sediment class distribution will alter leading to a change the physical benthic habitat that may be less suitable to the species presently occupying that area. Similarly, an increase in sediment accumulation could lead to the burial of benthic species, leading to increased mortality.

The results of Ramsey Sound case study are used as inputs for the species distribution modelling conducted in Chapter 6 using MaxEnt. Specifically, the MaxEnt model uses depth (bathymetry), mean and maximum bed shear stress and wave height as calculated by TELEMAC and TOMAWAC. As the MaxEnt model domain is different from TELEMAC model domain, the results of the unstructured mesh are interpolated onto the regular grid in order to be directly

used by MaxEnt. The TELEMAC base case provides the background conditions on which the MaxEnt model is trained, where upon the conditions of the turbine case are used to assess the change to the benthic environment.

Based on the research conducted in Chapter 4, a paper titled “Modelling the hydrodynamic and morphological impacts of a tidal stream development in Ramsey Sound” has been submitted to the Journal Renewable Energy for review.

## 7.4 Cumulative Impact Assessment of Tidal Energy in the Irish Sea

Assessments of tidal energy in the Irish Sea have previously been undertaken by Robins et al. (2015), Lewis et al. (2015) and Neil et al. (2014) but do not include the presence of tidal stream devices. Walkington & Burrows (2009) do include the presence of tidal turbines but only investigate each array in isolation. What differentiates the model used in this study compared to previous models, is the use of multiple types of turbine technology. Furthermore, the model used here is a significant improvement upon Walkington & Burrows (2009) in terms of model resolution and the method of representation of the tidal turbines. Walkington & Burrows (2009) represent the tidal array as a constant drag term neglecting the operation of the turbine and drag of the support structure.

A cumulative impact assessment of tidal energy in the Irish Sea has been undertaken using a high-resolution depth-averaged hydrodynamic model. Five of the eight tidal projects run quite independently of each other, although results show that Fair Head, Torr Head and Mull of Kintyre lie within each other’s zone of influence. Whilst not intended as an original objective, a second smaller coastal model was developed which included only these three projects. The results of the model are of great value to the regulators and the developers as it is the only detailed study of the cumulative impact assessment of Fair Head and Torr Head. Both developers of the two sites have not included an impact assessment on the other development in their Environmental Impact Assessment as they do not consider the other to be sufficiently along the consenting process to warrant investigation. Furthermore, there are no other published detailed studies of hydrodynamic modelling of this area.

Results of the second model show that the Mull of Kintyre project had very little impact on the energy production at Fair Head and Torr Head. Energy production slightly increased (+0.09%) at the Mull of Kintyre with the presence of the other two projects. For the two remaining projects, Fair Head had a greater impact on Torr Head than vice versa. Torr Head reduces energy production at Fair Head by 2%, whereas Fair Head reduces energy production by 17% at Torr Head. Whilst the economic viability of tidal energy was not considered within the remit of this study, it is clear that with a 17% reduction in energy production, Torr Head would lose a considerable portion of revenue. However, if Torr Head could still operate commercially despite the presence of Fair Head then there are environmental positives. The spatial extent of change to bed shear stress from operating Fair Head and Torr Head is similar to Fair Head operating alone. In both cases sediment would accumulate within the vicinity of the arrays with areas of erosion either side. The turbines are situated in an area of mainly gravel and exposed rock, meaning the impact of the erosion north of the two arrays would be minimal. However, sand is present between the coastline and the arrays meaning an erosion in this area is of greater consequence leading to a significant change in habitat. If the impact of the erosion in this area is deemed to be acceptable by the regulator, then the further presence of Torr Head would not lead to a significant additional impact.

Based on the research conducted in Chapter 5, a paper titled “Cumulative Impact Assessment of Tidal Stream Energy Extraction in the Irish Sea” has been published by the Journal of Ocean Engineering and is available: <http://doi.org/10.1016/j.oceaneng.2017.04.003>.

## 7.5 Modelling the Benthic Environment

Assessing the impact of tidal turbines on the benthic environment has not been considered a high research priority, meaning the only literature in this area is a conference paper by Bell et al (2011). This represents a significant gap in understanding around the subject, which this study aimed to fill. This study also improves upon the limitations of the Bell et al (2011) study whereby the impact of the tidal turbines was implemented through a constant percentage reduction in bed shear stress rather than model the tidal turbines.

From the modelling of the 10 MW tidal array at St David's Head, a spatial prediction of nine sessile species around Pembrokeshire was conducted using the species distribution model MaxEnt. The nine indicator species were chosen as they provided a range of representative species found within the Pembrokeshire Special Area of Conservation and the Skomer Marine Nature Reserve. Due to the close relationship between the benthos and the physical substrate, the predicted sediment distribution in Chapter 4 was qualitative in nature and was not used in the species distribution model. Instead, quantitative information about the sediment was required. A Random Forest model was used to make a spatial prediction of the sediment type fraction distribution based on observations. The model could be improved with more observations and acoustic back scatter data. However, this would require an expensive field campaign. Despite this limitation, the model does provide useful information and represents a methodology to enable developers to conduct desk based assessments of the sediment type fraction distribution using publicly available legacy data without expensive field campaigns.

The species distribution model was used to quantify the total area where the species were present. The impact of the tidal turbines was determined by the area of suitable habitat lost and new habitat created. As the area of change was small in comparison to the model domain, the calculated area of change was restricted to the extent of change in the bed shear stress. Whilst the environmental pressures on the marine renewable energy industry are significant and potentially prohibitive, the study shows that the 10 MW tidal array will not have a significant negative impact on the benthic environment at St David's Head. The model showed the presence of the tidal turbines resulted in a loss of habitat for each species, with the percentage difference of habitat lost ranging from 0.28% to 0.88%, which was not statistically significantly different from the total predicted distribution. This is a very positive result for the tidal development at St David's Head but caution should be applied before a generalisation is made towards the whole tidal industry. Case studies of this type are site specific and results are pertinent to each site. The impact at one site does not necessarily reflect the impact at another. Modelling is a cost-effective method for resource and impact assessments but must be used to complement physical observations as validated model results are crucial to determining the true impact. Whilst it has

been shown the impact of MCT at Strangford Loch and OpenHydro at EMEC is negligible (Keenan et al., 2011; Broadhurst & Orme, 2014), this does not represent the impact of a small tidal array for example at St David's Head. Furthermore, a small array at St David's Head does not reflect the potential impact of a 100MW tidal array, for example the MeyGen tidal farm in the Pentland Firth. Until a larger sample of sites is available, with devices deployed in the water, then a fuller assessment of validated results will not be possible. However, it is possible to build a picture of what the impact may be, even if small, and more importantly where.

An important result of the study was that the spatial extent of change to the benthic environment extended beyond the direct hydrodynamic wake of the array. Plots of the mean change in velocity or changes in the amplitude of harmonic constants provide useful information about the changes to the hydrodynamic conditions, but used alone would not indicate the true extent of the change to the benthic environment. The largest change to the hydrodynamics occurred within the vicinity of the tidal array, yet the main impact of the tidal turbines on the benthic habitat occurred further away in the more benign conditions. It shows that plots of the range of difference do provide a closer prediction of the spatial extent of change. This is important information for developers and regulators as it shifts the focus of where to look for environmental change. If developers and regulators only use the extent of the wake effect as a measure of where to conduct environmental monitoring, then the true impact may not be recognised. As physical environmental monitoring is expensive, this type of modelling approach can be used to maximise its effectiveness by informing the selection of monitoring sites.

There are clear benefits to this modelling approach as it indicates that tidal turbine deployments exhibit less impact on the benthic communities than may have been anticipated. However, without devices in the water at St David's Head and post installation field observations there is presently no way to validate the model. But that does not mean the model cannot provide valuable insights. Furthermore, the results presented do not include a time component. It shows the probability of where a species might occur and how that distribution changes, but does not show the implication of this result. It does not take into account the age to maturity of the species. There is little or no information on this for most of the species



modelled. *Bugula turbinata* has an age to maturity of less than 1 month (Ryland, 1976), whereas for *Alcyonium digitatum* it is 2-3 years (Hartnoll, 1977). As only a small fraction of the total population along the north Pembrokeshire coast is lost, given enough time and the proximity of new potential habitats, all the species have the potential to recover (Harris, 2012). However, this is difficult to determine as it is not known if the change in habitat would actually kill any of the species.

## 7.6 Limitations & Further Research

The combination of hydrodynamic numerical modelling and species distribution modelling used in this study has clear benefits, but it has highlighted a number of limitations that should be addressed in the future. The conclusions of this study are based upon the model predictions of a proposed tidal development. As neither this, nor any other tidal array has yet been built, there are no post installation observations of array-scale interaction from which to truly determine what impact a tidal array will have on the benthic environment. Once the tidal array is built, a field campaign can be conducted and the conclusions of this study examined.

One of the limitations of the species distribution model was the suspended sediments. It is expected that the presence of tidal turbines would alter suspended sediment loads. The model included observed suspended sediments but because there were no post-installation observations or model predictions the suspended particulate matter was the one variable that could not be altered. Whilst in this instance it is believed that the results would not have widely changed, the question remains to what extent would the results have changed. A full morphodynamic model, using a coupled SISYPHE-TELEMAC-TOMAWAC model, would answer this question and address other questions. SISYPHE is the bed evolution and suspended sediments module of the TELEMAC system. A SISYPHE model was not developed within this study due to time restrictions and insufficient observation data to provide accurate boundary forcing conditions or information regarding the vertical bed structure (i.e. grain size and depth of the erodible layer). If this information was available, the model could calculate the suspended sediments loads and allow the blockage effect from the tidal array to be further investigated by quantifying the change in the sediment transport rates. Furthermore, it could investigate how bed forms changed as a result of the

presence of the tidal array. The coastal model of Ramsey Sound quantified the change in bed shear stress due to the presence of the tidal array. However, this was only the bed shear stress due to skin friction. The model did not quantify the change in bed shear stress due to the variation in bed forms. It is important to note that in order to quantify the change in sediment transport rates and calculate suspended sediment loads, a field measurement campaign would be required to provide sufficient information to validate the model.

As the impact of the tidal array was found to be limited to the tidally dominated area, the effects on bed shear stress due to waves were ignored. The results of the species distribution model highlighted that the impact to the benthic environment extends beyond the direct wake of the tidal array and into areas of wave domination. As such, the natural variation in bed shear stress due to waves may well mask the impact of the tidal turbines. A fully coupled wave and tidal hydrodynamic model, using TELEMAC2D-TOMAWAC, could provide a better understanding of the total combined wave-tidal bed shear stress. As wave-current interactions can alter the tidal resource (Hashemi et al., 2015b), the coupled wave-tide model would provide a clearer indication as to the extent of change in bed shear stress which in turn can be fed into the species distribution model. Furthermore, it would also provide a better indication of the changes in the morphodynamics when further coupled with the SISYPHE model.

The aim of the coastal model was to investigate the impact of the proposed 10MW tidal array at St David's Head. The scope never extended to finding out what the maximum number of turbines that could be accommodated within the St David's Head lease site would be. Using the methodology set out in Robins et al (2014), the TELEMAC model combined with the SISYPHE model could be extended such that the maximum number of turbines could be determined without the changes to the suspended sediments exceeding natural variation. Equally, the aim of the species distribution model was to investigate the impact of the proposed 10MW tidal array and not determine the maximum number of turbines that could be accommodated without adversely affecting the benthic environment. An interesting question then presents itself: how does the maximum number of turbines as determined by the morphodynamic model vary from the maximum number of turbines as determined by the species distribution model?

The strength of the species distribution model is its ability to predict the impact of the tidal turbines spatially. Where it falls short is in its ability to determine the temporal impact. Whilst the model shows that habitat is lost and also new potential habitat is created, it does not show the implication of this result. It does not take into account the age to maturity of the species or how quickly a species can inhabit a new area. A potential solution is to use a coupled ecosystem-hydrodynamic model, such as ERSEM-GETM.

## 7.7 Conclusion

The principal aim of this study was to investigate the interaction between tidal stream arrays and the benthic environment. As the marine environment is already under considerable pressure, tidal stream developments must show they can be operated without any additional detrimental impact on the environment. Case studies of this type are site-specific and results are pertinent to each site. However, a more general conclusion can be applied to the whole tidal stream industry. This study presented an integrated approach using hydrodynamic modelling and species distribution modelling that developers and regulators can use to assess the impact of tidal turbines on the benthic environment. Modelling is a cost-effective method for resource and impact assessments but must be used to complement physical observations as validated model results are crucial to determining the true impact. It is possible, using the presented methodology, to site and size a tidal turbine development such that it does not have an adverse impact on the benthic environment.

As the greatest impact of a tidal stream device is very localised, tidal stream arrays need to be represented as individual devices where the extraction of energy mimics the real operation of a tidal turbine over a tidal cycle. Representing the influence of the combined array over a single area is a misrepresentation as it does not include the intra-array effects and leads to an over-estimation in the reduction in tidal velocities. Furthermore, the drag from the support structure needs to be included otherwise the impact would not be sufficiently representative as it would underestimate the impact of the tidal turbine, especially at velocities higher than the turbine's rated output.

The Ramsey Sound case study is a prime example as to why high resolution hydrodynamic models are required. Ramsey Sound is a complex environment

and encompasses many bathymetric features that significantly shape the hydrodynamics in the region. A high-resolution model was required to ensure the interaction with key bathymetric features of the environment was correctly resolved. Ramsey Sound is an area of high eddy generation and the presence of the tidal array directly influences the creation and propagation of those eddies. As a result, the zone of influence of the tidal stream array was larger than just the direct wake effect. If tidal arrays can be sited in less turbulent environments such that they do not influence areas of eddy generation, then the impacts could be reduced. However, the sites of interest around the UK are typically in turbulent environments meaning high-resolution models are required, at an appropriate scale, to enable the complex features of the environment to be correctly resolved for detailed site investigations.

Changes in bed shear stress can provide a useful insight into the potential long-term impact on the sedimentary processes. Tidal stream arrays are likely to act as a barrier to sediment transport by reducing the bed shear stress within the vicinity of the array, lead to an accumulation of finer sediment. In addition, bed shear stress may increase in areas, leading to an erosion of the seabed. The overall result is a potential change in the sediment class distribution that could lead to a change in the physical benthic habitat such that it is no longer favourable to the species presently occupying that area.

Within the limitations of the modelling approaches, a 10 MW tidal stream array at St David's Head was shown not to adversely affect the benthic environment. It was evident that this was to be expected as the indicator species investigated were not present within the vicinity of the array where the greatest change to the hydrodynamics occurred. Species that are likely to occur within tidal stream sites are already adapted to living under extreme conditions. The study showed that the spatial extent of change to the benthic habitat extended beyond the direct hydrodynamic wake of the array. Instead, the main impact of the tidal turbines on the benthic habitat occurred further away, in bays and inlets, where sediments and nutrients are transported into the more benign conditions. If developers and regulators only use the extent of the wake effect as a measure of where to conduct environmental monitoring, then the true impact may not be recognised.

Whilst the development of a 10 MW array is the likely to be the next step in the development of the tidal stream industry, it still represents a small-scale

deployment. The seabed was found to not significantly alter within the presence of the array at St David's Head. As array sizes increase, along with the number of deployments, the risk of change increases. Cumulative impact assessments of tidal stream developments need to be undertaken as the influence of one tidal stream development can adversely affect another. Furthermore, the impact on sites in close geographical proximity may not be equal. Hydrodynamic modelling offers the possibility to investigate how the cumulative power production could be maximised whilst minimising the environmental impact. In the Irish Sea case study, if Torr Head could still operate commercially in the presence of Fair Head, then the additional environmental impact of Torr Head, such as the change in bed shear stress, is small. Whilst the deployment of tidal stream extraction remains small, the risk of interaction is small. As the tidal stream industry grows and the technology matures, sites with lower peak velocities could be exploited. Thus, the risk of interaction will grow when more intermediary sites are developed.

# Appendix A

## File Format of Turbine Parameter Input File (.txt)

### File Format:

NARR

NSOM

TARR, NT, RDIAM, MDIAM, LMON, U\_Cut, U\_Des, CD, CTo, CPo, P\_Rated, RHO

XSOM(1,1), XSOM(1,2), ... , XSOM(1,NSOM)

YSOM(1,1), YSOM(1,2), ... , YSOM(1,NSOM)

TARR, NT, RDIAM, MDIAM, LMON, U\_Cut, U\_Des, CD, CTo, CPo, P\_Rated, RHO

XSOM(2,1), XSOM(2,2), ... , XSOM(2,NSOM)

YSOM(2,1), YSOM(2,2), ... , YSOM(2,NSOM)

...

...

...

TARR, NT, RDIAM, MDIAM, LMON, U\_Cut, U\_Des, CD, CTo, CPo, P\_Rated, RHO

XSOM(NARR,1), XSOM(NARR,2), ... , XSOM(NARR,NSOM)

YSOM(NARR,1), YSOM(NARR,2), ... , YSOM(NARR,NSOM)

### Number Format:

- NARR – Integer
- NSOM – Integer
- TARR – Integer
- NT – Double Precision

- RDIAM – Double Precision
- MDIAM – Double Precision
- LMON – Double Precision
- U\_Cut – Double Precision
- U\_Des – Double Precision
- CD – Double Precision
- CTo – Double Precision
- CPo – Double Precision
- P\_Rated – Double Precision
- RHO – Double Precision
- XSOM – Double Precision
- YSOM – Double Precision

# Appendix B

## User-Modified Fortran Code

```
!                                     *****
!                                     SUBROUTINE DRAGFO
!                                     *****
!
!      & (FUDRAG, FVDRAG)
!
!*****
! TELEMAC2D   V6P1                      21/08/2010
!*****
!
!brief      ADDS THE DRAG FORCE OF VERTICAL STRUCTURES IN THE
!+          MOMENTUM EQUATION.
!code
!+ FU IS THEN USED IN THE EQUATION AS FOLLOWS :
!+
!+  $DU/DT + U \text{ GRAD}(U) = - G * \text{GRAD}(\text{FREE SURFACE}) + \dots + FU\_IMP * U$ 
!+
!+ AND THE TERM  $FU\_IMP * U$  IS TREATED IMPLICITLY.
!
!warning    USER SUBROUTINE
!
!history    J-M HERVOUET
!+         01/03/1990
!+         V5P2
!+
!
!history    N.DURAND (HRW), S.E.BOURBAN (HRW)
!+         13/07/2010
!+         V6P0
!+ Translation of French comments within the FORTRAN sources into
!+ English comments
!
!history    N.DURAND (HRW), S.E.BOURBAN (HRW)
!+         21/08/2010
!+         V6P0
!+ Creation of DOXYGEN tags for automated documentation and
!+ cross-referencing of the FORTRAN sources
!
!history    D.HAVERSON
!+         12/07/2013
!+         V6P3
!+ Calculates drag from multiple types of tidal arrays in multiple
!+ locations. Turbine parameters read from external test file.
!
!~~~~~
!| FUDRAG      |<--| DRAG FORCE ALONG X
!| FVDRAG      |<--| DRAG FORCE ALONG Y
!~~~~~
!
!      USE BIEF
!      USE DECLARATIONS_TELEMAC2D
!
!      IMPLICIT NONE
```



```

INTEGER LNG, LU
COMMON/INFO/LNG, LU
!
!+-----+
!
TYPE (BIEF_OBJ), INTENT(INOUT) :: FUDRAG, FVDRAG
!+-----+
!
INTEGER IELEM, I, J, K, I4, DISCLIN, NSOM, TARR
INTEGER :: NARR=0
!
INTEGER :: NTAR=0
DOUBLE PRECISION UNORM, AIRE, SOM, X4, Y4, AOA, YAWX, YAWY, CT, A_Struc, A_Turb, CP
DOUBLE PRECISION NT, RDIAM, MDIAM, LMON, U_Cut, U_Des, CD, CTo, CPo, P_Rated, RHO
DOUBLE PRECISION P_Var(146,12), XSOM(146,4), YSOM(146,4)
DOUBLE PRECISION, PARAMETER :: PI=3.141592653589793D0

DOUBLE PRECISION P_DSUM
EXTERNAL P_DSUM

! IMPORTANT: Array size of XSOM & YSOM has to be equal to (NARR,NSOM)
! IMPORTANT: NSOM has to be the same for all arrays

SAVE NARR, NSOM, P_Var, XSOM, YSOM

INTRINSIC ATAN2, SIN, COS
!
!-----
! Define Parameters and location(s) for Array(s)
!-----
!
! NARR      Number of arrays
! TARR      Type of Array (1 = tidal or 2 = wind)
! NT        Number of Turbines
! RDIAM     Rotor Diameter (m)
! MDIAM     Monopile Diameter (m)
! LMON      Length of Monopile in water column (m)
! U_Cut     Cut in speed of rotor (m/s)
! U_Des     Design speed of rotor (aka rated speed) (m/s)
! CD        Coefficient of Drag of monopile
! CTo       Maximised Coefficient of Thrust of Rotor
! CPo       Maximised Coefficient of Power of Rotor
! P_Rated   Rated Power of Turbine (W)
! RHO       Density of sea water (kg/m^3)
!
! Define location of Array (in mercator coordinates)
! IMPORTANT: DRAGFORCE IS SET IN A QUADRILATERAL DEFINED BY NUMBER
!            OF DEFINED NODES (NSOM)
! Node 1 (XSOM(1),YSOM(1)) represents bottom left, counting counterclockwise
!-----

open (unit=99, file="./RS_array3_9turbines.txt")

IF (NARR.EQ.0) THEN
  READ(99,*) NARR
  READ(99,*) NSOM
  WRITE(*,*) "Read NARR and NSOM", NARR, NSOM
  DO K=1,NARR
    READ(99,*) P_Var(K,:)
    ! WRITE(*,*) "Read Parameters", P_Var
    READ(99,*) XSOM(K,:)
    READ(99,*) YSOM(K,:)
    ! WRITE(*,*) "Read XSOM", XSOM(K,:)
    ! WRITE(*,*) "Read YSOM", YSOM(K,:)
  ENDDO
  WRITE(*,*) "For Array 1:"
  WRITE(*,*) "Read Parameters", P_Var(1,:)
  WRITE(*,*) "Read XSOM", XSOM(1,:)
  WRITE(*,*) "Read YSOM", YSOM(1,:)
  WRITE(*,*) "For Array 2:"
  WRITE(*,*) "Read Parameters", P_Var(2,:)
  WRITE(*,*) "Read XSOM", XSOM(2,:)
  WRITE(*,*) "Read YSOM", YSOM(2,:)
  WRITE(*,*) "For Array 3:"
  WRITE(*,*) "Read Parameters", P_Var(3,:)
  WRITE(*,*) "Read XSOM", XSOM(3,:)
  WRITE(*,*) "Read YSOM", YSOM(3,:)
ENDIF
!
!-----

```

```

!      COMPUTES THE MASSE INTEGRALS
!-----
CALL VECTOR (T1, '=', 'MASBAS', UN%ELM, 1.D0,
&           S, S, S, S, S, S, MESH, .FALSE., S)
!
CALL CPSTVC (UN, FUDRAG)
CALL CPSTVC (VN, FVDRAG)
CALL OS ('X=C', FUDRAG, FUDRAG, FUDRAG, 0.D0)
CALL OS ('X=C', FVDRAG, FVDRAG, FVDRAG, 0.D0)
!-----
!      AIRE COMPUTATION
!-----
AIRE=0.D0
!
DO J=1, NARR
  AIRE=0.D0
  DO I=1, BIEF_NBPTS (11, MESH)
    IF (INPOLY (X (I), Y (I), XSOM (J, :), YSOM (J, :), NSOM)) THEN
      AIRE = AIRE + T1%R (I)
    ENDIF
  ENDDO
!-----
!      QUASI-BUBBLE POINTS
!-----
IF (FU%ELM.EQ.12) THEN
  DISCLIN=11
  CALL CHGDIS (FUDRAG, DISCLIN, 12, MESH)
  CALL CHGDIS (FVDRAG, DISCLIN, 12, MESH)
!
  DO IELEM = 1, NELEM
    I4=IKLE%I (IELEM+3*NELMAX)
    X4=(X (IKLE%I (IELEM))) +
&     X (IKLE%I (IELEM+ NELMAX)) +
&     X (IKLE%I (IELEM+2*NELMAX)) /3.D0
    Y4=(Y (IKLE%I (IELEM))) +
&     Y (IKLE%I (IELEM+ NELMAX)) +
&     Y (IKLE%I (IELEM+2*NELMAX)) /3.D0
    IF (INPOLY (X4, Y4, XSOM, YSOM, NSOM)) THEN
      AIRE = AIRE + T1%R (I4)
    ENDIF
  ENDDO
ENDIF
!-----
!      PARALLELISATION CORRECTION OF AREA COMPUTATION
!-----
!      In Parallel the area may be split into several domains
!
IF (NCSIZE.GT.0) AIRE=P_DSUM (AIRE)
IF (AIRE.GT.1.D-6) THEN
  SOM = 1.D0 / AIRE
ELSE
  IF (LNG.EQ.1) WRITE (LU, *) 'DRAGFO : AIRE DE LA ZONE NULLE'
  IF (LNG.EQ.2) WRITE (LU, *) 'DRAGFO: AREA OF ZONE EQUAL TO ZERO'
  CALL PLANTE (1)
  STOP
ENDIF
!-----
!      DRAG FORCE COMPUTATION
!-----
DO I=1, BIEF_NBPTS (11, MESH)
  IF (INPOLY (X (I), Y (I), XSOM (J, :), YSOM (J, :), NSOM)) THEN
    UNORM = SQRT (UN%R (I)**2+VN%R (I)**2)
    PRINT*, UN%R (I), VN%R (I), UNORM
!
    TARR = P_Var (J, 1)
    NT = P_Var (J, 2)
    RDIAM = P_Var (J, 3)
    MDIAM = P_Var (J, 4)
    LMON = P_Var (J, 5)
    U_Cut = P_Var (J, 6)
    U_Des = P_Var (J, 7)
    CD = P_Var (J, 8)
    CTo = P_Var (J, 9)
    CPo = P_Var (J, 10)
    P_Rated = P_Var (J, 11)
    RHO = P_Var (J, 12)

```

```

!           WRITE(*,*)"Parameters for Array:", J, NT, RDIAM
!
!   If modelling a monopile of a wind turbine, set LMON to zero,
!   the drag will be applied over the entire length within the
!   water column (HN%R(I)).
!
!           IF (LMON.GT.0) THEN
!               LMON = LMON
!           ELSE
!               LMON = HN%R(I)
!           ENDIF
!           PRINT*, J, LMON
!
!           A_Struc = MDIAM*LMON
!           A_Turb  = PI*(RDIAM/2)**2
!           PRINT*, J, A_Struc, A_Turb
!
!   Calculating Coefficient of Thrust
!   NOTE: In this if-then loop, use UNORM for a rotor that can yaw,
!         or use UN%R(I) if the device is fixed at 90 degrees
!         or use VN%R(I) if the device is fixed at 0 degrees
!
!           IF (TARR.EQ.1) THEN
!               IF (ABS (UNORM) .LE.U_Cut) THEN
!                   CT = 0.D0
!               ELSEIF (ABS (UNORM) .GT.U_Cut .AND. ABS (UNORM) .LE.U_Des) THEN
!                   CT = CTo
!               ELSEIF (ABS (UNORM) .GT.U_Des) THEN
!                   CT = (CTo/CPo)*((2*P_Rated)/(RHO*A_Turb*(UNORM)**3))
!               ENDIF
!           ELSEIF (TARR.EQ.2) THEN
!               CT = 0.D0
!           ENDIF
!           PRINT*, J, UNORM, CT
!
!           AOA=ATAN2 (ABS (VN%R(I)), ABS (UN%R(I))) ! Angle of Attack
!           YAWX=COS (AOA) ! Resolving Yaw error in X
!           YAWY=SIN (AOA) ! Resolving Yaw error in Y
!           PRINT*, UN%R(I), VN%R(I), AOA
!           PRINT*, J, AOA, YAWX, YAWY
!
!           FUDRAG%R(I) = -( (0.5D0*NT*(ABS (UN%R(I))) * ((A_Struc*CD) +
& (A_Turb*CT*YAWX))) / HN%R(I)) * SOM
!           FVDRAG%R(I) = -( (0.5D0*NT*(ABS (VN%R(I))) * ((A_Struc*CD) +
& (A_Turb*CT*YAWY))) / HN%R(I)) * SOM
!           !WRITE(*,*)"Calculating Drag for array:", J, FUDRAG%R(I), AIRE
!
!-----
!           POWER COMPUTATION
!-----
!   Power calculation using power coefficient as calculated by Plew and
!   Stephens (2013)
!   NOTE: Results outputted in private array 1. Use N in steering file
!   to output results.
!
!           IF (TARR.EQ.1) THEN
!               IF (ABS (UNORM) .LE.U_Cut) THEN
!                   CP = 0.D0
!               ELSEIF (ABS (UNORM) .GT.U_Cut .AND. ABS (UNORM) .LE.U_Des) THEN
!                   CP = CPo
!               ELSEIF (ABS (UNORM) .GT.U_Des) THEN
!                   CP = (2*P_Rated)/(RHO*A_Turb*(UNORM)**3)
!               ENDIF
!           ELSEIF (TARR.EQ.2) THEN
!               CP = 0.D0
!           ENDIF
!
!           PRIVE%ADR(1)%P%R(I) = (NT*0.5D0*RHO*A_Turb*CP*UNORM**3)/1000
!
!           ENDIF
!       ENDDO
!   ENDDO
!
!           PRINT*, UN%R(I), VN%R(I)
!           PRINT*, AIRE, FUDRAG%R(I), FVDRAG%R(I)
!-----
!
!   RETURN
!   END

```

# Appendix C

## Telemac Steering File for Idealised Case Study

```
-----/
/   Telemac v7p1r0
/   01 Jun 2016
/   Idealised Channel 2D Steering File
-----/
DEBUGGER=0
-----/
/   COMPUTER INFORMATIONS
-----/
GEOMETRY FILE = './IC_mesh_v3.slf'
BOUNDARY CONDITIONS FILE = './IC_mesh_v3_Q_BC.cli'
PREVIOUS COMPUTATION FILE = './results/IC_mesh_v3_1d.slf'
RESULTS FILE = './results/IC_mesh_v3_9turbines.slf'
FORTRAN FILE = './fortran/dragfo.f'
-----/
/   GENERAL INFORMATIONS - OUTPUTS
-----/
TITLE = 'Idealised Channel'
VARIABLES FOR GRAPHIC PRINTOUTS = 'H,U,V,S,B,N'
GRAPHIC PRINTOUT PERIOD = 900
LISTING PRINTOUT PERIOD = 900
TIME STEP = 1
NUMBER OF TIME STEPS = 18000
MASS-BALANCE = YES
INFORMATION ABOUT SOLVER = YES
-----/
/   INITIAL CONDITIONS
-----/
PARALLEL PROCESSORS = 16
COMPUTATION CONTINUED = YES
INITIAL TIME SET TO ZERO = YES
INITIAL CONDITIONS = 'CONSTANT ELEVATION'
INITIAL ELEVATION = 0
-----/
/   BOUNDARY CONDITIONS
-----/
VELOCITY PROFILES = 1
/PRESCRIBED VELOCITIES = 0; 2.7
PRESCRIBED ELEVATIONS = 0.0; 0.0
PRESCRIBED FLOWRATES =0.0; 405000
-----/
/   Tidal Array
```

```
/-----/
/dragfo.f subroutine must be implemented
VERTICAL STRUCTURES = YES
/-----/
/  PHYSICAL PARAMETERS
/-----/
LAW OF BOTTOM FRICTION = 5
FRICTION COEFFICIENT = 0.04
TURBULENCE MODEL = 3
VELOCITY DIFFUSIVITY = 1E-6
/-----/
/  NUMERICAL PARAMETERS
/-----/
NUMBER OF PRIVATE ARRAYS = 1
TREATMENT OF THE LINEAR SYSTEM = 2
CONTINUITY CORRECTION = NO
TYPE OF ADVECTION = 1;5
SUPG OPTION = 1;2
SOLVER ACCURACY = 1.E-4
DISCRETIZATIONS IN SPACE = 11;11
PROPAGATION = YES
SOLVER = 3
PRECONDITIONING = 2
IMPLICITATION FOR DEPTH = 0.6
IMPLICITATION FOR VELOCITY = 0.6
BOTTOM SMOOTHINGS = 1
MAXIMUM NUMBER OF ITERATIONS FOR SOLVER = 100
FREE SURFACE GRADIENT COMPATIBILITY = 0.9
/END OF STEERING FILE
```

# Appendix D

## Telemac Steering File for Ramsey Sound Case Study

```
/-----/
/   Telemac v7plr0
/   05 Apr 2016
/   Ramsey Sound 2D Steering File
/-----/
DEBUGGER=0
TITLE = 'RS_tides_2D_tpxo8_v19'
/-----/
/   File Locations
/-----/
/STEERING FILE = './RS_tides_2D.cast'
PREVIOUS COMPUTATION FILE = './results/RS_mesh_v19_hc_v7plr0_spinup.slf'
RESULTS FILE = './results/RS_mesh_v19_hc_v7plr0_array.slf'
GEOMETRY FILE = './RS_mesh_v19.slf'
BOUNDARY CONDITIONS FILE = './RS_mesh_v19_BC.cli'
FORTRAN FILE = './fortran/princi_hc_v7plr0_v4.f'
/ with mapping file, at each boundary node free surface elevation
/ is prescribed from either harmonic constituents or liquid boundary file
/ without mapping file, the normal Telemac boundary treatment
/ is applied
/ free surface elevation from harmonic constituents
FORMATTED DATA FILE 1 = './RS_mesh_v19_mapping.dat'
FORMATTED DATA FILE 2 = './RS_mesh_v19_hc_8dp.dat'
/-----/
/   Parallel & Previous Computation
/-----/
COMPUTATION CONTINUED = YES
INITIAL TIME SET TO ZERO = YES
PARALLEL PROCESSORS = 16
/-----/
/   Initial Conditions
/-----/
CORIOLIS = YES
CORIOLIS COEFFICIENT = 0.00011778
SPHERICAL COORDINATES = YES
LATITUDE OF ORIGIN POINT = 50.0
LONGITUDE OF ORIGIN POINT = 0
ORIGINAL HOUR OF TIME = 00;00;00
ORIGINAL DATE OF TIME = 2012;05;15
SPATIAL PROJECTION TYPE = 3
GEOGRAPHIC SYSTEM = 5
ZONE NUMBER IN GEOGRAPHIC SYSTEM = 30
```

```

INITIAL CONDITIONS = 'CONSTANT ELEVATION' /if used, define INIT ELEV
INITIAL ELEVATION = -2 /flat bdry start, average.
PRESCRIBED ELEVATIONS = 0
OPTION FOR LIQUID BOUNDARIES = 2;2
/-----/
/   Timestep and Output Options
/-----/
TIME STEP = 1
NUMBER OF TIME STEPS = 2592000 /30 days
GRAPHIC PRINTOUT PERIOD = 600
LISTING PRINTOUT PERIOD = 600
VARIABLES FOR GRAPHIC PRINTOUTS = 'U,V,H,B,S,N'
MASS-BALANCE = YES
/-----/
/   Tidal Array
/-----/
/   Note: For tidal array to be taken into account, the subroutine
/         dragfo.f must be implemented
VERTICAL STRUCTURES = YES
/-----/
/   Physical Parameters
/-----/
LAW OF BOTTOM FRICTION = 5 /Nikuradse
FRICTION COEFFICIENT = 0.04
TURBULENCE MODEL = 3
VELOCITY DIFFUSIVITY = 1E-6
/-----/
/   Numerical Parameters
/-----/
NUMBER OF PRIVATE ARRAYS = 1
ADVECTION = YES
ADVECTION OF U AND V = YES
ADVECTION OF H = YES
DIFFUSION OF VELOCITY = YES
CONTINUITY CORRECTION = YES
TREATMENT OF THE LINEAR SYSTEM = 2
DISCRETIZATIONS IN SPACE = 11;11
MATRIX STORAGE = 1
IMPLICITATION FOR DEPTH = 0.6
IMPLICITATION FOR VELOCITY = 0.6
MASS-LUMPING ON H = 1
MASS-LUMPING ON VELOCITY = 1
MAXIMUM NUMBER OF ITERATIONS FOR SOLVER = 200
SOLVER = 1
PRECONDITIONING = 2
INITIAL GUESS FOR H = 1
INITIAL GUESS FOR U = 1
FREE SURFACE GRADIENT COMPATIBILITY = 0.9
TIDAL FLATS = YES
OPTION FOR THE TREATMENT OF TIDAL FLATS = 1
TREATMENT OF NEGATIVE DEPTHS = 1
H CLIPPING = YES
MINIMUM VALUE OF DEPTH = 0.01
BOTTOM SMOOTHINGS = 0
/END OF STEERING FILE

```

# Appendix E

## Telemac Steering File for Irish Sea Case Study

```
-----/
/   Telemac v7plr0
/   18 Apr 2016
/   Celtic Sea 2D Steering File
-----/
DEBUGGER=0
TITLE = 'CS_tides_2D_hc_v2'
-----/
/   File Locations
-----/
/STEERING FILE = './CS_tides_2D_hc.cast'
PREVIOUS COMPUTATION FILE = './results/CS_mesh_v2_hc_spinup.slf'
RESULTS FILE = './results/CS_mesh_v2_hc_30d_array.slf'
GEOMETRY FILE = './CS_mesh_v2.slf'
BOUNDARY CONDITIONS FILE = './CS_mesh_v2_BC.cli'
FORTRAN FILE = './fortran/princi_hc_v7plr0_v4.f'
/ with mapping file, at each boundary node free surface elevation
/ is prescribed from either harmonic constituents or liquid boundary file
/ without mapping file, the normal Telemac boundary treatment
/ is applied
/ free surface elevation from harmonic constituents
FORMATTED DATA FILE 1 = './CS_mesh_v2_mapping.dat'
FORMATTED DATA FILE 2 = './CS_mesh_v2_hc_8dp.dat'
-----/
/   Parallel & Previous Computation
-----/
COMPUTATION CONTINUED = YES
INITIAL TIME SET TO ZERO = YES
PARALLEL PROCESSORS = 16
-----/
/   Initial Conditions
-----/
CORIOLIS = YES
CORIOLIS COEFFICIENT = 0.00011778
SPHERICAL COORDINATES = YES
LATITUDE OF ORIGIN POINT = 50.0
LONGITUDE OF ORIGIN POINT = 0
ORIGINAL HOUR OF TIME = 00;00;00
ORIGINAL DATE OF TIME = 2012;05;15
SPATIAL PROJECTION TYPE = 3
GEOGRAPHIC SYSTEM = 5
ZONE NUMBER IN GEOGRAPHIC SYSTEM = 30
```



```

INITIAL CONDITIONS = 'CONSTANT ELEVATION' /if used, define INIT ELEV
INITIAL ELEVATION = -2 /flat bdry start, average.
PRESCRIBED ELEVATIONS = 0
OPTION FOR LIQUID BOUNDARIES = 2;2;2
/-----/
/   Timestep and Output Options
/-----/
TIME STEP = 1
NUMBER OF TIME STEPS = 2592000 /30 days
GRAPHIC PRINTOUT PERIOD = 600
LISTING PRINTOUT PERIOD = 600
VARIABLES FOR GRAPHIC PRINTOUTS = 'U,V,H,B,S,N'
MASS-BALANCE = YES
/-----/
/   Tidal Array
/-----/
/   Note: For tidal array to be taken into account, the subroutine
/         dragfo.f must be implemented
VERTICAL STRUCTURES = YES
/-----/
/   Physical Parameters
/-----/
LAW OF BOTTOM FRICTION = 5 /Nikuradse
FRICTION COEFFICIENT = 0.04
TURBULENCE MODEL = 3
VELOCITY DIFFUSIVITY = 1E-6
/-----/
/   Numerical Parameters
/-----/
NUMBER OF PRIVATE ARRAYS = 1
ADVECTION = YES
ADVECTION OF U AND V = YES
ADVECTION OF H = YES
DIFFUSION OF VELOCITY = YES
CONTINUITY CORRECTION = YES
TREATMENT OF THE LINEAR SYSTEM = 2
DISCRETIZATIONS IN SPACE = 11;11
MATRIX STORAGE = 1
IMPLICITATION FOR DEPTH = 0.6
IMPLICITATION FOR VELOCITY = 0.6
MASS-LUMPING ON H = 1
MASS-LUMPING ON VELOCITY = 1
MAXIMUM NUMBER OF ITERATIONS FOR SOLVER = 200
SOLVER = 1
PRECONDITIONING = 2
INITIAL GUESS FOR H = 1
INITIAL GUESS FOR U = 1
FREE SURFACE GRADIENT COMPATIBILITY = 0.9
TIDAL FLATS = YES
OPTION FOR THE TREATMENT OF TIDAL FLATS = 1
TREATMENT OF NEGATIVE DEPTHS = 1
H CLIPPING = YES
MINIMUM VALUE OF DEPTH = 0.01
BOTTOM SMOOTHINGS = 0
/END OF STEERING FILE

```

# References

Abbott, M. and Basco, D. (1997) *Computational Fluid Dynamics: An introduction for Engineers*. 1 ed Harlow: Longman Pub Group.

Agnostini, V., Escobar-Briones, E., Cresswell, I., Gjerde, K., Niewijk, D.J.A., Polacheck, A., Raymond, B., Rice, J., Roff, J.C., Scanlon, K.M. and Spalding, M., 2008. Global Open Oceans and Deep Sea-habitats (GOODS) bioregional classification. In United Nations Conference of the Parties to the Convention on Biological Diversity (CBD) (p. 94).

Ahmadian, R. Falconer, R. and Bockelmann-Evans, B. (2012) Far-field modelling of the hydro-environmental impact of tidal stream turbines, *Renewable Energy*, 38(1), pp.107-116.

Aitchison, J. (1986) *The Statistical Analysis of Compositional Data*. London: Chapman and Hall.

Allee, R.J., David, A.W. and Naar, D.F. (2011) Two Shelf-Edge Marine Protected Areas in the Eastern Gulf of Mexico. *Seafloor Geomorphology as Benthic Habitat: GeoHAB Atlas of Seafloor Geomorphic Features and Benthic Habitats*, pp.435.

Anderson, T.J., Cochrane, G.R., Roberts, D.A., Chezar, H. and Hatcher, G. (2007) A rapid method to characterize seabed habitats and associated macro-organisms. *Mapping the seafloor for habitat characterization: Geological Association of Canada Special Paper*, 47, pp.71-79.

Andersson, M.H., Berggren, M., Wilhelmsson, D. and Öhman, M.C. (2009) Epibenthic colonization of concrete and steel pilings in a cold-temperate embayment: a field experiment. *Helgoland Marine Research*, 63(3), pp.249.

Arntz, W.E., Gili, J.M., Reise, K. (1999) Unjustifiably ignored: reflections on the role of benthos in marine ecosystems. In: Gray, J.S. (Ed.). *Biogeochemical Cycling and Sediment Ecology*. Kluwer Academic, Dordrecht, pp.105-124.

- Auster PJ, Malatesta RJ, Langton RW, Watling L, Valentine PC, et al. (1996) The impact of mobile fishing gear on seafloor habitats in the Gulf of Maine (Northwest Atlantic): implications for conservation of fish populations. *Rev. Fish Sci*, 4, pp.185-202.
- Backer, L. and McGillicuddy, D. (2006) Harmful algal blooms. *Oceanography*, 19(2), pp.94-106.
- Ball, B.J., Fox, G. and Munday, B.W. (2000) Long and short-term consequences of a Nephrops trawl fishery on the benthos and environment of the Irish Sea. *ICES J. Mar. Sci.* 57, pp.1315-20.
- Bell, C. and Carlin, L. (1998) Generation of UK tidal stream atlases from regularly gridded hydrodynamic modelled data. *Journal of Navigation*, 51(1), pp.73-78.
- Bell, M.C., Grist, E.P.M., Baston, S., Rouse, S., Spencer Jones, M., Porter, J.S., Want, A., Harris, R.E. and Side, J.C. (2001) Hydrokinetic energy as an ecological factor – how might wave and tidal energy extraction affect the distribution of marine organisms?, in *Proc. ICES Annual Science Conference*, Poland.
- Berdalet, E., Fleming, L.E., Gowen, R., Davidson, K., Hess, P., Backer, L.C., Moore, S.K., Hoagland, P. and Enevoldsen, H., 2015. Marine harmful algal blooms, human health and wellbeing: challenges and opportunities in the 21st century. *Journal of the Marine Biological Association of the United Kingdom*, 96(01), pp.61-91.
- Berenbrock, C. and Tranmer, A.W. (2008). Simulation of flow, sediment transport, and sediment mobility of the lower Coeur d'Alene River, Idaho. US Geological Survey.
- Betz, A. (1920). Das Maximum der theoretisch möglichen Ausnützung des Windes durch Windmotoren. *Zeitschrift für das gesamte Turbinenwesen*, 26(307-309), p.8.
- Black and Veatch (2005) Phase 2: UK tidal stream resource assessment. Technical report to Carbon Trust, Report submission 107799/D/2200/03.
- BlueKenue™, Canadian National Research Council, [Online], Available: [http://www.nrc-cnrc.gc.ca/eng/solutions/advisory/blue\\_kenue\\_index.html](http://www.nrc-cnrc.gc.ca/eng/solutions/advisory/blue_kenue_index.html).
- Borja, Á., Dauer, D.M., Elliott, M. and Simenstad, C.A. (2010) Medium-and long-term recovery of estuarine and coastal ecosystems: patterns, rates and restoration effectiveness. *Estuaries and Coasts*, 33(6), pp.1249-1260.
- Bowers, D.G., Macdonald, R.G., McKee, D., Nimmo-Smith, W.A.M. and Graham, G.W. (2013) On the formation of tide-produced seiches and double high waters in coastal seas. *Estuarine, Coastal and Shelf Science*, 134, pp.108-116.

- Breen, P., Brown, S., Reid, D. and Rogan, E., 2017. Where is the risk? Integrating a spatial distribution model and a risk assessment to identify areas of cetacean interaction with fisheries in the northeast Atlantic. *Ocean & Coastal Management*, 136, pp.148-155.
- Breiman, L. (2001) Random forests. *Machine learning*, 45(1), pp.5-32.
- British Broadcasting Centre (2010) Severn barrage tidal energy scheme scrapped by Huhne. BBC News. [Online]. 18 October. Available: <http://www.bbc.co.uk/news/uk-england-somerset-11564284>.
- British Geological Survey, Offshore GeoIndex, [Online], Available: <http://www.bgs.ac.uk/geoindex/>.
- British Oceanographic Data Centre, [Online], Available: <http://www.bodc.ac.uk/>.
- Broadhurst, M. and Orme, C.D.L. (2014). Spatial and temporal benthic species assemblage responses with a deployed marine tidal energy device: A small scaled study. *Marine environmental research*, 99, pp.76-84.
- Bryden, I.G., Couch, S.J. and Harrison, G. (2006) Overview of the issues associated with energy extraction from tidal currents. In *World renewable energy congress IX* (Ed. AAM Sayigh), Florence, Italy.
- Bulleri, F. and Airoidi, L. (2005) Artificial marine structures facilitate the spread of a non-indigenous green alga, *Codium fragile* ssp *tomentosoides*, in the north Adriatic Sea. *Journal Applied Ecology*, 42, pp.1063–72.
- Burd, B.J., Macdonald, R.W., Johannessen, S.C. and Van Roodselaar, A. (2008) Responses of subtidal benthos of the Strait of Georgia, British Columbia, Canada to ambient sediment conditions and natural and anthropogenic depositions. *Marine Environmental Research*, 66, pp.S62-S79.
- Busby, J.R. (1991) BIOCLIM – a bioclimate analysis and prediction system. *Nature conservation: cost effective biological surveys and data analysis* (ed. by C.R. Margules and M.P. Austin), pp. 64–68.
- Callaway, A. (2015) Interview on species distribution modelling with MaxEnt with D. Haverson, 28 August.
- Carpenter, G., Gillison, A.N. and Winter, J. (1993) DOMAIN: a flexible modelling procedure for mapping potential distributions of plants and animals. *Biodiversity & Conservation*, 2(6), pp.667-680.

Chen, C., Liu, H., and Beardsley, R. C. (2003) An unstructured, finite-volume, three-dimensional primitive equation ocean model: Application to coastal ocean and estuaries, *Journal of Atmospheric and Oceanic Technology*, 20, pp.159–186.

Climate Change Act 2008. (c.27). London: The Stationary Office.

Coates, D.A., Kapasakali, D.A., Vincx, M. and Vanaverbeke, J. (2016) Short-term effects of fishery exclusion in offshore wind farms on macrofaunal communities in the Belgian part of the North Sea. *Fisheries Research*, 179, pp.131-138.

Coccioni, R. (2000) Benthic foraminifera as bioindicators of heavy metal pollution. *Environmental micropaleontology*, pp. 71-103.

Coggan, R., Froján, C.R.B., Diesing, M. and Aldridge, J. (2012) Spatial patterns in gravel habitats and communities in the central and eastern English Channel. *Estuarine, Coastal and Shelf Science*, 111, pp.118-128.

Collie, J.S., Escanero, G.A. and Valentine, P.C. (1997) Effects of bottom fishing on the benthic megafauna of Georges Bank. *Marine Ecology Progress Series*, 155, pp.159-172.

Copernicus Marine environment monitoring service, [Online], Available: <http://marine.copernicus.eu/>.

Costello, M.J. (2009) Distinguishing marine habitat classification concepts for ecological data management. *Marine ecology progress series*, 397, pp.253-268.

Covich, A.P., Palmer, M.A. and Crowl, T.A. (1999) The role of benthic invertebrate species in freshwater ecosystems: zoobenthic species influence energy flows and nutrient cycling. *BioScience*, 49(2), pp.119-127.

Cox, A.T. and Swail, V.R. (2001). A global wave hindcast over the period 1958-1997- Validation and climate assessment. *Journal of Geophysical Research*, 106(C2), pp.2313-2329.

Cramer, J.S. (2003) *Logit models: from economics and other fields*. Cambridge Univ. Press, pp.66–67.

Crown Estate (2015) *Offshore wind operational report*. London, Crown Estate.

Crown Estate: Wave and Tidal, [Online], Available: <https://www.thecrownestate.co.uk/energy-minerals-and-infrastructure/wave-and-tidal/>.

Cutler, D.R., Edwards Jr, T.C., Beard, K.H., Cutler, A., Hess, K.T., Gibson, J. and Lawler, J.J. (2007) Random forests for classification in ecology. *Ecology*, 88(11), pp.2783-2792.

Dalton, G.J., Alcorn, R. and Lewis, T. (2010) Case study feasibility analysis of the Pelamis wave energy convertor in Ireland, Portugal and North America. *Renewable Energy*, 35(2), pp.443-455.

Davidson, K., Gowen, R.J., Harrison, P.J., Fleming, L.E., Hoagland, P. and Moschonas, G. (2014) Anthropogenic nutrients and harmful algae in coastal waters. *Journal of environmental management*, 146, pp.206-216.

Davies, A.M. and Jones, J.E. (1992). A three dimensional model of the M2, S2, N2, K1 and O1 tides in the Celtic and Irish Seas. *Progress in Oceanography*, 29(3), pp.197-234.

Denderen, P.D., Rijnsdorp, A.D. and Kooten, T. (2016) Using marine reserves to manage impact of bottom trawl fisheries requires consideration of benthic food-web interactions. *Ecological Applications*.

Department of Energy & Climate Change (2011), UK Renewable Energy Road Map, [Online], Available: [https://www.gov.uk/government/uploads/system/uploads/attachment\\_data/file/48128/2167-uk-renewable-energy-roadmap.pdf](https://www.gov.uk/government/uploads/system/uploads/attachment_data/file/48128/2167-uk-renewable-energy-roadmap.pdf).

Desplanque, C. and Mossman, D.J., 2001. Bay of Fundy tides. *Geoscience Canada*, 28(1).

Doodson, A.T. (1921) The harmonic development of the tide-generating potential. *Proceedings of the Royal Society of London. Series A, Containing Papers of a Mathematical and Physical Character*, 100(704), pp.305-329.

DP Marine Energy Ltd (2013) West Islay Environment Statement, [Online], Available: [http://marine.gov.scot/datafiles/lot/DP\\_ME/Environmental\\_Statement/](http://marine.gov.scot/datafiles/lot/DP_ME/Environmental_Statement/)

Draper, S., Adcock, T.A., Borthwick, A.G. and Houlsby, G.T. (2014). Estimate of the tidal stream power resource of the Pentland Firth. *Renewable Energy*, 63, pp.650-657.

Easton, M.C., Harendza, A., Woolf, D.K. and Jackson, A.C. (2011) Characterisation of a tidal energy site: hydrodynamics and seabed structure. In 9th European Wave and Tidal Energy Conference, Southampton, UK.

Eleftheriou, A. (2013) *Methods for the study of marine benthos*. 4<sup>th</sup> Edition, Chichester, John Wiley & Sons.

Elith, J., Graham, C. H., Anderson, R. P., Dudík, M., Ferrier, S., Guisan, A., Hijmans, R. J., Huettmann, F., Leathwick, J. R., Lehmann, A., Li, J., Lohmann, L. G., Loiselle, B. A., Manion, G., Moritz, C., Nakamura, M., Nakazawa, Y., Overton, J. McC., Peterson, A. T., Phillips, S. J., Richardson, K. S., Scachetti-Pereira, R., Schapire, R. E., Soberón, J.,

Williams, S., Wisz, M. S. and Zimmermann, N. E. (2006) Novel methods improve prediction of species' distributions from occurrence data. *Ecography*, 29, pp.129-151.

Elith, J. and Leathwick, J.R. (2009) Species distribution models: ecological explanation and prediction across space and time. *Annual review of ecology, evolution, and systematics*, 40, pp.677-697.

Elith, J., Phillips, S.J., Hastie, T., Dudík, M., Chee, Y.E. and Yates, C.J. (2011). A statistical explanation of MaxEnt for ecologists. *Diversity and distributions*, 17(1), pp.43-57.

EMEC (2009) Assessment of Tidal Energy Resource, [Online], Available: <http://www.emec.org.uk/assessment-of-tidal-energy-resource/>.

EMEC: Our History, [Online], Available: <http://www.emec.org.uk/about-us/emec-history/>.

EMECO, European Marine Ecosystem Observatory data portal, [Online], Available: <http://www.emecodata.net/>

Engel, J., Kvitek, R. (1998) Impacts of otter trawling on a benthic community in Monterey Bay National Marine Sanctuary. *Conservation Biology*, 12, pp.1204-14.

EUNIS, European Nature Information System, [Online], Available: <http://eunis.eea.europa.eu/index.jsp>.

Evans, P., Armstrong, S., Wilson, C., Fairley, I., Wooldridge, C. and Masters, I. (2013) Characterisation of a highly energetic tidal energy site with specific reference to hydrodynamics and bathymetry. In *Proceedings of the 10th European Wave and Tidal Energy Conference (EWTEC)*, Aalborg, Denmark (pp. 26-37).

Evans, P., Mason-Jones, A., Wilson, C., Wooldridge, C., O'Doherty, T. and O'Doherty, D. (2015) Constraints on extractable power from energetic tidal straits. *Renewable Energy*, 81, pp.707-722.

Ezhova, E., Dorokhov, D., Sivkov, V., Zhamoida, V., Ryabchuk, D. and Kocheshkova, O. (2012) Benthic habitats and benthic communities in Southeastern Baltic Sea, Russian sector. *Seafloor Geomorphology: Benthic Habitat*, pp.613-621.

Fairley, I., Neill, S., Wrobelowski, T., Willis, M. and Masters, I. (2011) Potential array sites for tidal stream electricity generation off the pembrokehire coast. In *Proceedings of the 9th European Wave and Tidal Energy Conference*, Southampton, UK, pp.5-9.

Fairley, I., Evans, P., Wooldridge, C., Willis, M. and Masters, I. (2013) Evaluation of tidal stream resource in a potential array area via direct measurements. *Renewable Energy*, 57, pp.70-78.

Fairley, I., Masters, I. and Karunaratna, H. (2015) The cumulative impact of tidal stream turbine arrays on sediment transport in the Pentland Firth. *Renewable Energy*, 80, pp.755-769.

Ferreira, J.G., Andersen, J.H., Borja, A., Bricker, S.B., Camp, J., Da Silva, M.C., Garcés, E., Heiskanen, A.S., Humborg, C., Ignatiades, L. and Lancelot, C. (2011) Overview of eutrophication indicators to assess environmental status within the European Marine Strategy Framework Directive. *Estuarine, Coastal and Shelf Science*, 93(2), pp.117-131.

Fischer, H.B. EJ List, E.J., Koh, R.C.Y., Imberger, J. and Brooks, N.H. (1979) *Mixing in inland and coastal waters*. Academic Press, San Diego, CA.

Folk, R.L. (1954). The distinction between grain size and mineral composition in sedimentary rock nomenclature. *Journal of Geology*, 62(4), pp.344-359.

FORCE (2009) NS Power and OpenHydro successfully deploy in-stream tidal turbine in the Bay of Fundy [Press release]. [12 Nov 2009]. Available: <http://fundyforce.ca/ns-power-and-openhydro-successfully-deploy-in-stream-tidal-turbine-in-the-bay-of-fundy/>.

Ford, R., Pain, C.C., Piggott, M.D., Goddard, A.J.H., De Oliveira, C.R.E. and Umpleby, A.P. (2004) A nonhydrostatic finite-element model for three-dimensional stratified oceanic flows. Part I: model formulation. *Monthly Weather Review*, 132(12), pp.2816-2831.

Frid, C.L. (2011). Temporal variability in the benthos: Does the sea floor function differently over time?. *Journal of Experimental Marine Biology and Ecology*, 400(1), pp.99-107.

Frid, C., Andonegi, E., Depestele, J., Judd, A., Rihan, D., Rogers, S.I. and Kenchington, E., (2012). The environmental interactions of tidal and wave energy generation devices. *Environmental Impact Assessment Review*, 32(1), pp.133-139.

Friedlander, A.M., Brown, E.K., Jokiel, P.L., Smith, W.R. and Rodgers, K.S. (2003) Effects of habitat, wave exposure, and marine protected area status on coral reef fish assemblages in the Hawaiian archipelago. *Coral Reefs*, 22(3), pp.291-305.

Frontalini, F. and Coccioni, R. (2011) Benthic foraminifera as bioindicators of pollution: a review of Italian research over the last three decades. *Revue de micropaléontologie*, 54(2), pp.115-127.

Galland, J.C., Goutal, N. and Hervouet, J.M., 1991. TELEMAC: A new numerical model for solving shallow water equations. *Advances in Water Resources*, 14(3), pp.138-148.



Garrett, C. and Cummins, P. (2008) Limits to tidal current power, *Renewable Energy*, 33, pp.2485-2490.

George, K.J. (1980) Anatomy of an amphidrome. *Hydrographic Journal*, 18, pp.5-12.

Getsiv-Clemons, J.E.R., Wakefield, W.W., Stewart, I.J. and Whitmire, C.E. (2011) Using meso-habitat information to improve abundance estimates for West Coast groundfish: a test case at Heceta Bank, Oregon. Baker (Eds.), *Seafloor Geomorphology as Benthic Habitat: GeoHab Atlas of Seafloor Geomorphic Features and Benthic Habitats*, Elsevier, Amsterdam.

Glasby, T.M., Connell, S.D., Holloway, M.G. and Hewitt, C.L. (2007) Nonindigenous biota on artificial structures: could habitat creation facilitate biological invasions?, *Marine Biology*, 151, pp.887–95.

Gordon, D.C. and Longhurst, A.R., 1979. The environmental aspects of a tidal power project in the upper reaches of the Bay of Fundy. *Marine Pollution Bulletin*, 10(2), pp.38-45.

Gray, J. S. (1997). Marine biodiversity: Patterns, threats and conservation needs. *Biodiversity and Conservation*, 6, pp.153–175.

Guillou, N., Chapalain, G. and Neill, S.P. (2016) The influence of waves on the tidal kinetic energy resource at a tidal stream energy site. *Applied Energy*, 180, pp.402-415.

Gunn, K. and Stock-Williams, C. (2013). On validating numerical hydrodynamic models of complex tidal flow. *International Journal of Marine Energy*, 3, pp.82-97.

Harris, P.T. (2012) On seabed disturbance, marine ecological succession and applications for environmental management: a physical sedimentological perspective. *Sediments, Morphology and Sedimentary Processes on Continental Shelves: Advances in Technologies, Research and Applications (Special Publication 44 of the IAS)*, 44, p.389.

Harris, P.T. and Baker, E.K. (2012). *Seafloor Geomorphology as Benthic Habitat: GeoHab Atlas of seafloor geomorphic features and benthic habitats*. Elsevier, London, pp.871-890.

Hartnoll, R.G. (1977) Reproductive strategy in two British species of *Alcyonium*. In *Biology of benthic organisms*, (ed. B.F. Keegan, P.O Ceidigh & P.J.S. Boaden), New York: Pergamon Press, pp. 321-328.

Hashemi, M.R., Neill, S.P. and Davies, A.G. (2015a) A coupled tide-wave model for the NW European shelf seas. *Geophysical & Astrophysical Fluid Dynamics*, 109(3), pp.234-253.

Hashemi, M.R., Neill, S.P., Robins, P.E., Davies, A.G. and Lewis, M.J. (2015b) Effect of waves on the tidal energy resource at a planned tidal stream array. *Renewable Energy*, 75, pp.626-639.

Hastie, T.J. and Tibshirani, R.J. (1990) *Generalized additive models*. Vol. 43. Washington. Chapman & Hall/CRC.

Hawkins, D.M. (2004) The problem of overfitting. *Journal of chemical information and computer sciences*, 44(1), pp.1-12.

Hervouet, J.M., 2007. *Hydrodynamics of free surface flows: modelling with the finite element method*. John Wiley & Sons.

Hinchey, E.K., Schaffner, L.C., Hoar, C.C., Vogt, B.W. and Batte, L.P. (2006) Responses of estuarine benthic invertebrates to sediment burial: the importance of mobility and adaptation. *Hydrobiologia*, 556(1), pp.85-98.

Houlsby, G.T., Draper, S. and Oldfield, M.L.G. (2008) Application of linear momentum actuator disc theory to open channel flow. Report no. OUEL, 2296(08).

Huang, Z., Brooke, B. and Li, J. (2011) Performance of predictive models in marine benthic environments based on predictions of sponge distribution on the Australian continental shelf. *Ecological Informatics*, 6(3), pp.205-216.

Hussain, S.S., Winrow-Giffin, A., Moran, D., Robinson, L.A., Fofana, A., Paramor, O.A. and Frid, C.L. (2010) An ex ante ecological economic assessment of the benefits arising from marine protected areas designation in the UK. *Ecological Economics*, 69(4), pp.828-838.

IPCC (2014) *Climate Change 2014: Synthesis Report*. Contribution of Working Groups I, II and III to the Fifth Assessment Report of the Intergovernmental Panel on Climate Change [Core Writing Team, R.K. Pachauri and L.A. Meyer (eds.)]. IPCC, Geneva, Switzerland.

IT Power Consulting Ltd, *Seaflow – 300kW Marine Current Turbine Tidal Energy Pilot Project*, UK. [Online], Available: <http://www.itpower.co.uk/our-projects/tidal-energy/seaflow-300kw-marine-current-turbine-tidal-energy-pilot-project-uk/>.

Jackson, A. (2004) *Nemertesia ramose*: A hydroid. In Tyler-Walters H. and Hiscock K. (eds) *Marine Life Information Network: Biology and Sensitivity Key Information Reviews*,

[online]. Plymouth: Marine Biological Association of the United Kingdom. Available: <http://www.marlin.ac.uk/species/detail/1318>.

Jaynes, E.T. (1957). Information theory and statistical mechanics. *Phys. Rev.* 106, pp.620–630.

Joint Nature Conservation Committee (a) Pembrokeshire Marine Special Area of Conservation, [Online], Available: <http://jncc.defra.gov.uk/protectedsites/sacselection/sac.asp?EUcode=UK0013116>.

Joint Nature Conservation Committee (b) UK Biodiversity Action Plan priority marine species, [Online], Available: <http://jncc.defra.gov.uk/page-5167>.

Jones, J.E. (1983) Charts of the O1, K1, N2, M2 and S2 tides in the Celtic Sea including M2 and S2 tidal currents. Institute of Oceanographic Sciences, Report No.169.

Keenan, G., Sparling, C., Williams, H. and Fortune, F. (2011) SeaGen environmental monitoring programme final report. Royal Haskoning: Edinburgh, UK, January.

Khan, M.N. and Mohammad, F. (2014) Eutrophication: challenges and solutions. In *Eutrophication: Causes, Consequences and Control*, Springer Netherlands, pp.1-15.

Kim, G., Lee, M.E., Lee, K.S., Park, J.S., Jeong, W.M., Kang, S.K., Soh, J.G. and Kim, H., 2012. An overview of ocean renewable energy resources in Korea. *Renewable and Sustainable Energy Reviews*, 16(4), pp.2278-2288.

Kirby, R. and Retiere, C. (2009) March. Comparing environmental effects of Rance and Severn barrages. In *Proceedings of the Institution of Civil Engineers-Maritime Engineering*, 162 (1), pp.11-26.

Kostylev, V.E., Todd, B.J., Fader, G.B.J., Courtney, R.C., Cameron, G.D.M., Pickrill, R. A. (2001) Benthic habitat mapping on the Scotian Shelf based on multibeam bathymetry, surficial geology and seafloor photographs. *Marine Ecology Progress Series*, 219, pp.121–137.

Kramer, S., Piggott, M.D., Hill, J., Kregting, L., Pritchard, D. and Elsaesser, B. (2014). The modelling of tidal turbine farms using multi-scale, unstructured mesh models. In *Proceedings of the 2nd International Conference on Environmental Interactions of Marine Renewable Energy Technologies*, Stornoway, UK.

Lark, R.M., Dove, D., Green, S.L., Richardson, A.E., Stewart, H. and Stevenson, A. (2012) Spatial prediction of seabed sediment texture classes by cokriging from a legacy database of point observations. *Sedimentary Geology*, 281, pp.35-49.

- Last, P.R., Lyne, V.D., Williams, A., Davies, C.R., Butler, A.J. and Yearsley, G.K. (2010) A hierarchical framework for classifying seabed biodiversity with application to planning and managing Australia's marine biological resources. *Biological Conservation*, 143(7), pp.1675-1686.
- Lawrence, K.E., Summers, S.R., Heath, A.C.G., McFadden, A.M.J., Pulford, D.J. and Pomroy, W.E., 2016. Predicting the potential environmental suitability for *Theileria orientalis* transmission in New Zealand cattle using maximum entropy niche modelling. *Veterinary parasitology*, 224, pp.82-91.
- Lewis, M., Neill, S.P., Robins, P.E. and Hashemi, M.R. (2015). Resource assessment for future generations of tidal-stream energy arrays. *Energy*, 83, pp.403-415.
- Liaw, A. and Wiener, M. (2002) Classification and regression by randomForest. *R news*, 2(3), pp.18-22.
- Liu, C., Berry, P.M., Dawson, T.P. and Pearson, R.G. (2005) Selecting thresholds of occurrence in the prediction of species distributions. *Ecography*, 28(3), pp.385-393.
- London Array (2014) London Array to stay at 630MW, [Press Release], 19 Feb, [Online], Available: <http://www.londonarray.com/project/london-array-to-stay-at-630mw/>.
- Long, D. (2006) BGS Detailed Explanation of Seabed Sediment Modified Folk Classification.
- Luderer, G., Krey, V., Calvin, K., Merrick, J., Mima, S., Pietzcker, R., Van Vliet, J. and Wada, K. (2014) The role of renewable energy in climate stabilization: results from the EMF27 scenarios. *Climatic change*, 123(3-4), pp.427-441.
- Madden, C.J. and Grossman, D.H. (2004) A framework for a coastal/marine ecological classification standard. NatureServe, Arlington, VA.
- Magagna, D. and Uihlein, A. (2015) Ocean energy development in Europe: Current status and future perspectives. *International Journal of Marine Energy*, 11, pp.84-104.
- Mallet, D. and Pelletier, D. (2014) Underwater video techniques for observing coastal marine biodiversity: a review of sixty years of publications (1952–2012). *Fisheries Research*, 154, pp.44-62.
- Martin-Short, R., Hill, J., Kramer, S.C., Avdis, A., Allison, P.A. and Piggott, M.D. (2015) Tidal resource extraction in the Pentland Firth, UK: Potential impacts on flow regime and sediment transport in the Inner Sound of Stroma. *Renewable Energy*, 76, pp.596-607.

Masters, I. Malki, R. Williams, A. and Croft, N. (2013) The influence of flow acceleration on tidal stream turbine wake dynamics: A numerical study using a coupled BEM-CFD model, *Applied Mathematical Modelling*, 37, pp.7905-7918.

McBreen, F. and Joint Nature Conservation Committee (2011). UK SeaMap 2010: predictive mapping of seabed habitats in UK waters.

McGlathery, K.J., Sundbäck, K. and Anderson, I.C. (2007). Eutrophication in shallow coastal bays and lagoons: the role of plants in the coastal filter. *Marine Ecology Progress Series*, 348, pp.1-18.

McGrath, C. (2013). Fairhead Tidal Environmental Impact Assessment Scoping Document, [Online], Available: <https://tethys.pnnl.gov/publications/fairhead-tidal-environmental-impact-assessment-scoping-document>

Merow, C., Smith, M.J. and Silander, J.A. (2013) A practical guide to MaxEnt for modeling species' distributions: what it does, and why inputs and settings matter. *Ecography*, 36(10), pp.1058-1069.

Meygen (2015) Phase 1a Construction April newsletter, [Online], Available: <http://www.meygen.com/wp-content/uploads/MEY-1A-70-PRE-001-AprilConstructionNewsletter.pdf>.

Miller, R.G., Hutchison, Z.L., Macleod, A.K., Burrows, M.T., Cook, E.J., Last, K.S. and Wilson, B. (2013) Marine renewable energy development: assessing the Benthic Footprint at multiple scales. *Frontiers in Ecology and the Environment*, 11(8), pp.433-440.

Minchinton, W.E. (1979) Early tide mills: some problems. *Technology and Culture*, 20(4), pp.777-786.

Ministry of Fuel and Power (1945). Severn barrage scheme, Non-parliamentary papers.

Moffitt, S.E., Hill, T.M., Roopnarine, P.D. and Kennett, J.P. (2015) Response of seafloor ecosystems to abrupt global climate change. *Proceedings of the National Academy of Sciences*, 112(15), pp.4684-4689.

Mork, G., Barstow, S., Kabuth, A. and Pontes, M.T. (2010) Assessing the global wave energy potential. In ASME 2010 29th International Conference on Ocean, Offshore and Arctic Engineering, pp. 447-454. American Society of Mechanical Engineers.

Moulin, C. (1995). Anisotropie de la Dispersion pour le Transport Bidimensionnel dans le Systeme TELEMAC, EDF Internal Report, HE-43/95/016/A, Department Laboratoire National d'Hydraulique, EDF Chatou, Paris.

Moulinec, C., Denis, C., Pham, C.T., Rougé, D., Hervouet, J.M., Razafindrakoto, E., Barber, R.W., Emerson, D.R. and Gu, X.J. (2011) TELEMAC: An efficient hydrodynamics suite for massively parallel architectures. *Computers & Fluids*, 51(1), pp.30-34.

Myers, L.E. and Bahaj, A.S. (2012) An experimental investigation simulating flow effects in first generation marine current energy converter arrays. *Renewable Energy*, 37(1), pp.28-36.

Nakagawa, S. and Cuthill, I.C. (2007) Effect size, confidence interval and statistical significance: a practical guide for biologists. *Biological Reviews*, 82(4), pp.591-605.

Nautricity (2013) Environmental Appraisal for the Argyll Tidal Demonstrator Project, [Online], Available:

[http://www.nautricity.com/docs/014\\_036\\_\\_argylltidal\\_environmentalappraisal\\_dec13\\_lores3\\_1392661149.pdf](http://www.nautricity.com/docs/014_036__argylltidal_environmentalappraisal_dec13_lores3_1392661149.pdf)

NBN, National Biodiversity Network Gateway, [Online], Available: <http://www.nbn.org.uk/>.

Neill, S. Litt, E. Couch, S. and Davies, A. (2009) The impact of tidal stream turbines on large-scale sediment dynamics, *Renewable Energy*, 34, pp.2803-2812.

Neill, S.P., Jordan, J.R. and Couch, S.J. (2012) Impact of tidal energy converter (TEC) arrays on the dynamics of headland sand banks. *Renewable Energy*, 37(1), pp.387-397.

Neill, S.P., Hashemi, M.R. and Lewis, M.J. (2014) Optimal phasing of the European tidal stream resource using the greedy algorithm with penalty function. *Energy*, 73, pp.997-1006.

Neill, S.P., Vögler, A., Goward-Brown, A.J., Baston, S., Lewis, M.J., Gillibrand, P.A., Waldman, S. and Woolf, D.K. (2017) The wave and tidal resource of Scotland. *Renewable Energy*: in press. Available online 16 March 2017.

Niclasen, B.A. and Simonsen, K. (2007) Validation of the ECMWF analysis wave data for the area around the Faroe Islands. *Societas Scientiarum Færoensis*.

Nickerson, R.S. (2000) Null hypothesis significance testing: a review of an old and continuing controversy. *Psychological methods*, 5(2), p.241.

O'Rourke, F., Boyle, F. and Reynolds, A. (2010). Tidal current energy resource assessment in Ireland: Current status and future update. *Renewable and Sustainable Energy Reviews*, 14(9), pp.3206-3212.

Openhydro (2016) Brimms Tidal Array Environmental Statement, Volume 2, Chapter 5. [Online]. Available: <http://www.openhydro.com/download/brims/Brims-ES-Volume-2-A-CH-5-May-2016.pdf>.

ORJIP Ocean Energy (2015) The Forward Look; an Ocean Energy Environmental Research Strategy for the UK, [Online], Available: <http://www.orjip.org.uk/documents>.

OSU Tidal Data Inversion, [Online], Available: <http://volkov.oce.orst.edu/tides/>.

Page, H.M., Dugan, J.E., Culver, C.S. and Hoesterey, J.C. (2006) Exotic invertebrate species on offshore oil platforms. *Marine Ecology - Progress Series*, 325, pp.101–07.

Parker, B.B. (2007) Tidal analysis and prediction. US Department of Commerce, National Oceanic and Atmospheric Administration, National Ocean Service, Centre for Operational Oceanographic Products and Services.

Phillips, S.J., Anderson, R.P. and Schapire, R.E. (2006) Maximum entropy modelling of species geographic distributions. *Ecological modelling*, 190(3), pp.231-259.

Phillips, S. J. and Dudík, M. (2008), Modelling of species distributions with Maxent: new extensions and a comprehensive evaluation. *Ecography*, 31, pp.161–175.

Pingree, R.D. and Griffiths, D.K. (1979). Sand transport paths around the British Isles resulting from M 2 and M 4 tidal interactions. *Journal of the Marine Biological Association of the United Kingdom*, 59(02), pp.497-513.

Pingree, R.D. and Griffiths, D.K. (1987) Tidal friction for semidiurnal tides. *Continental shelf research*, 7(10), pp.1181-1209.

Plew, D.R. and Stevens, C.L. (2013) Numerical modelling of the effect of turbines on currents in a tidal channel – Tory Channel, New Zealand, *Renewable Energy*, 57, p269-282.

PMMS (Project Management Support Services) Ltd. (2006). Skerries Tidal Stream Array: Environmental Impact Assessment Scoping Report. Report by TÜV SÜD PMSS. pp 84.

Pugh, D. (1987) *Tides, surges, and mean sea level*, John Wiley & Sons, Chichester, ISBN 0 471 91505 X.

Rastogi, A.K. and Rodi, W. (1978) Predictions of heat and mass transfer in open channels. *Journal of the Hydraulics division*, 104(3), pp.397-420.

Reddy, S. and Dávalos, L.M. (2003) Geographical sampling bias and its implications for conservation priorities in Africa. *Journal of Biogeography*, 30(11), pp.1719-1727.

Reiss, H., Cunze, S., König, K., Neumann, H. and Kröncke, I. (2011) Species distribution modelling of marine benthos: a North Sea case study. *Mar Ecol Prog Ser*, 442, pp.71–86.

Remya, K., Ramachandran, A. and Jayakumar, S. (2015) Predicting the current and future suitable habitat distribution of *Myristica dactyloides* Gaertn. using MaxEnt model in the Eastern Ghats, India. *Ecological Engineering*, 82, pp.184-188.

REN21 (2016) *Renewables 2016 Global Status Report*, Paris: REN21 Secretariat. ISBN 978-3-9818107-0-7.

RenewableUK (2015) *Wave and Tidal Energy in the UK – Capitalising on Capability*, [Online], Available: <http://www.renewableuk.com/en/publications/index.cfm/>.

reNEWS (2014) MCT loses vital Skerries cash, 18<sup>th</sup> June, [Online], Available: <http://renews.biz/68698/mct-loses-vital-skerries-cash/>.

Retiere, C. (1994) Tidal power and the aquatic environment of La Rance. *Biological journal of the Linnean society*, 51(1-2), pp.25-36.

Robins, P.E., Neill, S.P. and Lewis, M.J. (2014) Impact of tidal-stream arrays in relation to the natural variability of sedimentary processes. *Renewable Energy*, 72, pp.311-321.

Robins, P.E., Neill, S.P., Lewis, M.J. and Ward, S.L. (2015) Characterising the spatial and temporal variability of the tidal-stream energy resource over the northwest European shelf seas. *Applied Energy*, 147, pp.510-522.

Robinson, I.S. (1979) The tidal dynamics of the Irish and Celtic Seas. *Geophysical Journal International*, 56(1), pp.159-197.

Robinson, I.S. (1981) Tidal vorticity and residual circulation. *Deep Sea Research Part A. Oceanographic Research Papers*, 28(3), pp.195-212.

Roche, R.C., Walker-Springett, K., Robins, P.E., Jones, J., Veneruso, G., Whitton, T.A., Piano, M., Ward, S.L., Duce, C.E., Waggitt, J.J. and Walker-Springett, G.R. (2016) Research priorities for assessing potential impacts of emerging marine renewable energy technologies: Insights from developments in Wales (UK). *Renewable Energy*, 99, pp.1327-1341.

Roelvink, J.A. and Van Banning, G.K.F.M. (1995) Design and development of DELFT3D and application to coastal morphodynamics. *Oceanographic Literature Review*, 11(42), p.925.

Rogers, C.S. (1990) Responses of coral reefs and reef organisms to sedimentation. *Marine ecology progress series*. Oldendorf, 62(1), pp.185-202.



Rolet, C., Spilmont, N., Davout, D., Goberville, E. and Luczak, C. (2015) Anthropogenic impact on macrobenthic communities and consequences for shorebirds in Northern France: A complex response. *Biological Conservation*, 184, pp.396-404.

Rourke, F.O., Boyle, F. and Reynolds, A. (2010) Marine current energy devices: current status and possible future applications in Ireland. *Renewable and Sustainable Energy Reviews*, 14(3), pp.1026-1036.

Ryland, J.S. (1976). *Physiology and ecology of marine bryozoans*. *Advances in Marine Biology*, 14, pp.285-443.

Saint-Venant, A.J.C, (1871) Théorie du mouvement non-permanent des eaux, avec application aux crues des rivières et à l'introduction des marées dans leur lit. *Compte-Rendu à l'Académie des Sciences de Paris*, 73, pp147-154.

Samaras, A. G., Gaeta, M. G., Moreno Miquel, A., and Archetti, R. (2016) High resolution wave and hydrodynamics modelling in coastal areas: operational applications for coastal planning, decision support and assessment, *Nat. Hazards Earth Syst. Sci. Discuss.*, doi:10.5194/nhess-2016-63, in review.

Savidge, G., Ainsworth, D., Bearhop, S., Christen, N., Elsaesser, B., Fortune, F., Inger, R., Kennedy, R., McRobert, A., Plummer, K.E. and Pritchard, D.W. (2014) Strangford Lough and the SeaGen tidal turbine. *Marine Renewable Energy Technology and Environmental Interactions*, pp.153-172.

Scottish Government (2016) *Marine Spatial Planning*, [Online], Available: <http://www.gov.scot/Topics/marine/science/MSInteractive/Themes/msp>.

Scottish Power Renewables. (2010). *Sound of Islay Environmental Statement*. Report by Royal Haskoning and Scottish Power Renewables.

Scottish Power Renewables (2013) *Update on Argyll Array Offshore Wind Farm*, [Press Release], 13 December, [Online], Available: <http://www.argyllarray.com/news-detail.asp?item=195>.

Serhadlioglu, S. (2014) *Tidal stream resource assessment of the Anglesey Skerries and the Bristol Channel* (Doctoral dissertation, University of Oxford).

Shields, M.A., Dillon, L.J., Woolf, D.K. and Ford, A.T. (2009) Strategic priorities for assessing ecological impacts of marine renewable energy devices in the Pentland Firth (Scotland, UK). *Marine Policy*, 33(4), pp.635-642.

Shields, M.A., Woolf, D.K., Grist, E.P., Kerr, S.A., Jackson, A.C., Harris, R.E., Bell, M.C., Beharie, R., Want, A., Osalusi, E. and Gibb, S.W. (2011) *Marine renewable energy: The*

ecological implications of altering the hydrodynamics of the marine environment. *Ocean & Coastal Management*, 54(1), pp.2-9.

Shipton, M. (2014) Four key figures in Hafren Power resign, Wales Online, [Online], [14 Jan 2014], Available: <http://www.walesonline.co.uk/business/four-key-figures-hafren-power-6504734>.

Short, F.T. and Wyllie-Echeverria, S. (1996) Natural and human-induced disturbance of seagrasses. *Environmental conservation*, 23(01), pp.17-27.

Simons, D.G. and Snellen, M. (2009) A Bayesian approach to seafloor classification using multi-beam echo-sounder backscatter data. *Applied Acoustics*, 70(10), pp.1258-1268.

Synderman, M. and Wiseman, C. (1996) *Guide to marine life: Caribbean, Bahamas, Florida*. New York: Aqua Quest Publications.

Soulsby, R. (1997) *Dynamics of marine sands: a manual for practical applications*. Thomas Telford Publications, London, ISBN 0 7277 2584 X, 1997.

Soulsby, R. (2006) Simplified calculation of wave orbital velocities. Technical Report, HR Wallingford.

Sparks -McConkey, P.J. and Watling, L. (2001) Effects on the ecological integrity of a soft-bottom habitat from a trawling disturbance. *Hydrobiologia*, 456, pp.73-85.

Stein, J.E., Collier, T.K., Reichert, W.L., Casillas, E., Hom, T. and Varanasi, U. (1992) Bioindicators of contaminant exposure and sublethal effects: studies with benthic fish in Puget Sound, Washington. *Environmental Toxicology and Chemistry*, 11(5), pp.701-714.

Stephens, D. and Diesing, M (2015) "Towards Quantitative Spatial Models of Seabed Sediment Composition". *PLoS ONE* 10(11): e0142502.

Stockwell, D. (1999) The GARP modelling system: problems and solutions to automated spatial prediction, *International Journal of Geographical Information Science*, 13(2), pp.143-158.

TELEMAC-MASCARET, [Online], Available: <http://www.openTELEMAC.org/>.

Tethys: Project Site Annex IV Map viewer, [Online], Available: [https://tethys.pnnl.gov/map-viewer-marine-energy?f\[0\]=type%3Aannex\\_iv\\_site](https://tethys.pnnl.gov/map-viewer-marine-energy?f[0]=type%3Aannex_iv_site).

Thiébot, J., du Bois, P.B. and Guillou, S. (2015) Numerical modelling of the effect of tidal stream turbines on the hydrodynamics and the sediment transport—Application to the Alderney Race (Raz Blanchard), France. *Renewable Energy*, 75, pp.356-365.

Thrush, S.F. and Dayton, P.K. (2002) Disturbance to marine benthic habitats by trawling and dredging: implications for marine biodiversity. *Annual Review of Ecology and Systematics*, pp.449-473.

Tidal Energy Ltd (2012) Environmental Scoping Report, [Online], Available: <http://www.tidalenergyltd.com/>.

Tidal Energy Ltd (2015) Wales steps forward in marine renewable energy as the country's first full scale tidal energy demonstration device is installed, [Press Release], 14 December, [Online], Available: <http://www.tidalenergyltd.com/?p=2418>.

Tidal Lagoon Power (2015) The Return of British Sea Power: Consent for World's First Tidal Lagoon Power Plant Opens New Door in Global Effort to Address Climate Change [Press release]. [9 Jun 2015]. Available: <http://www.tidallagoonpower.com/news/>.

Tidal Ventures (2015) Torr Head Tidal Energy Array EIA, [Online], Available: <http://www.tidalventures.com/downloads/environmentalstatement/>

Trivellato, F. and Raciti Castelli, M. (2014) On the Courant–Friedrichs–Lewy criterion of rotating grids in 2D vertical-axis wind turbine analysis. *Renewable Energy*, 62, pp. 53-62.

Tyler-Walters, H. (2008) *Mytilus edulis* Common mussel. In Tyler-Walters H. and Hiscock K. (eds) *Marine Life Information Network: Biology and Sensitivity Key Information Reviews*, [Online]. Plymouth: Marine Biological Association of the United Kingdom. Available from: <http://www.marlin.ac.uk/species/detail/1421>.

Uihlein, A. and Magagna, D. (2016) Wave and tidal current energy—A review of the current state of research beyond technology. *Renewable and Sustainable Energy Reviews*, 58, pp.1070-1081.

UK Government (2013) Wave and tidal energy: part of the UK's energy mix, [Online], Available: <https://www.gov.uk/wave-and-tidal-energy-part-of-the-uks-energy-mix>.

UK Marine Industries Alliance, A strategy for Growth for the UK Marine Industries (2011), [Online], Available:

[https://www.gov.uk/government/uploads/system/uploads/attachment\\_data/file/31813/1-1310-strategy-for-growth-uk-marine-industries.pdf](https://www.gov.uk/government/uploads/system/uploads/attachment_data/file/31813/1-1310-strategy-for-growth-uk-marine-industries.pdf).

Van der Meer, J. (1997) Sampling design of monitoring programmes for marine benthos: a comparison between the use of fixed versus randomly selected stations. *Journal of Sea Research*, 37(1-2), pp.167-179.

- van Nieuwkoop, J.C., Smith, H.C., Smith, G.H. and Johanning, L. (2013) Wave resource assessment along the Cornish coast (UK) from a 23-year hindcast dataset validated against buoy measurements. *Renewable energy*, 58, pp.1-14.
- Violeau, D., Bourban, S., Cheviet, C., Markofsky, M., Petersen, O., Roberts, W., Spearman, J., Toorman, E., Vested, H.J. and Weilbeer, H. (2002) Numerical simulation of cohesive sediment transport: intercomparison of several numerical models. *Proceedings in Marine Science*, 5, pp.75-89.
- Wadey, M.P., Brown, J.M., Haigh, I.D., Dolphin, T. and Wisse, P. (2015). Assessment and comparison of extreme sea levels and waves during the 2013/2014 storm season in two UK coastal regions. *Natural Hazards and Earth System Sciences Discussions*, 3(4), pp.2665-2708.
- Walkington, I. and Burrows, R. (2009) Modelling tidal stream power potential. *Applied Ocean Research*, 31(4), pp.239-245.
- Warwick, R.M. and Uncles, R.J. (1980) The distribution of benthic macrofauna associations in the Bristol Channel in relation to tidal stress. *Marine Ecology Progress Series*, 3, pp.97-103.
- Warren, I.R. and Bach, H.K. (1992) MIKE21: a modelling system for estuaries, coastal waters and seas. *Environmental Software*, 7(4), pp. 229-240.
- West, A.M., Kumar, S., Brown, C.S., Stohlgren, T.J. and Bromberg, J., 2016. Field validation of an invasive species Maxent model. *Ecological Informatics*, 36, pp.126-134.
- Whiles, M.R. and Wallace, J.B. (1995) Macroinvertebrate production in a headwater stream during recovery from anthropogenic disturbance and hydrologic extremes. *Canadian Journal of Fisheries and Aquatic Sciences*, 52(11), pp.2402-2422.
- Wilson, C.A.M.E., Bates, P.D. and Hervouet, J.M. (2002) Comparison of turbulence models for stage-discharge rating curve prediction in reach-scale compound channel flows using two-dimensional finite element methods. *Journal of Hydrology*, 257(1), pp.42-58.
- Wilson, S., Bourban, S. and Couch, S. (2012). Understanding the interactions of tidal power projects across the UK continental shelf. In 4th International Conference on Ocean Energy, Dublin.
- Woolf, D.K. (2013) The strength and phase of the tidal stream. *Int. J. Marine Energy*, 3, p.4.

Woolf, D.K., Easton, M.C., Bowyer, P.A. and McIlvenny, J. (2014) The physics and hydrodynamic setting of marine renewable energy. In *Marine Renewable Energy Technology and Environmental Interactions* (pp. 5-20). Springer Netherlands.

World Health Organisation (2005) *Millennium Ecosystem Assessment, Ecosystems and Human Well-being: Synthesis*. Island Press, Washington, DC.

Yang, X.Q., Kushwaha, S.P.S., Saran, S., Xu, J. and Roy, P.S., 2013. Maxent modeling for predicting the potential distribution of medicinal plant, *Justicia adhatoda* L. in Lesser Himalayan foothills. *Ecological engineering*, 51, pp.83-87.

Yates, N., Burrows, R., Walkington, I. and Hedges, T. (2010) Studies on tidal power from estuaries of North-West England, in *Proc. 1st IAHR Europe Congress*, Edinburgh, Scotland.

Young, E.F., Aldridge, J.N. and Brown, J. (2000) Development and validation of a three-dimensional curvilinear model for the study of fluxes through the North Channel of the Irish Sea. *Continental Shelf Research*, 20(9), pp.997-1035.

Zaniewski, A.E., Lehmann, A. and Overton, J.M. (2002) Predicting species spatial distributions using presence-only data: a case study of native New Zealand ferns. *Ecological modelling*, 157(2), pp.261-280.

Zhang W., Xia H., Wang B. (2009) Numerical Calculation of the Impact of Offshore Wind Power Stations on Hydrodynamic Conditions. In: *Advances in Water Resources and Hydraulic Engineering*. Springer, Berlin, Heidelberg.

Zheng, X., Huang, L., Lin, R. and Du, J. (2015) Roles of epiphytes associated with macroalgae in benthic food web of a eutrophic coastal lagoon. *Continental Shelf Research*, 110, pp.201-209.